Investigating the role of innate lymphoid cells in targeted radiotherapy in lung cancer

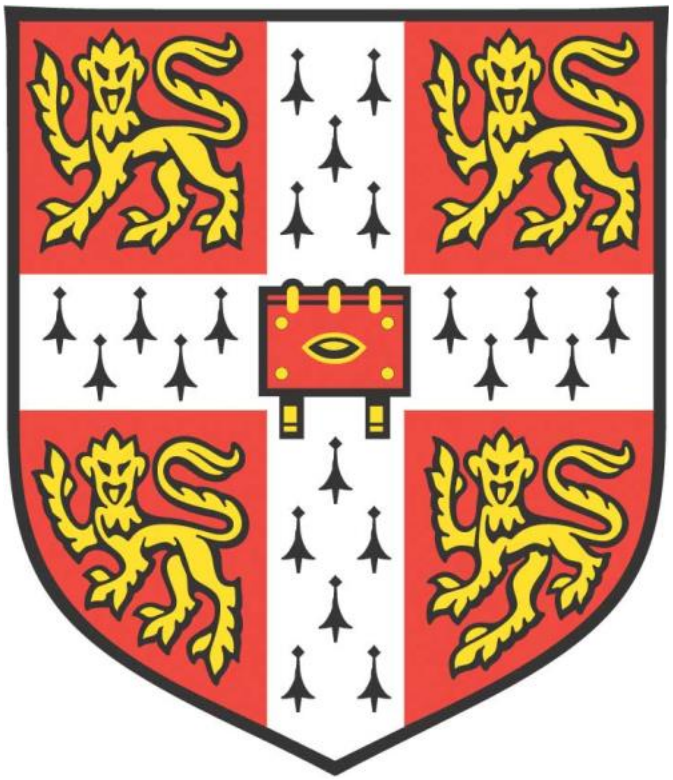

Shaun Png Ren Jie

Cancer Research UK Cambridge Institute

Homerton College

University of Cambridge

This dissertation is submitted for the degree of Doctor of Philosophy

September 2022

Declaration

This thesis is the result of my work. The inducible antigen construct discussed in Chapter 5 was designed by Dr Julie Stockis. No other work in the thesis was carried out in collaboration except as specified in the text.

I state that my dissertation is not substantially the same as any work that I have submitted before, or is being concurrently submitted for any degree, diploma or other qualification at the University of Cambridge or any other University or similar institution.

This thesis does not exceed the word limit of 60,000 prescribed by the Degree Committee of Clinical Medicine and Clinical Veterinary Medicine, excluding the figures, tables and references.

Shaun Png

Investigating the role of innate lymphoid cells in targeted radiotherapy in lung cancer

Shaun Png

Summary

Radiotherapy is a mainstay of lung cancer treatment, and its role in regulating immune responses to promote anti-cancer response is increasingly appreciated. However, it is still not fully understood how radiotherapy modulates the immune microenvironment in lung cancer. In the lung, ILC2s are critical innate lymphocytes that modulate Type 2 immunopathology, but their role in modulating the immune response to lung cancer is not fully understood. Furthermore, it is unclear how ILC2s respond to targeted lung radiotherapy. In this thesis, I characterised the response of ILC2s to lung radiotherapy and elucidate their response alongside the general immune response in targeted radiotherapy to lung cancer. Finally, I aimed to establish a model to study the role of ILC2s in modulating the adaptive immune response in the primary lung cancer context.

I established a model of targeted lung irradiation using a preclinical treatment platform known as the Small Animal Radiation Research Platform (SARRP) and monitored immune responses. In the naïve setting, targeted lung irradiation was observed to deplete ILC2s in the long term, but this was not observed in the majority of immune cells studied. Irradiated ILC2s expressed the activation marker OX40L, though this was not accompanied by increased production of Type 2 cytokines. In the tumour setting, ILC2s also express OX40L but do not appear to contribute to anti-tumour immunity. Probing the overall immune response to targeted lung radiotherapy in the tumour context demonstrated the importance of both the innate and adaptive immune response in radiotherapy-induced anti-tumour immunity. Dendritic cells (DCs) and adaptive CD4+ and CD8+ T-cells were activated and are crucial for anti-tumour immune responses. Innate NK cells are also important as their depletion reduced the effectiveness of radiotherapy.

To study the role of ILC2s in the regulation of adaptive immune responses in cancer, I validated an inducible antigen-expressing cassette and confirmed its functionality both i*n vitro* and *in vivo*. Expression of the antigen by tumour cells elicited adaptive CD4+ and CD8+ T-cell responses. I have also derived primary lung cancer cell lines to be used in combination with the cassette and demonstrate their capacity to engraft in the lung upon orthotopic implantation. Further work is needed to refine the orthotopic model of primary lung cancer, and to incorporate the cassette into the cell line. This could then be used alongside ILC2-deficient mouse models to study the role of ILC2s in modulating the adaptive immune response in lung cancer.

Acknowledgements

First off, I would like to thank Tim Halim for his supervision over the past 4 years and for providing me with the opportunity to do a PhD in this lab. Thank you for allowing me the freedom and confidence to navigate my way through the project, and for providing advice whenever things didn't go the way we wanted. Thank you for always providing a global perspective of the work that we do in the lab and for always entertaining my silly questions. Most importantly, thank you for creating this wonderful lab environment, and I will never forget the 4 years that I've spent in the Halim Lab.

Secondly, I would like to thank all members of the Halim Lab, both past and present, for being a constant source of support during my time here. Thank you, Martijn, for being an instrumental mentor during the early years of my PhD. Thank you, Julie, for being a role model that I could always turn to whenever I needed help. You have been a guardian angel for me and everyone else in the lab. Thank you, Celine, for being the backbone of the lab, for the technical support and training, and for being a colleague and friend I could always whine to. Thank you, Julia, Silvain and Liang for always being available for a chat or coffee. Thank you, my fellow students (and allies!) Shwetha, Sheng, Thomas, Bella, Stela, Charlotte and Weike for being such a supportive bunch, and for being a part of this journey with me.

I would also like to thank my friends and colleagues at the CRUK CI. Thank you Sabrina and Erica for the help with the SARRP, and even more so for being amazing colleagues whom I could always chat with freely. Thank you, Sheng, Thomas, Ming Li and Vincenzo for always listening to my rants and for being available for coffee and chats. Thank you to the core facilities for their support, in particular Flow Cytometry, RICS, Imaging and Histopathology. A special shoutout to all members of the BRU, which have been crucial in providing support for the extensive mouse work in my project. I would also like to thank the scientific administration team, in particular, Ann. Thank you, Ann, for being the reason I was able to come to Cambridge to do this PhD, and for providing support during difficult times. I would also like to extend my gratitude to the CRUK for their funding, without which the work done in this project would not have been possible.

Finally, I would like to thank my friends and family for their unwavering support throughout my time abroad. While I have been living abroad for the past 7 years, I have never felt lonely because I know all of you had my back and I could always turn to you all for support. I am extremely grateful for this. I would like to thank my partner Ke Xuan, for being my biggest supporter throughout this journey. Thank you for being with me at the highest of highs and the lowest of lows, and for reminding me that I am more than enough as a scientist and a person.

Contribution to publication

Schuijs, M.J., **Png, S.**, Richard, A.C. *et al.* ILC2-driven innate immune checkpoint mechanism antagonizes NK cell antimetastatic function in the lung. *Nat Immunol* **21,** 998–1009 (2020). https://doi.org/10.1038/s41590-020-0745-y

My contribution to this manuscript involved studying the role of Group 2 innate lymphoid cells (ILC2) in promoting lung metastatic cancer via eosinophil-mediated metabolic control of Natural killer (NK) cell function. These data are not included in this thesis but are occasionally referenced.

Contents

Abbreviations

3DCRT	3-dimensional conformation radiation therapy
ALK	Anaplastic lymphoma kinase
AM	Alveolar macrophages
APC	Antigen presenting cells
APL	Acute promyelocytic leukaemia
ATR	Ataxia telangiectasia and Rad3-related
cDC	Conventional DCs
CFSE	Carboxyfluorescein succinimidyl ester
CGRP	Calcitonin gene-related peptide
CHILP	Common helper innate lymphoid progenitor
CILP	Common innate lymphoid progenitor
CLP	Common lymphoid progenitors
COPD	Chronic obstructive pulmonary disease
COX2	Cyclooxygenase 2
CRTH2	Chemoattractant receptor-homologous molecule expressed on TH2 cells
CT	Computed tomography
CTLA4	Cytotoxic T-lymphocyte-associated protein 4
DC	Dendritic cells
DMSO	Dimethyl sulfoxide
dKP	derived KP
EGFR	Epithelial growth factor receptor
FALC	Fat-associated lymphoid cluster
FGFR1	Fibroblast growth factor receptor 1
Foxp3	Forkhead box P3
FTY720	Fingolimod
GATA3	GATA Binding Protein 3
G-CSF	Granulocyte stimulating factor
GEMM	Genetically engineered mouse models
GM-CSF	Granulocyte-macrophage colony-stimulating factor
Gy	Gray
HDM	House dust mite
HMGB1	High mobility group box protein 1
IAV	Influenza A virus
ICD	Immunogenic cell death
IFNβ	Interferon beta
IFNγ	Interferon gamma
IGRT	Image-guided radiotherapy
ILC	Innate lymphoid cell
iILC2	Inflammatory ILC2
ILCP	ILC progenitor
ILC2P	ILC2 progenitor
Ih2	Innate helper 2
IM	Interstitial macrophages
IMRT	Image modulated radiation therapy
iNH	Immature Natural helper
iNOS	Inducible nitric oxide synthase
iOVA	Inducible OVA
ITR	Inverted terminal repeats
JAK2	Janus kinase 2

K	*Kras*$^{LSL\text{-}G12D}$
KP	*Kras*$^{LSL\text{-}G12D}$*p53*$^{fl/fl}$
LCC	Large cell carcinoma
LKB1	Liver kinase B1
LSIG	Lin-Sca1+ID2+Gata3+ cells
LTi	Lymphoid tissue inducer
LUAD	Lung adenocarcinoma
LUSC	Lung squamous cell carcinoma
MAPK	Microtubule associated protein kinase
MDSC	Myeloid-derived suppressor cells
MHC	Multiple histocompatibility complex
mLN	Mediastinal lymph nodes
MDSC	Myeloid-derived suppressor cells
mTOR	mammalian target of rapamycin
NH	Natural helper
NMUR	Neuromedin U receptor
Nrp1	Neuropilin-1
NSCLC	Non-small cell lung cancer
OVA	Ovalbumin
PDAC	Pancreatic ductal adenocarcinoma
PD-1	Programmed cell death protein 1
PD-L1	Programmed cell death ligand 1
PGD2	Prostaglandin D2
PGE2	Prostaglandin E2
PMA	Phorbol 12-myristate 13-acetate
PTEN	Phosphatase and tensin homolog
Rb1	Retinoblastoma protein
RORα	RAR-related orphan receptor alpha
RORγt	RAR-related orphan receptor gamma
ROS	Reactive oxygen species
RTK	Receptor tyrosine kinases
rtTA	Reverse-tetracycline controlled transactivator
SABR	Stereotactic ablative radiotherapy
SARRP	Small animal radiation research platform
SCFA	Short-chain fatty acid
SCLC	Small cell lung cancer
SPC	Surfactant protein C
TAM	Tumour associated macrophages
TCR	T-cell receptor
TGFβ	Transforming growth factor beta
TME	Tumour microenvironment
TLR4	Toll-like receptor 4
TNFα	Tumour necrosis factor alpha
TP53	Tumour protein 53
TRE	Tetracycline responsive element
Treg	Regulatory T-cells
tTS	Tetracycline-controlled transcriptional silencer
Trex1	Three Prime Repair Exonuclease 1
WT	Wild type
VCAM-1	Vascular cell adhesion protein 1
VMAT	Volumetric modulated arc therapy

Chapter 1: General introduction

1.1 Lung cancer

1.1.1 Epidemiology of lung cancer

Lung cancer is the most common cancer and the leading cause of cancer deaths in the world, with 2.1 million new cases and 1.8 million deaths reported in 2018 (Bray et al. 2018). Furthermore, lung cancer contributes to a sixth of all cancer deaths (Sung et al. 2021). In 2020, there were approximately 370,000 and 100,000 deaths from lung cancer in Europe and the USA respectively (Sung et al. 2021). Despite advances in recent years in lung cancer treatments, the 5-year survival rate in the US has remained low at about 15-20% in the last decade, with developing countries displaying even lower survival rates (Bray et al. 2018). Notably, the majority of lung cancer incidences are diagnosed only after metastasis has taken place, thereby contributing to lower survival rates (Cronin et al. 2018), highlighting the need for improvements in early detection.

The importance of environmental factors in lung cancer development cannot be overstated, and tobacco smoking remains the largest risk factor for lung cancer (Wild et al. 2015; Stanaway et al. 2018). In high-income countries, efforts to reduce smoking rates were fundamental in reducing lung cancer incidences and improved survival, but this is less so in low-income countries in part due to reduced healthcare access and public initiatives (Thai et al. 2021). Other factors associated with lung cancer incidences include, but are not limited to, age, sex, race and socioeconomic status, air pollution, genetics and diet and these have been extensively reviewed elsewhere (Bade and Dela Cruz 2020).

Lung cancer can be broadly characterised into 2 subtypes; non-small cell lung cancer (NSCLC) and small cell lung cancer (SCLC). NSCLC accounts for approximately 85% of lung cancer cases, with SCLC encompassing the remaining 15% (Lemjabbar-Alaoui et al. 2015). NSCLCs can be further characterised into 3 distinct subtypes; lung adenocarcinoma (LUAD), lung squamous cell carcinoma (LUSC) and large cell carcinoma (LCC), with LUAD being the most common type of lung cancer. SCLC is the most aggressive subtype of lung cancer, and patients observe a 5-year survival rate of less than 7 years (Karachaliou et al. 2016).

Table 1 compares some key traits of both lung cancer types. While the staging of both cancer subtypes slightly defer, severity in both cases is in part determined by the spread to the other lung lobes, lymph nodes and distant organs. Smoking remains the main risk factor for both cancer types (Lemjabbar-Alaoui et al. 2015). This is particularly true for SCLC, where most diagnosed patients are

heavy (10-20 pack years) or former smokers (Alexandrov et al. 2016). The cell of origin of SCLC remains unknown, with neuroendocrine progenitors being the most likely candidate (Sutherland et al. 2011). Adenocarcinomas and squamous cell carcinomas are postulated to derive from alveolar Type 2 epithelial cells expressing surfactant protein C (SPC) (Mainardi et al. 2014) and tracheal basal cell progenitors (Rock et al. 2009) respectively, while LCC describes lung cancer bearing no resemblance to previously stated lung cancer types (Pelosi et al. 2015)

SCLCs present with large numbers of genetic alterations. This includes mutations facilitating the overexpression of oncogenes, suppression of tumour suppressor genes, and altered expression of receptor tyrosine kinases (RTK) (D'Angelo and Pietanza 2010). Recent characterisation of the genomic profile of SCLCs has demonstrated universal inactivation of genes encoding tumour protein 53 (Tp53) and retinoblastoma protein (Rb1) (George et al. 2015), and copy number alterations have been found in Janus kinase 2 (JAK2), Fibroblast growth factor receptor 1 (FGFR1) and *MYC* genes (Voortman et al. 2010). For NSCLCs, mutations in the genes *KRAS* and *TP53* are key oncogenic drivers and are thereby utilised in several genetically engineered mouse models (GEMM) of lung cancer. Mutations in the genes encoding Anaplastic lymphoma kinase (ALK) and Epithelial growth factor receptor (EGFR) are also observed (Paez et al. 2004; Kwak et al. 2010), rendering these appropriate targets for therapeutics (Herbst, Morgensztern, and Boshoff 2018). Other mutations observed in NSCLCs are implicated in various metabolic and signalling pathways, including the genes encoding microtubule associated protein kinase (MAPK), Wnt, mammalian target of rapamycin (mTOR), and cell cycle and RTK signalling pathways (Ding et al. 2008; Cancer Genome Atlas Research, Network 2014). Hence, despite several shared mutations between both cancer types, there exists clear differences in the mutational landscape. The remainder of the introduction for this thesis will be predominantly focused on NSCLC.

Table 1: Summary of the comparison between NSCLC and SCLC.

Cancer type	**Staging**	**Origin**	**Associated mutations**	**Risk factors (shared)**
SCLC	Limited Stage Extensive Stage	Neuroendocrine progenitor cells	*TP53* *RB1* *JAK2* *FGFR* *MYC* *PARP1* *EZH2*	Smoking (main) Genetics Diet and Alcohol Air pollution Occupation-related factors
NSCLC	Stage I Stage II Stage IIIa Stage IIIb Stage IV	**Adenocarcinoma**: Type 2 epithelial cells **Squamous cell carcinoma**: Tracheal basal cell progenitors	*KRAS* *TP53* *ALK* *EGFR* *LKB1/STK11*	

1.1.2 Modelling lung cancer in preclinical mouse models

Preclinical studies in mice have greatly improved our knowledge of lung cancer. This is facilitated primarily by the introduction of tumour cells and xenografts into mice to promote lung cancer development and the use of GEMMs.

Primary lung cancer can be mimicked in mice via the implantation of tumour cells directly into the lungs of syngeneic mice. In the C57BL/6 background, the LL/2 Lewis Lung carcinoma and CMT167 lung carcinoma are 2 common murine lung cell lines. Both of these are of epithelial origin are and considered adenocarcinomas. The implantation of these cell lines into the lungs of syngeneic C57BL/6 mice mimic primary lung tumours (Li et al. 2017; Doki et al. 1999). Notably, these lung tumour cells can also be injected subcutaneously to induce solid lung tumours, though this does not replicate the lung microenvironment. However, the introduction of well-established late stage cancer cell lines into tissues does not mimic the natural progression of cancer from a neoplastic state. Apart from primary lung tumours, the study of lung metastasis can be achieved via the introduction of tumour cells into the tail vein of the mice. For instance, lung metastatic seeding occurs when B16 melanoma cells are introduced via the tail vein (Overwijk and Restifo 2001). Alternatively, lung metastasis also occurs when orthotopically injected tumour cells in other tissues metastasise to the lungs. In the 4T1 model for instance, the injection of 4T1 breast cancer cells into the mammary fat pad of syngeneic BALB/C mice leads to lung metastasis formation (Yang, Zhang, and Huang 2012).

While the use of mouse cell lines comes with relative ease of handling and high reproducibility, these often do not accurately mimic human cancers. The use of xenografts or human-derived cell lines better mimics the intrinsic features observed in human cancers. Common human cell lines used in the study of adenocarcinomas include A549, H1298 and HCC827 (Kellar, Egan, and Morris 2015) and implantation of these cells to the lungs of immune-deficient mice is used as models for NSCLCs (Cui et al. 2006; Justilien and Fields 2013). Apart from human-derived cell lines, patient-derived xenografts are also utilised, which also require the use of immune-deficient mice. However, poor engraftment rates are common (Olson et al. 2018). Crucially, these models are limiting because they do not mimic the natural immunosuppressive microenvironment of cancer, as immune-deficient mice are required in these models.

The above models described are limited because tumour cells are transplanted, which does not mimic primary tumour development. Hence, GEMMs confer an advantage to study how primary tumour develops via the presence of driver mutations within these mouse models. One of the earliest GEMMs for lung cancer is the *Kras*$^{LSL\text{-}G12D/+}$ (K) mouse model, which develop lung tumours

due to the expression of mutant Kras protein (Jackson et al. 2001, 2005). In the presence of Cre recombinase, the stop codon flanked by loxP sites in the *Kras* gene is removed, allowing for the expression of mutant Kras to drive lung adenocarcinoma development. KP mice are developed from a cross between K mice and *Trp53*$^{fl/fl}$ mice, which contains loxP sites flanking the exons of the gene encoding the Trp53 protein, creating null alleles. KP mice develop tumours faster than K mice due to the combined effects of mutant *Kras* gene expression and null expression of *Trp53* (DuPage, Dooley, and Jacks 2009).

Activating mutations in Kras have also been utilised in combination with other activating or inactivating mutations to model lung cancer development, such as Phosphatase and tensin homolog (PTEN) and Liver kinase B1 (LKB1) (Ji et al. 2007; Iwanaga et al. 2008). In addition, other mouse models of lung cancer incorporate mutations in other NSCLC-associated genes seen in humans such as *ALK* and *EGFR* (Regales et al. 2007; Soda et al. 2008). Of note, EML4-ALK is a fusion protein derived from chromosomal inversion leading to human NSCLC, and a mouse model of EML4-ALK expression specific to lung alveolar cells drives lung adenocarcinoma (Soda et al. 2008). Similarly, GEMMs for SCLC involve inducing mutations in relevant genes, such a *Trp53 and Rb1* (Meuwissen et al. 2003). Hence, a wide variety of preclinical mouse models are available to study lung cancer, and these have proven useful in providing insight to lung cancer development.

1.1.3 Therapeutic approaches: surgery, chemotherapy, immunotherapy and radiotherapy

Surgery and resection of Stage I and II NSCLC is the preferred method of treatment (Ko, Raben, and Formenti 2018). Surgery is also used in Stage III NSCLC, but typically in combination with chemotherapy (Lemjabbar-Alaoui et al. 2015). Notably, chemotherapy can be used alongside surgery as an adjuvant to minimise lung cancer relapse (Zappa and Mousa 2016). Surgery can be utilised for limited-stage SCLC as well (Lemjabbar-Alaoui et al. 2015).

Chemotherapy is typically used in Stage III and IV NSCLC. As mentioned, surgery alongside chemotherapy is considered standard treatment for Stage III NSCLC (Lemjabbar-Alaoui et al. 2015). The use of chemotherapy in Stage IV NSCLC is also common, as surgery is no longer an option at that stage. In limited stage SCLC, chemotherapy alone improves survival but improved outcomes are observed when combined with surgery (Videtic et al. 2003). The platinum-based DNA alkylating agent cisplatin is typically the preferred choice in Stage IV NSCLCs to tackle rapidly dividing lung cancer cells (Dasari and Tchounwou 2014; Zappa and Mousa 2016). However, NSCLC cells are able to gain resistance to cisplatin (Sarin et al. 2017; Gao et al. 2019). Therefore, cisplatin is typically used alongside a wide range of other chemotherapeutic agents that exert their anti-tumour effect

through other mechanisms. For instance, Gefitinib is an EGFR inhibitor and is effective against NSCLCs with aberrant EGF signalling (Nurwidya, Takahashi, and Takahashi 2016). On the other hand, drugs such as Paclitaxel inhibit mitotic progression of cancer cells through interactions with microtubules necessary for cell division (Weaver 2014).

More recently, immunotherapeutic approaches that exploit the anti-cancer function of the immune system have gained popularity, with immune checkpoint regulators Programmed cell death protein 1 (PD-1) and Cytotoxic T-lymphocyte-associated protein 4 (CTLA-4) being extremely popular targets in multiple clinical trials (Corrales et al. 2018; Herbst, Morgensztern, and Boshoff 2018). PD-1 and CTLA-4 are expressed on the surface of T-cells and function as "breaks" to limit the function of T-cells. The blockade of these receptors is thought to reenergise the function of T-cells and promote their anti-tumour activity. Programmed cell death ligand 1 (PD-L1) expressed on tumour cells can interact with PD-1 on T-cells to inhibit their anti-tumour function, thereby favouring tumour immune escape (Iwai et al. 2002). Similarly, CTLA-4 is expressed on activated T-cells and its interaction with ligands CD80 or CD86 on antigen-presenting cells (APCs) inhibits T-cell function (Alegre, Frauwirth, and Thompson 2001). The use of immunotherapeutic agents is dependent on the staging and severity of lung cancer (Doroshow et al. 2019). Nivolumab, Atezolizumab and Pembrolizumab are key immunotherapeutic drugs which have been approved in the treatment of various lung cancer subtypes, with all three drugs targeting the PD-1/PD-L1 pathway (Garon et al. 2015; Santini and Rudin 2017; Zhang and Chen 2018). Critically, the success of immunotherapy with drugs targeting PD-L1 is highly dependent on PD-L1 expression within NSCLCs (Reck et al. 2016). Apart from PD1/PD-L1 and CTLA4, a myriad of drugs targeting other immune checkpoint blockades have demonstrated their potential in various clinical trials (Zappa and Mousa 2016).

While surgical resection is regarded as the standard of care for early-stage NSCLC, radiotherapy is used when lung cancer patients are inoperable due to certain risk factors like age, emphysema and heart disease (Timmerman et al. 2006). Radiotherapy is also administered in late-stage and metastatic NSCLC and extensive-stage SCLC (Lemjabbar-Alaoui et al. 2015). Recent advances in radiotherapy techniques, such as 3-dimensional conformation radiation therapy (3DCRT), Image modulated radiation therapy (IMRT) and Stereotactic ablative radiotherapy (SABR), incorporate the acquisition of 3D images of patients by Computed tomography (CT) scans to guide precise tumour targeting during treatment (Bucci, Bevan, and Roach 2005) and these newer methods have improved prognosis and survival in patients compared to standard radiation (Cheng et al. 2019). Despite these successes, problems such as recurrences of tumours and the formation of metastasis have yet to be adequately addressed (Ko, Raben, and Formenti 2018).

The method of radiation and the selected dose is dependent on the staging and severity of the disease, and hence is given with the intent to either cure the patient as much as possible (curative radiotherapy) or to relieve the symptoms and pain of incurable disease (palliative radiotherapy). SBRT is typically given as a curative form of radiotherapy. This involves a high dose, fractionated regimen and is becoming the preferred method of treatment for inoperable patients with early-stage NSCLCs (Louie et al. 2015). Multiple trials utilising SBRT against primary lung tumours in NSCLC highlight that fractionated regimen totalling 45-60 Gray (Gy) reported local tumour control of 80-98% (Timmerman et al. 2010; Nagata et al. 2011). Nevertheless, radiation toxicity typically encompassing pneumonitis and fibrosis remains a key concern in such high-dose radiation regimens and remains an area of improvement (Timmerman et al. 2006; Nagata et al. 2009). Whilst SBRT was initially used in the treatment of primary tumours, research has now demonstrated its promise in metastatic lung cancer (Rusthoven et al. 2009; Iyengar et al. 2018; Palma et al. 2019). On the other hand, palliative radiotherapy is given in much lower doses, albeit in a fractionated form as well (Bezjak et al. 2002; Cross et al. 2004; Senkus-Konefka et al. 2005). Naturally, lower doses of radiation correspond to significantly reduced treatment-related toxicity (Cross et al. 2004). While radiotherapy is classically known for its anti-tumour effects through the killing of rapidly dividing cells by DNA damage, it is now widely appreciated that radiation plays an important role in modulating the immune system, which could either promote or inhibit tumour progression (Ko, Raben, and Formenti 2018). The modulation of the immune system by radiotherapy will be further discussed in subsequent chapters.

Importantly, the treatment of lung cancer in practice utilises a combination of the methods I have discussed thus far. A study in humans demonstrated that radiotherapy induces a response of metastatic NSCLC to CTLA-4 blockade, whereas the response is not seen with CTLA-4 blockade alone (Formenti et al. 2018). Hence, the use of combination treatment strategies might be required to unlock the potential for immunotherapy in lung cancer. More recently, the Phase III study Checkmate 9LA looking at the combination of Nivolumab (anti-PD-1) and Ipilimumab (anti-CTLA-4) alongside platinum-based chemotherapy observed improved overall survival for Stage IV/recurrent NSCLC patients and has now been approved as first-line treatment for NSCLC (Reck et al. 2020), further demonstrating the potential of combination treatment to promote better disease control.

1.2 The immune microenvironment in lung cancer

The use of treatment modalities like radiotherapy and immunotherapy against lung cancer, both of which rely upon the immune system to induce anti-tumour responses, reflect the importance of the lung immune microenvironment in supporting tumour growth itself. In this subchapter, I focus on the lung tumour immune microenvironment (TME) and the ways cancer in the lung exploits some of these components to support tumour growth.

1.2.1 Factors influencing the tumour immune microenvironment

The immune system remains a double-edged sword in cancer. Though the immune system is inherently capable of fighting cancer by inducing direct tumour killing, cancer cells can also exploit the immune system to support its continued survival and proliferation by generating a pro-tumourigenic TME. This is achieved by promoting pro-tumour responses and inhibiting anti-tumour responses within the cancer microenvironment. Cancer-derived mutations play a key role in the development of TME. It has long been known that cancer-driven inflammation promotes tumour development (Mantovani et al. 2008), and the mutations that drive cancer further promote inflammation within the TME. Neoantigen burden in NSCLC patients is linked to T-cell infiltration and activation within the tumour microenvironment (McGranahan et al. 2016), and specific mutational signatures are associated with suppression of anti-tumour immune response. For instance, genetic ablation of LKB1 is shown to promote the recruitment of neutrophils, which produce T-cell suppressive factors to suppress anti-tumour immunity (Koyama et al. 2016). Other cancer-intrinsic and extrinsic factors, including hypoxia, the microbiota and non-immune cells within the cancer microenvironment contribute to the development and maintenance of the tumour immune microenvironment and these have been extensively reviewed elsewhere and will not be further discussed (Altorki et al. 2019; Milette et al. 2019; Ramirez-Labrada et al. 2020).

1.2.2 Innate immunity in lung cancer

Neutrophils are the most prevalent immune cell type in NSCLC (Kargl et al. 2017). While the bactericidal properties of neutrophils in the lung are well understood, the role of neutrophils in NSCLC remains polarised. On one hand, reactive oxygen species (ROS) production by neutrophils, which is typically associated with bactericidal activity, can induce epithelial mutagenesis and drive cancer formation within the lung (Canli et al. 2017). On the other hand, a subset of neutrophils in early stage NSCLCs displayed antigen-presentation properties and promoted T-cell responses

(Eruslanov et al. 2014; Singhal et al. 2016), highlighting the anti-tumour function of neutrophils in early stage NSCLCs. However, neutrophils in NSCLC are typically associated with worse prognosis as high neutrophil-lymphocyte ratios are a useful prognostic marker in determining the outcomes of NSCLC (Akinci Ozyurek et al. 2017). Neutrophils appear to adopt N1/N2 polarisation states, where the N1 and N2 state is associated with anti-tumour and pro-tumour function respectively. Transforming growth factor beta (TGFβ) accumulation in tumours appear to polarise neutrophils to pro-tumour N2 neutrophils (Fridlender et al. 2009). Notably, the classification of neutrophils into either N1 or N2 states represent a gross oversimplification of how neutrophils behave in cancer (i.e. polarisation, maturation states) and the field has gradually shunned away from this classification. Neutrophils have also been observed to accumulate within the pre-metastatic niche within the lung. While the bulk of literature in mouse models demonstrate that neutrophils can promote lung metastasis formation (Coffelt et al. 2015; Wculek and Malanchi 2015), some literature suggests neutrophils exhibit anti-metastatic potential within the lung (Granot et al. 2011). These differences might be attributed to the timing of neutrophil depletion in these studies and the type of cancer model used. Altogether, the role of neutrophils in lung cancer appears to be dependent on the stage of the tumour, and they contribute to the pre-metastatic niche within the lung microenvironment.

Other immune cells in the innate immune compartment contribute to the development of the TME. Tumour associated macrophages (TAM) typically exhibit anti-inflammatory phenotypes and favour tumour progression. Indeed, depletion of TAMs in a mouse model of lung cancer slows down the growth of lung carcinoma (Fritz et al. 2014). Alveolar macrophages (AM) also appear to favour lung metastasis, as they accumulate in the pre-metastatic lung and favour cancer colonisation through production of leukotrienes (Nosaka et al. 2018) and dampening anti-tumour CD4+ T-cell responses (Sharma et al. 2015).

γδ T-cells are an innate subset of T-cells present in several tissues, including the lung. Though γδ T-cells exhibit both pro and anti-tumour functions in multiple mouse model of cancer, they appear to contribute to the development of a pro-tumourgenic TME in the lung, in part via the production of IL-17 (Silva-Santos, Mensurado, and Coffelt 2019). For instance, IL-17 production by γδ T-cells increases Granulocyte-stimulating factor (G-CSF) levels within the lung to recruit neutrophils that exhibit pro-tumour function (Coffelt et al. 2015). Interestingly, a recent paper also highlighted the interactions of γδ T-cells with the lung microbiome to promote lung cancer (Jin et al. 2019), highlighting the importance of immune-microbiota interactions in cancer.

Natural killer (NK) cells, a member of the innate lymphoid cell (ILC) family, are also widely implicated in NSCLCs. These cells exhibit direct cytotoxic activity against tumour cells, and their

activation is dependent on the absence of major histocompatibility complex (MHC) molecules on the cell surface, as well as on the combination of activating and inhibitory signals derived from their activating and inhibitory receptors respectively. NK cells in human NSCLCs have been demonstrated to be dysfunctional, as intratumoural NK cells appear to have reduced capacity for degranulation and Interferon gamma (IFNγ) production, which is a key cytokine involved in anti-tumour immunity (Platonova et al. 2011). Indeed, this might be attributed to the enrichment of non-cytotoxic $CD56_{bright}$ NK cells within NSCLCs, which play a more immunoregulatory role as compared to their $CD56_{dim}$ counterparts (Carrega and Ferlazzo 2017). The suppression of NK cell function in the pre-metastatic niche in mouse models of lung cancer has also been observed (Sceneay et al. 2012), highlighting the importance of this cytotoxic effector population in both primary NSCLC and metastatic seeding of lung tumours.

1.2.3 Adaptive immunity in lung cancer

Though strictly an innate immune cell type, DCs play an integral role in the activation of the adaptive T-cell compartment. In the lung TME, DCs exhibit an immunosuppressive phenotype and upregulate the immune checkpoint molecule B7H3, triggering the production of anti-inflammatory IL-10 (Schneider et al. 2011). CD8+ T-cells are major producers of IFNγ and are key in mediating anti-tumour responses. CD8+ T-cells, alongside the likes of NK cells, play an important role in the destruction of tumour cells as they exhibit cytotoxic activity but their anti-tumour function is also compromised in NSCLC (Trojan et al. 2004). This is in part due to the upregulation of inhibitory receptors in the tumour context (Thommen et al. 2015). Notably, upregulation of PD-1 on CD8+ T-cells is correlated with their dysfunction in human NSCLCs (Zhang et al. 2010), highlighting the relevance of immunotherapeutic treatments in promoting anti-tumour responses of CD8+ T-cells.

In the CD4+ T-cell compartment, conventional CD4+ T-cells that emerge from the thymus can polarise to different helper subsets T_H1, T_H2 and T_H17, which are characterised by the transcription factors T-bet, GATA binding protein 3 (GATA3) and RAR-related orphan receptor gamma (RORγt) respectively. On the other hand, Tregs are characterised by the expression of Forkhead box P3 (Foxp3), and they typically suppress conventional CD4+ T-cell function as well as the broader immune response. The traditional T_H1/T_H2 paradigm is used to describe the CD4+ T-cell infiltration in lung cancer and used as a determinant of lung cancer prognosis. In essence, the balance of the T_H1/T_H2 profile was a key determinant in cancer progression and outcomes (Duan et al. 2015), where a T_H1/T_H2 profile skewed towards T_H1 typically indicate reduced cancer progression and improved cancer prognosis. More recently, a new T_H17/Regulatory T-cells (Treg) axis has emerged, which also

serves as a prognostic indicator of NSCLC progression (Marshall et al. 2016), and higher T_H17/Treg ratios are associated with better prognosis in NSCLCs. Indeed, pro-inflammatory T_H17 cells have demonstrated anti-tumour function in lung cancer by supporting CD8+ T-cells (Orozco et al. 2009). Importantly, the accumulation of TGFβ in lung cancer appears to have opposing effects on T_H17 and Tregs, where Foxp3 induction by TGFβ inhibits T_H17 cell differentiation by antagonizing RORγt function (Zhou et al. 2008). Unsurprisingly, owing to their potent immunosuppressive properties, Tregs contribute to immune dysfunction in NSCLCs (Woo et al. 2001; Woo et al. 2002). NSCLCs have evolved ways to facilitate the recruitment and activation of these cells, such as via the production of Prostaglandin E2 (PGE2) by Cyclooxygenase 2 (COX2) (S. Sharma et al. 2005), highlighting the role of cancer-intrinsic factors driving the maintenance of the pro-tumourgenic TME. Tregs in lung cancer have been demonstrated to inhibit anti-tumour function of CD8+ T-cells and inhibit autologous CD4+ T-cell proliferation (Woo et al. 2002; Ganesan et al. 2013), further demonstrating their pivotal role in regulating anti-tumour responses. Figure 1.1 illustrates some of these key immune cells in the lung cancer microenvironment.

Hence, cancer exploits the immune system through a combination of inhibiting anti-tumour response and promoting pro-tumour immune responses through a myriad of immune cell types. At the same time, these responses can also be exploited by multiple treatment modalities discussed previously. In the next subchapter, I focus specifically on the interactions between radiotherapy and the immune system in cancer.

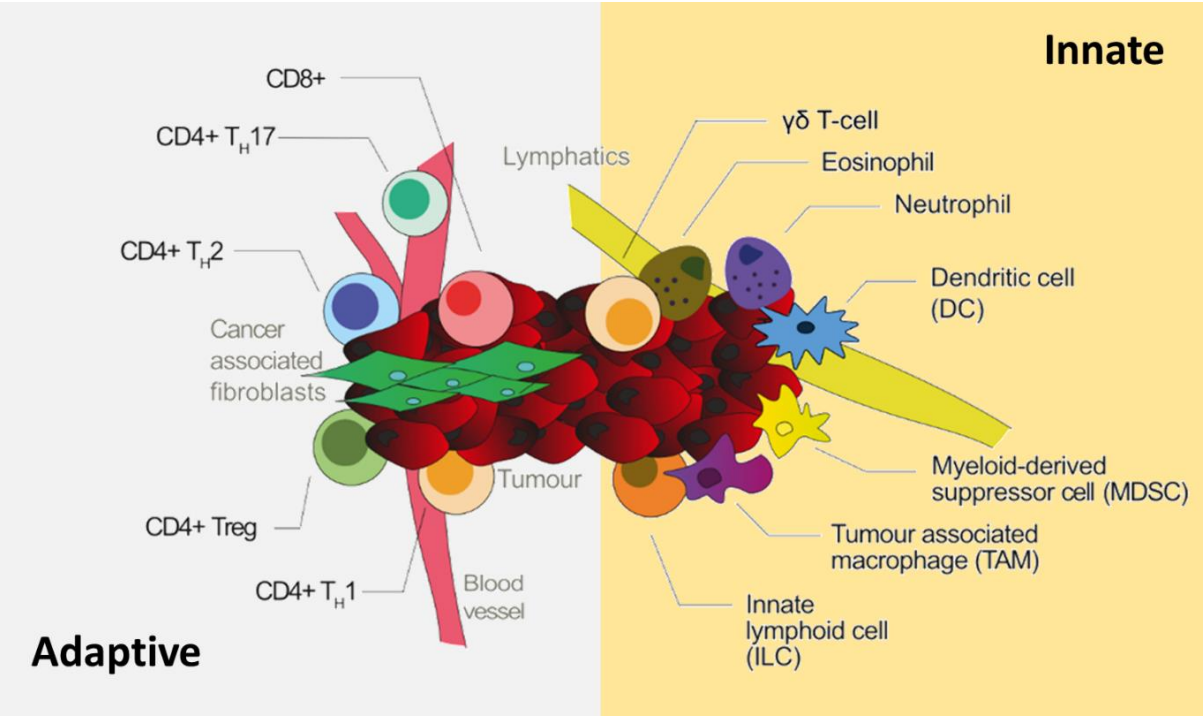

Figure 1.1 Immune microenvironment in lung cancer. The lung immune microenvironment is composed of both innate and adaptive immune cells that can contribute to both pro and anti-tumour responses.

1.3 Immune modulation by radiotherapy in cancer

Traditionally, DNA damage induced by radiotherapy has been the explanation for the anti-tumour response induced by radiotherapy. As some mutated cancer cells lose their ability to repair DNA damage, cell death via pathways like apoptosis or necrosis occurs (Sia et al. 2020). However, this traditional view of DNA damage as the sole reason for anti-tumour responses is insufficient to explain the abscopal effect (Golden and Apetoh 2015). The abscopal effect describes the off-target effect of radiotherapy, where targeted irradiation of a primary tumour leads to regression of tumours in a distant location. A landmark paper in 2004 demonstrated that this was attributed to the immune system (Demaria et al. 2004). Specifically, irradiation of a local tumour alongside treatment with Flt3L impaired the growth of a distant, non-irradiated tumour. This abscopal effect observed due to combined treatment was attributed to the activation of DCs. Since this discovery, the immune system's role in radiotherapy-induced anti-tumour immunity is increasingly appreciated, and the mechanisms behind this process are an active area of research.

1.3.1 Immunogenic cell death in radiotherapy

Immunogenic cell death (ICD) is a relatively newly defined form of cell death that takes into account the contribution of the immune system in promoting anti-tumour responses. Notably, the principles guiding the definitions of this process were initially derived from work in chemotherapeutic agents, but these principles apply just as well to radiotherapy. A review by Kroemer and Zitvogel nicely sums up the 3 necessary components of ICD (Kroemer et al. 2013): cell surface translocation of calreticulin, and extracellular release of High mobility group box protein 1 (HMGB1) and ATP. Calreticulin expression on the membrane surface acts as an "eat-me" signal, which is recognised by receptors expressed on phagocytic DCs. HMGB1 is recognised by Toll-like receptor 4 (TLR4) on DCs to optimise their cross-presentation function, allowing for the processing of extracellular antigens to be presented by MHC Class I molecules to CD8+ T-cells. Finally, ATP interacts with the receptor P2RX7 on DCs, facilitating IL-1β production necessary for the immune system to perceive cell death as immunogenic (Kroemer et al. 2013). Crucially, these processes are associated with the upregulation of DC function and anti-tumour CD8+ T-cells.

The evidence of ICD hallmarks in radiotherapy has been demonstrated by work from Formenti and Demaria in the TSA mammary carcinoma murine cell line. TSA cells were genetically engineered to express membrane luciferase to detect ATP release in the presence of luciferin, oxygen, and magnesium by bioluminescence. To detect cell surface calreticulin, TSA cells were modified to express calreticulin alongside a tag protein, which can be detected by flow cytometry upon binding

of fluorescent ligands to the tag. For detection of HMGB1, HMGB1 was genetically engineered to contain a red fluorescent protein (Golden et al. 2014). Radiotherapy *in vitro* demonstrated that all 3 components were present, and that these increased to a larger extent in combination with platinum chemotherapy (Golden et al. 2014).

Evidence of ICD has also been demonstrated in human cancer cell lines, emphasising the role of adaptive CD8+ cells. Using human MDA-MB-231 breast cancer, H522 lung cancer, and LNCaP prostate cancer cell lines, a dose-dependent release of ATP and HMGB1 was demonstrated upon irradiation, and consequently their susceptibility to killing by CD8+ T-cells. (Gameiro et al. 2014). *In vivo*, implanted LNCaP tumours upregulated calreticulin gene expression upon irradiation, which was accompanied by translocation to the cell surface as seen by an increase in calreticulin membrane staining. This surface expression of calreticulin also corresponded to increase sensitivity to CD8+ T-cell killing, substantiating the importance of ICD-induced CD8+ T-cell response in radiotherapy.

1.3.2 Adaptive immune activation

Supporting the notion that ICD is critical in inducing anti-tumour immunity by radiotherapy, activation of DCs and CD8+ T-cell responses in radiotherapy has been observed in many instances, and the mechanisms involved are being resolved. Early studies have demonstrated that in the subcutaneous B16 melanoma model, irradiation increased the number of APCs within the tumour-draining lymph node, likely due to the increase in antigen release by radiotherapy (Lugade et al. 2005)**.** This was accompanied by an increase of IFNγ production in T-cells.

Radiation was also observed to modulate the peptide repertoire and enhance MHCI expression to induce anti-tumour responses (Reits et al. 2006). Using MelJuSo human melanoma cell lines, a dose-dependent increase of MHCI on the tumour cell surface was observed *in vitro* after irradiation. In the *in vivo* setting, a similar trend was observed in irradiated kidneys. An expansion of the intracellular peptide pool was also observed, in part via increased synthesis and degradation of proteins induced by radiotherapy, which was dependent on the mTOR pathway. Notably, a high neoantigen burden is typically associated with T-cell immunoreactivity and improved clinical response to immune checkpoint blockade (McGranahan et al. 2016). Hence, the increase in both the quantity and variety of antigens likely promotes DC responses to radiotherapy.

The direct role of DCs in facilitating the activation of CD8+ T-cells in radiotherapy was first demonstrated in a paper published in 2012. With the B16 melanoma model, upregulation of the activation markers CD70 and CD86 on DCs was observed and activated DCs were important for

tumour control (Gupta et al. 2012). Once again, upregulation of IFNγ by CD8+ T-cells was observed. Depletion of lymphocyte subsets demonstrated that only CD8+ T-cells were important for the therapeutic effect of radiotherapy in this model. Notably, the activation status of DCs, rather than the amount of tumour-derived antigen, was a key determinant of induction of specific effector cells (Gupta et al. 2012). Further evidence of DCs priming adaptive CD8+ T-cells has since been shown. Using OVA-antigen expressing tumour cells, an increase in CFSE-labelled OVA-specific CD8+ T-cell proliferation was observed in the tumour-draining lymph nodes upon adoptive transfer after radiotherapy (Sharabi et al. 2015). Furthermore, priming of endogenous T-cells was also observed in secondary lymphoid tissues, as antigen-specific T-cells with a memory phenotype accumulated in irradiated mice at late time points after irradiation (Sharabi et al. 2015).

Radiotherapy also promotes adaptive immunity by modulating CD8+ T-cells accumulation through chemokine production. In the 4T1 breast cancer model, an accumulation of adoptively transferred CD8+ T-cells in the tumour was observed. This increase was attributed to CXCL16 expression and release by tumour cells upon irradiation, which was recognised by CXCR6-expressing CD8+ T-cells (Matsumura et al. 2008). In CXCR6-deficient mice, a reduction of CD8+ tumour infiltrating lymphocytes and reduction of anti-tumour efficacy of radiotherapy were observed (Matsumura et al. 2008). Apart from the upregulation of MHCI, radiation upregulates the expression of FAS receptor on tumour cells to facilitate their killing by cytotoxic CD8+ T-cells (Garnett et al. 2004). Notably, this expression does not necessarily lead to improved killing in all tumour cell types, suggesting that a combination of cell-intrinsic factors determines if cells are lysed by CD8+ T-cells.

As discussed, IFNγ is the prototypical cytokine associated with anti-tumour immunity. Indeed, reports have shown that IFNγ produced by T-cells is a response induced by radiotherapy (Lugade et al. 2005; A. Gupta et al. 2012). The role of IFNγ in facilitating anti-tumour immunity induced by radiotherapy has been studied, and IFNγ signalling in both tumour and host is demonstrated to be crucial in radiotherapy-mediated responses (Lugade et al. 2008). In IFNγ-deficient mice, Vascular cell adhesion protein 1 (VCAM -1) expression on tumour vasculature was observed to be reduced, altering the trafficking of T-cells into the tumour microenvironment. Furthermore, the chemoattractants CXCL9 and CXCL10 were reduced in irradiated tumours in IFNγ-deficient mice. In IFNγ-deficient tumour cells, radiation-induced upregulation of MHCI expression in tumour cells was reduced, in part due to altered STAT1 phosphorylation (Lugade et al. 2008). In all, DCs, CD8+ T-cells and IFNγ are key contributors to the anti-tumour response induced by radiotherapy.

In contrast to CD8+ T-cells, Tregs typically function to suppress anti-tumour immunity and promote cancer growth. While the understanding of Treg response to radiotherapy is significantly less

compared to CD8+ T-cells, they are suggested to be less radiosensitive compared to other lymphocytes, and therefore preferentially accumulate in irradiated tissues, thereby contributing to radioresistance (Kachikwu et al. 2011). Indeed, the accumulation of Tregs in response to radiotherapy has been observed in multiple cancer models (Klug et al. 2013; Muroyama et al. 2017). In mouse subcutaneous models of cancer, irradiated Tregs in tumours demonstrated upregulation of CTLA4 and 4-1BB, which are characteristic of an activated Treg phenotype. In addition, Treg accumulation in irradiated tumours was attributed to proliferation, as observed by increased Ki67 staining (Muroyama et al. 2017). Apart from enhanced Treg proliferation, the recruitment of Tregs in response to radiotherapy has also been reported. In a murine model of head and neck squamous cell carcinoma, CCL2 upregulation in response to radiotherapy was observed, alongside the accumulation of Tregs in a CCR2-dependent manner (Mondini et al. 2019).

1.3.3 Innate immune activation

While adaptive immunity has originally been the focus of radiotherapy-induced immune response, studies have now demonstrated the contributions of innate immunity. Monocytes and macrophages are important and appear to inhibit radiotherapy-induced anti-tumour immunity in general. In a pancreatic ductal adenocarcinoma (PDAC) mouse model, radiotherapy increases CCL2 within the tumour microenvironment, leading to the recruitment of CCR2+ monocytes (Kalbasi et al. 2017). While radiotherapy on its own did not induce an anti-tumour response, a combination of anti-CCL2 alongside radiotherapy observed a decrease in tumour burden. Notably, monocyte recruitment was associated with subsequent accumulation of TAMs (Kalbasi et al. 2017). CCR2-dependent recruitment of monocytes was also observed in the TC1 murine model of head and neck cancer, and recruited monocytes were thought to differentiate into Ly6C-CD64+ macrophages (Mondini et al. 2019). The increase in the concentration of serum CCL2 was attributed to tumour cells, and "myeloid-associated" cytokines granulocyte-macrophage colony-stimulating factor (GM-CSF) and tumour necrosis factor alpha (TNFα) were also observed. These cytokines were linked to the suppression of CD8+ T-cell activity via Tregs (Mondini et al. 2019).

Macrophages were demonstrated to limit the efficacy of radiotherapy in a model of mammary carcinoma growth. In this model, irradiation leads to the reduction of tumour burden, followed by a subsequent regrowth phase associated with an increase in CD11b+F4/80+ macrophages (Shiao et al. 2015). The combination of anti-CSF-1 to deplete macrophages alongside radiotherapy significantly reduced tumour burden in the regrowth phase (Shiao et al. 2015). It was also demonstrated that macrophages supported T_H2 CD4+ cells. The pro-tumour role of macrophages in radiotherapy is

supported by irradiation of macrophages *in vitro*, where irradiated macrophages retained their capacity to promote cancer cell invasion and angiogenesis (Pinto et al. 2016). Interestingly, macrophages can also exhibit anti-tumour function in low-dose irradiation (Klug et al. 2013). In the RT5 model of spontaneous pancreatic islet carcinogenesis, low-dose irradiation led to the recruitment of T-cells, which was dependent on inducible nitric oxide synthase (iNOS) production by macrophages. Depletion of macrophages or iNOS prevented the recruitment of T-cells after radiotherapy.

Myeloid-derived suppressor cells (MDSC), neutrophils, and eosinophils have also been implicated in immune responses induced by radiotherapy in cancer. A reduction of MDSC is linked to an increase in CD8+ T-cells in the CT26 model of colon carcinoma, and a single dose of 30Gy decreased the ratio of MDSC to CD8+ T-cells (Filatenkov et al. 2015). Eosinophils appear to support anti-tumour responses via CD8+ T-cells. In the subcutaneous B16 melanoma models, eosinophils were reported to be recruited by tumour-derived CCL11 upon radiotherapy. The depletion of eosinophils with an anti-SiglecF antibody alongside radiotherapy reduced the presence of CD8+ T-cells and a reduction in anti-tumour effectiveness (Cheng et al. 2021). Neutrophils are known to support metastatic seeding and it has been reported that radiotherapy enhances their pro-metastatic function in the lung. A single dose of 13Gy to the thorax region enhances lung metastasis in the 4T07 orthotopic breast cancer model (Nolan et al. 2022). This was attributed to radiation-induced neutrophil activation, which modulates the Notch signalling pathway in lung epithelial cells to promote metastasis (Nolan et al. 2022)

NK cell function is also influenced by radiotherapy. A notable example is ligands for the activating NKG2D receptor, which is upregulated by radiotherapy and hence, can stimulate NK cell function (Gasser et al. 2005). In the context of cancer, radiotherapy alongside ataxia telangiectasia and Rad3-related (ATR) inhibitors induces an anti-tumour response in a model of head and neck cancer. Radiotherapy upregulated the expression of IFNγ and the degranulation marker CD107a in NK cells, and depletion of NK cells decreased the effectiveness of irradiation (Patin et al. 2022). The importance of NK cells in radiotherapy has also been reported in pancreatic cancer. In human PDAC, radiotherapy induces CXCL8, leading to the recruitment of $CD56_{dim}$ NK cells that exert tumour control (Walle et al. 2022). Notably, no structural homologue of CXCL8 is present in mice, highlighting fundamental differences in the response to radiotherapy in both species (Walle et al. 2022).

1.3.4 Radiotherapy and immunotherapy combinations

Given the clear association between radiotherapy and immune activation, combinational treatments incorporating both immunotherapy and radiotherapy are increasingly explored to leverage the activation of the immune system. The use of immune checkpoint inhibitors remains one of the most popular approaches.

Notably, radiotherapy and immune checkpoint inhibitors were reported to activate non-redundant immune mechanisms in cancer. In the subcutaneous B16 melanoma model, radiation alongside dual checkpoint blockade with anti-PD1 and anti-CTLA4 treatment was observed to be more effective than dual checkpoint blockade on its own (Twyman-Saint Victor et al. 2015). On one hand, it was demonstrated that radiotherapy functions to increase the T-cell receptor (TCR) repertoire of intratumoural T-cells and allow for the selection and expansion of T-cell clones. On the other hand, blocking CTLA-4 and PD-L1 depletes Tregs and increases the proportion of CD8+ T-cells respectively (Twyman-Saint Victor et al. 2015). Indeed, preclinical studies using immune checkpoint blockade alongside radiotherapy have demonstrated promise (Sharabi et al. 2015; Twyman-Saint Victor et al. 2015; Niknam et al. 2018). In the context of human cancer, a number of clinical trials are currently ongoing and have been reviewed extensively (Spiotto, Fu, and Weichselbaum 2016; Wang et al. 2018; Buchwald et al. 2018).

Apart from the use of immune checkpoint inhibitors to target adaptive T-cells, other cell types can also be targeted. As discussed, DCs also play a central role in initiating the adaptive CD8+ T-cell response and could also be exploited to improve radiotherapy-induced anti-tumour responses. The use of FLT3L to enhance DC function alongside radiotherapy promoted survival in the LL/2 model of metastatic lung cancer (Chakravarty et al. 1999). While a formal role of DCs was not directly demonstrated, combination treatment did not impact survival in immunodeficient mice, implicating the role of the immune system. In addition, the adenosine signalling pathway is a crucial metabolic pathway regulating anti-tumour immunity on DCs, and the CD73 receptor is involved in the conversion ATP to adenosine. The use of anti-CD73 is shown to promote DC infiltration of irradiated tumours and promote tumour rejection (Wennerberg et al. 2020). In the TSA mammary adenocarcinoma model, anti-CD73 with radiotherapy promoted cDC1 recruitment to potentiate CD8+ T-cell response (Wennerberg et al. 2020).

Finally, immunotherapeutic approaches targeting innate immune cell types can be considered. MDSCs and macrophages are typically associated with pro-tumour function and can be targeted alongside radiotherapy. For instance, the use of anti-CCL2 to deplete monocytes recruitment and macrophages could potentially be used to improve radiotherapy outcomes (Kalbasi et al. 2017).

Furthermore, the influence of immune checkpoint inhibitors on innate immune cells could be taken into account. Myeloid cells also express PD-1, and targeted depletion of PD-1 on myeloid cells drives anti-tumour immunity, in part via an increase in effector memory T-cells (Strauss et al. 2020). NK cells also express PD-1, and the combination of ATR inhibitors and radiotherapy treatment alongside anti-PD1 and anti-TIGIT was more effective than treatment without immune checkpoint inhibitors in head and neck cancer. This was in part via the activation of NK cells (Patin et al. 2022).

1.3.5 Factors modulating radiotherapy efficacy

Several considerations have to be taken into account to maximise the effectiveness of radiotherapy, the most notable being the dose of irradiation administered. Classically, higher doses of irradiation are associated with a greater extent of DNA damage in cells, and in theory, increased cell death and higher effectiveness of radiotherapy. However, a major restriction in the use of high-dose radiation is the unintended consequence of irradiating healthy cells, leading to unintended side effects. For instance, in the context of lung irradiation, pneumonitis and fibrosis are common side effects (Lierova et al. 2018).

The selected dose also modulates the effectiveness of radiotherapy by modulating the immune response. Lymphocytes are also sensitive and can succumb to radiation, thereby limiting the effectiveness of anti-tumour immune responses. Interestingly, recent research has highlighted that T-cells within the tumour microenvironment are less sensitive to radiotherapy than expected. In a subcutaneous model of pancreatic cancer, intratumoural T-cells in the pre-irradiated tumour constitute 65-85% of total T-cells after radiotherapy, and these exhibited a memory phenotype (Arina et al. 2019). Crucially, these pre-existing T-cells are functional, as targeted irradiation alongside the use of fingolimod (FTY720) to block T-cell recruitment still demonstrated reduced tumour growth.

Notably, high-dose radiotherapy could attenuate radiotherapy-induced tumour immunogenicity via the induction of the DNA exonuclease Three Prime Repair Exonuclease 1 (Trex1). Cytosolic DNA release by radiotherapy is necessary for immune activation (M. Chen et al. 2020). At radiation doses above 12-18Gy, Trex1 was induced, leading to the degradation of cytosolic DNA release by radiotherapy, and downregulation of the Type 1 IFN pathway (Vanpouille-Box et al. 2017). Notably, Trex1 regulated the abscopal effect of radiation alongside immune checkpoint inhibitor treatment, suggesting that this could be targeted to improve abscopal responses. In addition, depending on the cell type, low or high-dose irradiation could differentially affect the response of the cell. As discussed, low dose irradiation appears to support macrophage anti-tumour function (Klug et al.

2013), whereas higher doses appear to promote macrophage pro-tumour function (Shiao et al. 2015).

The decision to choose single or fractionated regimens could also influence the efficacy of radiotherapy. Recently, fractionated regimens are preferred as they are typically more effective (Bezjak et al. 2002) and accompanied by fewer side effects (Cross et al. 2004). In the preclinical setting, fractionated regimens demonstrated better tumour control compared to single dose irradiation in B16-OVA murine melanoma tumours (Schaue et al. 2012). In the context of irradiation alongside immune checkpoint blockade, a fractionated 8Gy X 3 regimen, but not a single dose 20Gy regimen was demonstrated to induce an immune-mediated abscopal effect when combined with an anti-CTLA4 antibody (Dewan et al. 2009). This fractionated regimen has now been considered the standard for immunotherapy combinations (Sandra Demaria et al. 2021).

External factors independent of the dose or regimen also modulate the efficacy of radiotherapy. The metabolic status of the host and tumour can influence the efficacy of radiotherapy by influencing cancer cell radioresistance, and these include factors such as glucose metabolism and hypoxia (Tang et al. 2018). Of note, adrenergic stress reduces the efficacy of radiotherapy and the abscopal effect via the blunting of CD8+ T-cell responses. Mice housed at higher temperatures were observe to experience reduced adrenergic stress. Furthermore, mice housed at higher temperatures experienced greater abscopal effect compared to mice housed at lower temperatures when treated with radiotherapy (Chen et al. 2020). Blocking β-adrenergic signalling improved anti-tumour immunity and the abscopal effect. The surrounding stroma within the tumour microenvironment also contributes to the radioresistance of tumour cells and their contributions have been reviewed (Hellevik and Martinez-Zubiaurre 2014). Interestingly, low-dose radiation therapy of secondary tumours has been demonstrated to improve anti-tumour responses, in part via overcoming the inhibitory stroma (Barsoumian et al. 2020). This is accompanied by an influx of NK cells and M1-polarised macrophages that contribute to anti-tumour immunity (Barsoumian et al. 2020). Finally, the microbiota has also been recently implicated in modulating radiotherapy efficacy (Tonneau et al. 2021), though this is a field in its infancy and further work is warranted.

1.4 Introduction to ILC2s

ILC2s are part of the ILC family, which are a recently described subset of innate lymphocytes and knowledge of these cells, apart from NK and lymphoid tissue inducer (LTi) cells, has only emerged in the past 2 decades. These cells mount antigen-independent innate immune responses and are derived from lymphoid progenitor cells. ILC2s are the innate counterparts of adaptive CD4+ T_H2 cells and are potent producers of Type 2 cytokines. In this chapter, I provide an introduction of ILC2s and discuss their discovery, development and plasticity.

1.4.1 ILC2 discovery

Before the discovery of ILC2s, adaptive T_H2 cells were considered the primary drivers of Type 2 immunity. In the lungs, this knowledge is typically derived from studies looking at asthma and airway inflammation, where CD4+ T_H2 cells produce large amounts of Type 2 cytokines to support inflammation. These early studies in mouse models emphasised the importance of T_H2 cells. For instance, the adoptive transfer of T_H2 cells contributed to eosinophilic airway inflammation (Cohn et al. 1997). However, it was soon clear that the adaptive T_H2 cells cannot fully explain some of the phenotypes observed.

IL-25, IL-33 and TSLP have been identified as the prototypical epithelial-derived cytokines that are critical in initiating Type 2 immunity (McKenzie 2014). Crucially, studies in the early 2000s provided evidence that Type 2 responses induced by these cytokines occurred independently of adaptive immunity. IL-4 is known to be crucial for T_H2 cell development, but IL-33 administration induced airway inflammation in an IL-4-independent manner (Kurowska-Stolarska et al. 2008). In addition, IL-25 was able to drive eosinophilia and a T_H2-like inflammatory profile in B and T-cell deficient *Rag*$^{-/-}$ mice (Hurst et al. 2002). Thus, it was apparent that an unknown innate inflammatory mediator was responsible for driving Type 2 responses.

3 papers published in 2010 identified an innate Type 2 cytokine-producing population that contributed to Type 2 immune responses, which I will describe hereafter. In early 2010, this cell type was identified in fat-associated lymphoid clusters (FALC). These cells were cKit+Sca1+ cells and required IL-7 for their maintenance. Crucially, these cells were present in *Rag*$^{-/-}$ mice, and IL-33 exposure induced their production of IL-5 and IL-13 *in vitro* (Moro et al. 2009). These cells were termed natural helper (NH) cells, as these cells produced IL-13 necessary for *Nippostrongylus brasiliensis* expulsion from the gut (Moro et al. 2009). This IL-13-producing innate lymphocyte population was also described in 2 papers in the same year. The Locksley lab identified Lin- cells

which responded to IL-25 and IL-33 in *Rag*$^{-/-}$ mice. These cells were observed to differ from Type 2 cytokine-producing basophils and T_H2 cells based on transcriptomic data, and respond to IL-25 to contribute to immunity against helminth infection (Price et al. 2010). These cells were termed innate helper Type 2 (Ih2) cells in this paper. In addition, the McKenzie lab also identified IL-13-producing Lin- cells after IL-25 and IL-33 administration *in vivo* (Neill et al. 2010). These cells were also ICOS+ST2+IL7RB+. Notably, *Il7rb*$^{-/-}$ mice deficient in the IL-25 receptor demonstrated reduced helminth expulsion, corroborating the importance of IL-25 in the report from the Locksley lab. Here, these cells were termed nuocytes. The obvious similarities between nuocytes, Ih2 cells and NH cells discovered in mice were soon picked up in reviews published in 2011 (Koyasu and Moro 2011; Oliphant, Barlow, and McKenzie 2011) and were subsequently termed ILC2s based on their phenotypical and functional characteristics (Spits et al. 2013).

1.4.2 ILC2 development

All lymphocytes, including ILC2s, are derived from common lymphoid progenitors (CLP). A committed common innate lymphoid progenitor (CILP) population is derived from CLPs, and these can give rise to all ILC subsets including LTi and NK cells, but not adaptive B and T-cells. These cells express the integrin α4β7 (Artis and Spits 2015). Common helper innate lymphoid progenitors (CHILP) cells are a further committed precursor to ILC2s, and can give rise to all ILCs and LTi, but not NK cells (Klose et al. 2014), and these are defined by the expression of Id2. These cells give rise to a further committed precursor known as ILC progenitors (ILCP), which are defined by the acquisition of PLZF expression (Constantinides et al. 2014).

ILC2s are derived from ILCPs via an intermediate ILC2 progenitor (ILC2P) population. Literature first demonstrated the existence of these ILC2-committed precursors in the bone marrow that can give rise to ILC2s. These cells are defined as Lin-Sca-1+c-Kit-CD127+CD25+ST2+ cells and are termed immature NH cells (iNH) in this paper (Halim et al. 2012). They were observed to produce significantly fewer Type 2 cytokines compared to NH cells, and the adoptive transfer of these cells to immunodeficient NSG mice demonstrated their capacity to give rise to ILC2s (Halim et al. 2012). This progenitor population was also reported in the same year in a different paper. Hoyler et al. reported these cells in the bone marrow and were defined as Lin-Sca1+Id2+Gata3+ cells (LSIG) (Hoyler et al. 2012). Notably, LSIGs were shown to be able to generate ILC2s specifically, but not other ILC subsets both *in vitro* and *in vivo*. These bone marrow-derived ILC2-committed precursor populations were collectively termed preILC2s (Walker and McKenzie 2013), and are now defined as ILC2P. Both ILC1 and ILC3 subsets are also derived from ILCPs, but this will not be further discussed.

RAR-related orphan receptor alpha (RORα) and GATA3 are two critical transcription factors necessary for ILC2 development. ILC2s were reported to express RORα and *Rorα*$^{sg/sg}$ mice deficient in RORα do not have functional ILC2s (Halim et al. 2012). Notably, these mice retain adaptive T_H2 cells and ILC3s. These mice also presented defective immune responses to allergens. Wong et al. also demonstrated high RORα expression in ILC2s (Wong et al. 2012). In *Rorα*$^{sg/sg}$ mice, IL-25 injection did not lead to expansion of ILC2s. Furthermore, RORα functioned intrinsically to support ILC2 development, as irradiated mice reconstituted with an equal proportion of bone marrow cells from WT or *Rorα*$^{sg/sg}$ led to the generation of ILC2s only from WT mice (Wong et al. 2012). Finally, they also demonstrated that IL-7 and Notch signalling was also required for ILC2 development. GATA3 is also necessary for ILC2 development. Hoyler et al. definitively shown the importance of GATA3 in regulating ILC2 cell fate and maintenance using the *Id2*$^{CreERT2/+}$*Gata3*$^{fl/fl}$ mouse model, where targeted deletion of GATA3 occurred in all ILC subsets (Hoyler et al. 2012). When these mice were treated with tamoxifen, reduced ILC2 in the lamina propria was observed while ILC3s were not affected. In all, GATA3 and RORα are key players essential for the development of ILC2s.

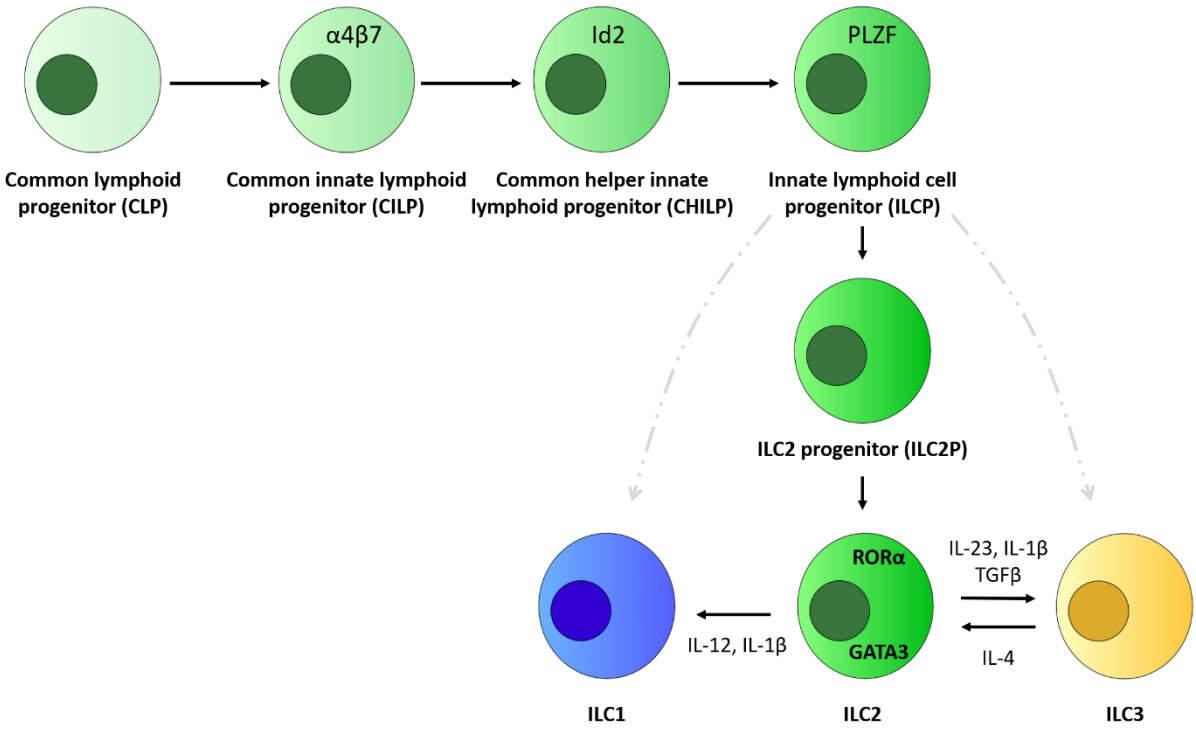

Figure 1.2 Developmental pathway of ILC2. CLPs go through a series of differentiation steps, giving rise to a series of increasingly committed precursor populations before eventually developing into ILC2s. ILC2s exhibit plasticity and can differentiate into ILC1 or ILC3 depending on the local cytokine environment.

1.4.3 ILC2 plasticity

Given the close developmental relationship of different ILC subsets, it is not surprising that these cells exhibit significant plasticity and develop characteristics of other ILC subsets depending on the signals within the microenvironment. Inflammatory ILC2 (iILC2) differ from IL-33 responsive ILC2s due to low ST2 expression, high IL-17RB expression, and expand in the presence of IL-25. These cells express higher levels of RORγt and can produce IL-17 upon restimulation by Phorbol 12-myristate 13-acetate (PMA) and ionomycin and T_H17-polarising conditions (Huang et al. 2015). These were thought to be transient progenitors of ILC2s. Interestingly, Notch signalling appears to do the reverse and drive the conversion of IL-33-repsonsive to iILC2 (Zhang et al. 2017).

ILC2s have been shown to convert to an ILC1-like phenotype. Cultures of human ILC2s in IL-2 with or without IL-25 or IL-33 revealed that a fraction of ILC2s expressed IFNγ (Lim et al. 2016). Notably, these cells also expressed T-bet. Culturing ILC2s in the presence of IL-12 also led to IFNγ production, highlighting an ILC1-like phenotype in the presence of Type 1-polarising conditions. Notably, cells from patients with a deficiency of IL-12RB1 also failed to generate plastic ILC2s (Lim et al. 2016). In addition, IL-1β is also implicated in the transdifferentiation of ILC2s to ILC1s in both mice and humans. Ohne et al demonstrated that IL-1β acts upstream of alarmin receptors ST2 and IL17RB, and stimulated the expression of these receptors (Ohne et al. 2016). Furthermore, IL-1β upregulated the expression of IL-12RB2 and T-bet and led to the production of IFNγ by transdifferentiated ILC2s when treated alongside IL-12. These changes were also demonstrated *in vivo* upon intranasal administration of IL-1β and IL-12. Finally, the conversion of ILC2s to ILC1 in the *in vivo* setting has also been demonstrated in the context of viral infection. In this context, ILC2s downregulate GATA3 expression, upregulate IL-12RB2 expression, and can contribute to anti-viral immunity (Silver et al. 2016).

More recently, human ILC2s have also been shown to convert to ILC3s. In response to *Candida albicans*, dermal ILC2s produced IL-17 and this was inhibited upon the addition of IL-23 and IL-1β antibodies (Bernink et al. 2019). Notably, differentiation of ILC2s to ILC3s was determined by reciprocal control of GATA3 and RORγt expression. IL-23 and TGFβ inhibit GATA3 expression, whereas IL-4 downregulates RORγt expression to maintain ILC2s (Bernink et al. 2019). These RORγt+ ILC2s were observed to express c-Kit and CCR6. The importance of IL-23, IL-1β and TGFβ in the differentiation of ILC2s to ILC3s was also shown in the context of nasal polyps (Golebski et al. 2019). Figure 1.2 summarises the developmental pathway of ILC2s.

1.5 ILC2s in lung disease and pathology

1.5.1 ILC2 in allergic airway inflammation

The bulk of our understanding of lung ILC2s is derived from models of allergic airway inflammation. Since their discovery, ILC2s have been recognised as important regulators of Type 2 immune responses, and they have now been demonstrated to be crucial in allergic airway inflammation. In earlier ovalbumin (OVA)-sensitisation and challenge models, ICOS+ST2+ ILC2s were observed to be the primary producers of IL-13, and the transfer of these cells into IL-13-deficient mice restored IL-25-induced airway hyperresponsiveness and eosinophilia (Barlow et al. 2012). The importance of cytokine production by ILC2s was substantiated by Halim et al. In the papain-induced airway inflammation model, an increase in ILC2s and eosinophilia was observed in *Rag*$^{-/-}$ mice. Experiments depleting and repleting ILC2s demonstrated the importance of ILC2s in eosinophilia and mucus production, and Type 2 cytokines by ILC2s were crucial in this process (Halim et al. 2012). In a separate report, *Il7rα*$^{-/-}$ mice deficient in ILC2s treated with OVA antigen and a cysteine protease did not display allergic airway inflammation. However, the adoptive transfer of ILC2s into these mice restored airway inflammation (Drake, Iijima, and Kita 2014). Hence, ILC2s are important in mediating immunity against allergic airway inflammation.

ILC2s in allergic airway inflammation have also demonstrated their capacity to prime and support adaptive CD4+ T-cell responses (Drake, Iijima, and Kita 2014; Halim et al. 2014; Mirchandani et al. 2014). *In vitro*, cocultures of ILC2s and CD4+ T-cells resulted in CD4+ T-cell proliferation and Type 2 cytokine production (Drake, Iijima, and Kita 2014). This was observed to be dependent on IL-4 as proliferation was reduced using IL-4-deficient ILC2s. Furthermore, direct contact via OX40L-OX40 interactions was necessary to promote CD4+ T-cell cytokine production (Drake, Iijima, and Kita 2014). *In vivo*, ILC2s are critical for the initiation of adaptive Type 2 immunity in the papain model of allergic lung inflammation. ILC2-derived IL-13 was required for the migration of CD40+ DCs to the draining lymph nodes, which contributes to T_H2 cell differentiation (Halim et al. 2014). IL-13 produced by ILC2s have also been shown to be crucial in inducing memory responses to papain, where IL-13 activated DCs produce CCL17 to recruit T_H2 cells (Halim et al. 2016). Notably, contrary to the previous report supporting a role for ILC2-derived IL-4 in promoting CD4+ T-cell response, IL-4 was not required to promote T_H2 responses in a papain protease allergen-driven model (Halim et al. 2014). In another study, blocking IL-4 in co-cultures of ILC2 and CD4+ T-cells was observed to only play a limited role in influencing CD4+ T-cell function, whereas IL-2 was necessary for ILC2-CD4+ T-cell crosstalk (Oliphant et al. 2014).

Alongside cytokine production, receptor-ligand interactions contribute to ILC2-mediated adaptive immune activation. ILC2s are capable of presenting antigens, and MHCII expression has been detected on ILC2s (Oliphant et al. 2014; Mirchandani et al. 2014) and shown to activate CD4+ T-cells (Mirchandani et al. 2014). In the context of *N.brasiliensis* infection, MHCII expression on ILC2s was instrumental for IL-13-dependent helminth expansion. Furthermore, costimulatory signalling molecules CD80 and CD86 on ILC2s also contribute to Type 2 cytokine expression (Oliphant et al. 2014). ILC2s also express PD-L1 and activated ILC2s upregulate PD-L1 expression (Schwartz et al. 2017). Crucially, PD-L1-PD-1 interactions were demonstrated to favour CD4+ T-cell T_H2 polarisation *in vitro* and *in vivo.* OX40L-OX40 interactions between ILC2 and CD4+ T-cells were first demonstrated to influence Type 2 responses, as an anti-OX40L blocking antibody blunted Type 2 cytokine production *in vitro* (Drake, Iijima, and Kita 2014). A clearer role of OX40-OX40L signalling between ILC2 and CD4+ T-cells was demonstrated in allergic airway inflammation *in vivo* (Halim et al. 2018). Specifically, OX40L on ILC2s and OX40 on CD4+ T-cells were necessary to promote adaptive T_H2 and Treg responses to IL-33. Thus, multiple receptor-ligand interactions facilitate ILC2-mediated activation of adaptive immune responses in the lung.

IL-33, IL-25 and TSLP are the prototypical alarmins that activate ILC2s to contribute to lung inflammation (McKenzie 2014; M. J. Schuijs and Halim 2018). These are typically released upon the damage of epithelial cells, and their role in ILC2 activation in allergic inflammation has been extensively studied (Schuijs and Halim 2018). Several cytokines and ligands are now shown to influence ILC2 activation in the context of lung inflammation. ILC2s produce IL-9, which acts in an autocrine loop to support both ILC2 accumulation and cytokine function during helminth function (Turner et al. 2013). IL-4 derived from basophils also support ILC2 induction of eosinophilic inflammation in the cysteine-protease model of inflammation (Motomura et al. 2014). Interestingly, the combination of IL-4 and IL-2 was observed to better induce ILC2 proliferation compared to the combination of IL-33 and IL-2, suggesting that IL-4 is a potent inducer of ILC2 function (Motomura et al. 2014). Alongside IL-33, TGFβ is an important cofactor for optimum ILC2 activation in the house dust mite (HDM)-induced model of allergic lung inflammation. HDM-induced TGFβ release promoted the accumulation of ILC2s specifically, but not T_H2 cells. Notably, TGFβ functions as a chemokine to attract ILC2s expressing the TGF-βRII receptor (Denney et al. 2015). In terms of ILC2 suppression, ILC2s can be suppressed by neutrophil-derived G-CSF, which functions to inhibit their production of Type 2 cytokines (Patel et al. 2019). The TL1A receptor DR3 is expressed on ILC2, and TL1A-DR3 signalling is shown to enhance ILC2 accumulation and allergic inflammation upon the treatment with OVA and papain (Hergen Spits and Mjösberg 2022). Interestingly, studies with DR3-deficient mice show that DR3 signalling is necessary for papain-induced allergic inflammation, but not in the case of

helminth or fungal infection. Thus, the relevance of certain ILC2 activating signals appears to be context-dependent. The receptor Chemoattractant receptor-homologous molecule expressed on TH2 cells (CRTH2) is also expressed on ILC2s, and accumulation of ILC2s and Type 2 immune response in the context of helminth infection was shown to be dependent on CRTH2 signalling (Wojno et al. 2015). This CRTH2 signalling axis is also observed in humans. Of note, CRTH2 is now a widely used marker for ILC2s in humans (Wojno et al. 2015).

The nervous system and metabolic factors are also demonstrated to modulate lung ILC2 function. ILC2s express the neuromedin U receptor (NMUR), which enhances ILC2-driven allergic lung inflammation (Wallrapp et al. 2017) upon binding to NMU. In the HDM model, IL-25 synergises with NMU to expand IL-25-responsive iILC2. In contrast, a different neuropeptide Calcitonin gene-related peptide (CGRP) restricts ILC2 response and Type 2 immunity (Nagashima et al. 2019). Finally, the role of metabolites in regulating lung ILC2s was recently reviewed (Spits and Mjösberg 2022). For instance, the short-chain fatty acid (SCFA) butyrate was shown to inhibit Type 2 cytokine production by ILC2s and reduce airway hyperreactivity (Thio et al. 2018). In all, ILC2 function in allergic airway inflammation is regulated by a myriad of factors within the local lung tissue microenvironment.

1.5.2 ILC2s in viral, bacterial, and chronic obstructive pulmonary disease

Apart from Type 2 immunopathology, ILC2s have also been implicated in viral infections. RSV infection induces TSLP-dependent activation of ILC2s in the lung, leading to upregulation of IL-13 and airway hyperreactivity (Stier et al. 2016). In neonatal mice, rhinovirus infection leads to IL-25 production and ILC2-dependent airway hyperresponsiveness (Hong et al. 2014). Furthermore, ILC2s can mediate wound healing responses after viral infection, and this will be further discussed in the next chapter. Thus, despite the prototypical role of ILC2s as master regulators of Type 2 immunopathology, they can also exert an influence on Type 1 immunopathology.

Viral-induced Type 1 immunity is capable of inhibiting Type 2 immune responses. Specifically, Type 1 and 2 interferons associated with Type 1 immune responses have been demonstrated to suppress ILC2 function. In the Influenza A virus (IAV) mouse model, IFNAR-deficient mice that lacked Type 1 IFN signalling presented exacerbated epithelial hyperplasia and thickening of the alveolar wall, which is associated with ILC2 function (Duerr et al. 2016). Interferon beta (IFNβ) was observed to directly regulate mouse and human ILC2s, as IFNβ blunted IL-33 mediated proliferation and cytokine release *in vitro*. This was mediated by the interferon stimulated gene ISGF3.

IFNγ release induced by bacteria or viral infections also restrains ILC2 function. In the H1N1 CA04 model of influenza, blocking IFNγ signalling resulted in increased ILC2 function, enhanced Type 2 immune response, and reduced immunopathology and epithelial lung tissue damage (Califano et al. 2018). This is in line with literature demonstrating the role of IFNγ in dampening ILC2 function and Type 2 immune responses (Moro et al. 2015; Duerr et al. 2016). Alongside viruses, bacteria-induced IFNγ also appears to suppress Type 2 ILC2. In the model of *N.brasiliensis* infection, coinfection with *Listeria monocytogenes*, which is a potent inducer of IFNγ, led to reduced accretion of ILC2, reduced IL-5 production by ILC2s, reduced eosinophilia and a reduction in Tregs (Molofsky et al. 2015).

The suppression of ILC2 function has also been demonstrated in chronic obstructive pulmonary disease (COPD). COPD is a chronic inflammatory lung condition characterised by obstructed airflow to the lung. Smoking is considered the leading cause of COPD, and exacerbations are linked to viral or bacterial infection (Kearley et al. 2015). While IL-33 release was critical in viral-exacerbated COPD infection in mice, IL-33 influenced macrophage and NK cell function to enhance Type 1 responses (Kearley et al. 2015). Crucially, IL-33-induced ILC2 activation was suppressed via cigarette smoke, skewing the inflammatory profile towards a Type 1-like response (Jing Chen et al. 2016; Chung et al. 2016; Meziani et al. 2018).

Finally, it is interesting to consider the interactions between lung ILC2s and the microbiota. Given the interactions of the microbiota and the lung immune system in maintaining pulmonary immunity (Lloyd and Marsland 2017), it is likely that ILC2s mediate tolerance and immunity to the lung microbiota in some way. Notably, in the context of the stomach, it has been demonstrated that commensal bacteria support ILC2 induction of humoral immune responses (D. Li et al. 2014). More work is needed to see if an ILC2-mediated humoral response induced by bacteria is present in the lung.

1.5.3 ILC2s in lung fibrosis and wound healing

A landmark paper in 2011 demonstrated for the first time the role of ILC2s in mediating wound healing responses in the lung (Monticelli et al. 2011). ILC2s were accumulated in response to influenza viral infection, and the depletion of ILC2s diminished lung function and wound healing responses. Crucially, this was dependent on ILC2-derived amphiregulin, which was able to restore airway integrity after influenza infection even in the absence of ILC2s (Monticelli et al. 2011).

Apart from wound healing responses, ILC2s are also implicated in various pulmonary fibrosis models. Injection of *Schistosoma mansoni* eggs induced collagen deposition within the lung, which

was significantly reduced in ILC2-deficient mice (Hams et al. 2014). Furthermore, enrichment of ILC2s and IL-25 was present in BAL fluid of patients with idiopathic pulmonary fibrosis (IPF), suggesting that an IL-25-ILC2 axis could be present, even though this relationship has not been explicitly demonstrated. ILC2s also contribute to bleomycin-induced lung fibrosis. *ST2*$^{-/-}$ mice lack IL-33 signalling and experience reduced ILC2 numbers and are protected from bleomycin-induced lung fibrosis (Li et al. 2014). Crucially, the adoptive transfer of ILC2s into control mice exacerbated bleomycin-induced lung fibrosis, highlighting a supportive role of ILC2S in promoting fibrosis.

The mechanisms regulating ILC2 pro-fibrotic function are gradually elucidated. The RNase Regnase-1 restrains ILC2 proliferation and activation to restrict fibrosis. In bleomycin-treated mice, the transfer of ILC2s from Regnase1-deficient mice displayed exacerbated fibrosis compared to mice transferred with WT ILC2s (Nakatsuka et al. 2020). More recently, a TGFβ1–Neuropilin-1 (Nrp1) axis was reported to enhance ILC2 function via the upregulation of the ST2 receptor, leading to enhanced bleomycin-induced lung fibrosis (Zhang et al. 2022) . Notably, Nrp1 expression in ILC2s is specific to lung ILC2s as ILC2s in other tissues displayed minimal expression on Nrp1, and this could be a promising target to suppress lung ILC2 function while sparing ILC2s in other tissues. Nevertheless, the mechanisms underlying the response of ILC2s in wound-healing and fibrosis are yet to be fully understood. Notably, the signals that differentiate wound-healing and fibrotic responses of ILC2s are unknown and this remains an area of further work.

1.6 ILC2s in cancer

While our understanding of ILC2s has come predominantly from studying them in the context of Type 2 inflammation, less is known about the role of ILC2s in cancer. Crucially, ILC2s display apparently contradicting functions to both inhibit and promote tumour growth depending on the tissue. It is likely that their function depends on the local microenvironment and the tissue in question. Here, I review some of the literature looking at ILC2s in the cancer context.

1.6.1 Anti-tumour role of ILC2s

One of the earliest reports studying the role of ILC2s cancer was published in 2012, where an anti-tumour function of ILC2 in the B16 model of lung metastasis was demonstrated (Ikutani et al., 2012). These IL-33-responsive ILC2s were observed to produce IL-5 in the lungs via the use of IL-5/Venus reporter mice. Though no direct link between ILC2-induced IL-5 production of eosinophil was demonstrated, an anti-tumour function of ILC2 via the recruitment of eosinophils was proposed.

The anti-tumour function of ILC2s has also been reported in subcutaneous cancer models. Using an IL-33-expressing EL-4 lymphoma lung cell cancer cell, it was demonstrated that IL-33-mediated inhibition of tumour growth was dependent on ILC2s, as adoptively transferred ILC2s to *Rag*$^{-/-}$*IL2rg*$^{-/-}$ mice was necessary to induce anti-tumour function (Kim et al., 2016). This was dependent on IL-33 induced activation of ILC2s, stimulating the production of CXCR2 ligands CXCL1 and CXCL2, which signal through CXCR2 on tumour cells to induce their apoptosis.

In 2020, an IL-33-ILC2 anti-tumour axis activating tissue-specific immunity in the context of PDAC was reported (Moral et al. 2020). In this model, ILC2s were observed to infiltrate the tumour microenvironment, and treatment with IL-33 led to the accumulation of ILC2 alongside CD8+ T-cells, contributing to anti-tumour immunity. Specifically, ILC2 production of CCL5 favoured the recruitment of CD103+ DCs, which promoted CD8+ T-cell anti-tumour activity. The report also demonstrated that ILC2 expressed the immune checkpoint receptor PD-1, and concomitant administration of IL-33 and anti-PD1 blocking antibody significantly reduced pancreatic tumour burden (Moral et al. 2020). This provided evidence that immunotherapeutic approaches targeting ILC2s could be employed to improve cancer outcomes. However, excessive IL-33 exposure was performed in this model to induce ILC2 activation, which is not representative of the actual microenvironment in PDAC.

The anti-tumour function of ILC2 in the context of lung cancer has also been reported (Saranchova et al. 2018). In this report, lung-derived IL-33-expressing TC1 and non-IL-33-expressing A9 cells were

used. Using a model of ILC2-deficiency where *Rorα*$^{-/-}$ mice are transplanted with WT bone marrow cells, ILC2-deficient mice displayed an increase in tumour burden when implanted with IL-33 expressing TC1 tumour cells. Crucially, this effect was not observed in non-IL-33-expressing A9 tumour cells, even though the trend was replicated when exogenous IL-33 was introduced. An increased spread to distal organs, including the lung (Saranchova et al. 2018), was also observed in ILC2-deficient mice. Finally, an ILC2-DC axis mediating anti-tumour activity was proposed, even though this was only demonstrated *in vitro* using a prostate cancer cell line.

1.6.2 Pro-tumour role of ILC2s

The bulk of ILC2-related literature in cancer suggest that ILC2 function to support cancer growth. This is unsurprising given that Type 2 immunity is typically associated with pro-tumour responses and ILC2s play a central role in promoting Type 2 immune responses.

A study in 2014 was one of the earliest postulating a pro-tumour function of ILC2 in cancer. In the 4T1 orthotopic model of triple negative breast cancer, 4T1 breast cancer cells produced IL-33 and exogenous IL-33 challenge accelerated primary tumour progression and facilitated an increase in metastatic dissemination to the lung and liver (Jovanovic et al. 2014). This was accompanied by a concomitant increase in immunosuppressive CD11b+CD11c-Gr-1+ MDSCs, immature DCs, IL-10-producing Tregs and ILC2s. While a direct link between ILC2s and increased tumour burden was not established, it was hypothesised that IL-13 release by ILC2 supports MDSCs production of nitric oxide synthase and arginase to maintain an immunosuppressive tumour microenvironment. In human breast cancer, malignant tissue displayed a higher percentage of ILC2s compared to benign tissues (Salimi et al. 2018). In addition, ILC2s in malignant breast cancer tissues showed a higher MHCII and KLRG1 expression, suggesting an activated phenotype, even though the significance of this is unclear. Notably, comparison of malignant tissue to benign tissue was not performed.

Further evidence of an ILC2-MDSCs axis involved in the promotion of tumour growth has been discovered in other cancers. ILC2s were reportedly upregulated in peripheral blood of patients diagnosed with acute promyelocytic leukaemia (APL), and this was accompanied by an increase in serum concentration IL-13 attributed to ILC2s (Trabanelli et al. 2017) . APL tumour cell-derived Prostaglandin D2 (PGD2) activates ILC2 via interaction with the receptor CRTH2. In addition, B7H6-NKP30 interactions contribute to ILC2 function. ILC2-derived IL-13 recruits MDSCs, which then favours an immunosuppressive environment for tumour growth. ILC2 and IL-25 were also observed to be associated with primary colorectal cancer in the *Apc*$^{1322T/+}$ mouse model of intestinal tumourigenesis (Jou et al. 2022). IL-25 is implicated in the development of intestinal tumours, as

exogenous IL-25 promotes tumour development alongside the accretion of ILC2s, and IL-25-deficiency increases survival of *Apc*$^{1322T/+}$ mouse. Crucially, ILC2s supports cancer development as ILC2-deficient *Il7rα*$^{Cre/+}$*Rorα*$^{fl/fl}$ *Apc*$^{1322T/+}$ mice had reduced tumour burden and improved life expectancy. Similar to the APL model, ILC2s promoted the recruitment of MDSCs via IL-13 and IL-4. In addition, they demonstrate that MDSC suppresses anti-tumour immunity, in part via the reduction of IFNγ production by CD8+ T-cells (Jou et al. 2022).

The ILC2-MDSC axis is also purported to play a role in bladder and prostate cancer. ILC2s were observed to be enriched in peripheral blood of prostate cancer, and MDSCs were observe to accumulate in a preclinical mouse model of prostate cancer (Trabanelli et al. 2017). In human bladder cancer, a low local T-cell/MDSC ratio was strongly associated with bladder tumour recurrence (Chevalier et al. 2017). In addition ILC2 was the most dominant ILC subset in urine of patients. However, these observations solely demonstrate correlation and it remains to see if such an axis is present in these cancers.

The majority of literature investigating the role of ILC2s in lung cancer suggest that they exert pro-tumourigenic function. We recently reported an ILC2-eosinophil-NK cell immune axis that promotes lung metastasis (Schuijs et al. 2020). Specifically, allergen-induced IL-33 activates lung ILC2s, leading to IL-5 mediated recruitment of eosinophils. The influx of highly glycolytic eosinophils perturbs NK cell metabolism, which compromises NK cell anti-tumour activity. Notably, we also demonstrate increased lung metastasis in the 4T1 model of breast cancer upon IL-33 administration, supporting a pro-tumour of ILC2s in metastasis of breast cancer as previously reported (Jovanovic et al. 2014). Others have also reported a role of ILC2s in restraining NK cell anti-tumour function, as ILC2s have also been reported to restrain NK cell anti-tumour immunity via direct CD39-CD73 interactions (Long et al., 2018). Similar to our findings, a later publication demonstrated a role of ILC2s in promoting lung metastasis in the B16 melanoma model of lung metastasis (Howard et al. 2021), which was one of the models we utilised. The authors reported the expression of PD-1 on ILC2 in tumour-bearing lungs, and blocking PD-1 on ILC2s promoted TNFα production that facilitated tumour apoptosis. In human lung cancer, an increase in the frequency of ILC2s in PBMC compared to healthy controls were observed, alongside elevated levels of IL-33 expression (Wu et al. 2017). Elevated levels of Type 2 cytokines were also observed, supporting the notion that enhanced Type 2 immunity is associated with worse prognosis for most cancers. Notably, an increase in MDSCs was also observed, suggesting that an ILC2-MDSC axis could also be present within lung cancer. Figure 1.3 summarises the literature investigating the pro and anti-tumour role of ILC2s in cancer.

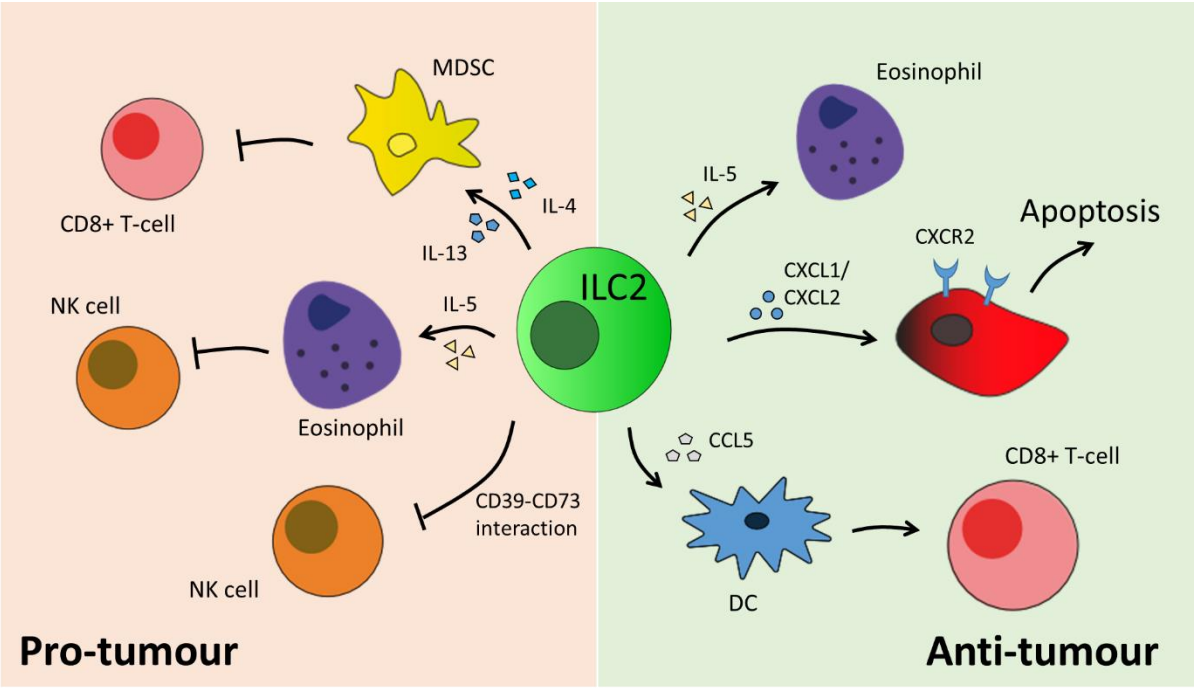

Figure 1.3 Summary of pro-tumour and ant-tumour effects of ILC2s in literature. ILC2 release of IL-5 activates eosinophils, which could either exert anti-tumour function or promote tumour growth via inhibiting NK cell function. ILC2s also inhibit NK cell function by direct CD39-CD73 interaction. ILC2s also promote MDSC function to inhibit anti-tumour function of CD8+ T-cells. ILC2s can also promote anti-tumour function via promoting CD8+ T-cell function via recruitment of DCs or by releasing CXCL1 or CXCL2 to induce apoptosis in tumour cells.

1.7 Aims and Hypothesis

Radiotherapy-induced activation of the immune response plays a key role in driving local and systemic anti-tumour immunity. Nevertheless, it is still not fully understood how radiotherapy modulates the immune microenvironment in lung cancer. ILC2s are a tissue-resident population of immune cells in the lung and they play an extensive role in mediating innate and adaptive Type 2 immunity. However, it is still not clear if this is also the case in the context of lung cancer, or if radiotherapy induces ILC2 activation. Hence, the aims of this thesis are as follows;

1. Characterise the response of ILC2s to targeted lung radiotherapy
2. Understand the response of the lung immune microenvironment to radiotherapy in the context of lung cancer
3. Establish a more refined *in vivo* model to study the immune-regulatory role of ILC2s in primary lung cancer

Chapter 2: Materials and Methods

2.1 *In vivo* animal studies

Wild type C57BL/6J (WT) mice were purchased from Charles Rivers Laboratories and housed in the Cancer Research UK Cambridge Institute (CRUK-CI) animal facility under specific pathogen-free conditions. *Il33*$^{cit/cit}$, *Il33*$^{cit/+}$, *Il7rα*$^{Cre/+}$, *Il7rα*$^{Cre/+}$*Rorα*$^{fl/fl}$, *Il7rα*$^{Cre/+}$*Tnfsf4*$^{fl/fl}$, *Rag2*$^{-/-}$, *Rag2*$^{-/-}$*Il2rg*$^{-/-}$, *Rag2*$^{-/-}$ OT-I and *Kras*$^{LSL\text{-}G12D/+}$*Trp53*$^{fl/fl}$ (KP) mice were bred in-house and maintained in the CRUK-CI facility. All mice were of the C57BL/6 background and housed in the CRUK-CI were kept between 19 and 23^{o}C with 45-65% humidity and a 12-hour light-dark cycle. Age-matched female mice between 7-12 weeks were used for all experiments. All animal work was conducted in accordance with the project licenses PD7484FB9 and PD993249 under the UK Home Office guidelines. All mice were sacrificed by Schedule 1 methods of either cervical dislocation or by rising concentration of CO_2, followed by a secondary method of confirmation.

2.2 *In vivo* experiments

Mice were anesthetised by isoflurane inhalation, followed by administration of mouse recombinant IL-33 (0.2µg, BioLegend, 12022-09) and OVA (50µg, Invivogen, vac-pova) in 40µl of PBS. For the treatment of KP mice, 2.5 x 10^7 PFU Adenoviral Cre (University of Iowa Viral Vector core) in 40µl of DMEM was administered intranasally in Containment level 2 conditions. IL-33R-Fc (10mg/kg, AstraZeneca) and anti-NK1.1 (50µg, Bio X cell, BE0003-1) were administered in 200µl of PBS intraperitoneally.

2.3 Tumour cell lines and tumour models

B16F10, B16F10-OVA (mCherry), B16F10-Luciferase, LL/2 Lewis Lung carcinoma, inducible OVA-expressing B16F10 (B16F10-iOVA) and derived KP (dKP) cells were tested negative for *Mycoplasma* and authenticated by short tandem repeat profiling. All tumour cells of the B16F10 background and LL/2 Lewis Lung carcinoma were grown in DMEM (ThermoFisher, 41965039) with 10% FCS and 100U/ml pencillin, 100µg/ml streptomycin (P/S) , while dKP cells were grown in RPMI 1640 (ThermoFisher, 21875034) with 10% FCS and P/S. All tumour cells were detached using 0.05% Trypsin-EDTA (ThermoFisher, 25300054), washed in PBS and resuspended in an appropriate volume before injection into mice. 1 × 10^5 cells for all cell lines in the B16F10 background and 1 × 10^6 of dKP cells were injected intravenously for the establishment of lung metastasis. At end point, lung

metastatic nodules were quantified by counting under a dissection microscope and lungs were collected for further processing.

In the subcutaneous model, 5×10^5 dKP were injected in 50µl of PBS into the right flank of mice. Protocol for the orthotopic injection of tumour cells was adapted from (Justilien and Fields 2013). Tumour cells were prepared by resuspending cells at a concentration of 1×10^5 dKP cells/10µl of matrigel diluted in PBS in a 1:1 ratio. Mice were first anaesthetised in an isoflurane chamber and anaesthesia was confirmed via a tail-pinch test. Anaesthetised mice were transferred onto a heating pad, kept on anaesthesia via a nose cone, and placed on the right lateral decubitus position. Hair covering the thorax region was shaved off to expose the skin, which was cleaned with Hibiscrub (Mölnlycke, 10009249) to reduce chances of infection. Tumour cell suspension was drawn into a 1ml syringe equipped with a 30-G hypodermic needle. The needle was advanced rapidly to a depth of approximately 5-7mm into the left lobe of the lung, approximately between the 4^{th} to 8^{th} rib, and 10µl of tumour cell suspension was injected. Upon removal of the needle, mice were kept on the left lateral decubitus position in a 37°C heating chamber and allowed to recover before transferring them back to their original cages. Mice were monitored daily for clinical signs (i.e weight loss, piloerection, lethargy) and tumour-bearing lungs were harvested at the appropriate time points. For optimisation experiments aiming to reduce leakage of tumour cells in the orthotopic model, LL/2 cells were prepared by resuspending cells at a concentration of 2×10^3 cells/5µl of matrigel diluted in PBS in a 1:1 ratio. A specialised glass syringe (Hamilton, 20701) equipped with the same 30-G hypodermic needle was used to inject 5µl of tumour cell suspension.

2.4 Targeted radiotherapy

The Xstrahl Small Animal Radiation Research Platform (SARRP) was used for all mouse treatments. Each mouse was kept anaesthetised on a mobile platform with isoflurane via a nose-cone connected to an external isoflurane source. Cone-beam CT was performed on all mice prior for treatment planning. CT images were obtained with a 60kVp and 0.8mA uncollimated beam. During the acquisition of CT images, the platform was rotated 360° and projections were acquired at 1° increments, with a total of 360 projections acquired at a rate of 6 projections/second. Muriplan software was used to select the targeted region of interest, and dose calculation was performed with the Monte Carlo algorithm. Targets were selected such that only the left lung was targeted, sparing the remaining lung lobes (see Results). A single beam of 220kV and 13mA was used for the targeted irradiation of all mice. For the 15Gy single dose regimen, a fixed 5 x 5mm collimator was used. For the 8.5Gy X 2 fractionated dose, a variable collimator adjusted to 8 x 5mm was used.

2.5 Single-cell preparation

Lung tissues were finely chopped with scissors and digested in 2ml of RPMI containing collagenase I (500U/ml, Life Technologies, 17100-017) and DNase I (0.2mg/ml, Sigma-Aldrich, DN25-1G) for 45 minutes at 37^{o}C on a shaking incubator (220 r.p.m). Digested lungs were filtered through a 70µm filter and subjected to 30% Percoll (Sigma-Aldrich, GE17-0891-09) centrifugation gradient, followed by treatment with red blood cell lysis buffer (1ml, 3 minutes, room temperature). Cells were spun and resuspended in 1ml of PBS to obtain single-cell suspension.

2.6 Cell line generation

B16F10 cells were transfected with the transposase-encoding PB7 vector (Yusa et al. 2011) and an inducible OVA (iOVA) vector carrying a doxycycline-sensitive OVA-expressing construct (see Results) using Lipofectamine 2000 (ThermoFisher, 11668030). Cells were kept and passaged for 2 weeks in selection media (DMEM 10% FCS, P/S, 2µg/ml puromycin, 1µg/ml tetracycline). Surviving stably transduced cells were expanded and sorted by fluorescence-activated cell sorting (FACS) with the BD FACS Aria II. Individual GFP+ cells were sorted at 1 cell/well in a 96-well plate and kept on selection media. Individual clones were screened for GFP with the MACSQuant VYB (see Results), and selected and expanded in selection media. Successfully amplified clones were frozen in 90% FCS/10% diemthyl sulfoxide (DMSO) freezing media.

The protocol for the generation of dKP cells was adapted from (Kasinski and Slack 2013). 10 weeks post-Cre treatment, KP mice were sacrificed by overdose of CO_2 and lungs were perfused with 10ml of cold PBS. Lungs were rinsed 4 times in PBS and minced until no large pieces were present, followed by addition of an equal volume of RPMI supplemented with 1mg/ml collagenase/dispase (Roche, 10269638001). The mixture was incubated for 1 hour at 37^{o}C in a 5% CO_2 chamber. Cells were removed intermittently from the top half of the supernatant every 10-15 minutes. Pooled supernatants were spun and the pellet was resuspended in RPMI 10% FCS media. Cells were transferred to 10cm sterile cell culture dishes coated with collagen (Bovine-Fisher, 50-260-230) and fibronectin (ThermoFisher, PHE-0023) and kept at 37^{o}C in a 5% CO_2 chamber. After 3 passages, individual epithelial-looking colonies were picked using a pipette and transferred to 96-well plates. Individual clones were gradually expanded in RPMI 10% FCS on non-coated plates. Validation of colonies was done by flow cytometry with the antibodies CD45-BV510, CD31-BV605 and EpCAM-BV711 (Table 1). Amplified clones have successfully propagated up to 15 passages and were frozen in 90% FCS/10% DMSO freezing media.

2.7 GFP expression assay

B16F10-iOVA cell lines were initially cultured on 6-well plates in the absence of tetracycline. Cells were transferred to 1µg/ml tetracycline-containing media or removed from tetracycline-containing media at the appropriate time points indicated in the results. Cells were passaged when 95-100% confluence was reached. Monitoring of GFP expression was performed using the MACSQuant VYB.

2.8 Cytotoxicity assay

Activated OVA-specific OT-I T-cells were obtained from the spleens of *Rag2*$^{-/-}$ OT-I mice. Briefly, spleens were first mashed through a 70µm cell strainer, centrifuged and resuspended in 40ml RPMI 10% FCS with + 50IU/ml IL-2 (Peprotech, 200-02) + 10nM SIINFEKL peptide (InvivoGen, vac-sin). Cells were kept in culture and expanded for up to 4 days to obtain activated OT-I T-cells. Activated OT-I cells were labelled with CFSE (ThermoFisher, C34554) at 1:1000 dilution and co-cultured with B16F10, B16F10-OVA or B16F10-iOVA cells with or without tetracycline in a 5:1 ratio. Annexin V dye (Satorius, 4641) was added to the co-culture to a final dilution of 1:200 to detect apoptotic cells. Co-cultures were imaged with the IncuCyte ZOOM and images were obtained every 15 minutes up to 22 hours. Quantification of tumour cell killing was performed with the IncuCyte ZOOM software.

2.9 Flow cytometry

The complete list of antibodies and fluorescent conjugates are shown in Table 1, and the gating strategy used to identify lymphoid and myeloid cells are shown in Figure 2.1 and 2.2 respectively. The gating strategy for ILC2s can be found in the Results section. Single cell suspensions were prepared as per chapter 2.5. A tenth of the total single cell suspension were incubated with the appropriate antibodies alongside side CD16/32 to block Fc receptors. The lineage cocktail for the lymphoid panel consisted of the following: CD5, CD19, F4/80, CD11b, CD11c, FcεRIa, Gr-1 and Ter119. The lineage cocktail for the myeloid panel consisted of the following: CD5, CD19, CD3, NK1.1 and B220. All lineage antibodies were conjugated to eF450. Intra-nuclear staining to detect transcription factors was done with the Foxp3/Transcription Factor Staining Buffer Set Kit (ThermoFisher, 00-5523-00). Intracellular staining to detect cytokines was performed using the Cytofix/Cytoperm kit (BD, 554714). For intracellular cytokine detection, single cells were stimulated with PMA and ionomycin plus protein transport inhibitor (ThermoFisher, 00-4975-03) at 1X concentration in RPMI 10% FCS for 3 hours at 37^{o}C. For the staining of OVA-specific CD4+ T-cells, I-A(b) HAAHAEINEA PE-labelled tetramers (NIH tetramer core facility) were incubated with single cell

suspensions at 37°C for 2 hours. Cells were analysed on the BD LSR Fortessa or BD FACS Symphony flow cytometers, and cell numbers were enumerated with CountBright beads (ThermoFisher, 01-1234-42). Analysis was performed using FlowJo X (FlowJo LLC).

2.10 IVIS imaging

A 15mg/ml D-luciferin solution (Perkin Elmer, 122799) was injected intraperitoneally in mice bearing B16F10-Luciferase tumour cells. Mice were weighed prior to injection and 10µl of D-luciferin was injected per gram of body weight. Mice were sacrificed 5 minutes after injection, dissected and imaged with the IVIS spectrum (Xenogen). Total photon emission from the left and right lung lobes was quantified separately with the Living Image software package (Xenogen).

2.11 Histology

Lung lobes and lung tumours were fixed in 10% neutral buffered formalin for 24 hours and transferred to 70% ethanol for an hour and up to 3 days. Tissues were embedded in paraffin and sectioned into 3µm slices. Slices were stained with H&E, Masson's Trichrome or Ki67. Slides were scanned with the Aperio AT2 scanner. Tissue embedding, sectioning, staining and scanning were all performed by the CRUK CI histology core facility. Scanned images were analysed using the HALO software (Indica Labs).

Quantification of tumour burden in the B16F10-OVA model of lung metastasis was done with a classifier tool on the HALO software. The software was trained to identify three features of tumour-bearing lungs: glass slide, tumour tissue, lung tissue (Figure 2.3). Percentage tumour area of the left lung lobe or right lobes was calculated by dividing the tumour area by the combined tumour and tissue area.

2.12 Statistics

Statistical analysis for experiments with only 2 groups were performed using unpaired two-tailed student's t-test. Statistical analysis with more than 2 groups were performed using one-way ANOVA with Tukey's or Dunnett's test. Statistical analysis with grouped data of more than 2 groups were performed using two-way ANOVA with Sidak's test. All statistical analysis was performed on Prism 8 (GraphPad Software). Significance was calculated as ns = not significant, * = $P \leq 0.05$, **= $P \leq 0.01$, *** = $P \leq 0.001$, **** = $P \leq 0.0001$, with $P \leq 0.05$ considered significant.

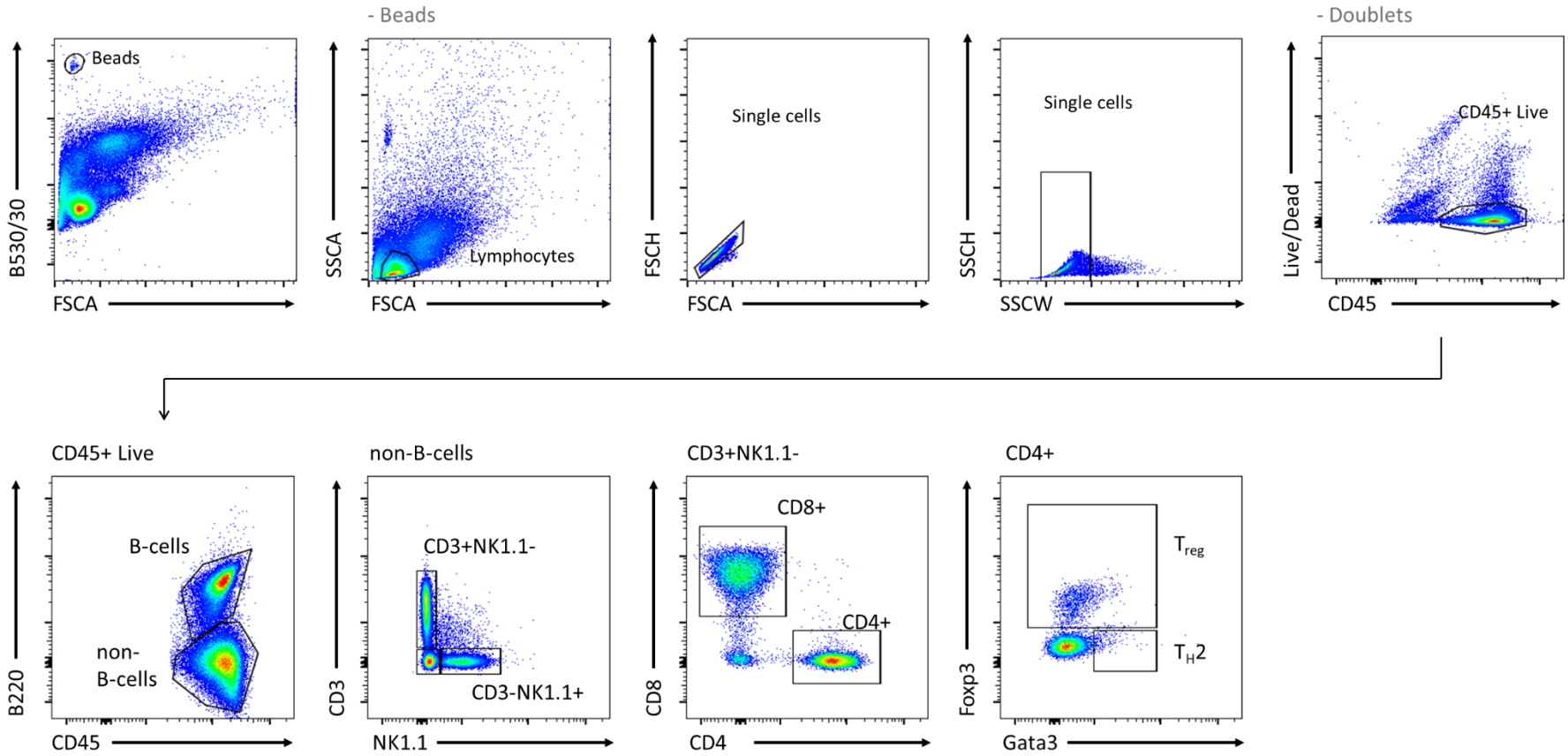

Figure 2.1. Lymphoid gating strategy. After the exclusion of counting beads, lymphocytes were gated based on their size profile and doublets were excluded via 2 consecutive size gates, followed by gating of CD45+ Live cells. B-cells were defined by expression of B220. B220- non-B-cells consisted of CD3-NK1.1+ NK cells and while CD3+NK1.1- cells consisted CD4+ and CD8+ T-cells. Within the CD4+ T-cell population, T_{regs} and T_H2 cells were defined via the expression of transcription factors Foxp3 and Gata3 respectively.

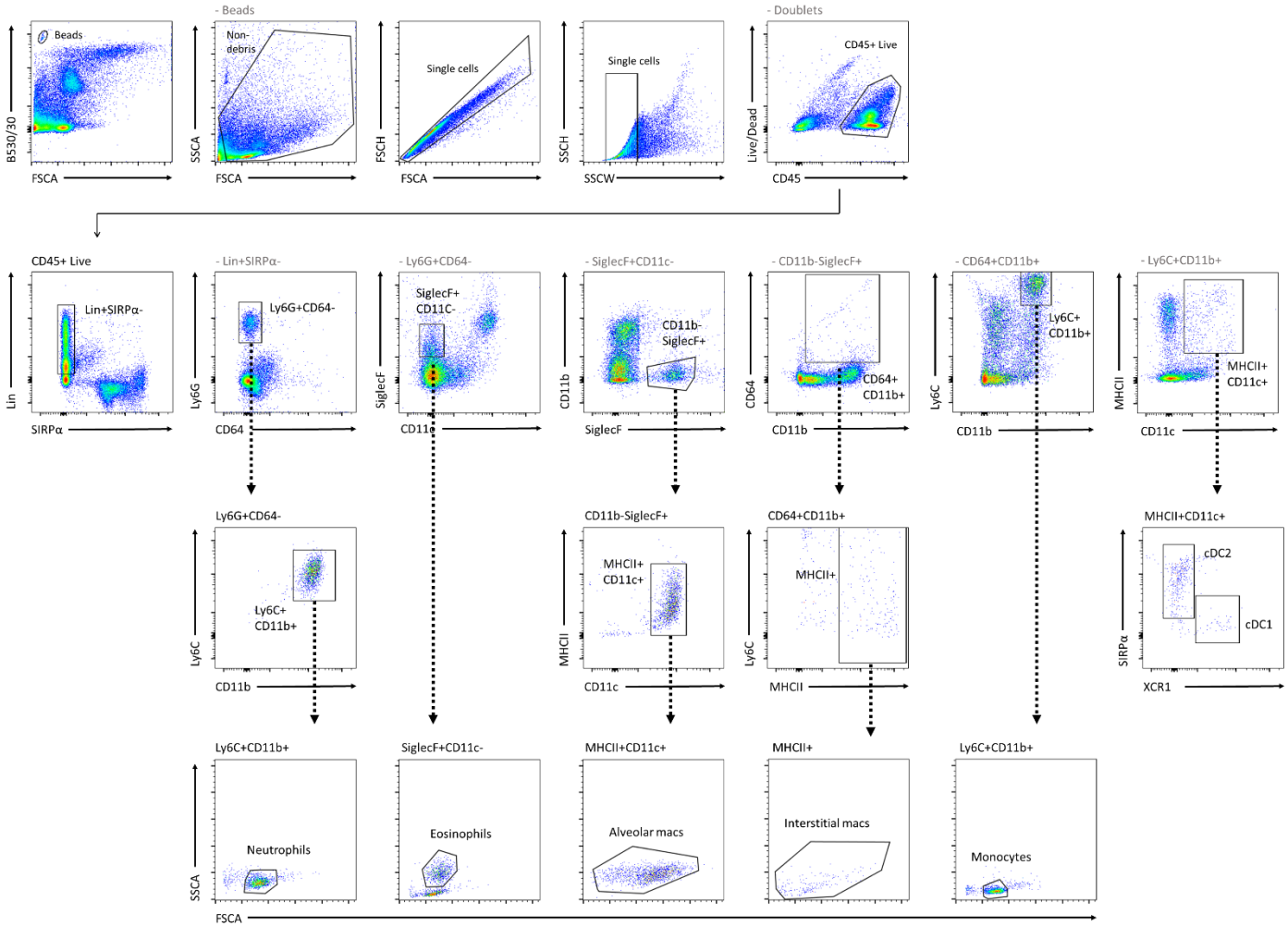

Figure 2.2. Myeloid gating strategy. After the exclusion of counting beads and debris via the B530/30 channel and size profile respectively, doublets were excluded via 2 consecutive size gates, followed by gating of CD45+ Live cells. Lin+ cells were excluded and neutrophils were identified by as Ly6G+CD64- cells, followed by expression of Ly6C and CD11b. After their exclusion, eosinophils were defined as SiglecF+CD11c- cells. Alveolar macrophages were defined as CD11b-SiglecF+CD11c+MHCII+ cells after the exclusion of eosinophils. Interstitial macrophages were defined as CD64+CD11b+MHCII+ cells after exclusion of alveolar macrophages, while monocytes were defined as CD11b+Ly6C+ cells after exclusion of interstitial macrophages. Finally, DCs were identified as CD11c+MHCII+ cells, and further sub-grouped into cDC1s or cDC2s via expression of XCR1 and SIRPα respectively.

Table 2. Antibody list for flow cytometry. Complete list of antibodies and conjugated fluorophores (excluding tetramers) used for flow cytometry.

Fluorophore	Protein	Clone	Manufacturer	Catalogue number	Dilution
AF488	CD172a	P84	ThermoFisher	144024	1:500
AF488	Foxp3	FJK-16S	ThermoFisher	53-5773-80	1:250
PerCP-ef710	CD8	53-6.7	ThermoFisher	46-0081-82	1:500
eF450	CD5	53-7.3	ThermoFisher	48-0051-82	1:2000
eF450	CD19	1D3	ThermoFisher	48-0199-42	1:2000
eF450	CD3e	145-2C11	ThermoFisher	48-0031-82	1:2000
eF450	NK1.1	PK136	ThermoFisher	48-5941-82	1:2000
eF450	B220	RA3-6B2	ThermoFisher	48-0452-82	1:2000
eF450	CD11b	M1/70	ThermoFisher	48-0112-82	1:2000
eF450	CD11c	N418	ThermoFisher	48-0114-82	1:2000
eF450	Gr-1	RB6-8C5	ThermoFisher	48-5391-82	1:2000
eF450	Ter119	TER-119	ThermoFisher	48-5921-82	1:2000
eF450	F4/80	BM8	ThermoFisher	48-4801-82	1:2000
eF450	FcεRIa	MAR-1	ThermoFisher	13-5898-82	1:2000
BV510	CD45	30-F11	BioLegend	103138	1:500
BV605	CD31	390	BioLegend	102427	1:500
SB600	SiglecF	1RNM44N	ThermoFisher	63-1702-82	1:500
BV650	RORyt	Q31 378	BD	563424	1:500
BV650	XCR1	ZET	BioLegend	148220	1:500
BV711	CD64	X54-5/7.1	BioLegend	139311	1:250
BV711	EpCAM	G8.8	BioLegend	118233	1:500
BV785	CD11b	M1/70	BioLegend	101243	1:500
BV785	IFNγ	XMG1.2	BioLegend	505838	1:250
BUV395	MHCII (I-A/I-E)	CI2G9	BD	743876	1:2000
BUV395	NK1.1	PK136	BD	564144	1:500
UV455	Live/Dead (Fixable)	-	ThermoFisher	65-0868014	1:500
eF660	Gata3	TWAJ	ThermoFisher	50-9966-42	1:250
APC	CD86	B7-2	ThermoFisher	17-1341-82	1:250
AF700	CD4	RM4-5	BioLegend	300526	1:500
AF700	CD11c	N418	BioLegend	337219	1:500
APC-ef780	B220	A3-6B2	ThermoFisher	47-0452-82	1:500
PE	CD80	B7-1	ThermoFisher	12-0801-81	1:250
PE	IL-13	13A	ThermoFisher	12-7133-82	1:250
PE	OX40L	RM134L	ThermoFisher	12-5905-82	1:250
PE-CF594	CD127	SB/199	BD	562419	1:500
PE-eF610	Ly6G	1A8-Ly6G	ThermoFisher	61-9668-82	1:1000
PE-Cy7	CD3e	145-2C11	ThermoFisher	25-0031-82	1:500
PE-Cy7	Ly6C	HK1.4	ThermoFisher	25-5932-82	1:2000
-	CD16/32	-	BioLegend	101320	1:500

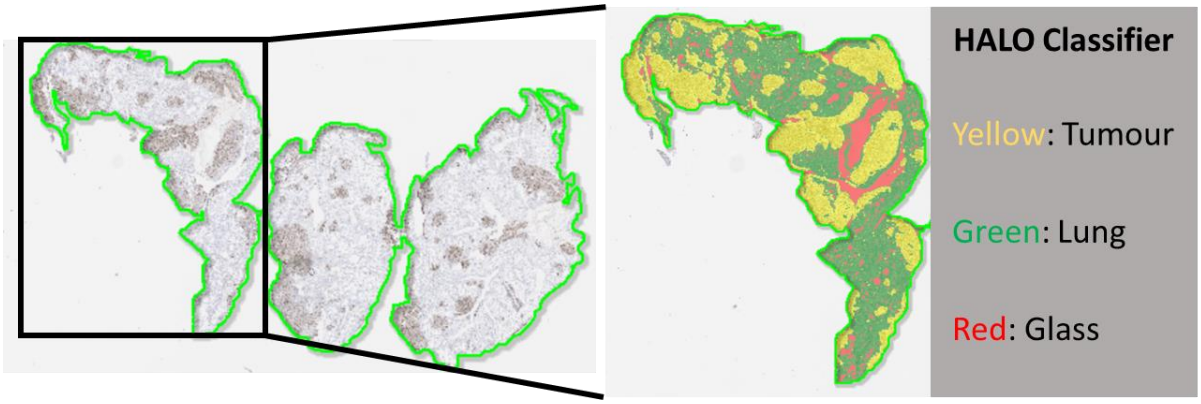

Figure 2.3. Trained HALO classifier for the quantification of lung tumours. The HALO classifier was used to identify 3 distinct regions on the Ki67-stained slide: tumour tissue, lung tissue and glass.

Chapter 3: Characterising ILC2 response to targeted lung radiotherapy

3.1 Introduction

It is widely appreciated that radiotherapy induces changes within the immune microenvironment of the irradiated tissue. I discussed previously the role of radiotherapy in inducing pro-tumour or anti-tumour responses by modulating the immune system. Whilst radiotherapy is typically used to target cancer cells within the tissue, an understanding of how radiotherapy modulates immune cells within the lung microenvironment could provide insight into how these neighbouring immune cells respond to radiotherapy. As previously discussed, an improved understanding of radiotherapy-induced immune interactions has allowed for improved treatment outcomes in radiotherapy-immunotherapy combinational therapy (Formenti et al. 2018).

Furthermore, in the context of the lung, radiation-induced pneumonitis and fibrosis are typical side-effects that occur due to the irradiation of bystander non-tumour tissues (Tsoutsou and Koukourakis 2006; Lierova et al. 2018). Whilst the progression of pneumonitis and fibrosis is typically linked to changes in the extracellular matrix and collagen deposition, the immune system also plays a key role in therapy-induced side effects (Gieseck, Wilson, and Wynn 2018). Thus, understanding the response of immune cells typically associated with Type 2 inflammation, such as ILC2s, to lung radiotherapy could elucidate the role of these immune cells in radiation-induced lung injury as well.

Preclinical radiotherapy treatment platforms have greatly improved knowledge in the field of radiation oncology. Such platforms allow for the irradiation of small rodents, typically mice, which have served as excellent preclinical models. A key benefit of such systems is that they mimic clinical radiation settings, and can perform both pre-treatment CT scans, as well as subsequent administration of radiotherapy (Wong et al. 2008). This allows for improved targeting of specific tissues as scanned CT images serve as a template for treatment planning.

An example of such a platform is the Small Animal Radiation Research Platform (SARRP). This platform has been used in the literature to target tumours in various tissues i.e. lung, pancreas and skin (Herter-Sprie et al. 2014; Kalbasi et al. 2017; Sharabi et al. 2015). Notably, studies using such radiation platforms typically monitor treatment outcomes and responses, while the immune compartment is often neglected. Furthermore, whilst some of these studies look at the innate immune response, the bulk of literature focuses on adaptive immune responses, which are recognised for its importance in radiotherapy-induced anti-tumour responses (Spiotto, Fu, and

Weichselbaum 2016). Nevertheless, there is a lack of studies focusing on immunophenotyping the response to radiotherapy, and even less is done in the context of the lung. In addition, as an emerging new cell type, the response of lung ILC2s to radiotherapy has not yet been investigated.

In this chapter, I discuss the use of the SARRP in profiling the immune response to targeted irradiation of mouse lungs. Firstly, I sought to establish a model of targeted lung irradiation using the SARRP. Subsequently, I aimed to carefully characterize the local immune response to targeted lung irradiation, focusing on lung ILC2. Finally, to investigate the potential role of ILC2s on radiation-induced lung fibrosis, I aimed to establish a model of lung fibrosis with the SARRP.

3.2 Results

3.2.1 Establishing a model of targeted lung irradiation using the Small Animal Radiation Research Platform (SARRP)

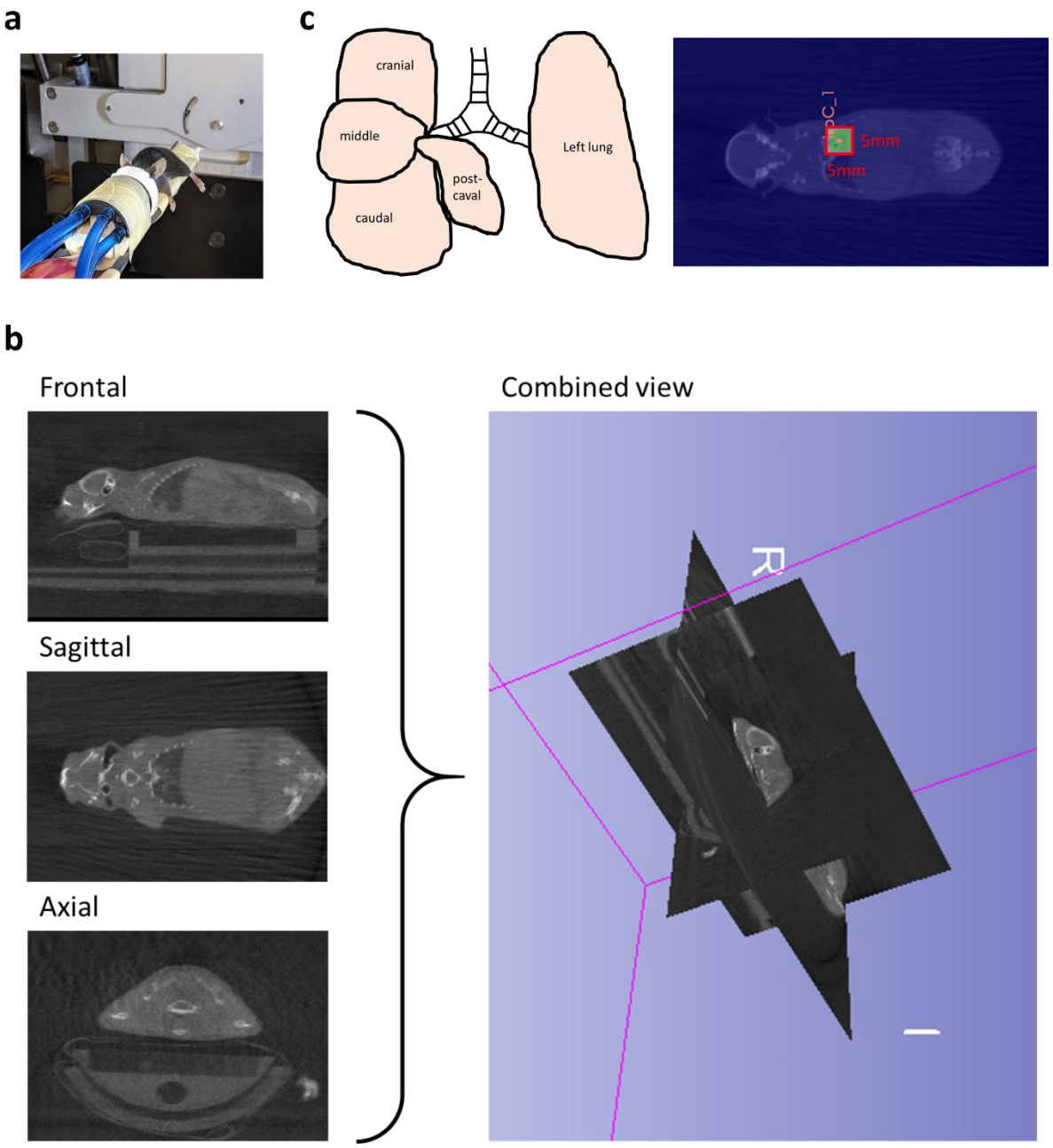

Figure 3.1 Method of targeted lung irradiation with the SARRP. (a) Mice are kept under anaesthesia and placed on a mobile platform within the SARRP. **(b)** Images from a CT scan showing 3 perspectives of an anaesthetised mouse obtained from the SARRP. A 3D reconstruction gives a combined view that allows for subsequent targeted irradiation. **(c)** The mouse lung contains 5 lobes in total, with the left lung composing a single left lobe (left). Targeted irradiation of the lung left lobe is achieved by selecting the region of interest in the scanned CT image. A 5 X 5mm region was targeted with a fixed collimator (right).

To study lung-specific immune responses, a model of targeted lung irradiation was established with the SARRP. As briefly discussed, the SARRP allows for image-guided radiation therapy (IGRT) to be performed. Essentially, IGRT involves the initial imaging of the target tissue (in this case a CT scan), after which the scanned image is used as a guide for radiation treatment planning.

The SARRP contains a mobile platform where the mouse is kept throughout the entire procedure (Figure 3.1a). A nose cone is embedded at the tip of the platform, and this is attached to an isoflurane source that is kept separate from the SARRP unit. This ensures that the mouse remains anaesthetized and asleep throughout the procedure. The SARRP comprises a CT scan function, which gives a 3D image of the mouse (Figure 3.1b). 3 different perspectives are displayed on the treatment planning software alongside the combined 3D image. Each of these individual perspectives can then be used to determine the site of irradiation. Before irradiation, a central point known as the isocentre is selected based on the scanned CT image. This is the central point where the radiation beam passes. Because each mouse is of a different size, and the way each mouse is placed on the platform varies, a new CT scan was performed each time to ensure accuracy in selecting the region of irradiation.

After initial trials and optimisation studies, I decided to specifically target the left lung lobe. This was achieved using a fixed collimator of size 5 X 5mm. As seen from the sagittal perspective, the region targeted is specific to the left lung lobe and the remaining lobes are spared in this set-up (Figure 3.1c, right). Unlike most preclinical studies which utilise whole thorax irradiation as a model for lung radiotherapy, I decided to target a single lobe to increase specificity. In addition, the left lung lobe was selected as it is the solitary lobe on the left side of the mouse, as compared to the right side with 4 different lobes (Figure 3.1c, left). The SARRP is also equipped with a rotating collimator head, which allows for irradiation to be given in an arc instead of a single stationary beam. This mimics volumetric modulated arc therapy (VMAT), which is sometimes used in clinical lung radiotherapy to improve the efficiency of the radiation beam, and thus reduce treatment lengths. However, previous work has demonstrated that irradiating in an arc in this set-up resulted in the irradiation of non-target lung tissue. Thus, I decided to simplify the model by performing irradiation with a single stationary beam. Further technical details of the SARRP will be provided in the Materials and Methods. This irradiation setup will be used in subsequent experiments unless stated otherwise.

3.2.2 Immunophenotyping the response to targeted lung irradiation

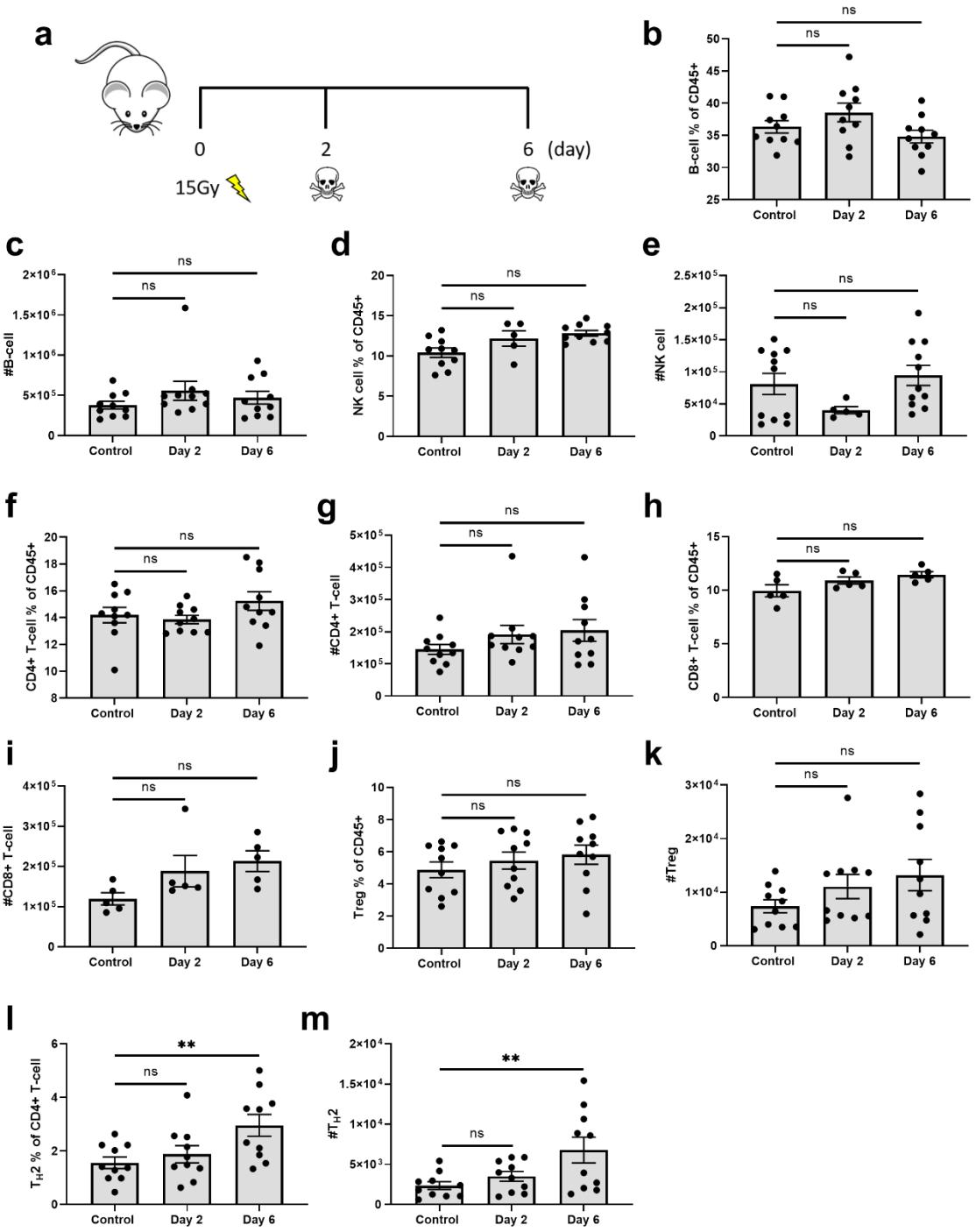

Figure 3.2 Lymphoid cell changes in response to targeted lung irradiation. (a) Mice were irradiated with 15Gy single dose irradiation and targeted left lung lobes were harvested 2 and 6 days post-irradiation. **(b-m)** Quantification of frequency and number of B-cells (n = 10, 10, 10), NK cells (n = 10, 5, 10), CD4+ T-cells (n = 10, 10, 10), CD8+ T-cells (n = 5, 5, 5), Tregs (n = 10, 10, 10) and T_H2 cells (n = 10, 10, 10) by flow cytometry. Bar graphs indicate the mean (± s.e.m) and data is combined of two independent experiments **(b-g, j-m)** or a single experiment **(h-i)**. Each data point represents a biological replicate. Statistical significance was calculated using one-way ANOVA and Dunnett's multiple comparison test, ns = not significant, **= $P \leq 0.01$.

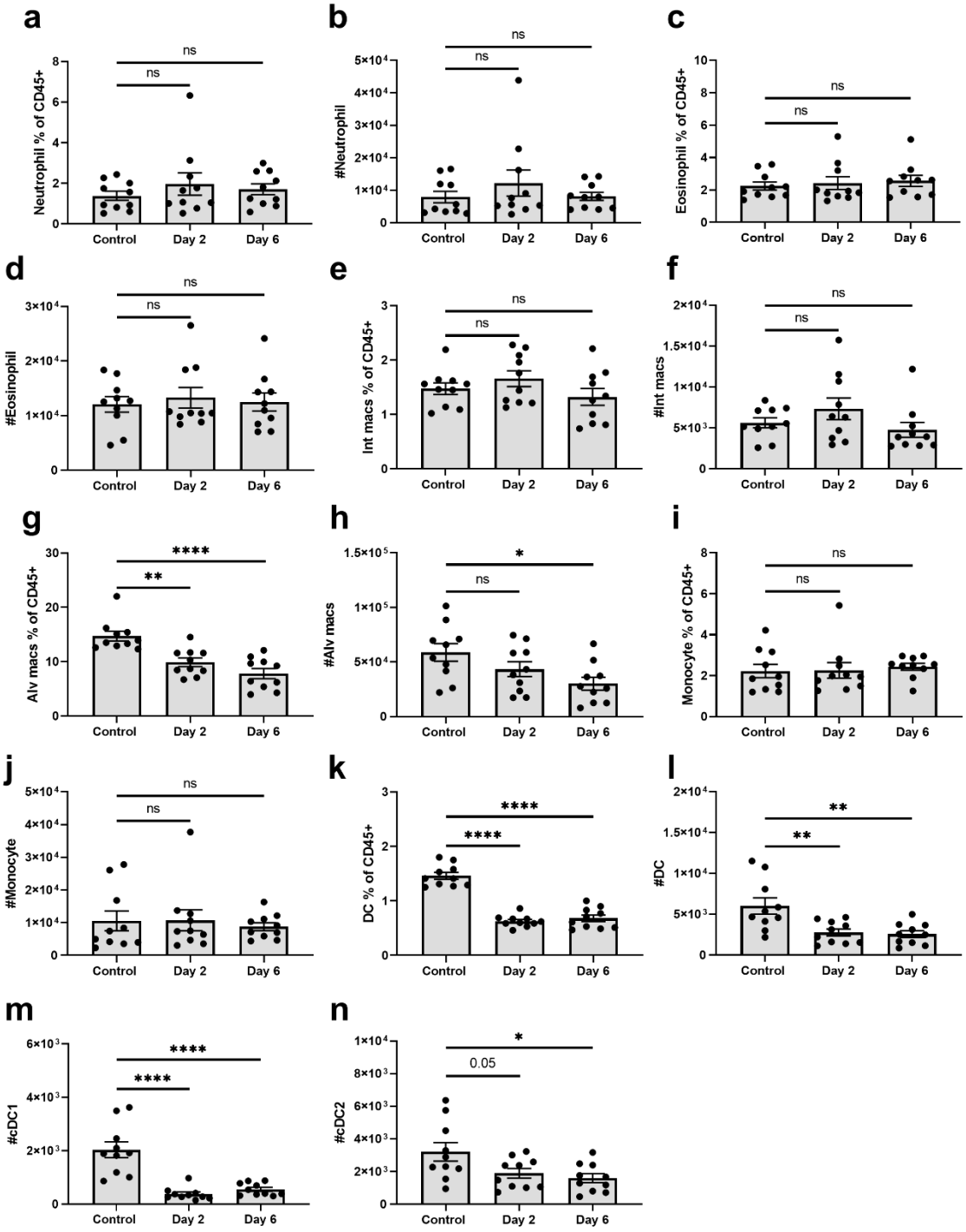

Figure 3.3 Myeloid cell changes in response to targeted lung irradiation. (a-n) Quantification of frequency and number of neutrophils, eosinophils, interstitial macrophages, alveolar macrophages, monocytes and dendritic cells by flow cytometry. **(a-n)** Bar graphs indicate the mean (± s.e.m) and n = 10 for each group and data is combined of two independent experiments. Each data point represents a biological replicate. Statistical significance was calculated using one-way ANOVA and Dunnett's multiple comparison test, ns = not significant, * = P ≤ 0.05, ** = P ≤ 0.01, *** = P ≤ 0.001, **** = P ≤ 0.0001.

I started with a single dose of 15Gy to the lung and monitored immune responses 2 and 6 days post-irradiation (Figure 3.2a). I hypothesised that these selected time points would encapsulate observable changes in both the innate and adaptive immune responses respectively, and I studied both myeloid and lymphoid cell populations at both time points using flow cytometry analysis. Myeloid and lymphoid flow cytometry panels previously described in Materials and Methods were used to quantify immune cell numbers of major immune cell populations.

Figure 3.2b-m demonstrates the changes in lymphoid cell populations, including B-cells, total CD4+ and CD8+ T-cells, NK cells, Tregs and CD4+ T_H2 cells. Immune cells were quantified as a frequency of total CD45+ leukocytes, as well as total cell numbers, and this will be used throughout the thesis. Interestingly, minimal changes in these lymphoid cell populations were observed. This was unexpected because radiotherapy is known to influence the immune microenvironment in tissues in different ways, including the depletion or recruitment of different immune cell types. Among these lymphoid cell populations studied, I only observed a significant increase in the frequency and number of T_H2 cells. Notably, this increase in T_H2 was only observed at 6 days post-irradiation, which is in line with the idea that adaptive immune responses induced by radiotherapy occur at later time points.

Figure 3.3 displays the changes in myeloid cell populations, specifically neutrophils, eosinophils, AMs, interstitial macrophages (IM), monocytes and DCs. Similar to the lymphoid compartment, most myeloid populations within the lung appear to remain stable after targeted irradiation. However, I observed the specific depletion of alveolar macrophages and both conventional DC1 and DC2 subsets (cDC). (Figure 3.3h-i, k-m). This decline was observed to occur rapidly, as both frequency and number of these cells were observed to fall as early as 2 days post-irradiation. The decline was observed to persist at 6 days post-irradiation. In all, I demonstrate that targeted radiotherapy to the left lobe leads to minimal changes in the overall lung immune microenvironment and that these changes were quantifiable by flow cytometry.

3.2.3 ILC2s are depleted and activated in response to targeted lung irradiation

With the establishment of the method of targeted irradiation, as well as validating the use of flow cytometry to quantify immune cell changes within the lung after irradiation, I focused on the response of ILC2s to targeted lung irradiation. A gating strategy was established within the lymphoid panel to identify this cell type (Figure 3.4). Live single and CD45+ cells were first identified. B-cells were subsequently excluded using B220, while T-cells and NK cells (including NK-like ILC1s) were

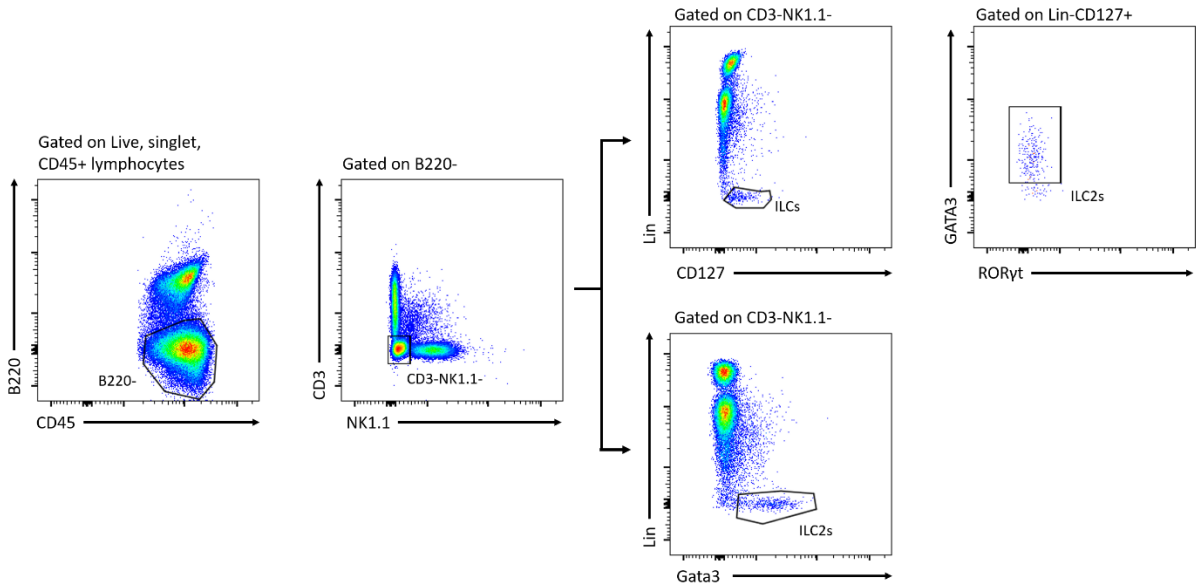

Figure 3.4 Quantifying lung ILC2s by flow cytometry analysis. ILC2s are initially gated on the CD45+B220-CD3-NK- subset, and further defined as Lin-CD127+Gata3+ cells (top). Alternatively, due to the absence of ILC3s within the lung, ILC2s can be gated directly as Lin-GATA3+ cells (bottom).

excluded using CD3 and NK1.1. Total ILCs, excluding ILC1s, were then defined as Lin- and CD127+ (Figure 3.4b, top). Lin- cells are immune cells negatively selected using a panel of several antibodies. These antibodies ruled out the presence of other cell types, including other lymphocytes, macrophages, granulocytes and erythrocytes. The total ILC population is also defined by IL-7R expression (H. Spits et al. 2013), which is necessary for their homeostatic maintenance and development. As the ILC1 population was previously excluded by NK1.1 expression, intracellular detection of GATA3 was used to identify ILC2s, and RORγt to identify ILC3s. Overall, ILC2s were defined as CD45+B220-CD3-NK1.1-Lin-CD127+GAT3A3+ cells. Notably, little to no ILC3S in the lungs were observed, as seen by the absence of RORγt cells. Moreover, I alternatively gated ILC2s as Lin-GATA3+ cells (Figure 3.4b, bottom) and observed that this gating strategy obtained similar numbers to the original gating strategy. This new simplified gating strategy will be used throughout the thesis for the identification of ILC2s.

Subsequently, I monitored ILC2 numbers in the experimental set-up shown in Figure 3.2a. With this gating strategy, a reduction in Lin-GATA3+ cells was observed (Figure 3.5a) and further quantification revealed a significant decline in both the frequency and number of ILC2s within the lung post-irradiation (Figure 3.5b-c). The decline in cell numbers was once again observed to occur as early as 2 days post-irradiation, which was similar to that observed for alveolar macrophages and DCs.

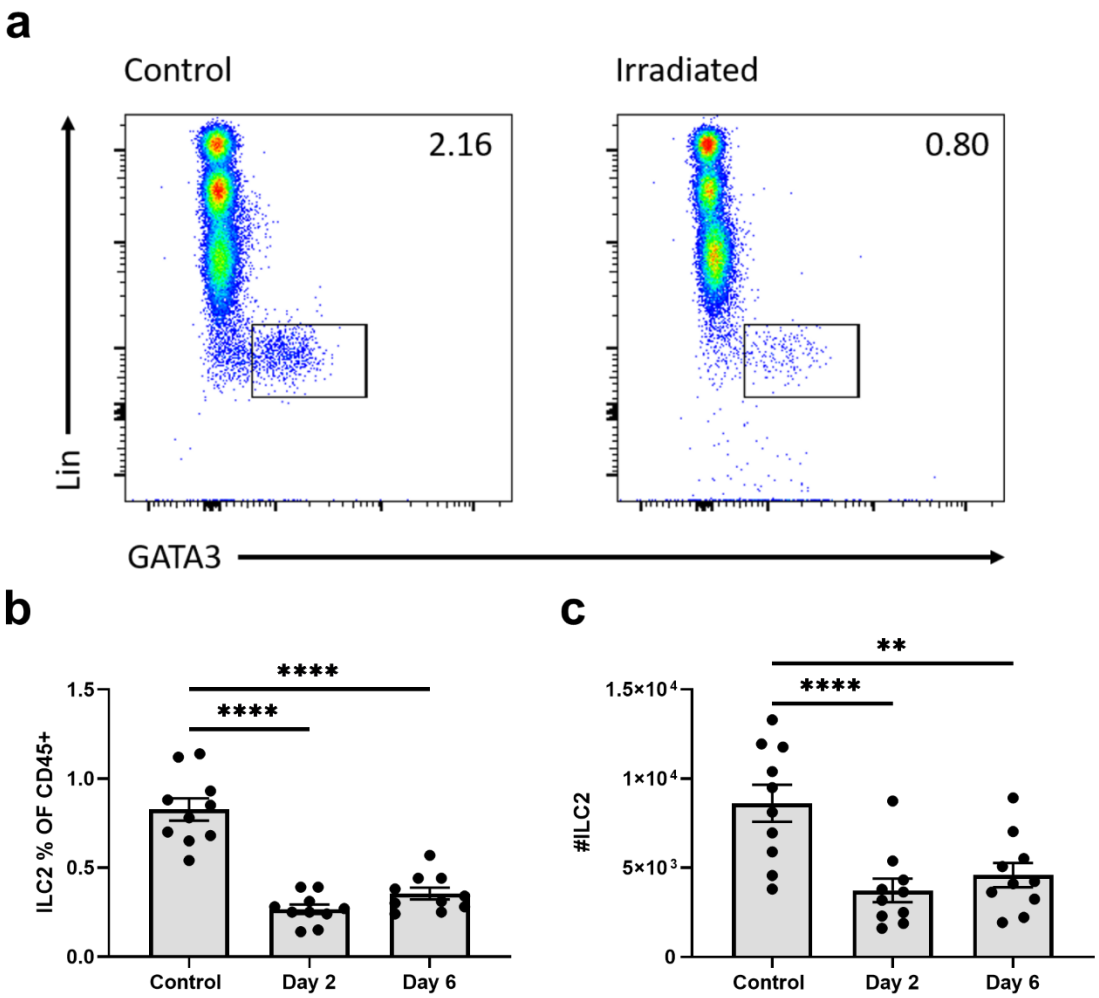

Figure 3.5 Targeted irradiation depletes lung ILC2s. **(a)** Representative gating demonstrating ILC2 numbers in control vs irradiated (Day 2) mice. **(b-c)** Quantification of frequency and number of ILC2s (n = 10 for each group). **(b-c)** Bar graphs indicate the mean (± s.e.m) and data is combined of two independent experiments. Each data point represents a biological replicate. Statistical significance was calculated using one-way ANOVA and Dunnett's multiple comparison test, ** = P ≤ 0.01, **** = P ≤ 0.0001.

Next, I investigated the activation status of ILC2. As discussed in the introduction, ILC2s are potent producers of Type 2 cytokines and express a number of cell surface receptors to regulate immune responses. One of these receptors is OX40L, and it has been shown that ILC2s upregulate OX40L in response to IL-33 in the context of Type 2 inflammation (Halim et al. 2018). As radiotherapy is known to induce cell death and release damage signals, possibly IL-33, I hypothesised that these signals could be picked up by ILC2s, thereby leading to their activation. Thus, I quantified OX40L expression by flow cytometry post-irradiation. Figure 3.6a-b demonstrates the gating strategy for OX40L on ILC2s, and a representative histogram of OX40L expression of ILC2s. A small but significant upregulation of OX40L on a fraction of ILC2s after radiotherapy was observed, and this was reflected by an increase in both the frequency and number of OX40L+ ILC2s (Figure 3.6c-d). This increase was observed as early as 2 days post-irradiation, which was similar to a time point previously reported after allergen-induced airway inflammation (Halim et al. 2018). Finally, ILC2 activation is typically

associated with an increase in the production of Type 2 cytokines, including IL-5 and IL-13. Thus I assessed Type 2 cytokine production, focusing on IL-13. Interestingly, no change in IL-13 production was observed (Figure 3.6e) in ILC2s after targeted lung radiotherapy and with restimulation of cells with PMA and ionomycin, suggesting that the increase in OX40L does not correlate with Type 2 cytokine production.

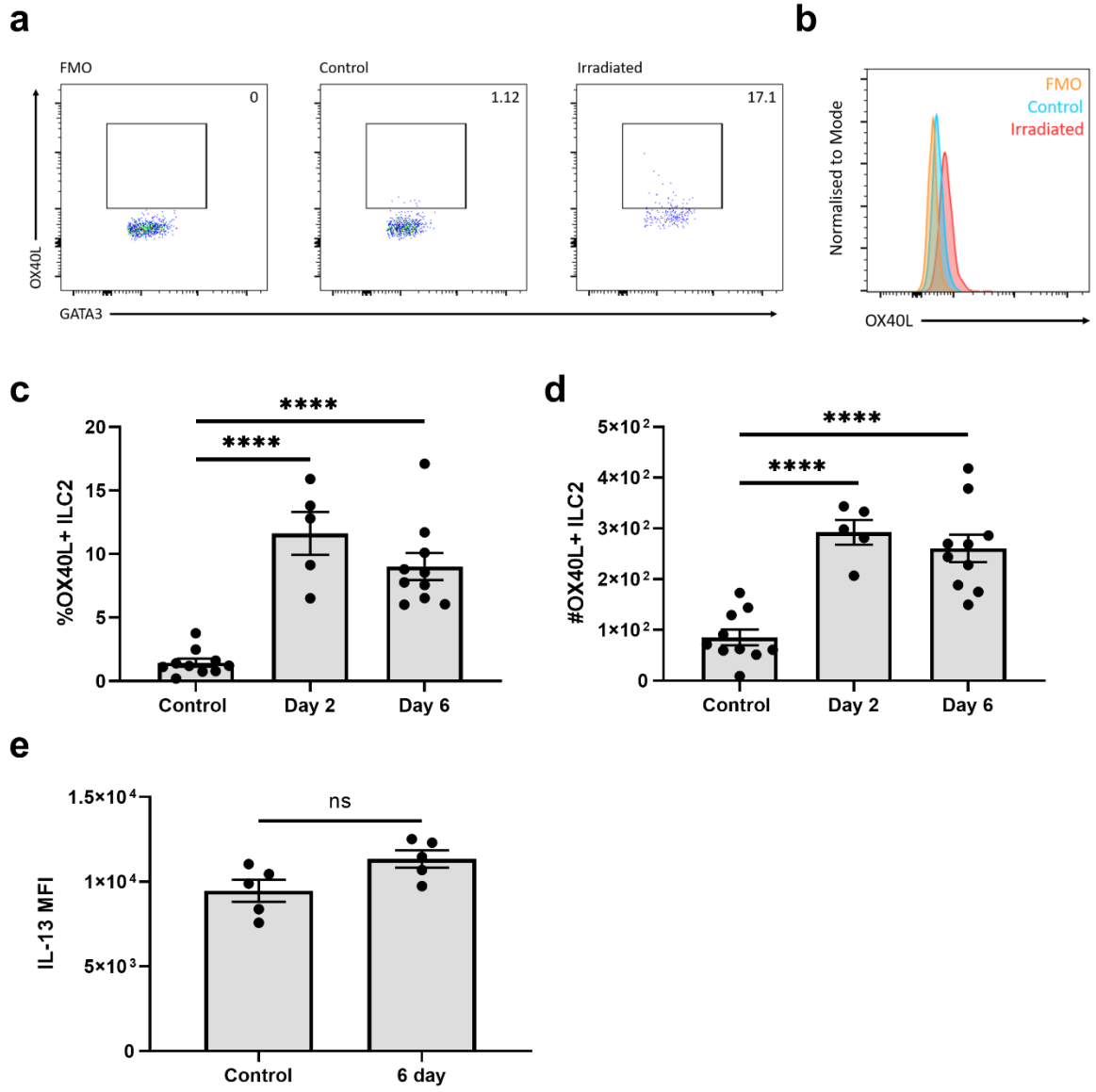

Figure 3.6 ILC2s upregulate OX40L in response to targeted lung irradiation. **(a)** Representative gating demonstrating the percentage of OX40L+ ILC2s in control and irradiated (Day 2) mice. **(b)** Representative histogram of OX40L in ILC2s in control and irradiated (Day 2) mice. **(c)** Quantification of frequency of OX40L+ ILC2 (n = 5, 10, 5). **(d)** Quantification of number of OX40L+ ILC2 (n = 5, 10, 5). **(e)** Quantification of MFI of IL-13 on ILC2s after restimulation for 3 hours with PMA + ionomycin (n = 5, 5). **(c-e)** Bar graphs indicate the mean (± s.e.m). Data is combined of two independent experiments **(c-d)** or a single experiment **(e)**. Each data point represents a biological replicate. Statistical significance was calculated was calculated using one-way ANOVA and Dunnett's multiple comparison test, ** = P ≤ 0.01, **** = P ≤ 0.0001 **(c-d)** or unpaired two-tailed t-test, ns = not significant **(e)**.

3.2.4 Monitoring short-term and long-term dynamics of ILC2s upon targeted irradiation

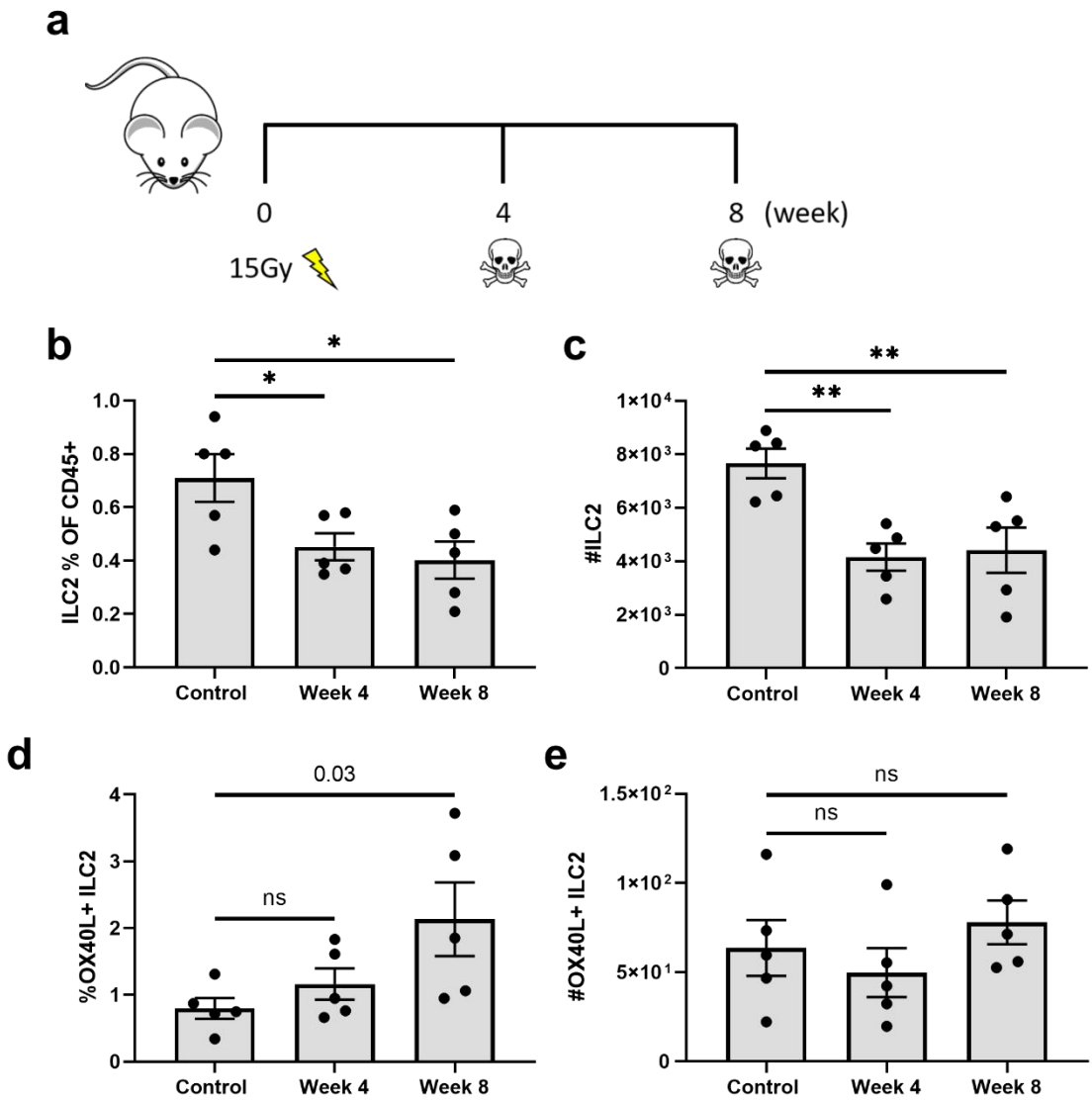

Figure 3.7 ILC2s remain depleted up to 8 weeks after targeted irradiation. (a) Mice were irradiated with 15Gy single dose irradiation and targeted left lung lobes were harvested 4 and 8 weeks post-irradiation. **(b-c)** Quantification of frequency and number of ILC2s. **(d-e)** Quantification of frequency and number of OX40L+ ILC2s**. (b-e)** Bar graphs indicate the mean (± s.e.m) and n = 5 for each group, and data is representative of a single experiment. Each data point represents a biological replicate. Statistical significance was calculated using one-way ANOVA and Dunnett's multiple comparison test, ns = not significant, * = $P \leq 0.05$, ** = $P \leq 0.01$.

The long-term dynamics of cell response to radiotherapy does not necessarily reflect what is observed in the short term. Indeed, while depletion of some radiosensitive cells is observed in the short-term acute response to radiotherapy, certain cell types are observed to rebound and exceed baseline levels in the long term after radiotherapy (Meziani et al. 2018). Hence, upon observing the short-term depletion and activation of ILC2, I sought to monitor ILC2 responses in the longer term. To that end, I quantified ILC2 numbers and OX40L expression 4 and 8 weeks post-irradiation (Figure 3.7a). Interestingly, the frequency and number of ILC2 numbers remained lower than non-irradiated

controls even at the 8-week time post-irradiation (Figure 3.7b-c), suggesting that ILC2s were not restored to naïve lung numbers even after the 8-week time point. Conversely, OX40L expression of ILC2s returned to baseline levels, suggesting transient activation of ILC2s in response to targeted lung radiotherapy (Figure 3.7d-e).

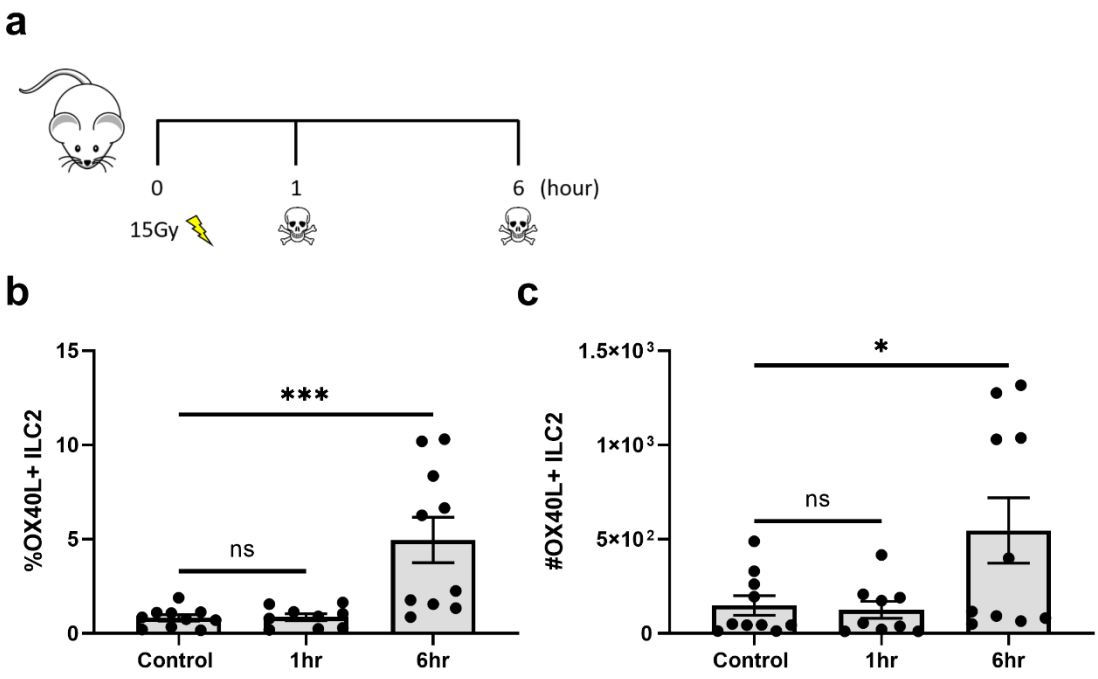

Figure 3.8 ILC2s upregulate OX40L rapidly in response to targeted lung irradiation. (a) Mice were irradiated with 15Gy single dose irradiation and targeted left lung lobes were harvested 1 and 6 hours post-irradiation. **(b-c)** Quantification of frequency and number of OX40L+ ILC2s. **(b-c)** Bar graphs indicate the mean (± s.e.m) and n = 10 for each group. Each data point represents a biological replicate. Data is combined of two independent experiments and statistical significance was calculated using one-way ANOVA and Dunnett's multiple comparison test, ns = not significant, * = P ≤ 0.05, *** = P ≤ 0.001.

Finally, I wondered if ILC2 activation could happen at even earlier time points. Hence, I monitored the kinetics of OX40L expression in ILC2s by radiotherapy at earlier time points 1 and 6 hours post-irradiation. Mice were irradiated and OX40L expression was monitored 1 and 6 hours post-irradiation (Figure 3.8a). Indeed, the upregulation of OX40L expression occurred as early as 6 hours post-irradiation, highlighting the rapid response of ILC2s to targeted lung radiotherapy. In all, radiotherapy results in a decline in ILC2 numbers which persists in the long term, while ILC2 expression of OX40L is a rapid but transient response to radiotherapy.

3.2.5 Radiotherapy-induced OX40L expression on ILC2s is dose-dependent

So far, the response of ILC2s to targeted lung irradiation has only been monitored in a single regimen of 15Gy. Notably, 15Gy is typically considered to be "high-dose". As discussed, several aspects have to be taken into account to determine the dose administered during radiotherapy. The list includes, but is not limited to, the toxicity of the given dose, the abscopal effect, and the

immunological profile of the tumour (i.e. immune “hot” or “cold” tumours) (Buchwald et al. 2018; Demaria et al. 2021). Notably, different immune cells respond differently to radiotherapy, which

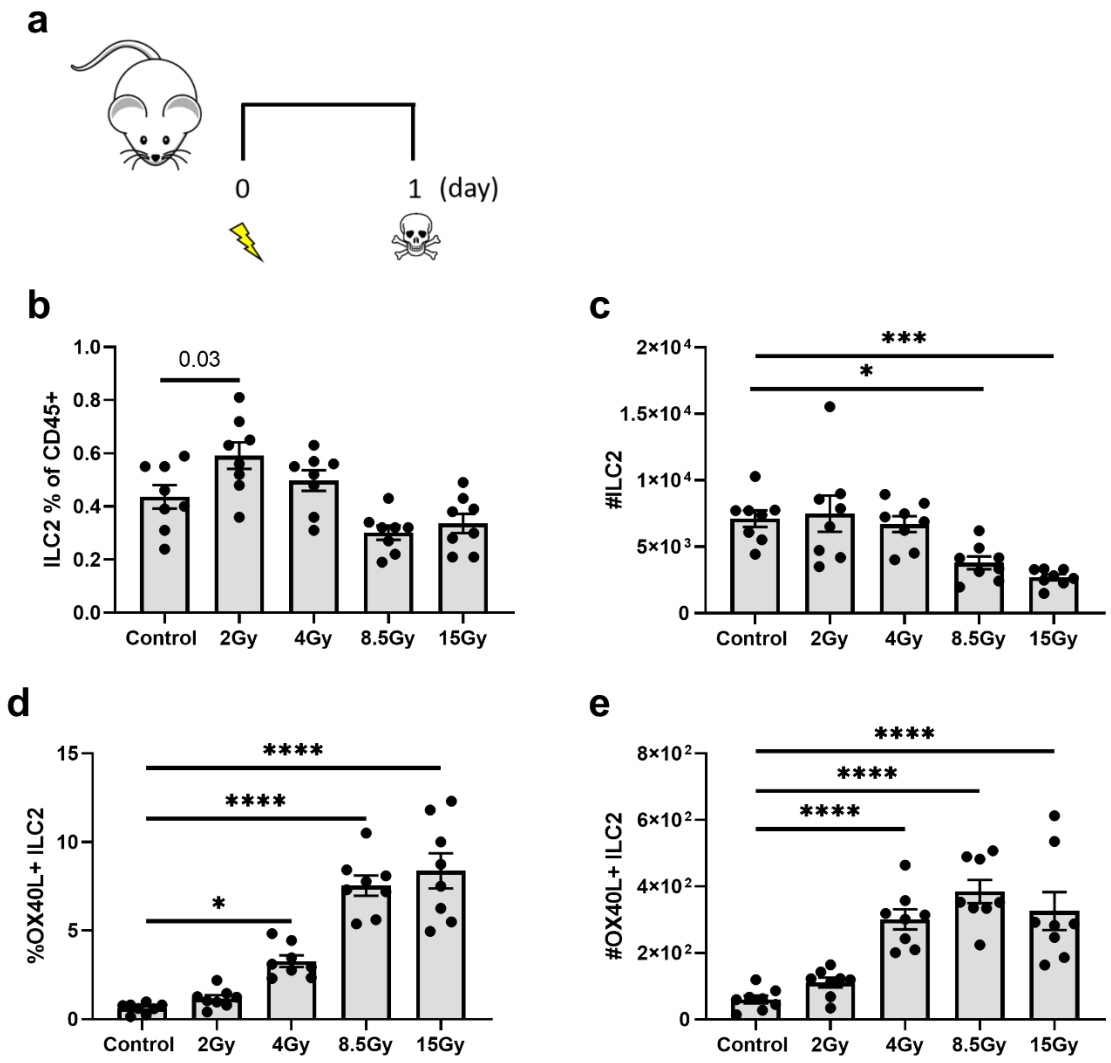

Figure 3.9 ILC2s upregulate OX40L in a dose-dependent manner. (a) Mice were irradiated with a single dose of irradiation at varying doses (2, 4, 8.5 or 15Gy) and irradiated left lung lobes were harvested 1 day post-irradiation. **(b-c)** Quantification of frequency and number of ILC2s. **(d-e)** Quantification of frequency and number of OX40L+ ILC2s. **(b-e)** Bar graphs indicate the mean (± s.e.m) and n = 8 for each group and data is combined of two independent experiments. Each data point represents a biological replicate. Statistical significance was calculated using one-way ANOVA and Dunnett’s multiple comparison, * = P ≤ 0.05, *** = P ≤ 0.001, * = P ≤ 0.0001.

could lead to differences in their subsequent function. For instance, depending on the administered dose of radiotherapy, macrophages respond differently to produce different cytokines (Wu et al. 2017). This is also the case for adaptive lymphocytes, where different radiation doses lead to differences in adaptive CD4+ T-cell response, which also later influence radiation-induced lung injury. (Wirsdorfer and Jendrossek 2016). Finally, the dose of radiotherapy administered also influences the expression of certain genes, which influences the outcome of radiation treatment. The most notable example is the DNA exonuclease Trex1 (Vanpouille-Box et al. 2017), which is

induced by high-dose radiotherapy and leads to attenuated adaptive immune response and thus, worsened cancer prognosis.

Thus, I questioned if the dose of radiotherapy administered differentially influenced ILC2 numbers and OX40L expression. To that end, I irradiated mice at different doses and monitored the response of ILC2 1 day post-irradiation (Figure 3.9a), where OX40L expression on ILC2s is expected. ILC2 numbers were observed to decrease in a dose-dependent manner. The frequency and number of ILC2s were relatively stable compared to non-irradiated controls up to 4Gy. However, a decline in ILC2 numbers was observed at 8.5Gy and 15Gy (Figure 3.9b-c). This suggests that a threshold dose of around 4Gy is necessary for the depletion of ILC2s. A significant upregulation of OX40L was also observed from 4Gy irradiation. Notably, a doubling in the frequency of OX40L+ ILC2 was observed at higher doses of 8.5Gy and 15Gy compared to 4Gy (Figure 3.9d), highlighting that OX40L expression on ILC2s is dose-dependent. In terms of cell numbers, the number of OX40L+ cells was observed to be similar at all 3 doses of 4, 8.5 and 15Gy. This is attributed to the corresponding decrease in ILC2 cell numbers alongside increased OX40L expression at higher doses of irradiation. In all, an intermediate dose of irradiation at 8.5Gy gave significant ILC2 activation compared to lower dose irradiation doses at 4Gy and below, whilst still preserving higher number of ILC2s compared to irradiation at a higher dose of 15Gy.

3.2.6 OX40L expression on ILC2s is partially dependent on IL-33

Next, I sought to investigate how radiotherapy promotes OX40L expression on ILC2s. Previously, Halim and colleagues have shown that intranasal administration of IL-33 to mice induced OX40L upregulation on lung ILC2s (Halim et al. 2018). Thus, I sought to investigate the importance of IL-33 in radiotherapy-induced upregulation of OX40L on ILC2. To that end, IL-33-deficient mice (*Il33*$^{cit/cit}$) and heterozygous controls (*Il33*$^{cit/+}$) (Hardman, Panova, and McKenzie 2013) were used. *Il33*$^{cit/+}$ mice harbour the fluorescent reporter citrine inserted downstream of the ATG start codon of the *Il33* locus, thereby allowing it to serve as a reporter for IL-33 expression. Notably, homozygous carriers of this allele are IL-33-deficient as the citrine reporter present in both alleles reporter disrupts IL-33 expression.

Il33$^{cit/cit}$ mice were irradiated alongside control *Il33*$^{cit/+}$ mice and OX40L expression on ILC2s was monitored (Figure 3.10a). As expected, no OX40L expression was detected on lung ILC2s in the absence of irradiation, regardless of the genotype of the mice. While there was an induction of OX40L expression in *Il33*$^{cit/+}$ controls, this was significantly reduced in *Il33*$^{cit/cit}$ mice (Figure 3.10b-c), suggesting that IL-33 contributes to radiotherapy-induced OX40L expression. Notably, the expression

of OX40L in *Il33*$^{cit/cit}$ was not reduced to baseline levels, suggesting an IL-33-independent mechanism of OX40L expression during radiotherapy.

To further validate the role of IL-33 in radiotherapy-induced OX40L expression, an IL-33 trap (IL-33R-Fc) that has been shown to neutralise allergen-mediated airway inflammation (Schuijs et al. 2020) was utilised. This trap functions by inhibiting IL-33 signalling through blockade of the IL-33 receptor. Mice were treated with the IL-33 trap by intranasal administration alongside targeted irradiation, and OX40L expression on ILC2s was monitored (Figure 3.10d). Unexpectedly, no difference in OX40L expression was observed after irradiation in the presence of the trap (Figure 3.10e-f). This could be explained by the inefficiency of the trap, or a cell-intrinsic role of IL-33 in mediating OX40L expression. Thus, the induction of OX40L expression on ILC2s by radiotherapy is in part IL-33-dependent.

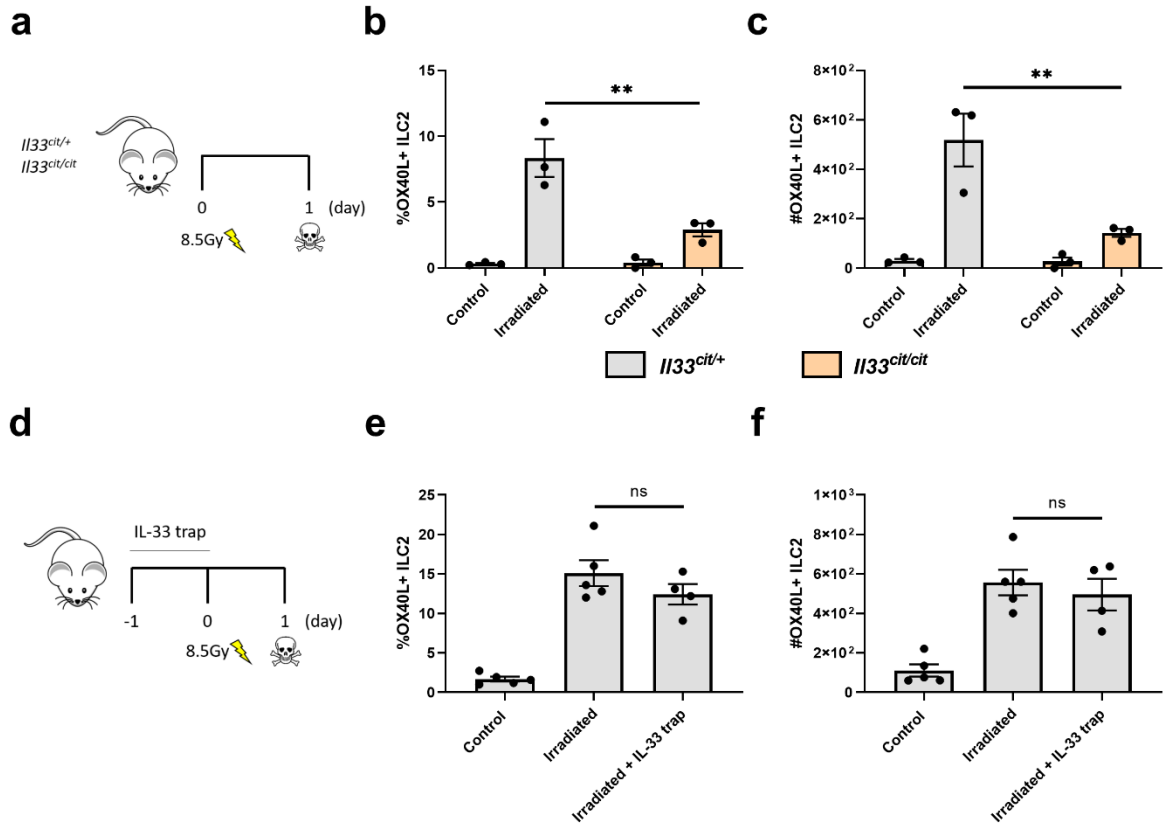

Figure 3.10 OX40L upregulation on ILC2s is partially dependent on IL-33. (a) *Il33*$^{cit/+}$ control and *Il33*$^{cit/cit}$ mice were irradiated with 8.5Gy single dose irradiation and irradiated left lung lobes were harvested 1 day post-irradiation. **(b)** Quantification of frequency of OX40L+ ILC2s (n = 3, 3, 3, 3). **(c)** Quantification of number of OX40L+ ILC2s (n = 3, 3, 3, 3). **(d)** Mice were treated with IL-33 trap alongside 8.5Gy single dose irradiation and irradiated left lobes were harvested 1 day post-irradiation. **(e)** Quantification of frequency of OX40L+ ILC2 (n = 5, 5, 4). **(f)** Quantification of number of OX40L+ ILC2s (n = 5, 5, 4). **(b-c, e-f)** Bar graphs indicate the mean (± s.e.m) and data is representative of a single experiment. Each data point represents a biological replicate. Statistical significance was calculated using two-way ANOVA and Sidak's comparison test, ns = not significant **(b-c)** and one-way ANOVA and Tukey's multiple comparison test, ns = not significant **(e-f)**.

3.2.7 Investigating a potential role of ILC2s in a model of radiotherapy-induced lung fibrosis

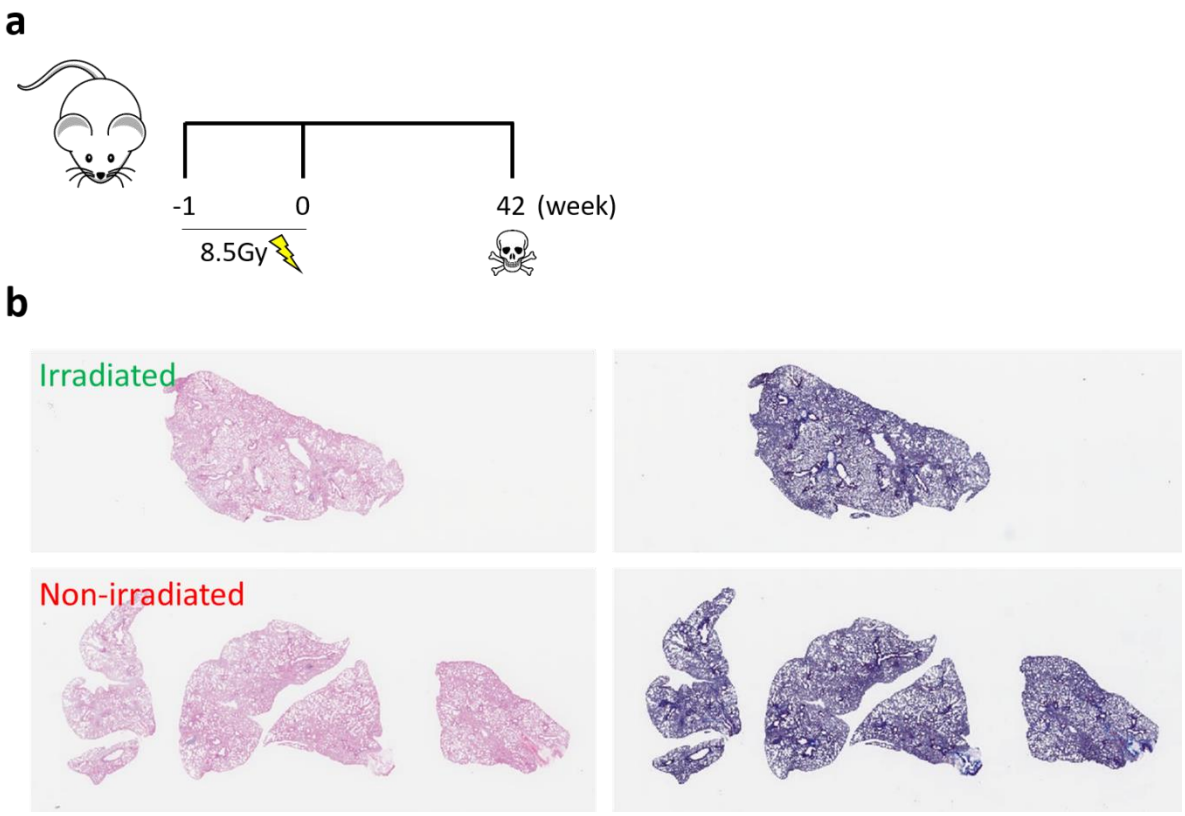

Figure 3.11 A fractionated 8.5Gy X 2 regimen does not induce lung fibrosis. (a) Mice were irradiated twice with 8.5Gy over 2 weeks, and lungs were harvested 42 weeks post-irradiation. **(b)** Representative H&E (left) and Masson Trichrome (MT) (right) sections from irradiated mice.

The observation of OX40L expression on ILC2s in response to targeted irradiation was interesting, as it suggests that ILC2s are activated in response to radiotherapy, and can potentially contribute to radiation-induced outcomes, like pneumonitis and fibrosis. As previously discussed, Type 2 immunity is associated with radiation-induced fibrosis, and lung ILC2s could potentially contribute to this response. Indeed, literature has demonstrated the supporting role of ILC2s in the bleomycin model of lung fibrosis. In this model, bleomycin-induced ILC2 activation and Type 2 cytokine production promote fibrotic progression (Li et al. 2014). More recently, another paper highlighted a mechanism of ILC2-mediated lung fibrosis and demonstrated that a TGFβ1–Nrp1 axis modulates and enhances ILC2 function via the upregulation of the IL-33 receptor ST2 (Zhang et al. 2022). Furthermore, apart from the lungs, ILC2s in other tissues have also demonstrated their ability to promote fibrosis and wound healing responses (Laurent et al. 2021). However, it remains to be seen if ILC2s could contribute to radiation-induced lung fibrosis.

I first set out to establish a model of lung fibrosis by targeted lung irradiation using the SARRP. A fractionated regimen of 8.5Gy X 2 was administered 1 week apart, and lungs were harvested 42

weeks (6 months) post-irradiation (Figure 3.11a). While the administered dose is lower compared to the typically high doses usually given to establish lung fibrosis, lower doses have also been observed to successfully induce fibrosis (Chen et al. 2016). This is in part due to increased susceptibility of the C57BL/6 strain to fibrosis (Jackson, Vujaskovic, and Down 2011). Nevertheless, I failed to observe clear signs of fibrosis in the targeted left lobe by H&E or Masson's Trichrome staining with this regimen (Figure 3.11b left and right respectively). Thus, further work is needed to establish a working model of radiation-induced lung fibrosis with the SARRP before the role of ILC2s could be studied.

3.3 Summary

While activation of immune responses in radiotherapy in the treatment of cancer is now increasingly appreciated, less is known about the immune response induced by radiotherapy in non-tumour naïve tissue. Furthermore, ILC2s are a more recently discovered cell type, and their response to targeted lung radiotherapy has yet to be to be investigated. In this chapter, I focused on the response of ILC2s to targeted irradiation in the naïve lung.

Using the SARRP, I first established a model of targeted lung irradiation. In this model, the lung left lobe was specifically targeted. I demonstrated that changes in major lung immune populations could be monitored by flow cytometry. Focusing on ILC2s, I observed that ILC2s were depleted at early time points after radiotherapy, and their numbers remained low even in the long term. Radiotherapy also induced expression of OX40L on ILC2, even though this expression was transient. ILC2 expression of OX40L was observed to occur in a dose-dependent manner, and radiotherapy-induced OX40L expression on ILC2s was partially dependent on the cytokine IL-33. Finally, to study the potential role of ILC2s in radiation-induced lung fibrosis, I tried to establish a model of lung fibrosis using the SARRP, but a fractionated regimen of 8.5Gy X 2 did not result in lung fibrosis 6 months post-irradiation.

Chapter 4: Dissecting the role of ILC2s and immune system in radiotherapy-mediated anti-tumour response in lung cancer

4.1 Introduction

Having looked at how targeted lung radiotherapy modulates the immune microenvironment in the healthy lung, specifically ILC2s, I now focus on immune modulation by radiotherapy in the context of lung cancer. Early preclinical mouse models studying the immune response in radiotherapy have mostly utilised subcutaneous models, in part due to the ease of administering radiotherapy and monitoring tumour progression. The main limitation of such models is that they do not mimic physiological conditions of the tumour, and thereby do not represent the actual microenvironment in which tumour cells reside.

As previously discussed, preclinical radiation treatment platforms are now equipped with dual CT scan and irradiation function, allowing for a better selection of specific target tissues. Indeed, this is subsequently accompanied by a greater volume of literature studying the anti-tumour response to targeted irradiation in the context of lung cancer (Herter-Sprie et al. 2014; Du et al. 2016; Liu et al. 2019). Despite this, most papers focus predominantly on the treatment outcomes induced by radiotherapy, whereas the immune responses behind these treatment outcomes is usually overlooked. Furthermore, little work has been done to immunophenotype myeloid and lymphoid populations within the lung tumour environment post-irradiation.

I have established in the previous chapter a method of targeted irradiation within the left lung lobe, and also demonstrate the use of flow cytometry to monitor changes in major immune populations within the lung post-irradiation. Evidence of ILC2 activation following targeted irradiation was seen in the previous chapter, suggesting that ILC2s could potentially contribute to the immune response against cancer upon radiotherapy.

In this chapter, I utilise this model of targeted irradiation in the B16F10-OVA model of lung metastasis to study the role of ILC2s and the broader immune system in radiotherapy-induced anti-tumour immunity. Firstly, I aimed to immunophenotype the immune response to radiotherapy in a metastatic model of lung cancer. Next, I aimed to study the contribution of ILC2s and the broader immune system to anti-tumour responses induced by radiotherapy. Finally, I sought to investigate the mechanisms underlying radiotherapy-induced anti-tumour immunity.

4.2 Results

4.2.1 ILC2s are enriched in the lung microenvironment in early stage B16F10 lung metastasis

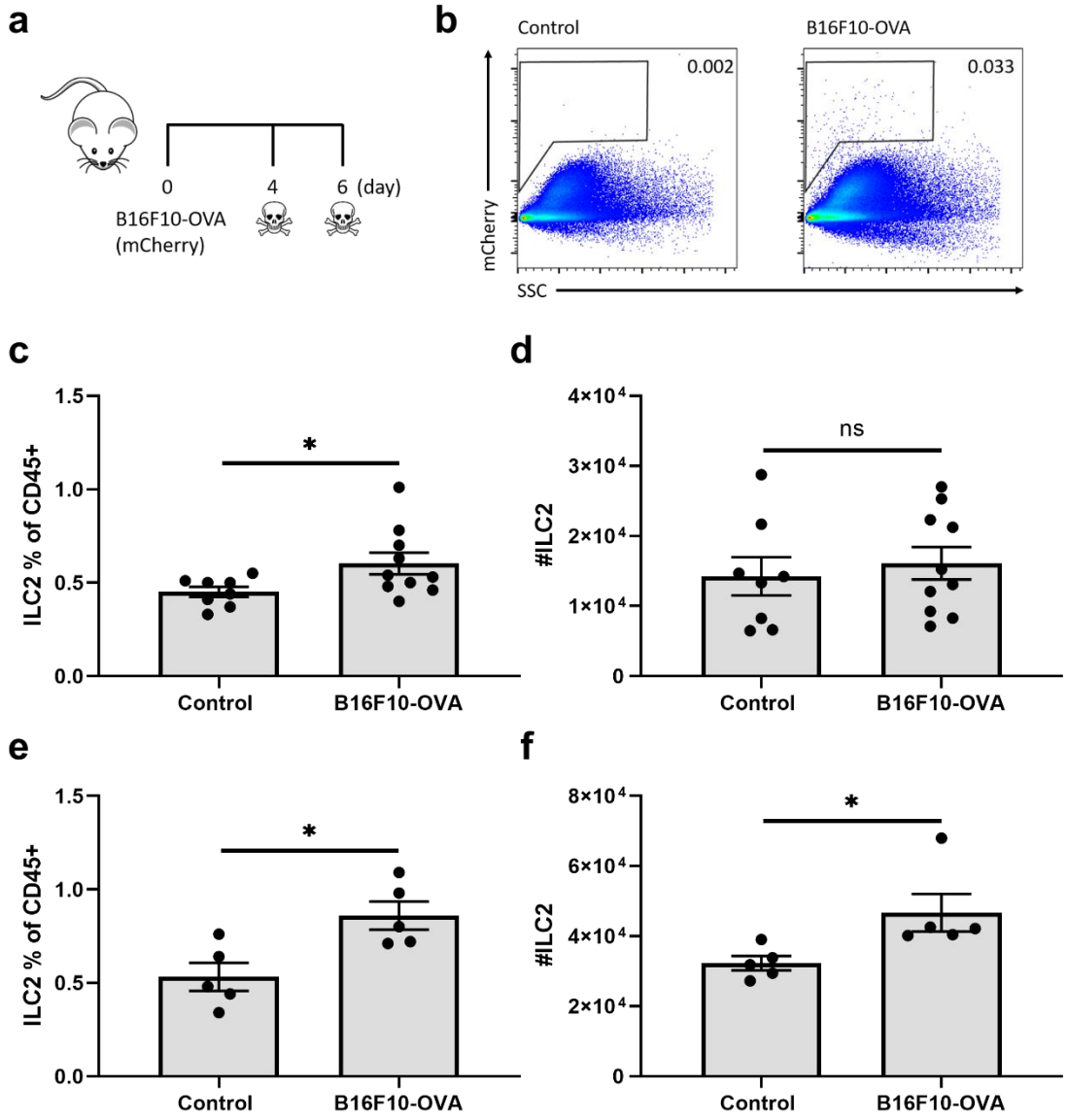

Figure 4.1 ILC2s are enriched within the lung microenvironment in early stage B16F10 lung metastasis. (a) Mice were injected with 1 X 10^5 B16F10-OVA cells intravenously and lungs were harvested 4 and 6 days post-injection. **(b)** Representative gating showing B16F10-OVA cells within the lung microenvironment 4 days post-injection. **(c)** Quantification of frequency of ILC2s 4 days post-injection (n = 4, 5). **(d)** Quantification of number of ILC2s 4 days post-injection (n = 4, 5). **(e-f)** Quantification of frequency and number of ILC2s 6 days post-injection (n =5 for each group). **(c-f)** Bar graphs indicate the mean (± s.e.m) and data is combined of two independent experiments **(c-d)** or a single experiment **(e-f)**. Each data point represents a biological replicate. Statistical significance was calculated using unpaired two-tailed t-test, ns = not significant, * = P ≤ 0.05.

I first sought to establish a lung cancer model to study radiotherapy-induced anti-tumour immune responses. For this, I decided to use the B16F10-OVA model of lung metastasis. While this tumour cell line has been extensively characterised in many studies, there is limited literature studying the role of radiotherapy in the lung metastatic cancer setting. Notably, our lab previously used this cell line to investigate the role of lung ILC2s in lung metastasis formation, although not in the context of radiotherapy (Schuijs et al. 2020). In this model, tumour cells are injected into the tail vein of mice, which leads to the subsequent establishment of metastatic lung tumours as circulating tumour cells seed in the lung microenvironment.

We have previously established in this model that tumour cells rapidly seed in the lung after tumour injection, as cells were observed to be present in the lung less than an hour post-tumour injection (Schuijs et al. 2020). Nevertheless, to avoid irradiation of the pre-metastatic niche, which has been shown to influence the seeding of tumour cells in the lung (Nolan et al. 2022), I sought to confirm the presence of tumour cells within the lung microenvironment at early time points. To that end, I injected B16F10-OVA cells into mice and harvested lungs 4 or 6 days post-injection (Figure 4.1a). Notably, the B16F10-OVA cells were tagged with a mCherry construct, allowing their detection by flow cytometry. As seen in Figure 4.1b, mCherry+ B16F10-OVA cells were present in the lung 4 days post-transfer, confirming that these tumour cells seed in the lung at early time points and that the 4-day time point post-tumour injection is an appropriate time point to irradiate the lung.

The lab has previously demonstrated the accretion of ILC2s in the context of early-stage primary lung cancer (unpublished data), suggesting that ILC2s could contribute to the early stages of lung cancer development. Hence, I questioned if ILC2s also accumulated in early metastatic lung cancer and probed the presence of ILC2s at both the 4 and 6-day time point post-tumour injection (Figure 4.1a). An increase in the percentage of ILC2s was observed at 4 days post-injection, even though this was not accompanied by an increase in cell numbers (Figure 4.1c-d). However, a more apparent increase in both the percentage and number of ILC2s was observed 6 days post-injection (Figure 4.1e-f). Overall, this highlights that the presence of tumour cells within the lung microenvironment is accompanied by a small but significant increase in the ILC2 population. Hence, the irradiation of tumour-bearing mice in subsequent experiments was done at relatively early time points, where I postulated that the local activation (see previous chapter) and expansion of ILC2s may influence radiotherapy-mediated anti-tumour responses within the lung tumour microenvironment.

4.2.2 Fractionated radiotherapy induces anti-tumour effect in the B16F10 model of lung metastasis

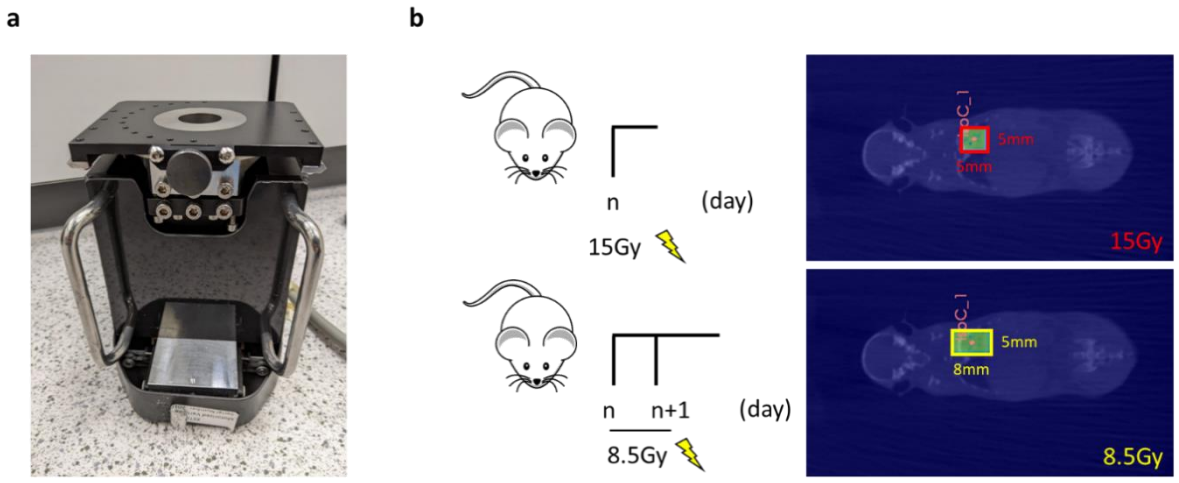

Figure 4.2 A modified lung irradiation setup to study the effectiveness of targeted lung radiotherapy. (a) A variable collimator was used (instead of a fixed collimator) to increase the targeted region of the lung. **(b)** A new dose of 8.5Gy was targeted to a larger area of the left lobe with the variable collimator adjusted to a size of 8 X 5mm (bottom) compared to the previous 5 X 5mm fixed collimator (top). A fractionated regimen of 8.5Gy is given twice (8.5Gy X 2)

A fixed collimator of size 5 X 5mm was used in the previous chapter to target the left lung. While the use of this collimator has allowed us to target the left lung to a sufficient depth to observe immune changes induced by targeted irradiation of the healthy lung, I decided to increase the surface area of targeted irradiation to target as much of the left lung as possible. To achieve this, a variable collimator was utilised (Figure 4.2a). Unlike the fixed collimator, which only allows a single standardised area to be irradiated (i.e 5 X 5mm), the variable collimator is adjustable and allows for flexibility over the area of irradiation. The area of irradiation was increased from the initial 5 X 5mm to 8 X 5mm length-wise (Figure 4.2b), which ensured that the non-targeted right lobes remain spared.

Furthermore, the irradiation regimen was altered to mimic radiation regimens used in the clinical setting. Previous experiments have mainly utilised a single dose of 15Gy. However, fractionated regimens and split-dose radiotherapy are typically more effective (Bezjak et al. 2002) and accompanied by fewer side effects (Cross et al. 2004). Hence, a fractionated regimen of 8.5Gy X 2 was selected (Figure 4.2b) and this regimen has been utilised in the clinic with minimal side effects (Cross et al. 2004). Furthermore, the utilised regimen is a form of palliative treatment intended to treat the symptoms of late stage or metastatic cancer. Hence, this regimen is more suited to this model of metastatic lung cancer. Notably, this regimen has also been previously adapted in other preclinical mouse studies studying anti-tumour responses in the context of the lung (Herter-Sprie et al. 2014), and no significant issues regarding unintended side effects were reported. Similar to the

15Gy single dose regimen, no significant health concerns nor clinical signs was observed, suggesting that this new regimen was safe for subsequent experiments.

The effectiveness of this new irradiation regimen to induce anti-tumour responses was studied in the B16F10 model of lung metastasis. To that end, irradiation was performed 4 and 5 days post-injection of tumour cells (Figure 4.3a). As previously shown, this time point corresponds to an increase in the frequency of ILC2 within the lung tumour microenvironment. Lung tissues were harvested on Day 18, which corresponds to the time point where mice typically succumb to lung metastasis based on initial optimisation experiments. Lung tumour burden in the irradiated left lobe was compared to non-irradiated right lobes. Importantly, the post-caval lobe was excluded from the analysis, as this lobe is typically present around the central region of the chest cavity and partially irradiated with this regimen. Tumour burden in the irradiated left lobe was observed to be significantly lower compared to non-irradiated right lobes (Figure 4.3b top) by visual qualification of the number of lung metastatic nodules. Tumour-bearing lungs were also sectioned and Ki67 staining was performed to detect proliferating tumour cells (Figure 4.3b bottom). A significantly lower tumour burden was also observed in the irradiated left lobe compared to non-irradiated right lobes using this approach. Thus, a fractionated 8.5Gy X 2 regimen induces anti-tumour responses in the B16F10-OVA model of lung metastasis.

To quantify the effectiveness of this irradiation regimen, a ratio of the measured metric between the irradiated left lobe to the non-irradiated right lobes was obtained. This allows for the non-irradiated lobes to function as an internal control. Two different metrics were utilised, namely the number of metastatic nodules, and the percentage tumour area as quantified by Ki67 staining. All visible surface lung metastatic nodules were counted visually, while the percentage tumour area was defined as the percentage of Ki67 staining to the total lung area as quantified by HALO analysis (see Materials and Methods). The ratio of lung metastatic nodules and percentage Ki67 staining are henceforth abbreviated the met ratio and tumour area ratio respectively. As seen in Figure 4.3c-d, irradiated tumour-bearing mice demonstrated a lower met ratio and tumour area ratio. This was expected given that radiotherapy decreases tumour burden in the targeted left lobe, thereby leading to the reduction in both ratios.

A slightly modified irradiation regimen was also utilised and the effectiveness of this regimen was evaluated. In this regimen, two fractions of 8.5Gy were administered a week apart (Figure 4.3e) and a similar reduction in tumour burden was observed (Figure 4.3f). Met ratios and tumour area ratios were quantified (Figure 4.3g-h), and a similar reduction in both ratios was observed. In all, both irradiation regimens demonstrated significant anti-tumour immunity in the B16F10-OVA model of

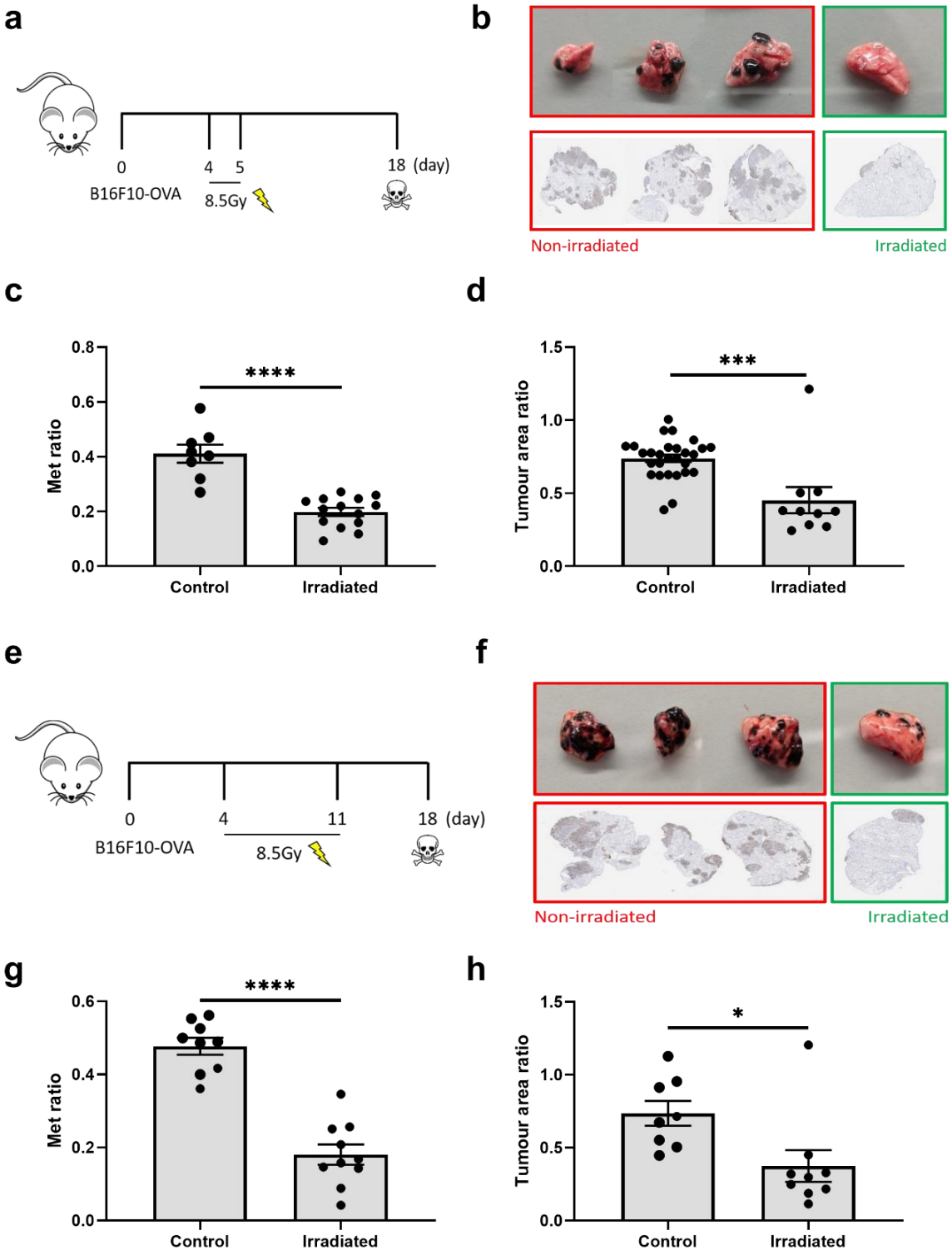

Figure 4.3 Two different regimens of fractionated radiotherapy induce an anti-tumour effect in the B16F10 model of lung metastasis. (a, e) Mice were injected with 1 X 10^5 B16F10-OVA cells intravenously and irradiated 4 and 5 days or 4 and 11 days post-injection respectively and lungs are harvested on Day 18. **(b, f)** Representative images of lungs (top) and histological staining of Ki67 tumour cells (bottom) on Day 18 for regimen shown in **a** and **e** respectively. **(c)** Quantification of lung metastatic nodule ratio (met ratio) for regimen **a** (n = 8, 14). **(d)** Quantification of tumour area ratio for regimen **a** (n = 28, 10). **(g)** Quantification of met ratio for regimen **e** (n = 9, 10). **(h)** Quantification of tumour area ratio for regimen **e** (n = 8, 9). **(c-d, g-h)** Bar graphs indicate the mean (± s.e.m) and data is combined of two to four independent experiments. Each data point represents a biological replicate. Statistical significance was calculated using unpaired two-tailed t-test, * = $P \leq 0.05$, *** = $P \leq 0.001$, **** = $P \leq 0.0001$.

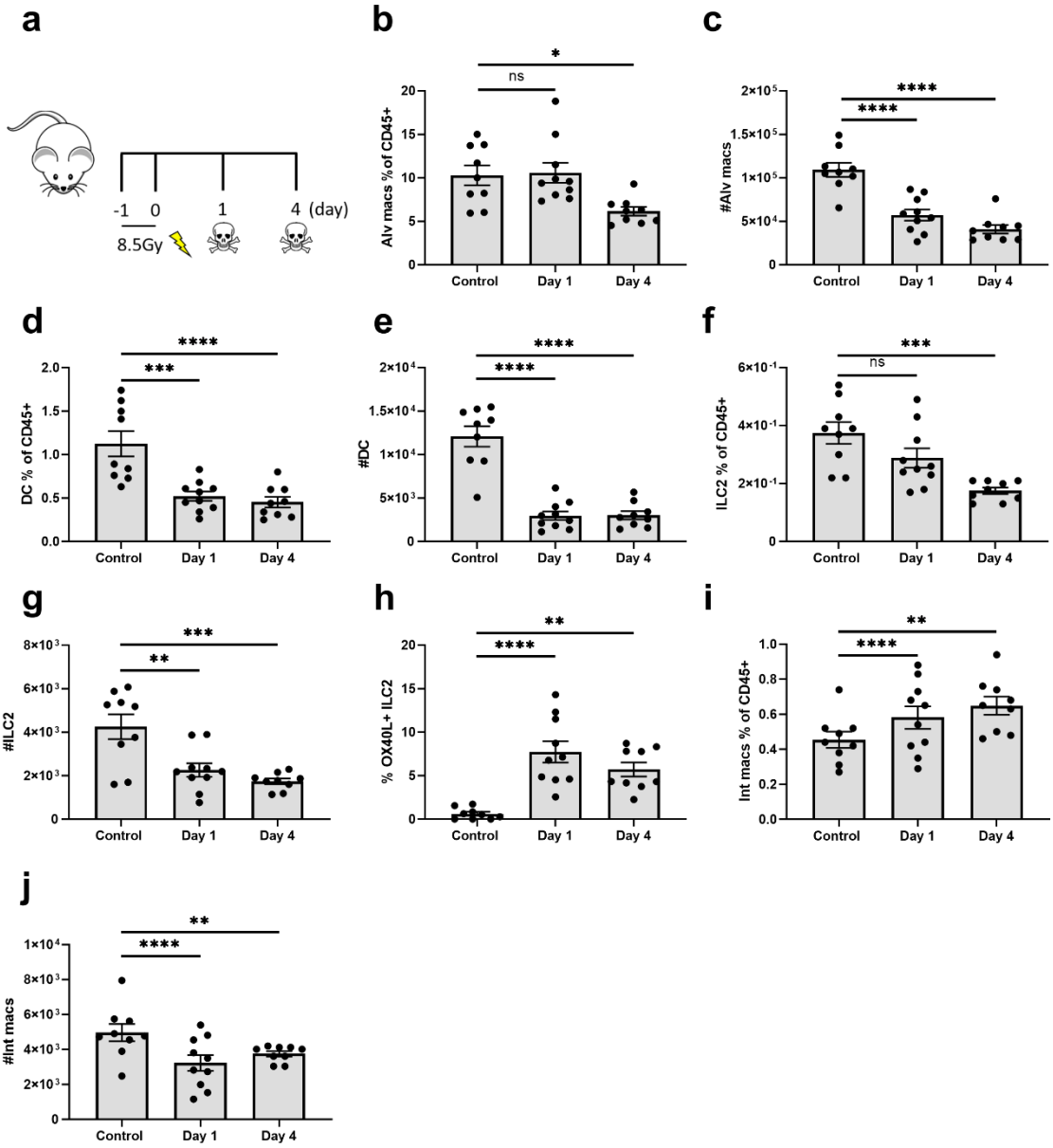

Figure 4.4 Lymphoid and myeloid cell changes in response to a new regimen in naïve mice are similar to the 15Gy single-dose regimen. (a) Mice were administered a fractionated dose of 8.5Gy X 2 on 2 consecutive days and targeted left lung lobes were harvested 1 or 4 days post-irradiation. **(b-j)** Quantification of frequency and number of alveolar macrophages, dendritic cells, ILC2s, OX40L+ ILC2s and interstitial macrophages by flow cytometry (n = 9, 10, 9). **(b-j)** Bar graphs indicate the mean (± s.e.m) and data is combined of two independent experiments. Each data point represents a biological replicate. Statistical significance was calculated using one-way ANOVA and Dunnett's multiple comparison, ns = not significant, * = P ≤ 0.05, ** = P ≤ 0.01, *** = P ≤ 0.001, **** = P ≤ 0.0001.

lung metastasis and these regimens will be used in subsequent experiments for the remainder of this chapter.

Next, I questioned if the 8.5Gy X 2 regimen induced similar immune changes in the naïve lung compared to the initial single dose 15Gy regimen. To that end, mice were irradiated with 8.5Gy for 2 consecutive days, and immune changes were probed 1 and 4 days after the final dose of irradiation was administered (Figure 4.4a). Importantly, similar immune changes were observed in this regimen,

with the majority of myeloid and lymphoid cell populations being relatively stable as demonstrated in Figure 3.2 and 3.3. Figure 4.4 summarises the main immune changes observed as a result of targeted radiotherapy with this new regimen, most of which was also previously observed in Figure 3.2 and 3.3. For myeloid cells, a decline in the frequency and number of tissue-resident AMs and DC was observed (Figure 4.4b-e). For lymphoid cells, a decline in ILC2 frequency and number was once again noted, alongside the expression of OX40L (Figure 4.4f-h). Interestingly, a decline in the number of IMs with this regimen was observed (Figure 4.4j), which was unchanged with the previous single dose 15Gy regimen. This likely suggests a dose-specific response to radiotherapy for IMs. Nevertheless, both the single, high dose 15Gy and the fractionated 8.5Gy X 2 regimen induces broadly similar changes in the immune microenvironment in the healthy lung.

4.2.3 ILC2s do not contribute to the anti-tumour response induced by radiotherapy

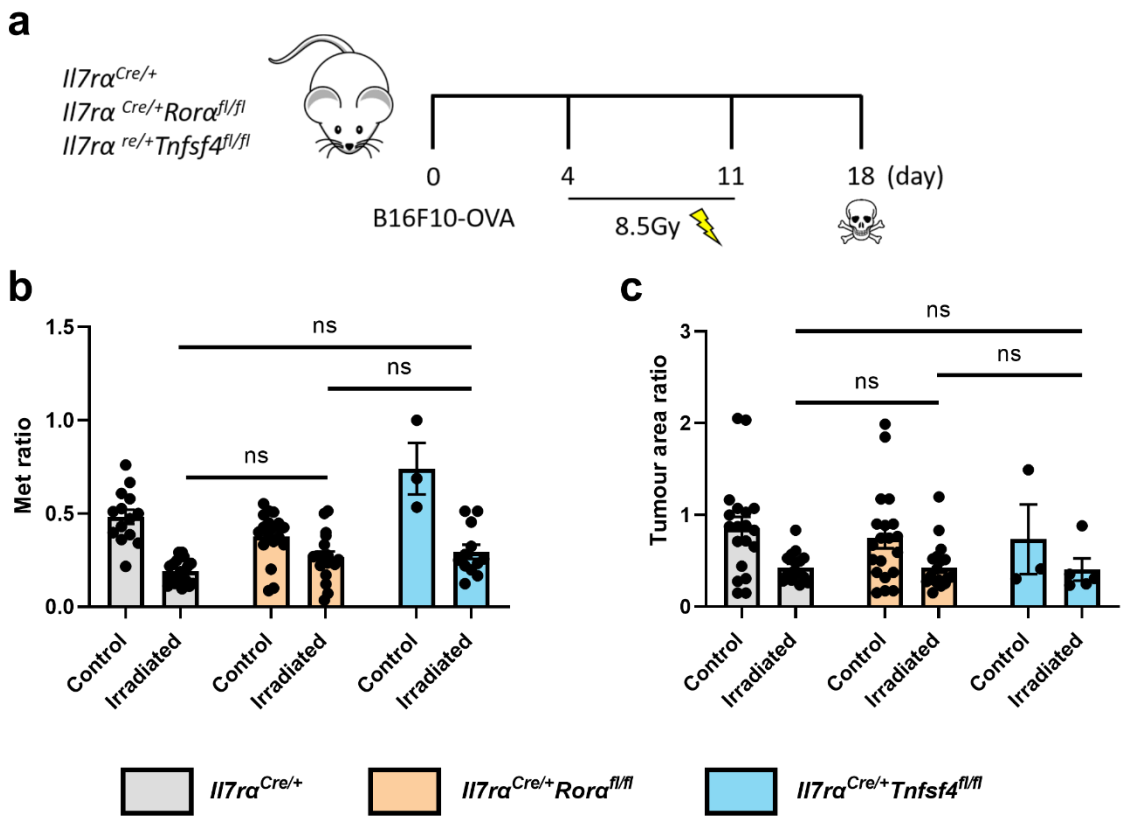

Figure 4.5 ILC2s do not contribute to the anti-tumour response induced by radiotherapy in the B16F10 model of lung metastasis. (a) *Il7rα*$^{Cre/+}$, *Il7rα*$^{Cre/+}$ *Rorα*$^{fl/fl}$ and *Il7rα*$^{Cre/+}$*Tnfsf4*$^{fl/fl}$ mice were injected with 1 X 10^5 B16F10-OVA cells intravenously and irradiated 4 and 5 days post-injection and lungs were harvested on Day 18. **(b)** Quantification of met ratio (n = 14, 20, 18, 18, 3, 12). **(c)** Quantification of tumour area ratio (n = 19, 16, 20, 19, 3, 5). **(b-c)** Bar graphs indicate the mean (± s.e.m). Data is pooled from two to four independent experiments for control and treated *Il7rα*$^{Cre/+}$ and *Il7rα*$^{Cre/+}$*Rorα*$^{fl/fl}$ mice for both lung metastatic nodule ratio and tumour area ratio, and treated *Il7rα*$^{Cre/+}$ *Tnfsf4*$^{fl/fl}$ lung metastatic nodule ratio. Data from control and treated *Il7rα*$^{Cre/+}$ *Tnfsf4*$^{fl/fl}$ tumour ratio and control *Il7rα*$^{Cre/+}$*Tnfsf4*$^{fl/fl}$ met ratio was obtained from a single experiment. Each data point represents a biological replicate. Statistical significance was calculated using two-way ANOVA and Sidak's multiple comparisons, ns = not significant.

The observation that targeted irradiation induces OX40L expression in ILC2s suggests that the ILC2 activation could induce immune modulation within the lung tumour microenvironment. I hypothesised that the activation of ILC2s by radiotherapy could modulate immune responses, and thereby influence radiotherapy-induced anti-tumour immunity. Hence, I utilised various mice strains and compared the effectiveness of radiotherapy in these different models (Figure 4.5a), namely *Il7rα*$^{Cre/+}$*Rorα*$^{fl/fl}$ mice, which are deficient in ILC2s, as well as *Il7rα*$^{Cre/+}$*Tnfsf4*$^{fl/fl}$ mice, which are ILC2-targeted OX40L-deficient mice. Heterozygous *Il7α*$^{Cre/+}$ mice were used as controls. Mice were irradiated with the 8.5Gy X 2 regimen for 2 consecutive days 4 days after tumour injection and lungs were harvested on Day 18, and the effectiveness of radiotherapy was quantified as previously described (Figure 4.5a). While radiotherapy was observed to be effective in all strains in both measured metrics, there was no difference in the met ratios or tumour area ratios in irradiated mice of both strains compared to irradiated controls (Figure 4.5b-c), suggesting that neither OX40L expression on ILC2s nor the presence of ILC2s influences the efficacy of radiotherapy in the B16F10-OVA model of lung metastasis. Notably, given that radiotherapy led to the significant depletion of ILC2s within the lung microenvironment, any observed effect of ILC2s activation on the tumour microenvironment by radiotherapy might have been diminished.

To more robustly assess putative roles of ILC2s in radiotherapy-induced immune modulation, ILC2 numbers were amplified prior to radiotherapy using exogenous IL-33 administration. As IL-33 priming of the pre-metastatic niche is known to influence seeding, mice were dosed after B16F10 adoptive transfer, which does not influence tumour progression (Schuijs et al. 2020). We previously validated that exogenous IL-33 administration induced the amplification of ILC2s in the lung, though this was also accompanied by infiltration of other immune cells (Schuijs et al. 2020). Mice were injected with B6F10-OVA cells and treated with IL-33 on 2 and 3 days after tumour injection before the irradiation on Day 4 and 5 (Figure 4.6a). The met ratios and tumour area ratios were enumerated and no significant difference between irradiated mice and irradiated mice pre-treated with IL33 was observed (Figure 4.6b and c), suggesting that IL-33 pre-treatment does not affect the efficacy of radiotherapy.

Finally, I sought an alternative method to quantify tumour burden in the lungs post radiotherapy by IVIS imaging. In this system, tumour cells are engineered to express luciferase, which catalyses the oxidation of D-luciferin. Light is released in this process, which can be detected by IVIS imaging. I utilised modified B16F10 cells that express luciferase (B16F10-Luc) and repeated the experiment (Figure 4.6a). Luciferin was injected into these mice before dissection. A representative image obtained by IVIS imaging is shown in Figure 4.6e, and the intensity of bioluminescence

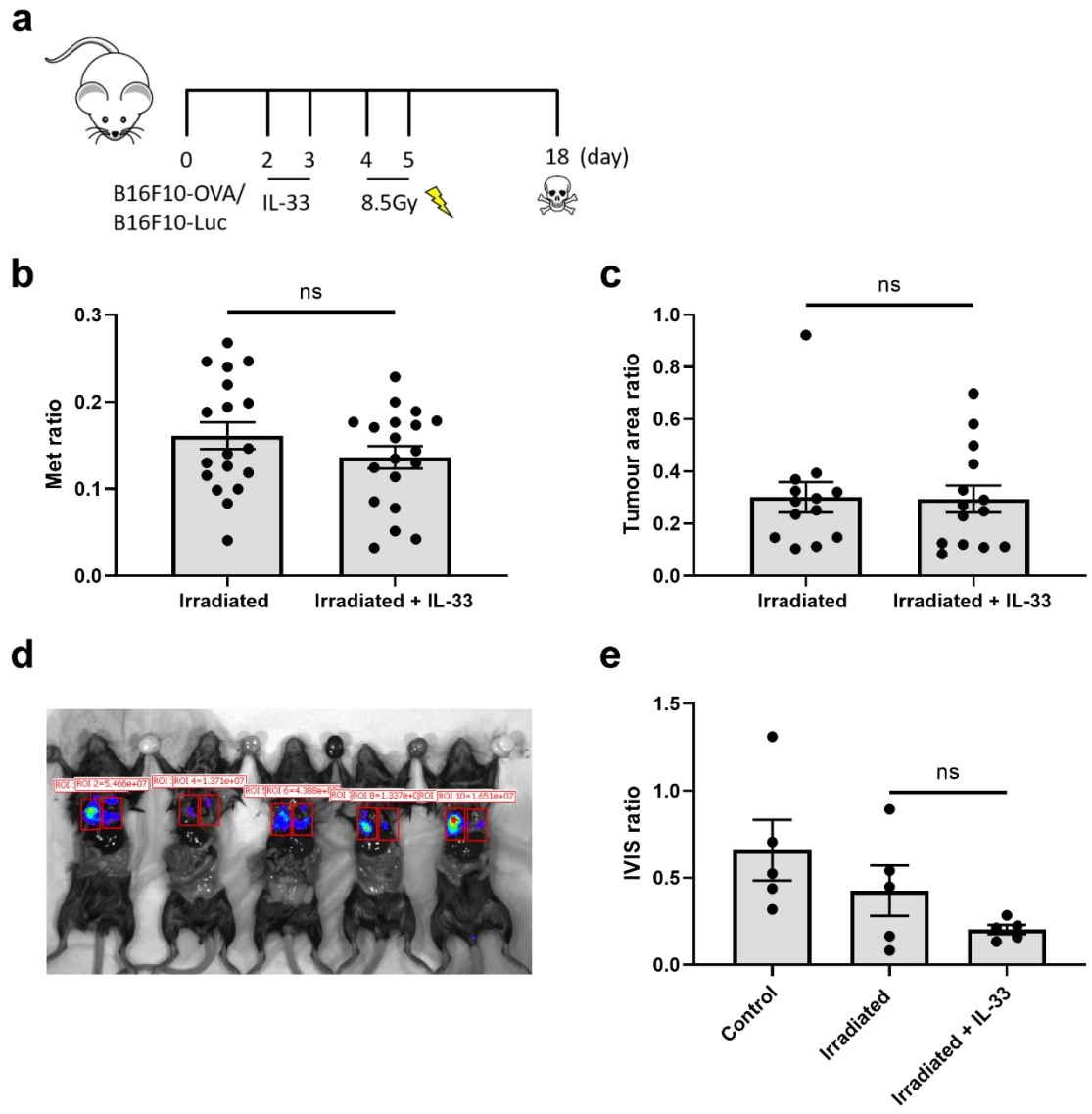

Figure 4.6 IL-33 treatment alongside radiotherapy does not modulate the effectiveness of radiotherapy. (a) WT mice were injected with either 1 X 10^5 B16F10-OVA cells or 1 X 10^5 B16F10-luciferase cells intravenously, treated with IL-33 2 and 3 days post-injection, irradiated 4 and 5 days post-injection, and lungs were harvested on Day 18. **(b)** Quantification of met ratio (n = 18, 19). **(c)** Quantification of tumour area ratio (n= 13, 14). **(d)** Representative image of quantification of signal in lung tumours in left and right lobes by IVIS imaging in tumour-bearing irradiated mice. **(e)** Quantification of IVIS ratio (n = 5, 5, 5). **(b-c, e)** Bar graphs indicate the mean (± s.e.m) and data is combined of three independent experiments **(b-c)** or a single experiment **(e)**. Each data point represents a biological replicate. Statistical significance was calculated using unpaired two-tailed t-test, ns = not significant **(b-c)** and one-way ANOVA and Tukey's multiple comparisons, ns = not significant **(e)**.

in the irradiated left lobe and non-irradiated right lobes was quantified separately. Similar to the other metrics, a ratio of the bioluminescence intensity (IVIS ratio) between the left and right lobes was obtained and no significant difference between irradiated mice and irradiated mice pre-treated with IL-33 was observed (Figure 4.6e). Notably, a significant decrease in the IVIS ratio between non-irradiated controls and irradiated mice was not observed, in part due to the variation between the calculated ratios. This suggests that the IVIS system was not the most optimal way to quantify

tumour burden in this model. In all, pre-treatment with IL-33 to expand ILC2 numbers does not influence the effectiveness of radiotherapy.

4.2.4 Immunophenotyping the response to targeted lung irradiation in the B16F10 model of lung metastasis

To obtain insight into important local immune changes that could contribute to radiotherapy-induced anti-tumour immunity, I performed immunophenotyping by flow cytometry to targeted radiotherapy in the context of this lung cancer model. To that end, the fractionated regimen of 8.5Gy X 2 was administered 4 days after tumour injection, and immune profile 1 and 4 days post-irradiation was monitored. Figure 4.7 and Figure 4.8 show changes in lymphoid and myeloid panel changes respectively.

For lymphoid cell number and frequencies, a relatively stable immune microenvironment was observed, which was similar to previous characterisation experiments. At the Day 4 time point, minimal differences were observed in the majority of lymphocyte populations. Interestingly, a small increase in the frequency of NK cells was seen, even though this was not accompanied by an increase in cell numbers (Figure 4.7d-e). This could be explained by a reduction in other cell populations within the CD45+ fraction, whilst NK cell numbers remain relatively stable. Indeed, a small decline in CD8+ T-cell numbers was observed, although this was not reflected in the frequency of this population out of the total CD45+ lymphocytes (Figure 4.7h-i). The unchanged frequency is likely due to a general decline in the total CD45+ population.

For myeloid cells, the trends were also similar to those observed in previous characterisation experiments. Like lymphoid cells, minimal differences in myeloid cell populations were observed 4 days post-irradiation. A decline in tissue-resident alveolar macrophages and DCs was observed once more (Figure 4.8e-f). Furthermore, a decline in the frequency and number of interstitial macrophages was observed, corroborating what was previously seen in the irradiation of the healthy lung with this regimen (Figure 4.8g-h). The frequency and number of said populations decreased as early as 1 day post-irradiation, and remained low after 4 days, further mimicking the trends observed in irradiation of the healthy lung. Overall, the immune changes observed after radiotherapy in the tumour context appear minimal, at least in the context of immune cell numbers. Notably, immune cell changes induced by radiotherapy with or without the presence of tumour appear to be similar. This suggests that irradiation of the lung microenvironment, rather than irradiation of tumour cells themselves, is the main driver of immune cell population changes within this model.

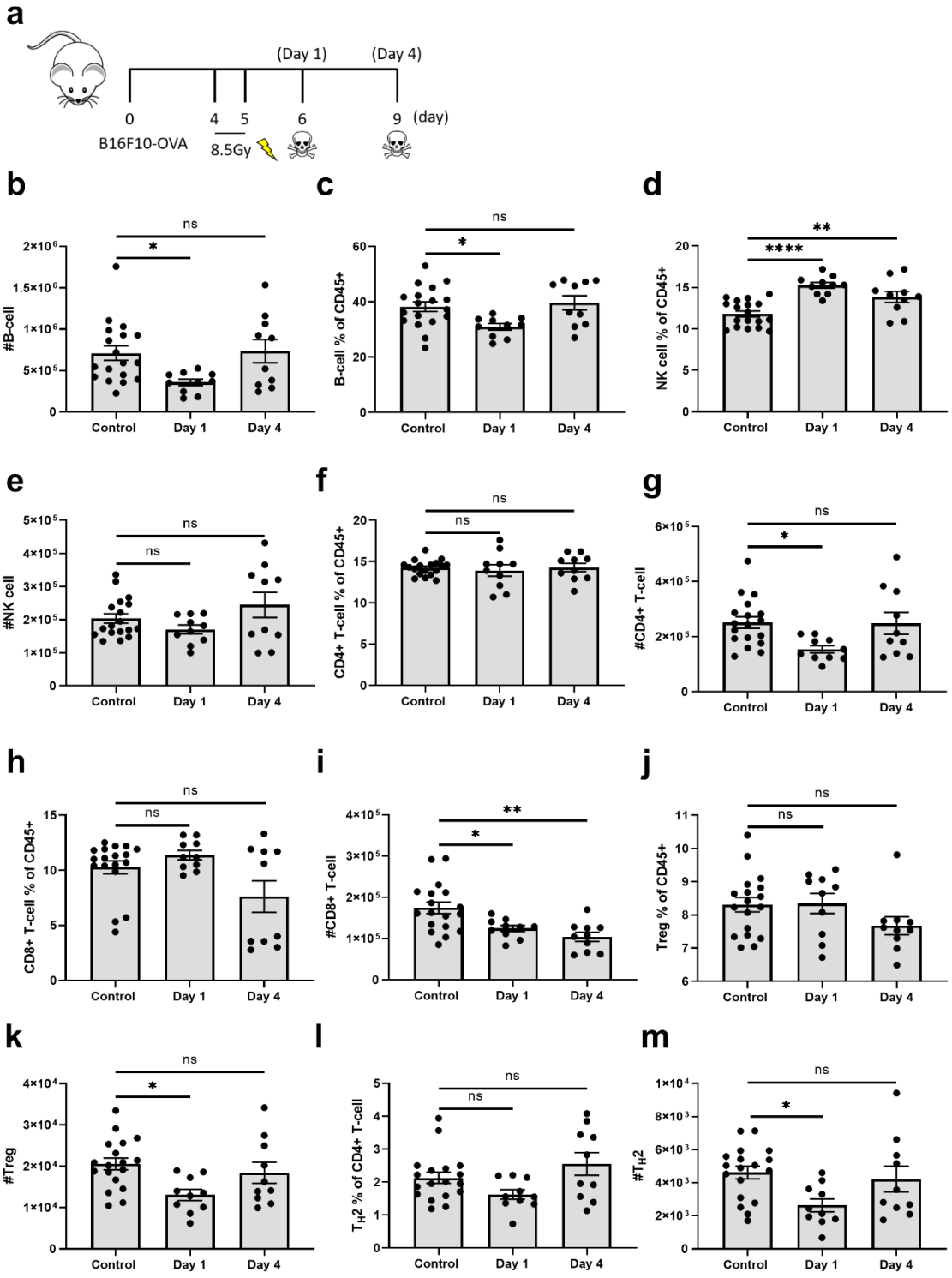

Figure 4.7 Lymphoid cell changes in response to radiotherapy in the B16F10-OVA model of lung metastasis. (a) WT mice were injected with 1 X 10^5 B16F10-OVA cells intravenously, irradiated 4 and 5 days post-injection, and targeted left lung lobes were harvested 1 (Day 1) and 4 (Day 4) days post-irradiation. **(b-m)** Quantification of frequency and number of B-cells, NK cells, CD4+ T-cells, CD8+ T-cells, Tregs and T_H2 cells by flow cytometry (n = 18, 10, 10). **(b-m**) Bar graphs indicate the mean (± s.e.m) and data is combined of two to four independent experiments**.** Each data point represents a biological replicate. Statistical significance was calculated using one-way ANOVA and Dunnett's multiple comparison test, ns = not significant, * = $P \leq 0.05$, ** = $P \leq 0.01$, **** = $P \leq 0.0001$.

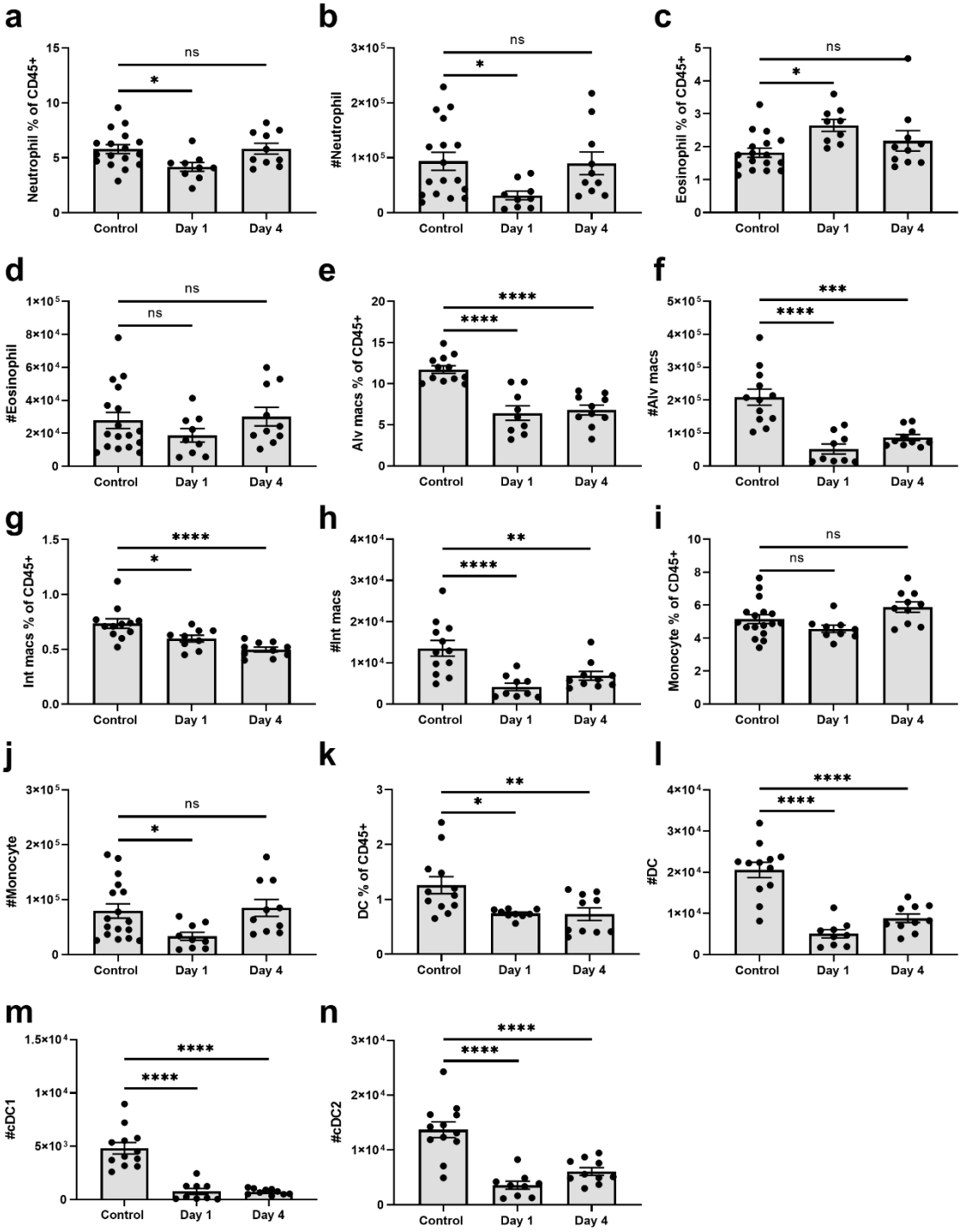

Figure 4.8 Myeloid cell changes in response to radiotherapy in the B16F10 model of lung metastasis. (a-n) Quantification of frequency and number of neutrophils (n = 17, 9, 10), eosinophils (n = 17, 9, 10), interstitial macrophages (n = 12, 9, 10), alveolar macrophages (n = 12, 9, 10), monocytes (17, 9, 10) and dendritic cells (12, 9, 10) by flow cytometry. **(a-n)** Bar graphs indicate the mean (± s.e.m) and data is combined of two to four independent experiments. Each data point represents a biological replicate. Statistical significance was calculated using one-way ANOVA and Dunnett's multiple comparison test, ns = not significant, * = P ≤ 0.05, ** = P ≤ 0.01, *** = P ≤ 0.001, **** = P ≤ 0.0001.

4.2.5 The adaptive immune response partially contributes to the anti-tumour function of radiotherapy

Whilst immunophenotyping the myeloid and lymphoid cell response to radiotherapy observed minimal immune changes, this has been predominantly focused on understanding broad changes in cell numbers, rather than individual cell function. Notably, the anti-tumour effect induced by radiotherapy suggests evidence of immune activation. As discussed, radiotherapy is crucial in promoting adaptive immune responses against cancer in multiple instances (Lugade et al. 2005; Reits et al. 2006), and DCs play a critical role in presenting antigens to activate these adaptive T-cells, particularly CD8+ T-cells, which could exert cytotoxic effects on tumour cells (A. Gupta et al. 2012). Hence, I first focused on studying the functional role of adaptive immunity in this model and initially focused on DC function in the tumour context after radiotherapy.

To that end, mice were irradiated 4 days post-tumour injection and lungs were harvested 1 day post-radiotherapy (Figure 4.9a). I postulated that similar to innate ILC2s which express OX40L at early time points post-irradiation, activation of DCs would be captured at early time points. DCs were defined as CD45+ cells, and further gated on CD11c+MHCII+ cells after the exclusion of other myeloid cells, including macrophages, which also express both CD11c and MHCII (see Materials and Methods, Figure 4.9b). DCs can be further categorised into either cDC1 or cDC2 via the expression of markers XCR1 and SIRPα respectively (Figure 4.9b). cDC1 and cDC2 are demonstrated to preferentially present to CD8+ and CD4+ T-cells respectively. The expression of CD80, which is a costimulatory marker for T-cells, was monitored by flow cytometry. Interestingly, an increase in the MFI of CD80 was observed in both cDC1 and cDC2 subsets post-irradiation (Figure 4.9c-e), suggesting their activation. Expression of MHCII was also monitored. Interestingly, upregulation of MHCII was observed specifically on the cDC1 subset (Figure 4.9f-g), suggesting a differential response to different DC subsets in response to radiotherapy.

Thereafter, I sought to confirm activation of the adaptive immune system. To that end, I probed the function of adaptive CD4+ and CD8+ T-cells post-irradiation. IFNγ is widely known to promote anti-tumour responses and is induced by radiotherapy, and critical for radiotherapy-induced anti-tumour immunity (Lugade et al. 2008; Liu et al. 2019). Hence, the production of IFNγ by CD4+ and CD8+ T-cells upon *in vitro* re-stimulation 4 days post-irradiation was measured, where activation of the adaptive immune system was expected (Figure 4.10a). An upregulation of IFNγ in both CD4+ (Figure 4.10b) and CD8+ T-cell subsets (Figure 4.10c) was observed, confirming that activation of DCs is accompanied by downstream activation of anti-tumour adaptive immunity.

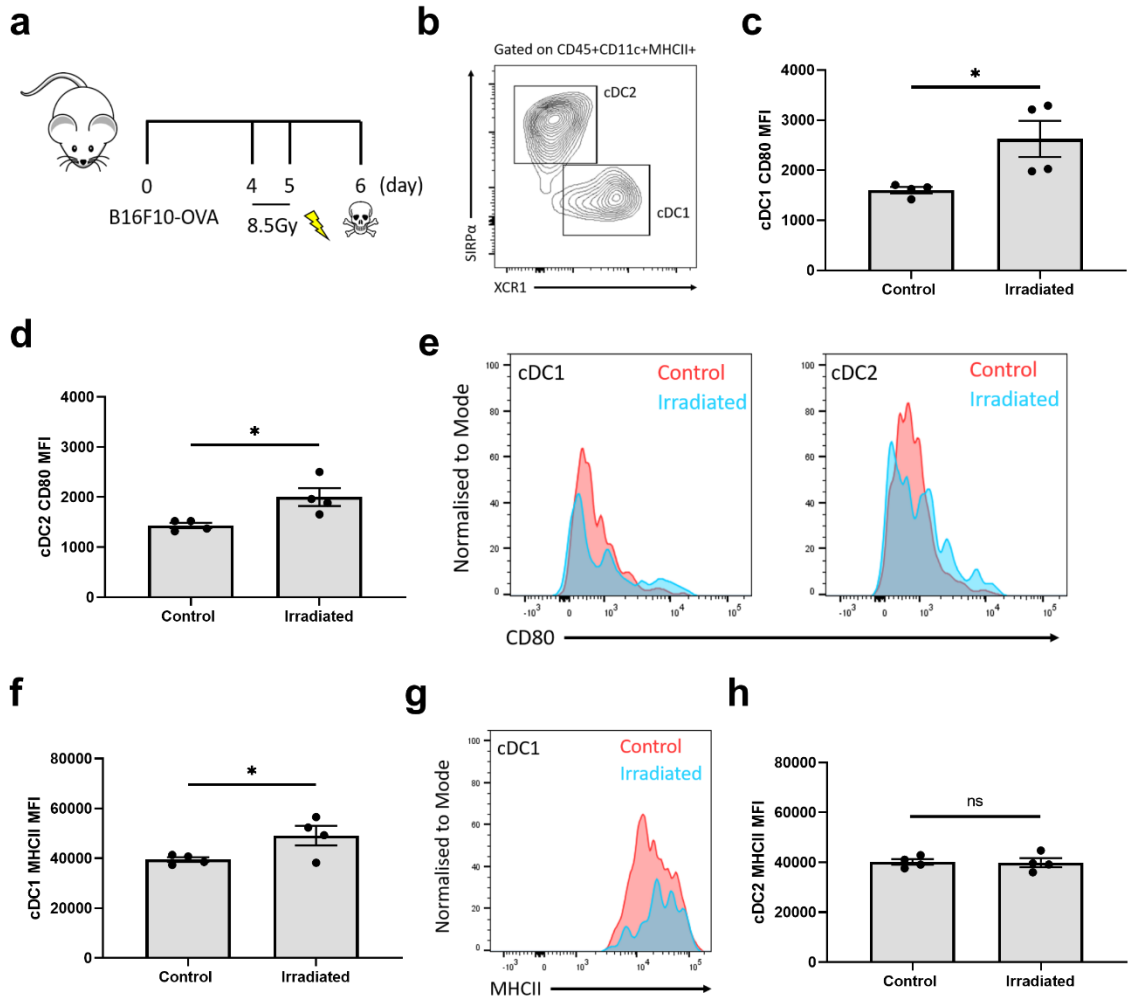

Figure 4.9 Dendritic cells are activated by radiotherapy. (a) WT mice were injected with 1 X 10^5 B16F10-OVA cells intravenously, irradiated 4 and 5 days post-injection, and targeted left lung lobes were harvested 1 day post-irradiation. **(b)** Representative flow cytometry plot demonstrating gating strategy of cDC1s and cDC2s. **(c-d)** Quantification of CD80 MFI in cDC1s and cDC2s. (**e)** Representative plots of CD80 in cDC1 and cDC2 in control and irradiated mice. **(f)** Quantification of MHCII MFI in cDC1s. (**g)** Representative plot of MHCII in cDC1 in control and irradiated mice. (**h)** Quantification of MHCII MFI in cDC2s. **(c-d, f, h)** Bar graphs indicate the mean (± s.e.m) and n = 4 for each group and data is representative of two independent experiments. Each data point represents a biological replicate. Statistical significance was calculated using unpaired two-tailed t-test, ns = not significant, * = P ≤ 0.05.

To confirm the importance of adaptive immunity in radiotherapy-induced anti-tumour immunity, I utilised *Rag2*$^{-/-}$ mice and compared the effectiveness of radiotherapy to that of WT mice (Figure 4.10d). *Rag2*$^{-/-}$ mice do not contain B or T-cells and present an inability to mount adaptive immune responses. These mice were subjected to irradiation along with WT controls, and the effectiveness of radiotherapy was quantified. Figures 4.10e and 4.10f demonstrate the met ratio and tumour area ratio respectively in control or irradiated WT or *Rag2*$^{-/-}$ mice. In WT mice, targeted irradiation results in the reduction of both met ratio and tumour area ratio, confirming the effectiveness of radiotherapy. Interestingly, while a reduction in met ratio was observed in *Rag2*$^{-/-}$ mice, this was not accompanied by a similar reduction in tumour area ratio. I postulated that this might be due to differences in the quantification method and the ability of each method to detect subtle differences

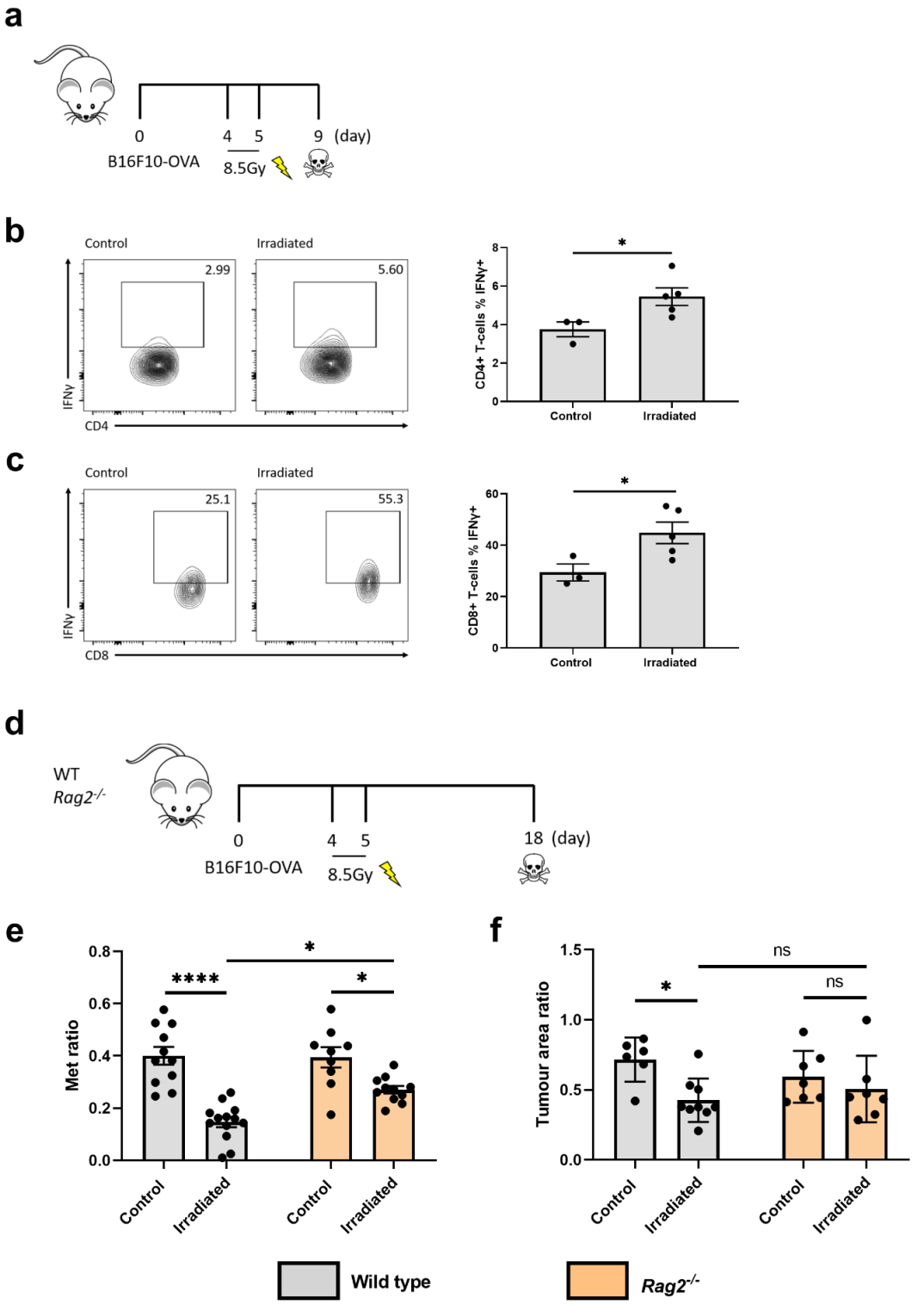

Figure 4.10 Anti-tumour function of radiotherapy is partially dependent on adaptive immunity. (a) Mice were injected with 1 X 10^5 B16F10-OVA cells intravenously, irradiated 4 and 5 days post-injection, and lungs were harvested 4 days post-irradiation. **(b)** Gating strategy and quantification of the frequency of IFNγ+ CD4+ T-cells (n = 3, 5). **(c)** Gating strategy and quantification of the frequency of IFNγ+ CD8+ T-cells after 3 hour restimulation with PMA and ionomycin (n = 3, 5). **(d)** WT or *Rag2*$^{-/-}$ mice were injected with 1 X 10^5 B16F10-OVA cells intravenously, irradiated 4 and 5 days post-injection, and lungs were harvested on Day 18. **(e)** Quantification of met ratio (n = 11, 13, 9, 11). **(f)** Quantification of tumour area ratio (n = 6, 9, 7, 7). **(b-c, e-f)** Bar graphs indicate the mean (± s.e.m) and data is of a single experiment **(b-c)** or combined of two to three independent experiments **(e-f)**. Each data point represents a biological replicate. Statistical significance was calculated using unpaired two-tailed t-test **(b-c)** or two-way ANOVA and Sidak's multiple comparison test **(e-f)**, ns = not significant, * = P ≤ 0.01, **** = P ≤ 0.0001.

in tumour burden (see Discussion and Conclusion).

Notably, while a reduction in the met ratio is observed in irradiated *Rag2*$^{-/-}$ mice compared to non-irradiated controls, the met ratio of irradiated *Rag2*$^{-/-}$ mice is still higher than that of irradiated WT mice (Figure 4.10e). However, this was not the case when quantification of tumour area was performed (Figure 4.10f). In all, the activation of DCs was observed in response to targeted radiotherapy to lung cancer, and quantification of tumour burden by the met ratio suggests that downstream adaptive immunity is necessary for radiotherapy-induced anti-tumour immunity.

4.2.6 NK cells contribute to the anti-tumour function of radiotherapy

Notably, *Rag2*$^{-/-}$ mice still displayed some degree of anti-tumour immunity, as reflected by a significant reduction in the met ratio in irradiated compared to non-irradiated *Rag2*$^{-/-}$ mice (Figure 4.10e). This suggests the presence of additional cell types that could contribute to radiotherapy-induced anti-tumour immunity. Whilst *Rag2*$^{-/-}$ mice are deficient in adaptive immune cells, innate NK cells are present. Importantly, NK cells also display anti-tumour function and cytotoxic activity against tumour cells. While radiotherapy is known to trigger anti-tumour responses predominantly via adaptive CD8+ T-cells, NK cell function can be influenced by radiotherapy as well(Chen et al. 2020). Furthermore, radiotherapy-induced NK cell activation has been shown to contribute to anti-tumour immunity (Barsoumian et al. 2020; Walle et al. 2022) in both mice and human studies. Thus, I sought to investigate if NK cells were also contributing to anti-tumour immunity in this model.

Alongside adaptive CD4+ and CD8+ T-cells, NK cells are also potent producers of IFNγ. Thus, I probed the capacity of NK cells to produce IFNγ post-irradiation upon *in vitro* restimulation after radiotherapy (Figure 4.11a-b). Similar to the adaptive immune compartment, IFNγ production was upregulated in response to irradiation (Figure 4.11c). Finally, I sought to confirm the importance of NK cells in radiotherapy-induced anti-tumour immunity. To that end, an anti-NK1.1 antibody that depletes NK cells in the lung was used alongside radiotherapy (Figure 4.11d). Interestingly, a similar trend to that of the irradiation of *Rag2*$^{-/-}$ mice was observed. The met ratio was observed to be higher in the irradiated group alongside anti-NK1.1 treatment, suggesting a reduction in the effectiveness of radiotherapy (Figure 4.13f). However, this was once again not observed in the tumour area ratio (Figure 4.13g). Overall, the met ratio suggests that NK cells also play a role in radiotherapy-induced anti-tumour immunity alongside the adaptive immune system.

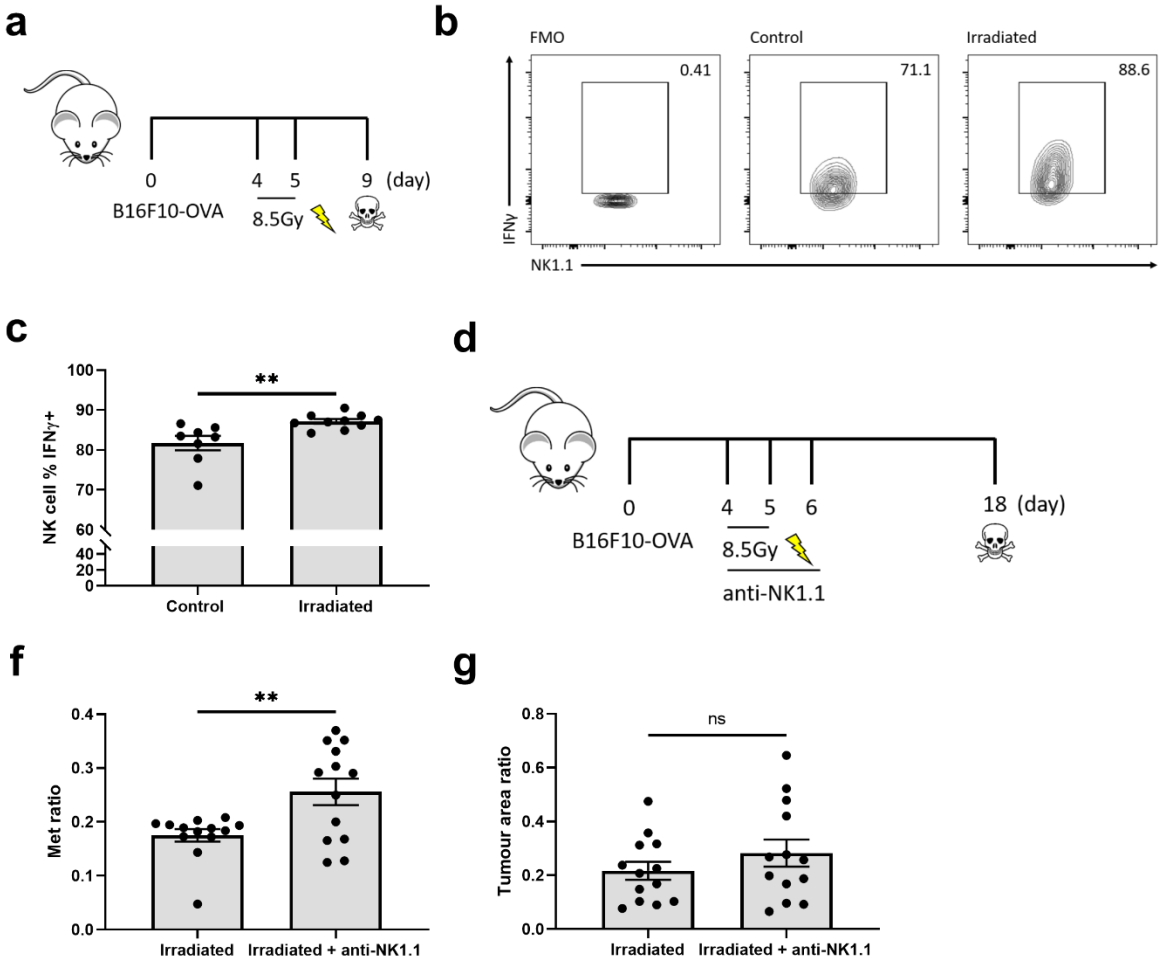

Figure 4.11 NK cells are activated and contribute to the anti-tumour function of radiotherapy. (a) WT mice were injected with 1 X 10^5 B16F10-OVA cells intravenously, irradiated 4 and 5 days post-injection, and lungs were harvested on Day 9. **(b)** Representative gating of IFNγ+ NK cells in control and irradiated mice. **(c)** Quantification of frequency of IFNγ+ NK cells after 3 hour restimulation with PMA and ionomycin (n = 8, 10). **(d)** Quantification of frequency of NK cells 1 and 4 days post-irradiation, as previously shown in Figure 2.7. **(e)** Mice were injected with 1 X 10^5 B16F10-OVA cells intravenously, treated with anti-NK.1.1 depleting antibody 4, 5 and 6 days post-injection, irradiated 4 and 5 days post-injection, and lungs were harvested on Day 18. **(f-g)** Quantification of met ratio and tumour area ratio (n= 13 for all groups). **(c-d, f-g)** Bar graphs indicate the mean (± s.e.m) and data is combined of two to three independent experiments. Each data point represents a biological replicate. Statistical significance was calculated using one ANOVA and Dunnett's multiple comparison test, ** = P ≤ 0.01, **** = P ≤ 0.0001 **(d)** and unpaired two-tailed t-test, ns = not significant, ** = P ≤ 0.01 **(c, f-g)**.

4.3 Summary

It remains to be fully understood the contributions of different immune cells within the lung tumour microenvironment in response to radiotherapy, as well as the mechanisms that contribute to radiotherapy-induced anti-tumour immunity. This includes the contribution of ILC2s, which are an important cell type mediating immune responses within the lung. In this chapter, I focused on the role of ILC2s and the broader immune system in radiotherapy-induced anti-tumour immunity.

I first characterised the B16F1-OVA model of lung metastasis and observed an accumulation of ILC2s post-tumour injection. The original single dose 15Gy regimen was modified to a fractionated 8.5Gy X 2 regimen, which induced similar immune changes to the original regimen. This modified regimen induced significant anti-tumour responses in the B16F10-OVA lung metastasis model. Whilst minimal changes in immune cell numbers were observed, activation of both innate and adaptive immunity was observed. While ILC2 expressed OX40L upon targeted radiotherapy, neither ILC2s nor OX40L activation on ILC2s influenced the effectiveness of radiotherapy. However, activation of DCs was observed, and downstream adaptive immunity was demonstrated to be important for radiotherapy-induced anti-tumour immunity. Interestingly, innate NK cells were also activated by targeted radiotherapy and contributed to anti-tumour responses. In all, I provide evidence for the role of both innate and adaptive immune system in targeted radiotherapy-induced anti-tumour immunity.

Chapter 5: Developing a model to study the role of ILC2s in modulating adaptive immune responses in primary lung cancer

5.1 Introduction

Current literature suggests that ILC2s can exhibit dual functions to either promote or inhibit cancer growth. Thus, further work is needed to dissect the multitude of ways ILC2s function to influence the outcome of cancer progression. Given the promiscuous nature of ILC2s and their ability to interact with and regulate a wide variety of cell types, including immune cells, it is likely that the nature of these interactions within the tumour microenvironment dictates cancer progression. Indeed, I previously discussed that ILC2s are key players in regulating both innate and adaptive immunity, and their interactions with both components of the immune system in the context of cancer likely influence cancer progression. For instance, ILC2 interactions with MDSCs are demonstrated to be pro-tumour (Trabanelli et al. 2017) in some cases, while ILC2 interactions with adaptive T-cells (Saranchova et al. 2018; Moral et al. 2020) appear to be anti-tumour in others.

As seen in the previous chapter, ILC2 numbers appear to increase in metastatic lung tumours in the B16F10 model. Furthermore, unpublished data from our lab demonstrate an accumulation of ILC2s in the early stages of the KP mouse model of primary lung cancer (data not shown). The accumulation of ILC2s is also observed in the context of human lung cancer (Wu et al. 2017). In addition, epidemiological evidence reveals that the prevalence of asthma is disproportionately higher in breast cancer patients with pulmonary metastasis (Taranova et al. 2008), suggesting a role of Type 2 immunity in supporting lung metastasis. Despite the clear enrichment and association of ILC2s in lung cancer, little is known about how ILC2s modulate immune responses and cancer progression within the lung.

As discussed in the introduction, our lab discovered an ILC2-eosinophil-NK cell innate immune axis that regulates lung metastasis using ILC2-deficient mouse models (Schuijs et al. 2020). Strikingly, this axis is independent of the adaptive immune system. Our results agree with another report suggesting a pro-tumour function of ILC2s, which can be reversed by PD-1 blockade (Howard et al. 2021), while also differing from other studies proposing an anti-tumour function of ILC2s (Saranchova et al. 2018). Notably, while Saranchova et al. suggests an anti-tumour function of ILC2s in metastatic lung cancer, their results highlighting ILC2-CD8+ T-cell interactions were demonstrated *in vitro* and on prostate cancer cells, rather than in the lung cancer setting (Saranchova et al. 2018).

In addition, I found no literature investigating the role of ILC2s in regulating the adaptive immune system on primary lung cancer. Altogether, this highlights a lack of understanding of the role of ILC2s in modulating adaptive immune responses, particularly in the context of primary lung cancer.

In this chapter, I discuss the development of a model to study the role of ILC2s in modulating adaptive immune responses in early-stage primary lung cancer. Firstly, I aimed to validate a doxycycline-controlled inducible OVA (iOVA) expression cassette and establish its functionality both *in vitro* and *in vivo*, with the intention of tracing ILC2-T-cell interactions at defined stages of lung cancer formation. Secondly, I aimed to establish an early stage, primary lung cancer cell from KP mice, which develops lung adenocarcinoma upon the administration of the Cre-recombinase. Finally, I aimed to establish an orthotopic model of lung cancer via intrathoracic injection of generated lung cancer cell lines.

5.2. Results

5.2.1 A model to study the role of ILC2s in modulating adaptive immune responses in primary lung cancer

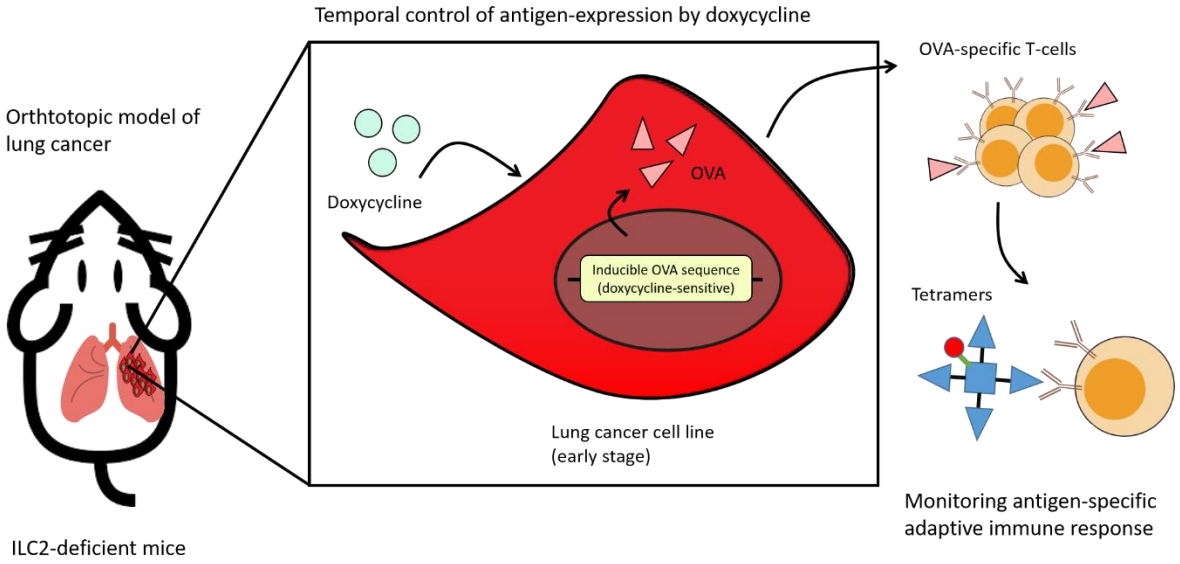

Figure 5.1 A model to study the role of ILC2s in modulating adaptive immune responses in lung cancer. Lung cancer cell lines containing a doxycycline-sensitive inducible OVA (iOVA) construct can be orthotopically implanted in control or ILC2-deficient mice. Expression of the antigen is controlled temporally via the administration of doxycycline, and expression of the OVA antigen generates OVA-specific adaptive T-cell responses. Adaptive T-cell responses can be monitored by tetramers detecting OVA-specific T-cells.

Figure 5.1 summarises the key components of a system developed to study the role of ILC2s in modulating adaptive immune responses in the context of primary lung cancer. In this model, I utilised the model antigen OVA to track OVA-specific immune responses. The use of the OVA antigen has proven to be an extremely useful tool in the study of antigen-specific immune responses. A key reason for this is that the generation of OVA-specific T-cell responses is detectable and quantifiable via the use of OVA-specific tetramers. These comprise fluorescently labelled tetrameric peptide-MHC complexes. Fluorescent-tagged tetramers, and thereby OVA-specific T-cells, can be detected by flow cytometry.

The induction of antigen-specific adaptive T-cell responses requires the expression of the OVA antigen by cancer cells. Unlike most cancer models that utilise constitutively expressed antigen, an inducible doxycycline-sensitive system was used. This allows for greater temporal control of antigen expression, and expression of antigens can be induced at certain stages of tumour development after the introduction of tumour cells into the mouse, rather than directly after tumour implantation. Another benefit of this system is that the expression of the antigen is reversible, unlike tamoxifen-inducible systems which are irreversible.

As previous unpublished data showed an enrichment in ILC2s in early lesions (data not shown), tumour cell lines derived from early stage tumours were selected to express this OVA construct. For this, the KP mouse model was selected and this will be discussed in subsequent paragraphs. Transfected cell lines could then be introduced into the lung intrathoracically to establish a model of primary lung cancer. After recovery from this procedure, mice will be placed on a doxycycline diet, triggering the expression of OVA in tumour cells. Tetramers will then be used to probe for T-cell-specific immune responses to the OVA antigen. If successful, this approach could be repeated in ILC2-deificient animals to study how ILC2s could contribute to adaptive immune responses. The remainder of this chapter discusses the steps taken to set up this model.

5.2.2 Validating an iOVA construct to monitor antigen-specific immune responses

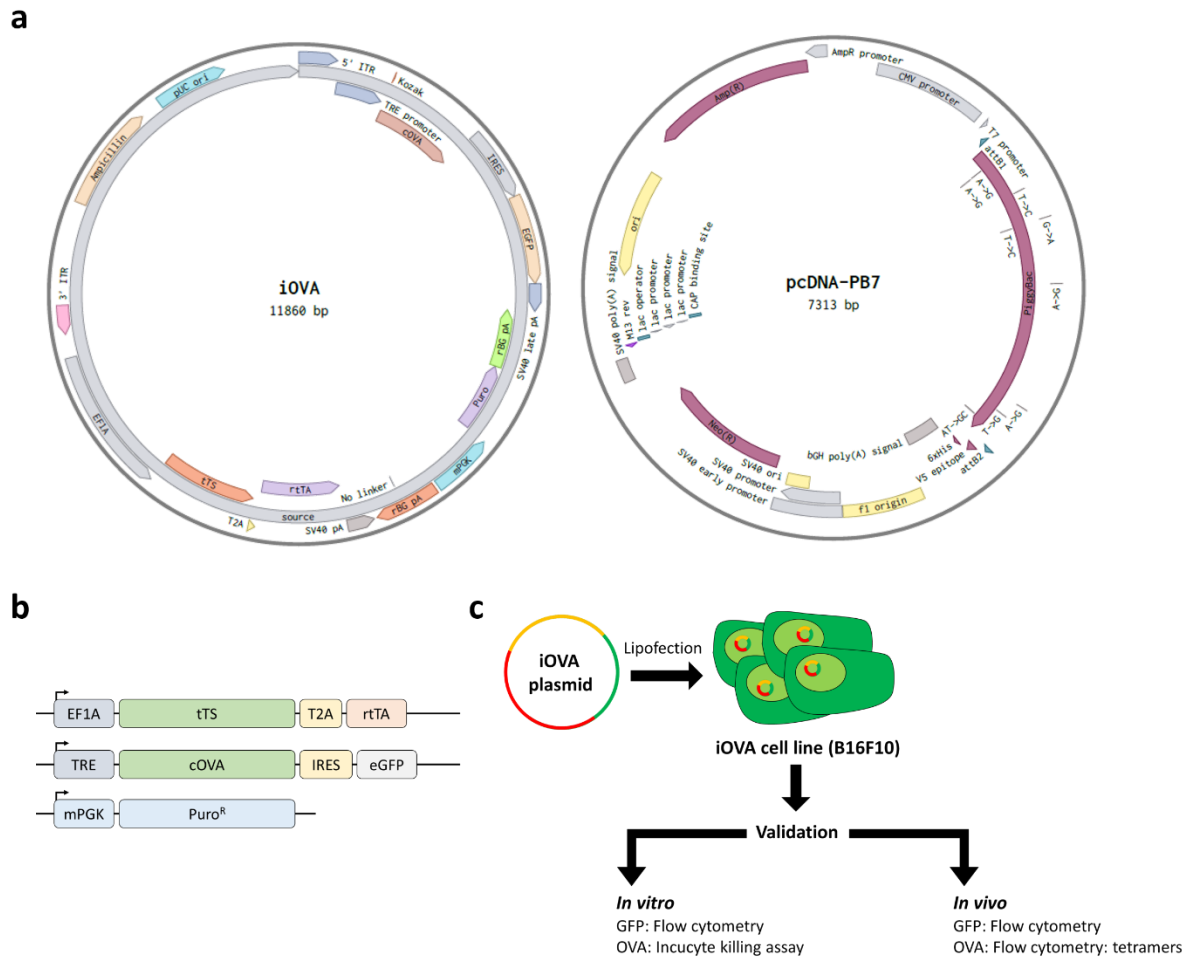

Figure 5.2 An iOVA construct to study antigen-specific immune responses. (a) Graphical representation of the iOVA plasmid (left) and the Piggybac-containing plasmid (right). Images were obtained from Benchling. **(b)** Graphical representation of key components of the iOVA plasmid. **(c)** Graphical representation of the workflow to validate the iOVA construct.

A plasmid containing an inducible OVA (iOVA) expression cassette (Figure 5.2a, left) was previously designed by a post-doc researcher within the lab. The plasmid was designed to contain inverted terminal repeat (ITR) sequences, which are positioned such that they flank the expression cassette. These flanking ITRs are recognised by the piggyBac transposase, which then facilitates the "cut and paste" of the expression cassette into the host genome. The piggyBac transposase is encoded by the PB7 plasmid (Yusa et al. 2011) (Figure 5.2a, right), and expression of the transposase is controlled by a mammalian CMV promoter, allowing for its use in murine cells. Thus, co-transfection of both the iOVA and PB7 plasmid within the host cell allows for the expression cassette to be inserted into the host genome.

The iOVA expression cassette contains 3 sequences of interest (Figure 5.2b). Firstly, expression of the tetracycline-controlled transcriptional silencer (tTS) and reverse tetracycline-controlled transactivator (rtTA) is controlled by the strong EF1A promoter. Secondly, the expression of cytoplasmic OVA (henceforth abbreviated OVA) and green fluorescent protein (GFP) is controlled by a tetracycline response element (TRE). In the absence of tetracycline, tTS binds to the TRE, thereby preventing the expression of both OVA and GFP. When tetracycline is present, rtTA binds to tetracycline, allowing it to bind to the TRE and displace the tTS, thus allowing for the expression of OVA and GFP. Finally, the cassette also contains a puromycin-resistance gene, which functions as a selection marker during the transfection process.

Figure 5.2c demonstrates the workflow to validate the functionality of the iOVA construct both *in vitro* and *in vivo*. To validate the function of OVA-expression in the tumour cell context, B16F10 cells were transfected to generate B16F10-iOVA cells. As seen previously, these cells can generate metastatic lung tumours, allowing the function of the construct to be validated in the lung. Finally, as the presence of tetracycline should result in the expression of both OVA and GFP, the expression of both was confirmed in both the *in vitro* and *in vivo* setting.

Figure 5.3a demonstrates the strategy to generate stably transfected B16F10-iOVA cells. Transfection of B16F10 cells was achieved with lipofectamine (see Materials and Methods). After transfection, cells were cultured in the presence of both puromycin and tetracycline to select for transfected cells and induce OVA and GFP expression. Transfected cells were then sorted 1-cell per well based on the expression of GFP (Figure 5.3b) by flow cytometry. Upon the expansion of single cells into a larger colony, individual clones were once again screened for GFP (Figure 5.3c). Selected clones expressing GFP were expanded before subsequent validation steps.

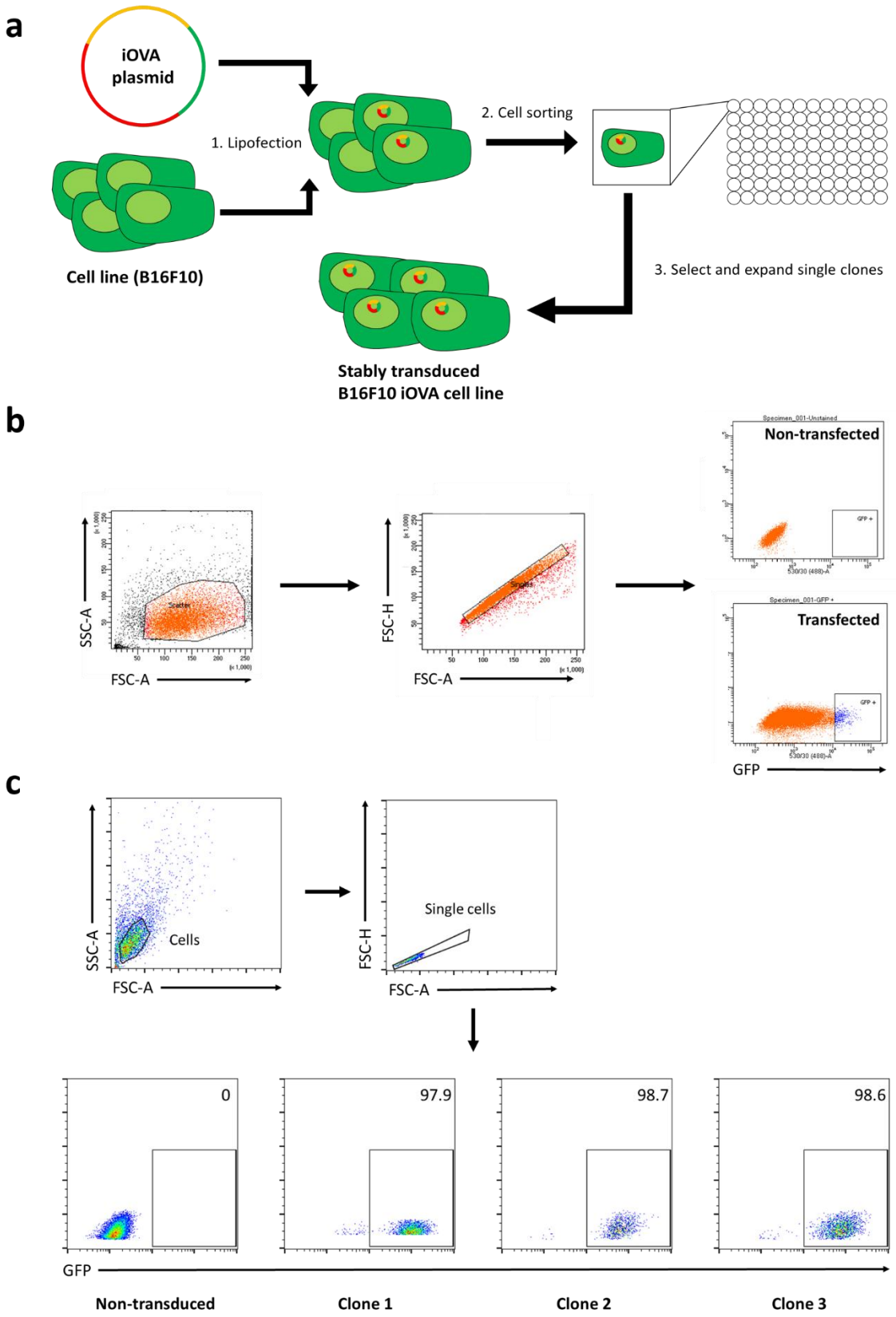

Figure 5.3 Generation of B16F10-iOVA cell lines. (a) Transfected B16F10-iOVA cell lines were sorted 1 cell per well in a 96-well plate and left in culture in selection media. Multiple clones were screened for the expression of GFP, and selected GFP+ clones were expanded to generate B16F10-iOVA cell lines. **(b)** Plots demonstrating the sort of GFP+ single cells. **(c)** Plots of 3 selected GFP+ B16F10-iOVA cell lines observed during the screening of individual clones.

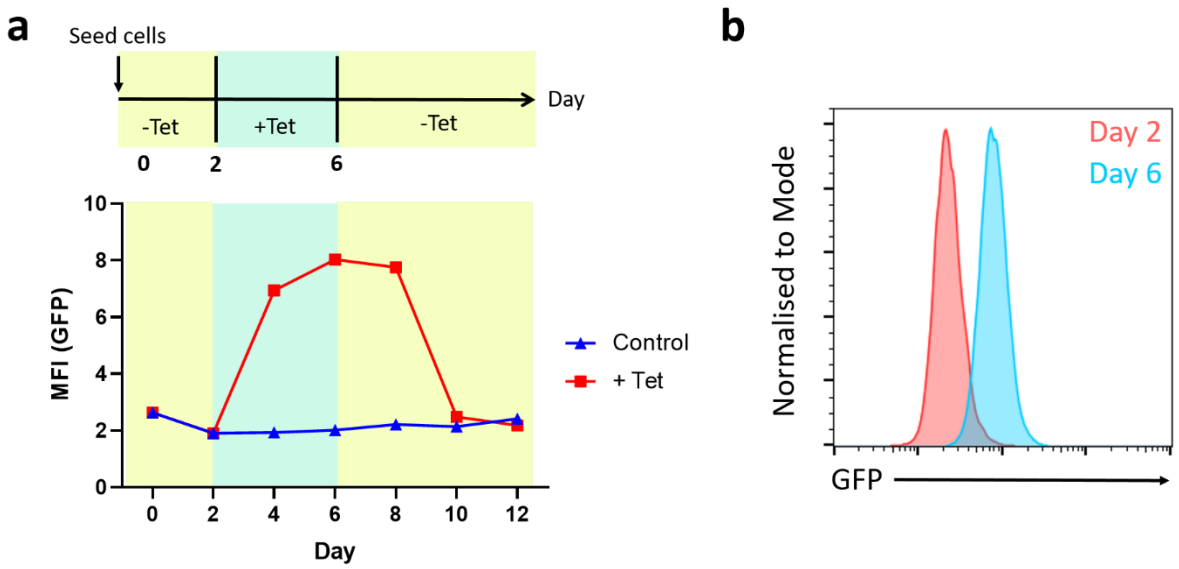

Figure 5.4 Validation of the iOVA construct by GFP expression in vitro. (a) B16F10-iOVA cells were initially seeded in the absence of tetracycline and transferred to tetracycline-containing media from Day 2 to 6. Cells were transferred back to non-tetracycline media on Day 6. MFI of GFP was monitored every 2 days throughout the experiment, and results demonstrate an increase and decrease in MFI in the presence or absence of tetracycline respectively. (**b)** Representative histogram of MFI of GFP on Day 2 and Day 6. **(a)** Data is indicative of a single experiment and one sample (n=1) was collected for each time point.

I first validated the tetracycline-responsiveness of OVA expression in newly generated B16F10-iOVA cells *in vitro*. A cell culture system was set up where cells were seeded in the absence of tetracycline from Day 0 to 2, followed by the introduction of tetracycline in the culture media from Day 2 to 6. Finally, cells were transferred to media without tetracycline for the remainder of the experiment up to Day 12 (Figure 5.4a). GFP expression was monitored every 2 days by flow cytometry. MFI of GFP was observed to increase on Day 4, 2 days after the introduction of tetracycline into the media. Notably, the MFI of GFP remained high on Day 8 2 days after the removal of tetracycline, likely due to a delay in the response of the system to the absence of tetracycline. Strikingly, GFP levels reverted to baseline levels of GFP at Day 10. Control B16F10-iOVA cells cultured in the absence of tetracycline maintained low baseline expression of GFP throughout the experiment. Figure 5.4b demonstrates the difference in GFP MFI on Day 2 and Day 6. Thus, the iOVA construct modulates GFP expression *in vitro* based on the presence or absence of tetracycline.

I then validated the expression of OVA and its ability to be detected by antigen-specific T-cells *in vitro*. Interactions between the OVA antigen and OVA-specific OT-I CD8+ T-cells have been well-characterised in literature (Moore, Carbone, and Bevan 1988; Kobori et al. 2010; Budhu et al. 2010). Notably, cultures of OVA-expressing tumour cells and OT-I CD8+ T-cells have demonstrated the capacity of OT-I CD8+ T-cells to kill these OVA-expressing cells *in vitro* (Kobori et al. 2010). Here, the Incucyte ZOOM (Gupta et al. 2018) was utilised to monitor specific killing of B16F10-iOVA tumour cells in the presence of OT-I CD8+ T-cells.

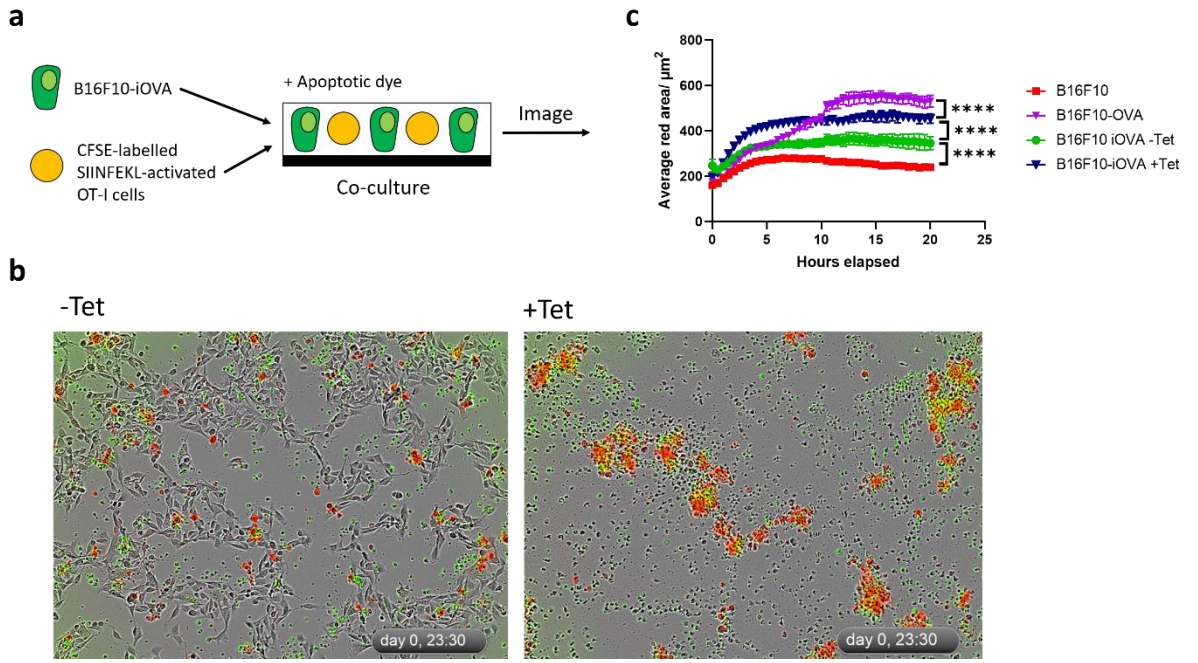

Figure 5.5 Validation of iOVA construct by OVA expression in vitro. (a) B16F10-iOVA cells previously seeded in media with or without tetracycline were cultured with CFSE-labelled, SIINFEKL-peptide activated OVA-specific OT-I T-cells. An apoptotic dye, which labels apoptotic cells red when viewed under the IncuCyte, was added to the culture for imaging. **(b)** Representative images of non-treated or tetracycline-treated B16F10-iOVA co-cultures obtained from the IncuCyte ZOOM 6 hours after co-culture. **(c)** Average red area (µm2) of the co-culture as quantified by the IncuCyte ZOOM. **(c)** Individual points indicate the mean (± s.e.m) of 3 technical replicates (n=3) and data is indicative of a single experiment**.** Statistical significance was calculated using one-way ANOVA and Tukey's multiple comparison test for the final time point for each condition, **** = P ≤ 0.0001.

Briefly, OT-I CD8+ T-cells were harvested from *Rag2*$^{-/-}$ OT-I mice, activated with the SIINFEKL-peptide, and labelled with the proliferation dye carboxyfluorescein succinimidyl ester (CFSE). B16F10-iOVA cells were then cultured in the presence of activated, labelled OT-I CD8+ T-cells. An Annexin V apoptotic dye was added to the co-culture, and cultures were imaged under the IncuCyte ZOOM (Figure 5.5a). CFSE-labelled OT-I CD8+ T-cells fluoresce green, whereas apoptotic cells fluoresce red. In the presence of tetracycline, greater killing of B16F10-iOVA cells was observed, as highlighted by a reduction in the number of adhering B16F10-iOVA cells in the culture (Figure 5.5b). Concomitantly, an increase in apoptotic staining was also observed. Notably, green CFSE-labelled OT-I CD8+ T-cells were observed to co-localise with red apoptotic cells, suggesting that increased apoptosis was attributed to an increase in killing.

The average red area was used as a measure of B16F10-iOVA killing, and by extension, the expression of OVA by B16F10-iOVA cells. Increased red staining was observed for B16F10-iOVA cells in the presence of tetracycline, compared to the absence of tetracycline, confirming the inducible expression of OVA in the presence of tetracycline. I also cultured parental B16F10 controls and constitutive OVA-expressing B16F10-OVA cells in the presence of OT-I CD8+ T-cells. Notably, the red area observed in B16F10 cells was significantly lower than in B16F10-iOVA cells cultured in the

absence of tetracycline, suggesting low levels of OVA expression in B16F10-iOVA cells at baseline. Nevertheless, the inducible expression of OVA in the presence of tetracycline was confirmed.

After validation of GFP and OVA expression *in vitro*, I validated the functionality of the iOVA construct *in vivo*, beginning with the detection of GFP. As seen in the previous chapter, B16F10 cells metastasise to the lung, serving as an ideal model to study if the inducible OVA construct functions within the lung tissue. Hence, B6F10-iOVA cells were injected into mice to establish metastatic lung tumours and mice were kept on a doxycycline diet (Figure 5.6a). I first checked if the addition of doxycycline affected the capacity of B16F10-iOVA cells to establish lung tumours, and observed no difference in the number of lung metastatic nodules in tumour-injected mice that were on a normal or a doxycycline diet (Figure 5.6b). I then assessed the frequency of GFP+ cells within the lung by flow cytometry. As seen in Figure 5.6c, tumour-bearing mice kept on a doxycycline diet had a significantly greater frequency of GFP+ cells, and this is quantified in Figure 5.6d. Thus, the iOVA construct responds to doxycycline *in vivo* to induce GFP expression.

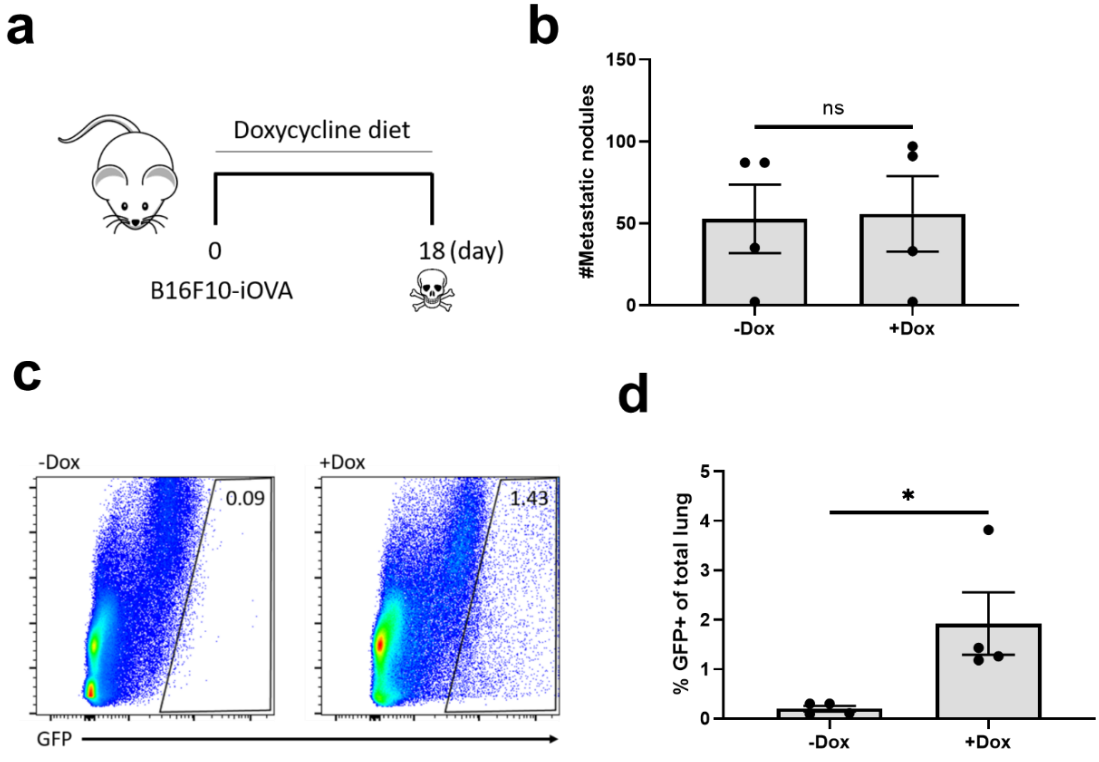

Figure 5.6 Validation of iOVA construct by GFP expression in vivo. (a) Mice were injected with 1 X 10^5 B16F10-iOVA cells intravenously and were kept on a doxycycline diet throughout the experiment. Lungs were harvested on Day 18. **(b)** Quantification of lung metastatic nodules in mice on normal or doxycycline diet (n=4, 4). **(c)** Representative plot of GFP+ cells from lungs of mice on normal or doxycycline diet. (**d)** Quantification of frequency of GFP+ cells from lungs of mice on normal or doxycycline diet (n = 4, 4). **(b, d)** Bar graphs indicate the mean (± s.e.m) and data is indicative of a single experiment. Each data point represents a biological replicate. Statistical significance was calculated using unpaired two-tailed t-test, ns = not significant, * = P ≤ 0.05.

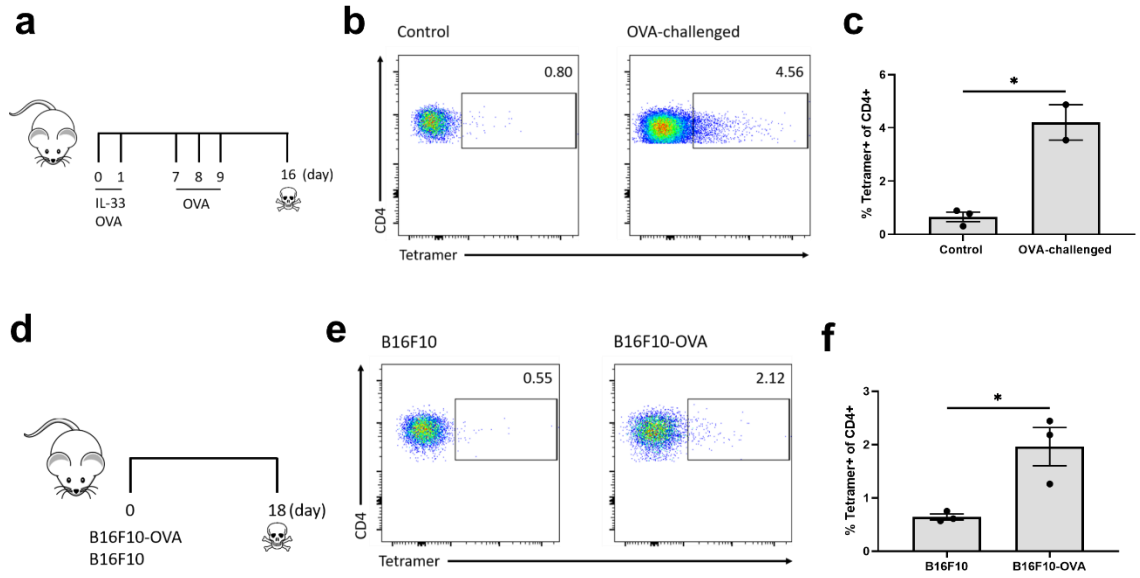

Figure 5.7 Tetramers detect OVA-specific T-cells in the lung in OVA-induced airway inflammation and the OVA-expressing B16F10 model of lung metastasis. (a) Mice were sensitised with OVA and IL-33 on Day 0 and 1, and further challenged with OVA on Day 7, 8 and 9. Lungs were harvested on Day 16. **(b)** Representative plots of Tetramer+ cells in control and OVA-challenged mice**. (c)** Quantification of frequency of Tetramer+ cells in control and OVA-challenged mice (n = 3, 2). **(d)** Mice were injected with 1 X 10^5 B16F10 or B16F10-OVA cells intravenously lungs were harvested on Day 18. **(e)** Representative plots of Tetramer+ cells in B16F10 control and B16F10-OVA mice**. (f)** Quantification of frequency of Tetramer+ cells in B16F10 control and B16F10-OVA mice (n = 3, 3). **(c,f)** Bar graphs indicate the mean (± s.e.m) and data is indicative of a single experiment. Each data point represents a biological replicate. Statistical significance was calculated using unpaired two-tailed t-test, * = P ≤ 0.05.

Next, I sought to validate the use of tetramers recognising OVA-specific T cells using two well established models. Firstly, an OVA-induced airway inflammation model was used. Mice were sensitised with IL-33 and OVA, followed by subsequent challenge with OVA 1 week after the initial sensitisation (Figure 5.7a). An increase in OVA-specific CD4+Tetramer+ cells was observed in OVA-challenged mice compared to controls (Figure 5.7c-d), demonstrating that Class II tetramers could pick up OVA-specific CD4+ T-cells in the context of OVA-induced airway inflammation. The ability of Class II tetramers to pick up OVA-specific T-cells in the tumour context was also tested. For this, B16F10-OVA cells constitutively expressing OVA was used to establish lung tumours, and their ability to induce OVA-specific T-cells was compared to parental B16F10. Similarly, an increase in OVA-specific CD4+Tetramer+ cells in B16F10-OVA cells was observed compared to controls (Figure 5.7e-f), suggesting that tetramers could pick up OVA-specific CD4+ T-cells in the tumour context as well.

Finally, the ability of Class II MHC tetramers to detect OVA-specific CD4+ T-cells induced by doxycycline in the B16F10-iOVA was tested. Mice were treated as previously described in Figure 5.6a, and tumour-bearing lungs were harvested. Strikingly, an increase in OVA-specific CD4+ tetramers+ was detected in mice on a doxycycline diet. This highlights that OVA expression is induced by doxycycline *in vivo*, and this induces OVA-specific CD4+ T-cells which can then be picked up by Class II MHC tetramers. Overall, this highlights the functionality of the iOVA construct both *in*

vitro and *in vivo*, and it's potential to detect adaptive T-cell responses in the context of lung tumours.

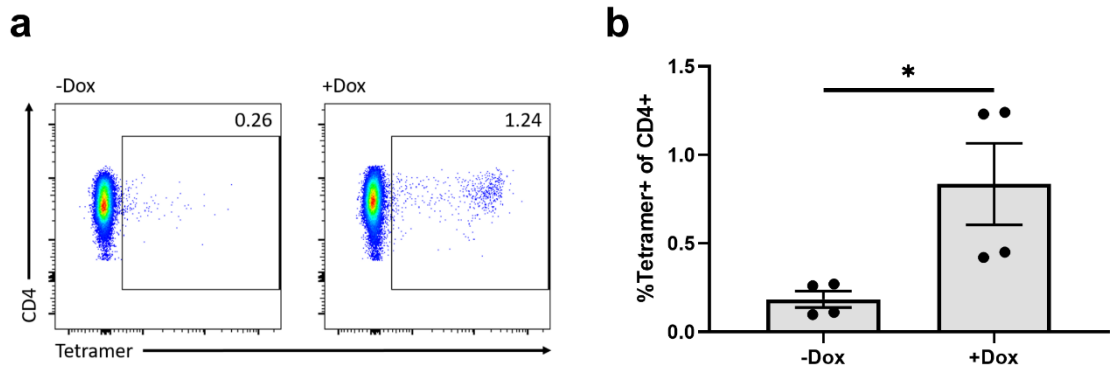

Figure 5.8 Tetramers detect OVA-specific T-cells in the lung in B161F10-iOVA model of lung metastasis. (a) Representative plots of tetramer+ cells in B16F10-iOVA tumour-bearing mice under normal or doxycycline diet. **(b)** Quantification of frequency of Tetramer+ cells in B16F10-iOVA tumour-bearing mice under normal or doxycycline diet (n = 4, 4). Bar graphs indicate the mean (± s.e.m) and data is indicative of a single experiment. Each data point represents a biological replicate. Statistical significance was calculated using unpaired two-tailed t-test, * = P ≤ 0.05.

5.2.3 Generating an early-stage lung cancer cell line from KP mice

The next objective was the generation of an early-stage lung cancer cell line. For this, I selected the KP mouse model of lung adenocarcinoma, which has been shown to capture certain aspects of human pulmonary carcinoma (Jackson et al. 2005). As discussed, the introduction of Cre recombinase results in the expression of mutant Kras, as well as the deletion of both p53 alleles, leading to the gradual development of primary lung adenocarcinoma. Notably, tumour progression and development in this model have been well-characterised histologically. A 4-stage grading system has been employed, with the earliest lesions designated Grade 1, and late-stage tumours and subsequent metastasis designated Grade 4 (DuPage, Dooley, and Jacks 2009). Early-stage Grade 1 lesions show up histologically 2-3 weeks post-Cre administration, though visible lesions on the surface of the lung only show up after 6-8 weeks. On the other hand, Grade 2 larger adenomas show up between 8-16 weeks. As I aimed to generate early-stage lung tumour cell lines, cell lines were derived from early Grade 2 larger adenomas.

KP mice were treated with Adeno-viral Cre recombinase (see Materials and Methods) and lung tissues were harvested 10 weeks post-treatment (Figure 5.9a). Small visible lesions were observed on the surface of the lung, confirming the development of tumours after Cre introduction. Cell lines were generated from these mice and further details are covered in the Material and Methods section. Briefly, total lung tissue was plated on collagen-coated plates, and tumour cells were allowed to expand. The emergence of cell clusters within the plate around 1-2 weeks (Figure 5.9b).

Notably, these cells were observed to look epithelial in nature, which is in agreement with literature on the epithelial nature of KP tumours cells (Kasinski and Slack 2013; Arnal-Estapé et al. 2020). The epithelial nature of these cells was confirmed by flow cytometry (Figure 5.9c), and they were confirmed to be CD45-CD31-EpCAM+. Importantly, these cells were capable of surviving more than 10 passages, highlighting that these cells were indeed transformed tumour cells. Cells were screened externally and were confirmed to be deficient in p53 at both alleles. However, the presence of the Kras-G12D mutation was not confirmed. This generated KP cell line is henceforth termed derived-KP (dKP) cells.

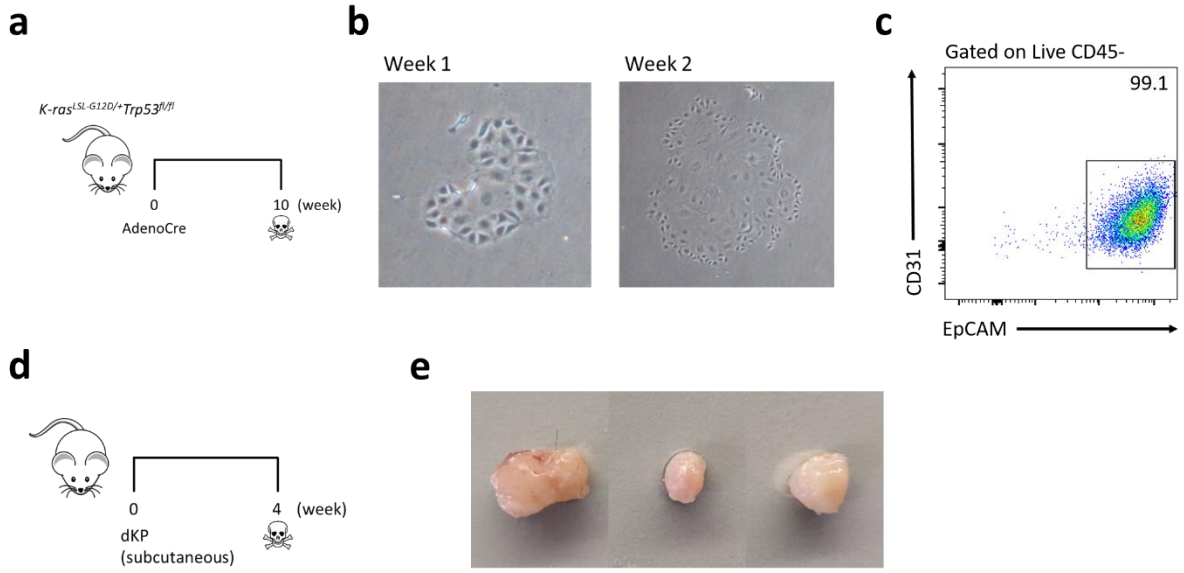

Figure 5.9 Derived cell lines from KP mice (dKP) are tumourigenic and form subcutaneous tumours (a) KP mice were treated with 2.5×10^7 pfu AdenoCre intranasally and lungs were harvested 10 weeks post-AdenoCre administration. **(b)** Representative images of dKP cells 1 and 2 weeks post-harvest. **(c)** Characterisation of EpCAM+ dKP cells by flow. cytometry. **(d)** Mice were injected with 5 X 10^5 dKP cells subcutaneously and tumours were harvested 4 weeks post-tumour administration. **(e)** Representative images of subcutaneous tumours derived from injected dKP cells.

The ability of dKP cells to generate tumours *in vivo* was assessed. To that end, dKP cells were injected subcutaneously and tumours were harvested 4 weeks post-tumour administration (Figure 5.9d). The presence of small tumours in mice implanted with this cell line was noted (Figure 5.9e), confirming that these cells were able to establish lesions *in vivo*. I also probed the ability of dKP cells to form metastatic lung tumours by intravenous injection, as previous studies using KP cells demonstrated their ability to metastasise to the lung (Maier et al. 2020). However, I failed to observe the establishment of any lung metastatic tumours in this model. This might be in part explained by the fact that dKP cells were derived from early-stage adenocarcinomas that have not yet acquired the capacity to metastasise and establish tumours in secondary sites.

5.2.4 Establishing an orthotopic model of lung cancer by intrathoracic injection

With the generation of dKP cells, the next step was to establish orthotopic lung tumours using these generated cell lines. Thus, I sought to establish a protocol for the intrathoracic injection of tumour cells in the lung. Current literature suggests two main ways to establish primary tumours within the lung tissue, namely via injection of tumours cells via the bronchi or trachea (Nakajima et al. 2014; Im et al. 2014) or directly into the lung via the intercostal space by intrathoracic injection (Onn et al. 2003; Cui et al. 2006; Im et al. 2014). As I hoped to establish solitary primary tumours within the lung, direct injection into the lung through the intercostal place was the method I decided to pursue, as injection in the bronchi or trachea typically results in the formation of multiple tumours within the lung. Furthermore, intrathoracic injections were typically less invasive and less technically challenging compared to injections into the bronchi or trachea. Thus, a protocol for intrathoracic injection of tumour cells into the lung was developed, and further details are indicated in the Materials and Methods sections. As this protocol was newly established, I first optimised the technique on dead mice.

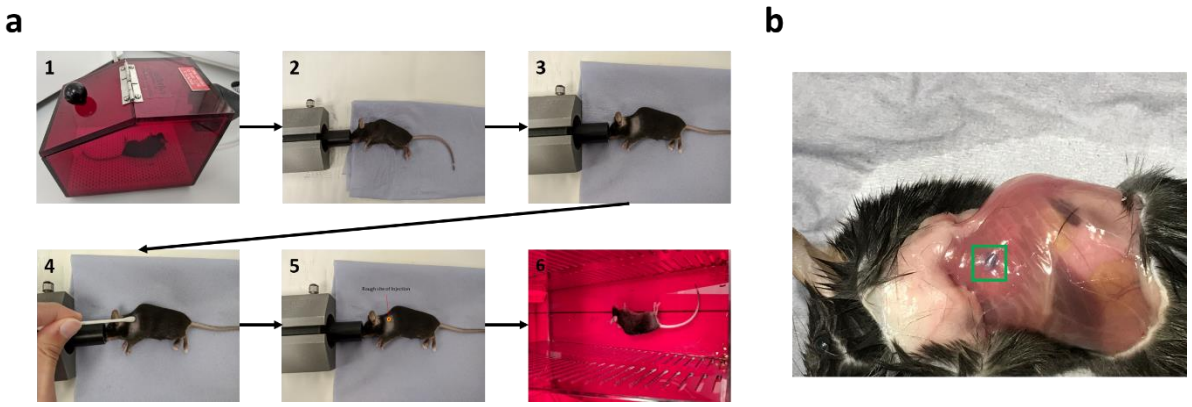

Figure 5.10 Establishing a protocol for intrathoracic injection of tumour cells into the lung left lobe. (a) Key steps in the intrathoracic injection of dKP cells into the mouse lung. **(b)** Representative image of injected trypan blue into dead mice. Green square indicates the presence of localised injected trypan blue within the lung.

A simplified workflow of the procedure is demonstrated in Figure 5.10a. Briefly, mice were anaesthetised in an isoflurane chamber. Once unconscious, they were transferred to an external nose cone and kept in the right lateral decubitus position and the hair surrounding the thorax was shaved off. After sterilisation, the needle was advanced 5-7mm into the left thorax and quickly removed after the injection. Optimisation of the procedure was performed with trypan blue, allowing us to observe the site of injection after the procedure was performed. As demonstrated in Figure 5.10b, injection of trypan blue with the established protocol resulted in the localisation of injected dye in the left lung lobe.

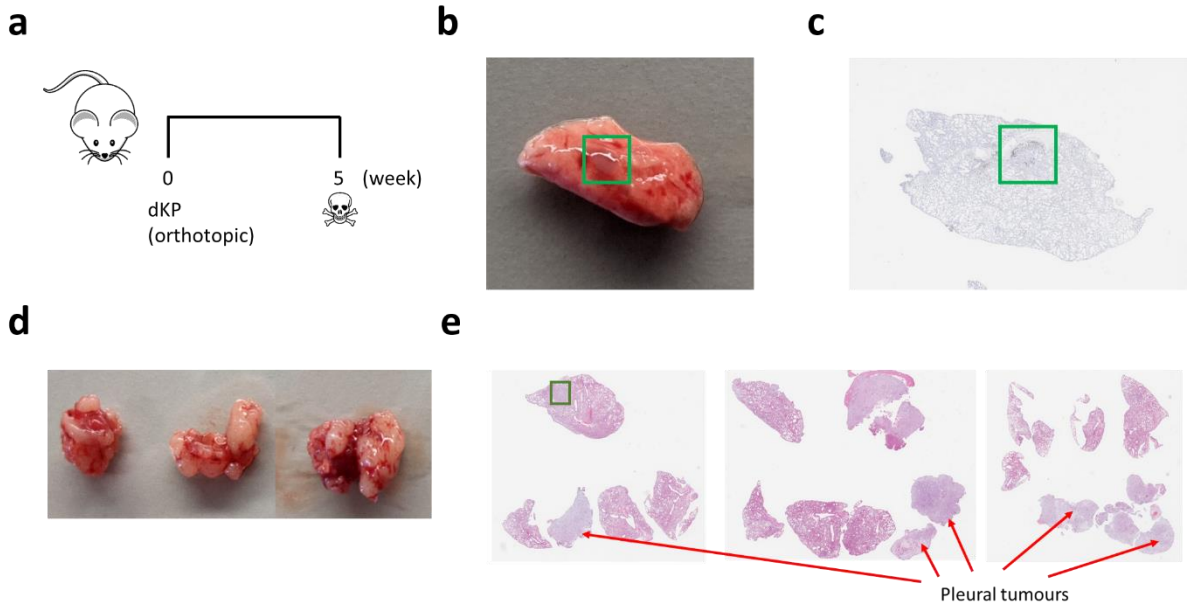

Figure 5.11 An orthotopic model of lung cancer by intrathoracic injection of dKP cells. (a) Mice were injected with 1 X 10^5 dKP cells intrathoracically and lungs were harvested 5 weeks post-tumour administration. **(b)** Representative image of orthotopically injected dKP cells within the left lobe. Green square indicates the presence of injected dKP cells. **(c)** Representative image of Ki67-stained lung left lobe section. Green square indicates the presence of injected dKP cells. **(d)** Representative images of pleural tumours obtained after orthotopic injection of dKP cells. **(e)** Representative H&E sections of total lung and pleural tumours. Green square indicates the presence of injected dKP cells and red arrows demonstrate examples of pleural tumours.

Finally, I sought to assess the ability of dKP cells to form orthotopic lung tumours via the established protocol. To that end, mice were injected and lung tissues were harvested 5 weeks post-injection (Figure 5.11a). The orthotopic implantation of dKP tumours resulted in the presence of localised tumour nodules within the lung, as seen visually and by histological Ki67 staining (Figure 5.11b, c). Notably, established tumour nodules were typically small and slow-growing. Importantly, the overwhelming majority of mice injected with tumour cells presented with a significant number of diffuse thoracic growth present within the chest cavity (Figure 5.11d, e), likely as a result of a leakage of tumour cells during the injection process. Compared to tumour nodules within the injected left lung, tumours in the pleural cavity were significantly larger, and led to mice reaching their humane end-point around 5-6 weeks post-injection.

To circumvent the leakage observed in these experiments, an increased concentration of matrigel was utilised, alongside decreasing the diameter of the needle from 27G to 30G, but leakage was still observed in these subsequent experiments. Attempts were also made to reduce the injected volume via the use of specialised glass syringes that could inject lower volumes not achievable with conventional 1ml syringes (see Materials and Methods). I tried these syringes in the LL/2 Lewis lung carcinoma model of cancer, where injection of significantly lower tumour cell numbers can establish tumours (Doki et al. 1999). In these experiments, volumes as low as 5µl were injected, but even

these led to the formation of tumours within the chest cavity (data not shown). Thus, despite these efforts, the leakage of tumour cells into the lung chest cavity remained a problem and this prevented further experiments aiming to study the role of ILC2s in mediating immune responses in this primary cancer.

5.3 Summary

The role of ILC2s in regulating adaptive immune responses in the context of cancer remains unclear. Furthermore, this is less so in the context of primary lung cancer. In this chapter, I describe an attempt to develop a model to study the role of ILC2s in regulating the adaptive immune response in early-stage primary lung cancer.

To study antigen-specific adaptive immune responses, an iOVA construct expressing the OVA antigen in the presence of tetracycline was validated in B16F10 cells both *in vitro* and *in vivo*. I confirmed via the detection of GFP and OVA-specific T-cell responses that the construct was tetracycline-sensitive. I also generated tumour cell lines from KP mice as a model for early-stage lung cancer. dKP cells were confirmed to be epithelial in origin and demonstrated their tumourigenicity *in vivo* in the subcutaneous setting. Finally, I established a protocol for the orthotopic implantation of lung tumour cells into the lung. Whilst solitary tumour nodules were established in the lung, this was accompanied by leakage of tumour cells into the chest cavity, which has prevented progress to study the role of ILC2s in mediating immune responses in this primary cancer.

Chapter 6: Discussion and Conclusion

6.1 ILC2s respond to targeted lung radiotherapy

Radiotherapy is widely used in the treatment of many cancers, and the role of radiotherapy-induced immune activation is increasingly appreciated. However, studies looking at irradiation in healthy non-tumour tissue remain few and far between. Importantly, the study of immune responses in healthy tissue could elucidate knowledge of the response of bystander immune cells in response to radiotherapy. In the context of the lung, understanding the response of healthy tissue allows us to understand the mechanisms of the side effects of radiotherapy, the most notable being radiation-induced lung fibrosis. Furthermore, ILC2s are a relatively new cell type and their response to radiotherapy is still elusive.

As radiotherapy has been shown to induce changes in the immune microenvironment in the tumour context, I hypothesised that targeted lung radiotherapy would induce major changes in the immune landscape within the lung. Interestingly, minimal changes in the major immune cell populations within the lung in the acute response post-radiotherapy was observed. Specifically, depletion of DCs and alveolar macrophages was observed, while the lymphocyte compartment remained relatively stable, with only a slight increase in CD4+ T_H2 cells. DCs and macrophages in the lung have been demonstrated to be radiosensitive, and irradiation of the thorax region has been shown to deplete both populations acutely (Hahn et al. 2011; Meziani et al. 2018). Notably, both populations are repopulated back to baseline levels at later time points that were not looked at in these experiments. The initial decline of these cells could be attributed to the tissue-resident nature of these cells (Kopf, Schneider, and Nobs 2014), and unlike most other cell types, are not rapidly recruited from circulation. For CD4+ T_H2 cells, the finding is similar to a previous study looking at the response of the lymphocyte component to radiotherapy in the lung, where they report an increase in CD4+ T_H2 IL-13+ cells (Paun, Kunwar, and Haston 2015). Interestingly, the reported increase in CD4+ T_H2 cells was observed as early as 1 day post-irradiation, even though changes in the adaptive immune compartment typically occur multiple days after the initial insult, suggesting that changes in the adaptive immune compartment could occur at even earlier time points.

A recent report also demonstrated the use of the SARRP to administer targeted irradiation to the healthy lung (Nolan et al. 2022). The report utilised high dose irradiation of 13Gy, which was of a similar dose to what was used in my experiments monitoring immune responses. Contrary to my findings, they observed no change in macrophage and DC populations in the lung 7 days post-irradiation. Furthermore, infiltration of neutrophils was observed, which led to neutrophil-mediated

responses that enhanced lung metastasis. These disparities might be attributed to differences in mice strain, where they utilised relatively radioresistant BALB/C mice (Jackson, Vujaskovic, and Down 2011). Strikingly, the paper also reported minimal immune changes in most immune cell populations post-irradiation as well, suggesting that a relatively stable immune microenvironment is maintained in the lungs after radiotherapy.

Quantification of ILC2s by flow cytometry revealed a reduction in their numbers after targeted lung irradiation, suggesting the radiosensitive nature of ILC2s. Notably, the kinetics of ILC2 decline is similar to that of alveolar macrophages and DCs. Like both of these cells, ILC2s are tissue-resident, and their persistent decline might be attributed to a lack of rapid recruitment from circulation to replace the depleted population. These results depart from existing literature, which suggests that lung-resident ILC2s are radioresistant (Bruce et al. 2017). Interestingly, the report also looked at ILC2s in the lamina propria and mediastinal lymph nodes (mLN), and show that ILC2s within these organs are more radiosensitive, leading to a sharper decline in numbers. These differences could be simply explained by differences in the irradiation setup. In their report, whole body irradiation at 950cGy was performed instead, instead of target lung irradiation. Nevertheless, further work is needed to study the radiosensitive or radioresistant nature of ILC2s in different tissues, as well as the global response of these ILC2s to non-specific whole-body irradiation.

To the best of my knowledge, this work is the first to observe evidence of ILC2 activation by targeted lung radiotherapy, as indicated by OX40L expression. My experiments reveal that OX40L expression induced by radiotherapy is transient, occurs rapidly post-irradiation, and occurs in a dose-dependent manner. Intriguingly, OX40L expression was not associated with an increase in IL-13 production, suggesting that OX40L expression does not necessarily correlate with Type 2 cytokine production in ILC2s. Notably, IL-33 is a key alarmin known to induce OX40L expression in ILC2s, and this is accompanied by the production of Type 2 cytokines (Halim et al. 2018). The absence of upregulation of Type 2 cytokines suggests that OX40L expression induced by radiotherapy could be independent of IL-33. Indeed, even though targeted irradiation of IL-33-deficient *Il33*$^{cit/cit}$ mice resulted in lower levels of OX40L expression compared to irradiated controls, residual OX40L expression was still observed compared to non-irradiated mice, suggesting the existence of an IL-33-independent mechanism of OX40L expression.

Interestingly, using an IL-33 trap that binds the IL-33R, OX40L expression was not abrogated on ILC2s and remained at similar levels in irradiated mice not treated with the trap. These results highlight an apparent contradictory role of IL-33 in OX40L expression on ILC2s induced by radiotherapy. While the exact reason for this remains unclear, a few possible hypotheses could

reconcile these differences. Firstly, the IL-33 trap binds to the ST2 receptor, which could suggest a cell-intrinsic role of IL-33 that regulates OX40L expression. A more likely explanation is the compensatory effect by other factors that lead to the same level of OX40L expression in mice treated with the IL-33 trap. This compensatory effect might not be evident in *Il33*$^{cit/cit}$ mice due to an intrinsic defect of ILC2s in these mice to respond to activating signals like IL-33 (Steer et al. 2020). Furthermore, given the observed dose-dependency of OX40L expression, it is likely that the magnitude of irradiation affects the extent of release of ILC2 activating signals by damaged cells, leading to different levels of OX40L activation on ILC2s. Alternatively, a technical explanation would be that the IL-33 trap might have been ineffective in neutralising IL-33, resulting in no decrease in OX40L expression. Hence, it still remains unclear the mechanism and implications of radiotherapy-induced OX40L expression on ILC2s.

To investigate the potential role of ILC2s in radiation-induced lung fibrosis, we tried to establish a model of lung fibrosis using the SARRP. Unfortunately, a fractionated regimen of 8.5Gy X 2 was insufficient to induce fibrosis, as observed in the lung 6 months post-irradiation. Thus, it is likely that a significantly higher dose is needed. Alternatively, fibrotic changes could be studied at much later time points. These initial results observing the decline of ILC2s cast doubt over their role in fibrotic progression. Notably, in previous literature demonstrating the role of ILC2s in the bleomycin model of lung fibrosis, ILC2s numbers typically increase and enhanced Type 2 cytokine production is observed. On the other hand, alongside the decline in ILC2 numbers induced by radiotherapy, no changes in IL-13 production was observed, as well as only a slight upregulation of OX40L. Despite this, it is still interesting to consider the dynamics of ILC2 responses at much later time points after radiotherapy. Noteworthily, ILC2 numbers was only monitored up to 8 weeks post-radiotherapy, even though the induction of fibrosis typically occurs from 6 months onwards. (Wirsdorfer and Jendrossek 2016). Indeed, literature has demonstrated that while radiotherapy leads to the decline of specific cell populations like alveolar macrophages acutely, this is accompanied by a strong rebound to much higher levels at much later time points during fibrotic progression (Meziani et al. 2018). Hence, it remains interesting to see if ILC2s could exhibit similar dynamics in response to targeted lung radiotherapy as well.

This model of targeted lung irradiation serves as a good starting point to study the response of ILC2s, as well as broader changes in the lung immune microenvironment. While immune changes have been monitored predominantly at a single dose of 15Gy, differential responses to variable doses of irradiation could be studied. With this model, deeper phenotyping of ILC2s could also be performed by flow cytometry to look at expression of different cell surface markers and cytokines. To understand how ILC2s modulate changes within the immune microenvironment, bulk RNA

sequencing of total immune cell populations could be performed on irradiated controls to irradiated ILC2-deficient mice to identify changes in immune signatures post-irradiation. Furthermore, to specifically study radiotherapy-induced changes in ILC2s, single-cell RNA sequencing on ILC2s can be performed. While much effort is focused on the immune compartment, radiotherapy modulates other cell populations within the lung microenvironment (i.e stromal and epithelial cells) and these other populations can be studied as well. Finally, the immune response induced with this model of targeted irradiation can also be studied in the context of lung tumours, and this was studied in Chapter 5 of the thesis.

6.2 Innate and adaptive immune responses drive radiotherapy-induced anti-tumour immunity

While the role of radiotherapy in the activation of the immune system is increasingly appreciated, it is still not fully understood how radiotherapy modulates the immune response in the context of lung cancer. Furthermore, while the dynamics of ILC2 activation in response to targeted radiotherapy in the healthy lung was studied, it is unclear if ILC2s could modulate anti-tumour responses induced by radiotherapy in this context.

To study radiotherapy-induced anti-tumour responses in the lung, I utilised the B16F10-OVA model of lung metastasis, where B16F10-OVA melanoma cells establish lung metastatic tumours after intravenous administration of tumour cells via the tail vein. Notably, these have been utilised previously in multiple studies examining the role of the immune system in modulating anti-tumour responses induced by radiotherapy (Lugade et al. 2005, 2008; Gupta et al. 2012), though these studies irradiate primary tumours formed in the subcutaneous setting. To the best of my knowledge, only one study has previously utilised the B6F10 cell line in the lung metastatic setting with radiotherapy, and they demonstrated the importance of adaptive CD8+ T-cell in mediating anti-tumour responses (Liu et al. 2019). Notably, minimal profiling of the immune system in response to radiotherapy in this setting has been performed. Thus, I investigated the role of the immune system and ILC2s in modulating anti-tumour responses induced by radiotherapy in this tumour model.

The observation that ILC2s accumulated in relatively early-stage tumours suggests that they likely exert immunomodulatory effects at these early time points, and I postulated that targeted irradiation at these time points could modulate ILC2 function, and thereby influence the tumour microenvironment and anti-tumour responses. However, differences in the anti-tumour efficacy of radiotherapy in a newly established 8.5Gy x 2 fractionated in ILC2-deficient mice strains was not observed, suggesting that ILC2s do not contribute to the anti-tumour efficacy of radiotherapy. As

discussed in the Results section, it is likely that depletion of ILC2s likely mitigated the potential impact of ILC2 activation, thereby minimising its influence on the tumour microenvironment. Hence, combined IL-33 administration to promote ILC2 expansion alongside targeted irradiation was performed, but no significant difference in the anti-tumour effect of radiotherapy was observed either. Notably, IL-33 influences the recruitment of a whole myriad of immune cells alongside ILC2s, which is a key limitation in studying ILC2-specific effects in response to radiotherapy on anti-tumour responses. In all, I found no evidence suggesting that ILC2s influence the anti-tumour response to targeted radiotherapy in this model.

Despite minimal changes in the immune microenvironment post-radiotherapy in the context of metastatic lung cancer, probing activation of the immune system highlighted the importance of the adaptive immune system. As discussed, DCs and CD8+ T-cells are key for the anti-tumour responses induced by radiotherapy as reflected by their activation, and the reduced anti-tumour response in immunodeficient *Rag2*$^{-/-}$ mice. While activation of DCs by radiotherapy has been previously reported (Gupta et al. 2012), upregulation of the T-cell co-stimulation marker CD80 on DCs has been reported to occur specifically in CD103+ cDC1s (Blair et al. 2020), which are known to be crucial for cross-presentation to CD8+ T-cells. Strikingly, similar to my findings that radiotherapy depletes DCs within the tumour microenvironment, a reduction of total DCs was reported, highlighting that the presence of a smaller population of activated DCs is sufficient in inducing anti-tumour immunity. While upregulation of CD80 on XCR1+ cDC1s was demonstrated, CD80 was observed to be upregulated on SIRPα+ cDC2s, highlighting that the upregulation of CD80 on DCs is not cDC1-specific. It has been shown that macrophages upregulate the pro-inflammatory marker CD80 in response to irradiation (Pinto et al. 2016), suggesting that CD80 upregulation could be a broad response of myeloid APCs to targeted irradiation. The upregulation of MHCII on cDC1s was also observed, though this was not observed on cDC2s. This finding was initially surprising, as cDC2s are typically known to preferentially present to CD4+ T-cells via MHCII-TCR interactions. Noteworthily, a recent report highlighted the importance of MHCII on cDC1s in facilitating early priming by CD4+ T-cells, which is crucial to license CD8+ T-cells for anti-tumour immunity (Ferris et al. 2020). This could explain the importance of MHCII upregulation on cDC1s in promoting radiotherapy-induced CD8+ T-cell response in this model.

Interrogating the innate immune compartment also revealed an important role of NK cells, which are also activated and contribute to radiotherapy-mediated anti-tumour immunity. Specifically, the upregulation of IFNγ on NK cells was observed, and depletion of NK cells with an anti-NK1.1 depleting antibody alongside radiotherapy decreased the anti-tumour response, as seen by an increase in the met ratio compared to mice treated with irradiation alone. I attempted to validate

the importance of NK cells using *Rag2*$^{-/-}$*Il2rg*$^{-/-}$ mice lacking both adaptive cells and NK cells, but observed severely increased tumour burden alongside an increase in mice succumbing to tumours at significantly earlier time points (data not shown). This was due to the importance of NK cells in mitigating metastatic tumour seeding (Lopez-Soto et al. 2017), and the large increase in tumour seeding prevented us from accurately assessing tumour burden in these mice. While NK cells are likely the key contributors to anti-tumour innate immune responses to radiotherapy, the role of ILC1s cannot be ruled out. Notably, ILC1s also express NK1.1 and its role cannot be excluded from NK cells by the gating strategy used. The use of other markers such as CD49a and CD49b could be used to distinguish these both populations (Gao et al. 2017). Furthermore, given that these cells could interconvert in the tumour context (Gao et al. 2017), it would be interesting to consider how these populations differ in contributing to immune responses against lung cancer. Nevertheless, given that NK cells are the predominant innate lymphocyte population within the lung, it is likely that NK cells are the NK1.1+ population contributing to radiotherapy-induced anti-tumour immunity.

Notably, experiments assessing the role of the immune system in modulating the effectiveness of radiotherapy demonstrated discrepancies in the met ratio and tumour area ratio. Specifically, while the met ratios highlight the importance of both the adaptive immune system and NK cells in radiotherapy-induced anti-tumour responses, this was not reflected in the tumour area ratio. Notably, both methods have been utilised in literature as a measure of tumour burden in the B16F10 model of lung metastasis, and both typically complement each other as a readout of tumour burden. While the visual counting of metastasis is a straightforward method to quantify tumour burden, a key limitation is that quantification is limited by what is observed on the surface of the lung. On the other hand, the use of Ki67 as a marker for tumour cells in the lung is limited by the fact that only a single slice of tissue is used as a readout. I postulated that these differences are likely due to very small differences in tumour burden. For instance, while the met ratio was enumerated to be higher in the irradiated group treated alongside anti-NK1.1, the size of remaining metastasis in the targeted lobe was observed to be significantly smaller, and these small differences might not have been picked up by tumour area quantification by HALO analysis. To reconcile the differences observed between both methods of quantification, targeted irradiation of the entire lung could be performed instead. This would eliminate the need for data to be expressed as a ratio. However, a key limitation would be the absence of a non-irradiated internal control, and variation in tumour burden in the absence of irradiation cannot be accounted for.

The use of IVIS imaging was attempted alongside quantification by met ratio and tumour area ratio in an experiment with IL-33. However, this was highly limited by significant variation observed between individual mice of the same group. As the left and right lung lobes were in close proximity

during the imaging process, separation of the left and right lung lobes prior to imaging could be performed. This could potentially supplement the quantification methods discussed above. Finally, while quantification of tumour burden in the left and right lung lobe separately allows for an internal control to be present, a potential limitation was that this neglects the potential abscopal effect of radiotherapy, whereby irradiation of tumour in one lung lobe could promote anti-tumour activity in the remaining lobes. Nevertheless, there is no clear evidence in literature highlighting the abscopal effect in the context of lung radiotherapy, as this is mostly seen in the subcutaneous setting.

The mechanism of NK cell activation by radiotherapy in the context of lung cancer in this model is also yet to be discovered. One hypothesis is that radiotherapy-mediated STING activation could be involved in mediating NK cell activation. STING is commonly implicated in radiotherapy-induced anti-tumour responses, leading to the activation of DCs and downstream adaptive CD8+ T-cells (Deng et al. 2014). Notably, NK cells have been shown to mediate STING-mediated anti-tumour responses (Marcus et al. 2018; Nicolai et al. 2020), and are demonstrated to be particularly important in the elimination of tumours that have evaded CD8+ T-cell detection via downregulation of MHC-I (Nicolai et al. 2020). However, it has yet to be shown if a radiotherapy-STING-NK cell axis is present within the lung tumour context that mediates anti-tumour response and this is an avenue that warrants further investigation. Apart from STING, radiotherapy is known to modulate the repertoire of NK cell ligands and NK cell receptor expression within the tumour microenvironment, which could influence NK cell anti-tumour function (Spiotto, Fu, and Weichselbaum 2016). For instance, a recent paper demonstrated that human NK cells in pancreatic cancer are activated by radiotherapy in a CXCL8-dependent manner, contributing to NK cell anti-tumour function (Walle et al. 2022). Thus, further work could focus on probing the cytokines released by radiotherapy, as well as further profiling lung NK cells to monitor differences in expression of activation markers induced by radiotherapy.

6.3 A model to study the role of ILC2s in modulating adaptive immune responses in primary lung cancer

ILC2s are known to regulate adaptive immune responses in the context of Type 2 inflammation, and extensive work has been done in such models to elucidate the mechanisms involved. However, less is known about how ILC2s regulate adaptive immune responses in the context of cancer, and even less so in the context of lung cancer. Hence, I developed a model to study the role of ILC2s in modulating adaptive immune responses in lung cancer.

I first validated an iOVA expression construct *in vitro* and *in vivo* and demonstrated inducible expression of both GFP and the OVA antigen. However, the *in vitro* killing assay of B16F10-iOVA cells demonstrated some baseline expression of OVA, as B16F10-iOVA cells cultured in the absence of tetracycline were more susceptible to killing by OVA-specific OT-I CD8+ T-cells as compared to parental B16F10 cells. This was unexpected, as while the rtTA alone was previously demonstrated to possess some "leakiness" in the absence of tetracycline (Zheng et al. 2000), the presence of an accompanying tTS component was reported to eliminate baseline "leakiness" (Zhu et al. 2001). A possible explanation was that standard FCS containing low levels of tetracycline was present in the culture during these experiments. Due to the sensitivity of this system, low levels of tetracycline present in culture would still be able to induced expression of the antigen. Alternatively, this could be due to a potential delay in the removal and degradation of OVA, as cells were previously cultured extensively in the presence of tetracycline during the transfection, selection and expansion process during the generation of these cells. Thus, these cells could be passaged in the absence of tetracycline to prevent OVA expression, as well as for previously expressed OVA to be removed and degraded. A potential improvement to such a system could be achieved by utilising a combination of both tetracycline and tamoxifen-controlled systems (Hegde et al. 2020). Tamoxifen-inducible systems, unlike tetracycline-inducible systems, are irreversible systems. In the presence of tamoxifen, the Cre recombinase induces cleavage of target sequences flanked by loxP sites, resulting in permanent removal of flanked sequences. In the paper referenced, a system combining both elements was utilised to control the expression of the OVA antigen, where the introduction of tamoxifen, as well as the absence of tetracycline, induces the expression of OVA.

While the ability of the iOVA construct to induce OVA expression was studied, the ability of B16F10-iOVA cells to stop the expression of OVA in the absence of tetracycline was not assessed. This could easily be achieved by setting up an *in vitro* culture similar to Figure 5.4 and then monitoring OVA expression by Western blot in a time-course experiment. Regardless, *in vitro* confirmation of GFP expression in Figure 5.4 would suggest reversibility of OVA expression as well, as the expression of both genes is controlled by the same promoter. Notably, the majority of literature using such systems typically look at responses induced by antigen expression, rather than the removal of said antigen. Nevertheless, a reversible system like this could potentially be used to study responses during the initial infection, as well as secondary immune responses and memory responses that occur after antigen re-exposure (Jellison Evan R. et al. 2012).

The ability of OVA expression to drive OVA-specific T-cells responses was also confirmed via the use of Class II MHC tetramers. Notably, antigen expression by tumours could induce antigen-specific T-cells responses, which could affect tumour progression depending on the nature of these responses.

Indeed, using a similar inducible antigen-expressing tumour model, it was shown that the induction of OVA by tetracycline induces CD8+ T-cell responses that decrease tumour burden in a model of hepatocellular carcinoma (McVey et al. 2022). On the other hand, we observed no difference in tumour burden *in vivo* with mouse kept on doxycycline diet in this model. This might be attributed to differences in the tumour model used, even though the literature suggests an important role of CD8+ T-cells in mediating anti-tumour responses in the B16F10 model of lung metastasis. Nevertheless, I have only profiled OVA-specific CD4+ T-cell responses, and further work is needed to carefully characterise the immune response driven by induction of OVA by tetracycline in this model.

dKP cells were also derived from KP mice, and their ability to form primary lung tumours by orthotopic lung implantation was assessed. A limitation of the orthotopic model of dKP cells was that these cells grew very slowly within the lung. This was expected as this cell line was derived from relatively early-stage tumours. To accelerate tumour growth, a greater number of cells could be injected. However, this could increase the chances of leakage of cells into the chest cavity, which is a problem further discussed in the next paragraph. Alternatively, the introduction of further mutations by genome-editing techniques could generate more aggressive versions of this cell line. Nevertheless, a careful balance has to be struck as the primary goal is the formation of early-stage primary lung tumours.

Another limitation of the orthotopic implantation of dKP cells is the leakage of tumours into the chest cavity. Notably, the establishment of tumours within the chest cavity led to mice succumbing to their humane endpoint much quicker than the time needed to establish sizeable tumours within the lung. This is likely due to the protocol that was established, which is minimally invasive and does not require incisions to be made. Thus, this setup is more prone to errors as I was unable to establish the exact position of the lung and the optimum depth at which the needle should be inserted. Several steps were taken to try to circumvent the leakage observed in these experiments. Firstly, the needle gauge was increased from 27G to 30G to allow for a more localised injection and hence reduce spreading and leakage. Secondly, the concentration of matrigel use was also increased to limit spreading. Finally, I also tried to reduce the volume of cells injected via the use of specialised glass syringes that could inject extremely lower volumes. In the LL/2 Lewis lung carcinoma model, which required the injection of a significantly less number of tumour cells to establish lung tumours, injection of lower volumes still led to the establishment of tumours within the chest cavity. Thus, despite these efforts, the leakage of tumour cells into the lung chest cavity remained a problem.

Moving forward, more in-depth surgical methods could be employed. Though more technically challenging, this could greatly improve the accuracy of injection to establish solitary tumours. These

procedures typically involve the incision of soft tissues to expose the thoracic rib and intercostal space to allow better visualisation of the lung (Justilien and Fields 2013). In a more surgically-advanced setting, thoracotomy could also be performed to expose the lung to achieve greater precision of injection (Im et al. 2014). Thus, with the right level of technical expertise, such procedures could be performed to combat issues of leakiness of tumour cells within the chest cavity.

The development of this model remains in its early stages. While I have validated the functionality of the iOVA construct, this needs to be tested in the context of the dKP cell line. Furthermore, optimisation of the orthotopic implantation procedure is necessary to ensure the establishment of local tumours by dKP cells within the lung. Once the above-mentioned steps are accomplished, implantation of the tumour cells into ILC2-deficient mice could be performed to elucidate the role of ILC2s in modulating the adaptive immune response in lung cancer.

Importantly, the use of radiotherapy as a treatment modality could be incorporated into this model. As discussed in previous chapters, radiotherapy induces the killing of tumour cells and antigen release into the surrounding microenvironment. Released antigens could then be processed by the endocytic pathway, and subsequently presented by MHCII to induce CD4+ T-cell responses (Roche and Furuta 2015). Thus, the role of ILC2s in modulating CD4+ T-cells responses could also be studied in the context of radiotherapy using such a model.

References

Akinci Ozyurek, B., T. Sahin Ozdemirel, S. Buyukyaylaci Ozden, Y. Erdogan, B. Kaplan, and T. Kaplan. 2017. "Prognostic Value of the Neutrophil to Lymphocyte Ratio (NLR) in Lung Cancer Cases." *Asian Pacific Journal of Cancer Prevention: APJCP* 18 (5): 1417–21.

Alegre, Maria-Luisa, Kenneth A. Frauwirth, and Craig B. Thompson. 2001. "T-Cell Regulation by CD28 and CTLA-4." *Nature Reviews. Immunology* 1 (3): 220–28.

Alexandrov, L. B., Y. S. Ju, K. Haase, P. Van Loo, I. Martincorena, S. Nik-Zainal, Y. Totoki, et al. 2016. "Mutational Signatures Associated with Tobacco Smoking in Human Cancer." *Science* 354 (6312): 618–22.

Altorki, N. K., G. J. Markowitz, D. Gao, J. L. Port, A. Saxena, B. Stiles, T. McGraw, and V. Mittal. 2019. "The Lung Microenvironment: An Important Regulator of Tumour Growth and Metastasis." *Nature Reviews. Cancer* 19 (1): 9–31.

Arina, A., M. Beckett, C. Fernandez, W. Zheng, S. Pitroda, S. J. Chmura, J. J. Luke, et al. 2019. "Tumor-Reprogrammed Resident T Cells Resist Radiation to Control Tumors." *Nature Communications* 10 (1): 3959.

Arnal-Estapé, Anna, Wesley L. Cai, Alexandra E. Albert, Minghui Zhao, Laura E. Stevens, Francesc López-Giráldez, Kiran D. Patel, et al. 2020. "Tumor Progression and Chromatin Landscape of Lung Cancer Are Regulated by the Lineage Factor GATA6." *Oncogene* 39 (18): 3726–37.

Artis, D., and H. Spits. 2015. "The Biology of Innate Lymphoid Cells." *Nature* 517 (7534): 293–301.

Bade, B. C., and C. S. Dela Cruz. 2020. "Lung Cancer 2020: Epidemiology, Etiology, and Prevention." *Clinics in Chest Medicine* 41 (1): 1–24.

Barlow, J. L., A. Bellosi, C. S. Hardman, L. F. Drynan, S. H. Wong, J. P. Cruickshank, and A. N. McKenzie. 2012. "Innate IL-13-Producing Nuocytes Arise during Allergic Lung Inflammation and Contribute to Airways Hyperreactivity." *The Journal of Allergy and Clinical Immunology* 129 (1): 191-8 e1-4.

Barsoumian, Hampartsoum B., Rishab Ramapriyan, Ahmed I. Younes, Mauricio S. Caetano, Hari Menon, Nathan I. Comeaux, Taylor R. Cushman, et al. 2020. "Low-Dose Radiation Treatment Enhances Systemic Antitumor Immune Responses by Overcoming the Inhibitory Stroma." *Journal for Immunotherapy of Cancer* 8 (2). https://doi.org/10.1136/jitc-2020-000537.

Bedford, James L., Vibeke Nordmark Hansen, Helen A. McNair, Alexandra H. Aitken, Juliet E. C. Brock, Alan P. Warrington, and Michael Brada. 2008. "Treatment of Lung Cancer Using Volumetric Modulated Arc Therapy and Image Guidance: A Case Study." *Acta Oncologica* 47 (7): 1438–43.

Bernink, Jochem H., Yoichiro Ohne, Marcel B. M. Teunissen, Jingya Wang, Jincheng Wu, Lisette Krabbendam, Christine Guntermann, et al. 2019. "C-Kit-Positive ILC2s Exhibit an ILC3-like Signature That May Contribute to IL-17-Mediated Pathologies." *Nature Immunology* 20 (8): 992–1003.

Bezjak, Andrea, Peter Dixon, Michael Brundage, Dong Sheng Tu, Michael J. Palmer, Paul Blood, Clive Grafton, et al. 2002. "Randomized Phase III Trial of Single versus Fractionated Thoracic Radiation in the Palliation of Patients with Lung Cancer (NCIC CTG SC.15)." *International Journal of Radiation Oncology*Biology*Physics* 54 (3): 719–28.

Blair, Tiffany C., Shelly Bambina, Alejandro F. Alice, Gwen F. Kramer, Terry R. Medler, Jason R. Baird, Miranda L. Broz, et al. 2020. "Dendritic Cell Maturation Defines Immunological Responsiveness of Tumors to Radiation Therapy." *Journal of Immunology* 204 (12): 3416–24.

Bray, F., J. Ferlay, I. Soerjomataram, R. L. Siegel, L. A. Torre, and A. Jemal. 2018. "Global Cancer Statistics 2018: GLOBOCAN Estimates of Incidence and Mortality Worldwide for 36 Cancers in 185 Countries." *CA: A Cancer Journal for Clinicians* 68 (6): 394–424.

Bruce, D. W., H. E. Stefanski, B. G. Vincent, T. A. Dant, S. Reisdorf, H. Bommiasamy, D. A. Serody, et al. 2017. "Type 2 Innate Lymphoid Cells Treat and Prevent Acute Gastrointestinal Graft-versus-Host Disease." *The Journal of Clinical Investigation* 127 (5): 1813–25.

Bucci, M. K., A. Bevan, and M. Roach 3rd. 2005. "Advances in Radiation Therapy: Conventional to 3D, to IMRT, to 4D, and Beyond." *CA: A Cancer Journal for Clinicians* 55 (2): 117–34.

Buchwald, Z. S., J. Wynne, T. H. Nasti, S. Zhu, W. F. Mourad, W. Yan, S. Gupta, S. N. Khleif, and M. K. Khan. 2018. "Radiation, Immune Checkpoint Blockade and the Abscopal Effect: A Critical Review on Timing, Dose and Fractionation." *Frontiers in Oncology* 8: 612.

Budhu, Sadna, John D. Loike, Ashley Pandolfi, Soo Han, Geoffrey Catalano, Andrei Constantinescu, Raphael Clynes, and Samuel C. Silverstein. 2010. "CD8+ T Cell Concentration Determines Their Efficiency in Killing Cognate Antigen-Expressing Syngeneic Mammalian Cells in Vitro and in Mouse Tissues." *The Journal of Experimental Medicine* 207 (1): 223–35.

Califano, D., Y. Furuya, S. Roberts, D. Avram, A. N. J. McKenzie, and D. W. Metzger. 2018. "IFN-γ Increases Susceptibility to Influenza A Infection through Suppression of Group II Innate Lymphoid Cells." *Mucosal Immunology*. https://doi.org/10.1038/mi.2017.41.

Cancer Genome Atlas Research, Network. 2014. "Comprehensive Molecular Profiling of Lung Adenocarcinoma." *Nature* 511 (7511): 543–50.

Canli, O., A. M. Nicolas, J. Gupta, F. Finkelmeier, O. Goncharova, M. Pesic, T. Neumann, et al. 2017. "Myeloid Cell-Derived Reactive Oxygen Species Induce Epithelial Mutagenesis." *Cancer Cell* 32 (6): 869-883 e5.

Carrega, P., and G. Ferlazzo. 2017. “Natural Killers Are Made Not Born: How to Exploit NK Cells in Lung Malignancies.” *Frontiers in Immunology* 8: 277.

Chakravarty, P. K., A. Alfieri, E. K. Thomas, V. Beri, K. E. Tanaka, B. Vikram, and C. Guha. 1999. “Flt3-Ligand Administration after Radiation Therapy Prolongs Survival in a Murine Model of Metastatic Lung Cancer.” *Cancer Research* 59 (24): 6028–32.

Chen, Jiarui, Xingyu Liu, Zihang Zeng, Jiali Li, Yuan Luo, Wenjie Sun, Yan Gong, Junhong Zhang, Qiuji Wu, and Conghua Xie. 2020. “Immunomodulation of NK Cells by Ionizing Radiation.” *Frontiers in Oncology* 10 (June): 874.

Chen, Jing, Yacheng Wang, Zijie Mei, Shimin Zhang, Jie Yang, Xin Li, Ye Yao, and Conghua Xie. 2016. “Radiation-Induced Lung Fibrosis in a Tumor-Bearing Mouse Model Is Associated with Enhanced Type-2 Immunity.” *Journal of Radiation Research* 57 (2): 133–41.

Chen, M., G. Qiao, B. L. Hylander, H. Mohammadpour, X. Y. Wang, J. R. Subjeck, A. K. Singh, and E. A. Repasky. 2020. “Adrenergic Stress Constrains the Development of Anti-Tumor Immunity and Abscopal Responses Following Local Radiation.” *Nature Communications* 11 (1): 1821.

Cheng, Jia-Nan, Wen Luo, Chengdu Sun, Zheng Jin, Xianghua Zeng, Peter B. Alexander, Zhihua Gong, et al. 2021. “Radiation-Induced Eosinophils Improve Cytotoxic T Lymphocyte Recruitment and Response to Immunotherapy.” *Science Advances* 7 (5). https://doi.org/10.1126/sciadv.abc7609.

Cheng, M., S. Jolly, W. O. Quarshie, N. Kapadia, F. D. Vigneau, and F. S. Kong. 2019. “Modern Radiation Further Improves Survival in Non-Small Cell Lung Cancer: An Analysis of 288,670 Patients.” *Journal of Cancer* 10 (1): 168–77.

Chevalier, Mathieu F., Sara Trabanelli, Julien Racle, Bérengère Salomé, Valérie Cesson, Dalila Gharbi, Perrine Bohner, et al. 8 2017. “ILC2-Modulated T Cell–to-MDSC Balance Is Associated with Bladder Cancer Recurrence.” *The Journal of Clinical Investigation* 127 (8): 2916–29.

Coffelt, S. B., K. Kersten, C. W. Doornebal, J. Weiden, K. Vrijland, C. S. Hau, N. J. M. Verstegen, et al. 2015. “IL-17-Producing Gammadelta T Cells and Neutrophils Conspire to Promote Breast Cancer Metastasis.” *Nature* 522 (7556): 345–48.

Cohn, L., R. J. Homer, A. Marinov, J. Rankin, and K. Bottomly. 1997. “Induction of Airway Mucus Production By T Helper 2 (Th2) Cells: A Critical Role for Interleukin 4 in Cell Recruitment but Not Mucus Production.” *The Journal of Experimental Medicine* 186 (10): 1737–47.

Constantinides, Michael G., Benjamin D. McDonald, Philip A. Verhoef, and Albert Bendelac. 2014. “A Committed Precursor to Innate Lymphoid Cells.” *Nature* 508 (7496): 397–401.

Corrales, Luis, Katherine Scilla, Christian Caglevic, Ken Miller, Julio Oliveira, and Christian Rolfo. 2018. “Immunotherapy in Lung Cancer: A New Age in Cancer Treatment.” In *Immunotherapy*, edited by Aung Naing and Joud Hajjar, 65–95. Cham: Springer International Publishing.

Cronin, K. A., A. J. Lake, S. Scott, R. L. Sherman, A. M. Noone, N. Howlader, S. J. Henley, et al. 2018. “Annual Report to the Nation on the Status of Cancer, Part I: National Cancer Statistics.” *Cancer* 124 (13): 2785–2800.

Cross, C. K., S. Berman, L. Buswell, B. Johnson, and E. H. Baldini. 2004. “Prospective Study of Palliative Hypofractionated Radiotherapy (8.5 Gy x 2) for Patients with Symptomatic Non-Small-Cell Lung Cancer.” *International Journal of Radiation Oncology, Biology, Physics* 58 (4): 1098–1105.

Cui, Zheng Yun, Jin Seok Ahn, Jee Yun Lee, Won Seog Kim, Ho Yeong Lim, Hyun Jung Jeon, Soo Won Suh, et al. 2006. “Mouse Orthotopic Lung Cancer Model Induced by PC14PE6.” *Cancer Research and Treatment: Official Journal of Korean Cancer Association* 38 (4): 234–39.

D’Angelo, S. P., and M. C. Pietanza. 2010. “The Molecular Pathogenesis of Small Cell Lung Cancer.” *Cancer Biology & Therapy* 10 (1): 1–10.

Dasari, S., and P. B. Tchounwou. 2014. “Cisplatin in Cancer Therapy: Molecular Mechanisms of Action.” *European Journal of Pharmacology* 740: 364–78.

Demaria, S., B. Ng, M. L. Devitt, J. S. Babb, N. Kawashima, L. Liebes, and S. C. Formenti. 2004. “Ionizing Radiation Inhibition of Distant Untreated Tumors (Abscopal Effect) Is Immune Mediated.” *International Journal of Radiation Oncology, Biology, Physics* 58 (3): 862–70.

Demaria, Sandra, Chandan Guha, Jonathan Schoenfeld, Zachary Morris, Arta Monjazeb, Andrew Sikora, Marka Crittenden, et al. 2021. “Radiation Dose and Fraction in Immunotherapy: One-Size Regimen Does Not Fit All Settings, so How Does One Choose?” *Journal for Immunotherapy of Cancer* 9 (4): e002038.

Deng, L., H. Liang, M. Xu, X. Yang, B. Burnette, A. Arina, X. D. Li, et al. 2014. “STING-Dependent Cytosolic DNA Sensing Promotes Radiation-Induced Type I Interferon-Dependent Antitumor Immunity in Immunogenic Tumors.” *Immunity* 41 (5): 843–52.

Denney, L., A. J. Byrne, T. J. Shea, J. S. Buckley, J. E. Pease, G. M. Herledan, S. A. Walker, L. G. Gregory, and C. M. Lloyd. 2015. “Pulmonary Epithelial Cell-Derived Cytokine TGF-Beta1 Is a Critical Cofactor for Enhanced Innate Lymphoid Cell Function.” *Immunity* 43 (5): 945–58.

Dewan, M. Zahidunnabi, Ashley E. Galloway, Noriko Kawashima, J. Keith Dewyngaert, James S. Babb, Silvia C. Formenti, and Sandra Demaria. 2009. “Fractionated but Not Single-Dose Radiotherapy Induces an Immune-Mediated Abscopal Effect When Combined with Anti-CTLA-4 Antibody.” *Clinical Cancer Research: An Official Journal of the American Association for Cancer Research* 15 (17): 5379–88.

Ding, L., G. Getz, D. A. Wheeler, E. R. Mardis, M. D. McLellan, K. Cibulskis, C. Sougnez, et al. 2008. “Somatic Mutations Affect Key Pathways in Lung Adenocarcinoma.” *Nature* 455 (7216): 1069–75.

Doki, Y., K. Murakami, T. Yamaura, S. Sugiyama, T. Misaki, and I. Saiki. 1999. “Mediastinal Lymph Node Metastasis Model by Orthotopic Intrapulmonary Implantation of Lewis Lung Carcinoma Cells in Mice.” *British Journal of Cancer* 79 (7–8): 1121–26.

Doroshow, D. B., M. F. Sanmamed, K. Hastings, K. Politi, D. L. Rimm, L. Chen, I. Melero, K. A. Schalper, and R. S. Herbst. 2019. “Immunotherapy in Non-Small Cell Lung Cancer: Facts and Hopes.” *Clinical Cancer Research: An Official Journal of the American Association for Cancer Research* 25 (15): 4592–4602.

Drake, L. Y., K. Iijima, and H. Kita. 2014. “Group 2 Innate Lymphoid Cells and CD4+ T Cells Cooperate to Mediate Type 2 Immune Response in Mice.” *Allergy* 69 (10): 1300–1307.

Du, S., V. Lockamy, L. Zhou, C. Xue, J. LeBlanc, S. Glenn, G. Shukla, et al. 2016. “Stereotactic Body Radiation Therapy Delivery in a Genetically Engineered Mouse Model of Lung Cancer.” *International Journal of Radiation Oncology, Biology, Physics* 96 (3): 529–37.

Duan, M. C., W. Han, P. W. Jin, Y. P. Wei, Q. Wei, L. M. Zhang, and J. C. Li. 2015. “Disturbed Th17/Treg Balance in Patients with Non-Small Cell Lung Cancer.” *Inflammation* 38 (6): 2156–65.

Duerr, C. U., C. D. McCarthy, B. C. Mindt, M. Rubio, A. P. Meli, J. Pothlichet, M. M. Eva, et al. 2016. “Type I Interferon Restricts Type 2 Immunopathology through the Regulation of Group 2 Innate Lymphoid Cells.” *Nature Immunology* 17 (1): 65–75.

DuPage, M., A. L. Dooley, and T. Jacks. 2009. “Conditional Mouse Lung Cancer Models Using Adenoviral or Lentiviral Delivery of Cre Recombinase.” *Nature Protocols* 4 (7): 1064–72.

Eruslanov, E. B., P. S. Bhojnagarwala, J. G. Quatromoni, T. L. Stephen, A. Ranganathan, C. Deshpande, T. Akimova, et al. 2014. “Tumor-Associated Neutrophils Stimulate T Cell Responses in Early-Stage Human Lung Cancer.” *The Journal of Clinical Investigation* 124 (12): 5466–80.

Ferris, S. T., V. Durai, R. Wu, D. J. Theisen, J. P. Ward, M. D. Bern, J. T. th Davidson, et al. 2020. “CDC1 Prime and Are Licensed by CD4(+) T Cells to Induce Anti-Tumour Immunity.” *Nature*. https://doi.org/10.1038/s41586-020-2611-3.

Filatenkov, Alexander, Jeanette Baker, Antonia M. S. Mueller, Justin Kenkel, G-One Ahn, Suparna Dutt, Nigel Zhang, et al. 2015. “Ablative Tumor Radiation Can Change the Tumor Immune Cell Microenvironment to Induce Durable Complete Remissions.” *Clinical Cancer Research: An Official Journal of the American Association for Cancer Research* 21 (16): 3727–39.

Formenti, S. C., N. P. Rudqvist, E. Golden, B. Cooper, E. Wennerberg, C. Lhuillier, C. Vanpouille-Box, et al. 2018. “Radiotherapy Induces Responses of Lung Cancer to CTLA-4 Blockade.” *Nature Medicine* 24 (12): 1845–51.

Fridlender, Z. G., J. Sun, S. Kim, V. Kapoor, G. Cheng, L. Ling, G. S. Worthen, and S. M. Albelda. 2009. “Polarization of Tumor-Associated Neutrophil Phenotype by TGF-Beta: ‘N1’ versus ‘N2’ TAN.” *Cancer Cell* 16 (3): 183–94.

Fritz, J. M., M. A. Tennis, D. J. Orlicky, H. Lin, C. Ju, E. F. Redente, K. S. Choo, et al. 2014. “Depletion of Tumor-Associated Macrophages Slows the Growth of Chemically Induced Mouse Lung Adenocarcinomas.” *Frontiers in Immunology* 5: 587.

Gameiro, Sofia R., Momodou L. Jammeh, Max M. Wattenberg, Kwong Y. Tsang, Soldano Ferrone, and James W. Hodge. 2014. “Radiation-Induced Immunogenic Modulation of Tumor Enhances Antigen Processing and Calreticulin Exposure, Resulting in Enhanced T-Cell Killing.” *Oncotarget* 5 (2): 403–16.

Ganesan, A. P., M. Johansson, B. Ruffell, A. Yagui-Beltran, J. Lau, D. M. Jablons, and L. M. Coussens. 2013. “Tumor-Infiltrating Regulatory T Cells Inhibit Endogenous Cytotoxic T Cell Responses to Lung Adenocarcinoma.” *Journal of Immunology* 191 (4): 2009–17.

Gao, Y., P. Dorn, S. Liu, H. Deng, S. R. R. Hall, R. W. Peng, R. A. Schmid, and T. M. Marti. 2019. “Cisplatin-Resistant A549 Non-Small Cell Lung Cancer Cells Can Be Identified by Increased Mitochondrial Mass and Are Sensitive to Pemetrexed Treatment.” *Cancer Cell International* 19: 317.

Gao, Yulong, Fernando Souza-Fonseca-Guimaraes, Tobias Bald, Susanna S. Ng, Arabella Young, Shin Foong Ngiow, Jai Rautela, et al. 2017. “Tumor Immunoevasion by the Conversion of Effector NK Cells into Type 1 Innate Lymphoid Cells.” *Nature Immunology* 18 (9): 1004–15.

Garnett, Charlie T., Claudia Palena, Mala Chakraborty, Kwong-Yok Tsang, Jeffrey Schlom, and James W. Hodge. 2004. “Sublethal Irradiation of Human Tumor Cells Modulates Phenotype Resulting in Enhanced Killing by Cytotoxic T Lymphocytes.” *Cancer Research* 64 (21): 7985–94.

Garon, E. B., N. A. Rizvi, R. Hui, N. Leighl, A. S. Balmanoukian, J. P. Eder, A. Patnaik, et al. 2015. “Pembrolizumab for the Treatment of Non-Small-Cell Lung Cancer.” *The New England Journal of Medicine* 372 (21): 2018–28.

Gasser, Stephan, Sandra Orsulic, Eric J. Brown, and David H. Raulet. 2005. “The DNA Damage Pathway Regulates Innate Immune System Ligands of the NKG2D Receptor.” *Nature* 436 (7054): 1186–90.

George, J., J. S. Lim, S. J. Jang, Y. Cun, L. Ozretic, G. Kong, F. Leenders, et al. 2015. “Comprehensive Genomic Profiles of Small Cell Lung Cancer.” *Nature* 524 (7563): 47–53.

Gieseck, Richard L., 3rd, Mark S. Wilson, and Thomas A. Wynn. 2018. “Type 2 Immunity in Tissue Repair and Fibrosis.” *Nature Reviews. Immunology* 18 (1): 62–76.

Golden, Encouse B., and Lionel Apetoh. 2015. “Radiotherapy and Immunogenic Cell Death.” *Seminars in Radiation Oncology* 25 (1): 11–17.

Golden, Encouse B., Derek Frances, Ilenia Pellicciotta, Sandra Demaria, Mary Helen Barcellos-Hoff, and Silvia C. Formenti. 2014. “Radiation Fosters Dose-Dependent and Chemotherapy-Induced Immunogenic Cell Death.” *Oncoimmunology* 3 (April): e28518.

Golebski, Korneliusz, Xavier R. Ros, Maho Nagasawa, Sophie van Tol, Balthasar A. Heesters, Hajar Aglmous, Chantal M. A. Kradolfer, et al. 2019. “IL-1β, IL-23, and TGF-β Drive Plasticity of Human ILC2s towards IL-17-Producing ILCs in Nasal Inflammation.” *Nature Communications* 10 (1): 1–15.

Granot, Z., E. Henke, E. A. Comen, T. A. King, L. Norton, and R. Benezra. 2011. “Tumor Entrained Neutrophils Inhibit Seeding in the Premetastatic Lung.” *Cancer Cell* 20 (3): 300–314.

Gupta, A., H. C. Probst, V. Vuong, A. Landshammer, S. Muth, H. Yagita, R. Schwendener, M. Pruschy, A. Knuth, and M. van den Broek. 2012. “Radiotherapy Promotes Tumor-Specific Effector CD8+ T Cells via Dendritic Cell Activation.” *Journal of Immunology* 189 (2): 558–66.

Gupta, Sarthak, Diana W. Chan, Kristien J. Zaal, and Mariana J. Kaplan. 2018. “A High-Throughput Real-Time Imaging Technique To Quantify NETosis and Distinguish Mechanisms of Cell Death in Human Neutrophils.” *Journal of Immunology* 200 (2): 869–79.

Hahn, I., A. Klaus, R. Maus, J. W. Christman, T. Welte, and U. A. Maus. 2011. “Dendritic Cell Depletion and Repopulation in the Lung after Irradiation and Bone Marrow Transplantation in Mice.” *American Journal of Respiratory Cell and Molecular Biology* 45 (3): 534–41.

Halim, T. Y. F., B. M. J. Rana, J. A. Walker, B. Kerscher, M. D. Knolle, H. E. Jolin, E. M. Serrao, et al. 2018. “Tissue-Restricted Adaptive Type 2 Immunity Is Orchestrated by Expression of the Costimulatory Molecule OX40L on Group 2 Innate Lymphoid Cells.” *Immunity* 48 (6): 1195-1207 e6.

Halim, T. Y., Y. Y. Hwang, S. T. Scanlon, H. Zaghouani, N. Garbi, P. G. Fallon, and A. N. McKenzie. 2016. “Group 2 Innate Lymphoid Cells License Dendritic Cells to Potentiate Memory TH2 Cell Responses.” *Nature Immunology* 17 (1): 57–64.

Halim, T. Y., C. A. Steer, L. Matha, M. J. Gold, I. Martinez-Gonzalez, K. M. McNagny, A. N. McKenzie, and F. Takei. 2014. “Group 2 Innate Lymphoid Cells Are Critical for the Initiation of Adaptive T Helper 2 Cell-Mediated Allergic Lung Inflammation.” *Immunity* 40 (3): 425–35.

Halim, Timotheus Y. F., Ramona H. Krauss, Ann C. Sun, and Fumio Takei. 2012. “Lung Natural Helper Cells Are a Critical Source of Th2 Cell-Type Cytokines in Protease Allergen-Induced Airway Inflammation.” *Immunity* 36 (3): 451–63.

Halim, Timotheus Y. F., Aric MacLaren, Mark T. Romanish, Matthew J. Gold, Kelly M. McNagny, and Fumio Takei. 2012. “Retinoic-Acid-Receptor-Related Orphan Nuclear Receptor Alpha Is Required for Natural Helper Cell Development and Allergic Inflammation.” *Immunity* 37 (3): 463–74.

Hams, E., M. E. Armstrong, J. L. Barlow, S. P. Saunders, C. Schwartz, G. Cooke, R. J. Fahy, et al. 2014. “IL-25 and Type 2 Innate Lymphoid Cells Induce Pulmonary Fibrosis.” *Proceedings of the National Academy of Sciences of the United States of America* 111 (1): 367–72.

Hardman, C. S., V. Panova, and A. N. McKenzie. 2013. “IL-33 Citrine Reporter Mice Reveal the Temporal and Spatial Expression of IL-33 during Allergic Lung Inflammation.” *European Journal of Immunology* 43 (2): 488–98.

Hegde, S., V. E. Krisnawan, B. H. Herzog, C. Zuo, M. A. Breden, B. L. Knolhoff, G. D. Hogg, et al. 2020. “Dendritic Cell Paucity Leads to Dysfunctional Immune Surveillance in Pancreatic Cancer.” *Cancer Cell* 37 (3): 289-307 e9.

Hellevik, Turid, and Iñigo Martinez-Zubiaurre. 2014. “Radiotherapy and the Tumor Stroma: The Importance of Dose and Fractionation.” *Frontiers in Oncology* 4 (January): 1.

Herbst, R. S., D. Morgensztern, and C. Boshoff. 2018. “The Biology and Management of Non-Small Cell Lung Cancer.” *Nature* 553 (7689): 446–54.

Herter-Sprie, G. S., H. Korideck, C. L. Christensen, J. M. Herter, K. Rhee, R. I. Berbeco, D. G. Bennett, et al. 2014. “Image-Guided Radiotherapy Platform Using Single Nodule Conditional Lung Cancer Mouse Models.” *Nature Communications* 5: 5870.

Hong, Jun Young, J. Kelley Bentley, Yutein Chung, Jing Lei, Jessica M. Steenrod, Qiang Chen, Uma S. Sajjan, and Marc B. Hershenson. 2014. “Neonatal Rhinovirus Induces Mucous Metaplasia and Airways Hyperresponsiveness through IL-25 and Type 2 Innate Lymphoid Cells.” *The Journal of Allergy and Clinical Immunology* 134 (2): 429–39.

Howard, Emily, Benjamin P. Hurrell, Doumet Georges Helou, Christine Quach, Jacob D. Painter, Pedram Shafiei-Jahani, Marshall Fung, et al. 2021. “PD-1 Blockade on Tumor Microenvironment-Resident ILC2s Promotes TNF-α Production and Restricts Progression of Metastatic Melanoma.” *Frontiers in Immunology* 12 (August): 733136.

Hoyler, Thomas, Christoph S. N. Klose, Abdallah Souabni, Adriana Turqueti-Neves, Dietmar Pfeifer, Emma L. Rawlins, David Voehringer, Meinrad Busslinger, and Andreas Diefenbach. 2012. “The Transcription Factor GATA-3 Controls Cell Fate and Maintenance of Type 2 Innate Lymphoid Cells.” *Immunity* 37 (4): 634–48.

Huang, Y., L. Guo, J. Qiu, X. Chen, J. Hu-Li, U. Siebenlist, P. R. Williamson, J. F. Urban Jr, and W. E. Paul. 2015. “IL-25-Responsive, Lineage-Negative KLRG1(Hi) Cells Are Multipotential ‘inflammatory’ Type 2 Innate Lymphoid Cells.” *Nature Immunology* 16 (2): 161–69.

Hurst, Stephen D., Tony Muchamuel, Daniel M. Gorman, Jonathan M. Gilbert, Theresa Clifford, Sylvia Kwan, Satish Menon, et al. 2002. “New IL-17 Family Members Promote Th1 or Th2 Responses in the Lung: In Vivo Function of the Novel Cytokine IL-25.” *Journal of Immunology* 169 (1): 443–53.

Ikutani, M., T. Yanagibashi, M. Ogasawara, K. Tsuneyama, S. Yamamoto, Y. Hattori, T. Kouro, et al. 2012. “Identification of Innate IL-5-Producing Cells and Their Role in Lung Eosinophil Regulation and Antitumor Immunity.” *Journal of Immunology* 188 (2): 703–13.

Im, Geun Ho, Moon-Sun Jang, Julius Juhyun Chung, Kyoung-Nam Kim, Jae-Hun Kim, Sun I. Kim, and Jung Hee Lee. 2014. “Improvement of Orthotopic Lung Cancer Mouse Model via Thoracotomy and Orotracheal Intubation Enabling in Vivo Imaging Studies.” *Laboratory Animals* 48 (2): 124–31.

Iwai, Yoshiko, Masayoshi Ishida, Yoshimasa Tanaka, Taku Okazaki, Tasuku Honjo, and Nagahiro Minato. 2002. “Involvement of PD-L1 on Tumor Cells in the Escape from Host Immune System and Tumor Immunotherapy by PD-L1 Blockade.” *Proceedings of the National Academy of Sciences* 99 (19): 12293.

Iwanaga, K., Y. Yang, M. G. Raso, L. Ma, A. E. Hanna, N. Thilaganathan, S. Moghaddam, et al. 2008. “Pten Inactivation Accelerates Oncogenic K-Ras-Initiated Tumorigenesis in a Mouse Model of Lung Cancer.” *Cancer Research* 68 (4): 1119–27.

Iyengar, P., Z. Wardak, D. E. Gerber, V. Tumati, C. Ahn, R. S. Hughes, J. E. Dowell, et al. 2018. “Consolidative Radiotherapy for Limited Metastatic Non-Small-Cell Lung Cancer: A Phase 2 Randomized Clinical Trial.” *JAMA Oncol* 4 (1): e173501.

Jackson, E. L., K. P. Olive, D. A. Tuveson, R. Bronson, D. Crowley, M. Brown, and T. Jacks. 2005. “The Differential Effects of Mutant P53 Alleles on Advanced Murine Lung Cancer.” *Cancer Research* 65 (22): 10280–88.

Jackson, E. L., N. Willis, K. Mercer, R. T. Bronson, D. Crowley, R. Montoya, T. Jacks, and D. A. Tuveson. 2001. “Analysis of Lung Tumor Initiation and Progression Using Conditional Expression of Oncogenic K-Ras.” *Genes & Development* 15 (24): 3243–48.

Jackson, Isabel L., Zeljko Vujaskovic, and Julian D. Down. 2011. “A Further Comparison of Pathologies after Thoracic Irradiation among Different Mouse Strains: Finding the Best Preclinical Model for Evaluating Therapies Directed against Radiation-Induced Lung Damage.” *Radiation Research* 175 (4): 510–18.

Jellison Evan R., Turner Michael J., Blair David A., Lingenheld Elizabeth G., Zu Li, Puddington Lynn, and Lefrançois Leo. 2012. “Distinct Mechanisms Mediate Naïve and Memory CD8 T-Cell Tolerance.” *Proceedings of the National Academy of Sciences* 109 (52): 21438–43.

Ji, H., M. R. Ramsey, D. N. Hayes, C. Fan, K. McNamara, P. Kozlowski, C. Torrice, et al. 2007. “LKB1 Modulates Lung Cancer Differentiation and Metastasis.” *Nature* 448 (7155): 807–10.

Jin, C., G. K. Lagoudas, C. Zhao, S. Bullman, A. Bhutkar, B. Hu, S. Ameh, et al. 2019. “Commensal Microbiota Promote Lung Cancer Development via Gammadelta T Cells.” *Cell* 176 (5): 998-1013 e16.

Jou, Eric, Noe Rodriguez-Rodriguez, Ana-Carolina F. Ferreira, Helen E. Jolin, Paula A. Clark, Kovilen Sawmynaden, Michelle Ko, et al. 2022. “An Innate IL-25–ILC2–MDSC Axis Creates a Cancer-Permissive Microenvironment for *Apc* Mutation–Driven Intestinal Tumorigenesis.” *Science Immunology*. https://doi.org/10.1126/sciimmunol.abn0175.

Jovanovic, Ivan P., Nada N. Pejnovic, Gordana D. Radosavljevic, Jelena M. Pantic, Marija Z. Milovanovic, Nebojsa N. Arsenijevic, and Miodrag L. Lukic. 2014. “Interleukin-33/ST2 Axis Promotes Breast Cancer Growth and Metastases by Facilitating Intratumoral Accumulation of Immunosuppressive and Innate Lymphoid Cells.” *International Journal of Cancer. Journal International Du Cancer* 134 (7): 1669–82.

Justilien, V., and A. P. Fields. 2013. “Utility and Applications of Orthotopic Models of Human Non-Small Cell Lung Cancer (NSCLC) for the Evaluation of Novel and Emerging Cancer Therapeutics.” *Current Protocols in Pharmacology / Editorial Board, S.J. Enna ... [et Al.]* 62: Unit 14 27.

Kachikwu, Evelyn L., Keisuke S. Iwamoto, Yu-Pei Liao, John J. DeMarco, Nzhde Agazaryan, James S. Economou, William H. McBride, and Dörthe Schaue. 2011. “Radiation Enhances Regulatory T Cell Representation.” *International Journal of Radiation Oncology, Biology, Physics* 81 (4): 1128–35.

Kalbasi, A., C. Komar, G. M. Tooker, M. Liu, J. W. Lee, W. L. Gladney, E. Ben-Josef, and G. L. Beatty. 2017. “Tumor-Derived CCL2 Mediates Resistance to Radiotherapy in Pancreatic Ductal Adenocarcinoma.” *Clinical Cancer Research: An Official Journal of the American Association for Cancer Research* 23 (1): 137–48.

Karachaliou, N., S. Pilotto, C. Lazzari, E. Bria, F. de Marinis, and R. Rosell. 2016. “Cellular and Molecular Biology of Small Cell Lung Cancer: An Overview.” *Transl Lung Cancer Res* 5 (1): 2–15.

Kargl, J., S. E. Busch, G. H. Yang, K. H. Kim, M. L. Hanke, H. E. Metz, J. J. Hubbard, et al. 2017. “Neutrophils Dominate the Immune Cell Composition in Non-Small Cell Lung Cancer.” *Nature Communications* 8: 14381.

Kasinski, A. L., and F. J. Slack. 2013. “Generation of Mouse Lung Epithelial Cells.” *Bio Protoc* 3 (15). https://www.ncbi.nlm.nih.gov/pmc/articles/PMC4880421.

Kearley, J., J. S. Silver, C. Sanden, Z. Liu, A. A. Berlin, N. White, M. Mori, et al. 2015. “Cigarette Smoke Silences Innate Lymphoid Cell Function and Facilitates an Exacerbated Type I Interleukin-33-Dependent Response to Infection.” *Immunity* 42 (3): 566–79.

Kellar, A., C. Egan, and D. Morris. 2015. “Preclinical Murine Models for Lung Cancer: Clinical Trial Applications.” *BioMed Research International* 2015: 621324.

Kim, J., W. Kim, U. J. Moon, H. J. Kim, H. J. Choi, J. I. Sin, N. H. Park, H. R. Cho, and B. Kwon. 2016. “Intratumorally Establishing Type 2 Innate Lymphoid Cells Blocks Tumor Growth.” *Journal of Immunology* 196 (5): 2410–23.

Klose, Christoph S. N., Melanie Flach, Luisa Möhle, Leif Rogell, Thomas Hoyler, Karolina Ebert, Carola Fabiunke, et al. 2014. “Differentiation of Type 1 ILCs from a Common Progenitor to All Helper-like Innate Lymphoid Cell Lineages.” *Cell* 157 (2): 340–56.

Klug, Felix, Hridayesh Prakash, Peter E. Huber, Tobias Seibel, Noemi Bender, Niels Halama, Christina Pfirschke, et al. 2013. “Low-Dose Irradiation Programs Macrophage Differentiation to an INOS+/M1 Phenotype That Orchestrates Effective T Cell Immunotherapy.” *Cancer Cell* 24 (5): 589–602.

Ko, E. C., D. Raben, and S. C. Formenti. 2018. “The Integration of Radiotherapy with Immunotherapy for the Treatment of Non-Small Cell Lung Cancer.” *Clinical Cancer Research: An Official Journal of the American Association for Cancer Research* 24 (23): 5792–5806.

Kobori, Hiroko, Masaaki Hashiguchi, Jinhua Piao, Moriyuki Kato, Patcharee Ritprajak, and Miyuki Azuma. 2010. "Enhancement of Effector CD8+ T-Cell Function by Tumour-Associated B7-H3 and Modulation of Its Counter-Receptor Triggering Receptor Expressed on Myeloid Cell-like Transcript 2 at Tumour Sites." *Immunology* 130 (3): 363–73.

Kopf, Manfred, Christoph Schneider, and Samuel P. Nobs. 2014. "The Development and Function of Lung-Resident Macrophages and Dendritic Cells." *Nature Immunology* 16 (1): 36–44.

Koyama, S., E. A. Akbay, Y. Y. Li, A. R. Aref, F. Skoulidis, G. S. Herter-Sprie, K. A. Buczkowski, et al. 2016. "STK11/LKB1 Deficiency Promotes Neutrophil Recruitment and Proinflammatory Cytokine Production to Suppress T-Cell Activity in the Lung Tumor Microenvironment." *Cancer Research* 76 (5): 999–1008.

Koyasu, Shigeo, and Kazuyo Moro. 2011. "Type 2 Innate Immune Responses and the Natural Helper Cell." *Immunology* 132 (4): 475–81.

Kroemer, G., L. Galluzzi, O. Kepp, and L. Zitvogel. 2013. "Immunogenic Cell Death in Cancer Therapy." *Annual Review of Immunology* 31: 51–72.

Kurowska-Stolarska, Mariola, Pete Kewin, Grace Murphy, Remo C. Russo, Bartosz Stolarski, Cristiana Couto Garcia, Mousa Komai-Koma, et al. 2008. "IL-33 Induces Antigen-Specific IL-5+ T Cells and Promotes Allergic-Induced Airway Inflammation Independent of IL-4." *Journal of Immunology* 181 (7): 4780–90.

Kwak, Eunice L., Yung-Jue Bang, D. Ross Camidge, Alice T. Shaw, Benjamin Solomon, Robert G. Maki, Sai-Hong I. Ou, et al. 2010. "Anaplastic Lymphoma Kinase Inhibition in Non–Small-Cell Lung Cancer." *The New England Journal of Medicine* 363 (18): 1693–1703.

Laurent, Paôline, Benoit Allard, Pauline Manicki, Valérie Jolivel, Emeline Levionnois, Mohamed Jeljeli, Pauline Henrot, et al. 2021. "TGFβ Promotes Low IL10-Producing ILC2 with Profibrotic Ability Involved in Skin Fibrosis in Systemic Sclerosis." *Annals of the Rheumatic Diseases* 80 (12): 1594–1603.

Lemjabbar-Alaoui, H., O. U. Hassan, Y. W. Yang, and P. Buchanan. 2015. "Lung Cancer: Biology and Treatment Options." *Biochimica et Biophysica Acta* 1856 (2): 189–210.

Li, Dong, Rodrigo Guabiraba, Anne-Gaëlle Besnard, Mousa Komai-Koma, Majid S. Jabir, Li Zhang, Gerard J. Graham, et al. 2014. "IL-33 Promotes ST2-Dependent Lung Fibrosis by the Induction of Alternatively Activated Macrophages and Innate Lymphoid Cells in Mice." *The Journal of Allergy and Clinical Immunology* 134 (6): 1422-1432.e11.

Li, H. Y., M. McSharry, B. Bullock, T. T. Nguyen, J. Kwak, J. M. Poczobutt, T. R. Sippel, et al. 2017. "The Tumor Microenvironment Regulates Sensitivity of Murine Lung Tumors to PD-1/PD-L1 Antibody Blockade." *Cancer Immunol Res* 5 (9): 767–77.

Lierova, A., M. Jelicova, M. Nemcova, M. Proksova, J. Pejchal, L. Zarybnicka, and Z. Sinkorova. 2018. "Cytokines and Radiation-Induced Pulmonary Injuries." *Journal of Radiation Research* 59 (6): 709–53.

Lim, Ai Ing, Silvia Menegatti, Jacinta Bustamante, Lionel Le Bourhis, Matthieu Allez, Lars Rogge, Jean-Laurent Casanova, Hans Yssel, and James P. Di Santo. 2016. "IL-12 Drives Functional Plasticity of Human Group 2 Innate Lymphoid Cells." *The Journal of Experimental Medicine* 213 (4): 569–83.

Liu, Y., W. N. Crowe, L. Wang, Y. Lu, W. J. Petty, A. A. Habib, and D. Zhao. 2019. "An Inhalable Nanoparticulate STING Agonist Synergizes with Radiotherapy to Confer Long-Term Control of Lung Metastases." *Nature Communications* 10 (1): 5108.

Lloyd, C. M., and B. J. Marsland. 2017. "Lung Homeostasis: Influence of Age, Microbes, and the Immune System." *Immunity* 46 (4): 549–61.

Long, Alan, Donye Dominguez, Lei Qin, Siqi Chen, Jie Fan, Minghui Zhang, Deyu Fang, Yi Zhang, Timothy M. Kuzel, and Bin Zhang. 2018. "Type 2 Innate Lymphoid Cells Impede IL-33–Mediated Tumor Suppression." *The Journal of Immunology*. https://doi.org/10.4049/jimmunol.1800173.

Lopez-Soto, A., S. Gonzalez, M. J. Smyth, and L. Galluzzi. 2017. "Control of Metastasis by NK Cells." *Cancer Cell* 32 (2): 135–54.

Louie, A. V., D. A. Palma, M. Dahele, G. B. Rodrigues, and S. Senan. 2015. "Management of Early-Stage Non-Small Cell Lung Cancer Using Stereotactic Ablative Radiotherapy: Controversies, Insights, and Changing Horizons." *Radiotherapy and Oncology: Journal of the European Society for Therapeutic Radiology and Oncology* 114 (2): 138–47.

Lugade, A. A., J. P. Moran, S. A. Gerber, R. C. Rose, J. G. Frelinger, and E. M. Lord. 2005. "Local Radiation Therapy of B16 Melanoma Tumors Increases the Generation of Tumor Antigen-Specific Effector Cells That Traffic to the Tumor." *Journal of Immunology* 174 (12): 7516–23.

Lugade, A. A., E. W. Sorensen, S. A. Gerber, J. P. Moran, J. G. Frelinger, and E. M. Lord. 2008. "Radiation-Induced IFN-Gamma Production within the Tumor Microenvironment Influences Antitumor Immunity." *Journal of Immunology* 180 (5): 3132–39.

Maier, B., A. M. Leader, S. T. Chen, N. Tung, C. Chang, J. LeBerichel, A. Chudnovskiy, et al. 2020. "A Conserved Dendritic-Cell Regulatory Program Limits Antitumour Immunity." *Nature* 580 (7802): 257–62.

Mainardi, S., N. Mijimolle, S. Francoz, C. Vicente-Duenas, I. Sanchez-Garcia, and M. Barbacid. 2014. "Identification of Cancer Initiating Cells in K-Ras Driven Lung Adenocarcinoma." *Proceedings of the National Academy of Sciences of the United States of America* 111 (1): 255–60.

Mantovani, A., P. Allavena, A. Sica, and F. Balkwill. 2008. "Cancer-Related Inflammation." *Nature* 454 (7203): 436–44.

Marcus, A., A. J. Mao, M. Lensink-Vasan, L. Wang, R. E. Vance, and D. H. Raulet. 2018. "Tumor-Derived CGAMP Triggers a STING-Mediated Interferon Response in Non-Tumor Cells to Activate the NK Cell Response." *Immunity* 49 (4): 754-763 e4.

Marshall, E. A., K. W. Ng, S. H. Kung, E. M. Conway, V. D. Martinez, E. C. Halvorsen, D. A. Rowbotham, et al. 2016. "Emerging Roles of T Helper 17 and Regulatory T Cells in Lung Cancer Progression and Metastasis." *Molecular Cancer* 15 (1): 67.

Martin-Orozco, N., P. Muranski, Y. Chung, X. O. Yang, T. Yamazaki, S. Lu, P. Hwu, N. P. Restifo, W. W. Overwijk, and C. Dong. 2009. "T Helper 17 Cells Promote Cytotoxic T Cell Activation in Tumor Immunity." *Immunity* 31 (5): 787–98.

Matsumura, S., B. Wang, N. Kawashima, S. Braunstein, M. Badura, T. O. Cameron, J. S. Babb, et al. 2008. "Radiation-Induced CXCL16 Release by Breast Cancer Cells Attracts Effector T Cells." *Journal of Immunology* 181 (5): 3099–3107.

McGranahan, N., A. J. Furness, R. Rosenthal, S. Ramskov, R. Lyngaa, S. K. Saini, M. Jamal-Hanjani, et al. 2016. "Clonal Neoantigens Elicit T Cell Immunoreactivity and Sensitivity to Immune Checkpoint Blockade." *Science* 351 (6280): 1463–69.

McKenzie, A. N. 2014. "Type-2 Innate Lymphoid Cells in Asthma and Allergy." *Annals of the American Thoracic Society* 11 Suppl 5 (December): S263-70.

McLaughlin, M., E. C. Patin, M. Pedersen, A. Wilkins, M. T. Dillon, A. A. Melcher, and K. J. Harrington. 2020. "Inflammatory Microenvironment Remodelling by Tumour Cells after Radiotherapy." *Nature Reviews. Cancer*. https://doi.org/10.1038/s41568-020-0246-1.

McVey, John C., Benjamin L. Green, Benjamin Ruf, Justin D. McCallen, Simon Wabitsch, Varun Subramanyam, Laurence P. Diggs, Bernd Heinrich, Tim F. Greten, and Chi Ma. 2022. "NAFLD Indirectly Impairs Antigen-Specific CD8+ T Cell Immunity against Liver Cancer in Mice." *IScience* 25 (2): 103847.

Meuwissen, Ralph, Sabine C. Linn, R. Ilona Linnoila, John Zevenhoven, Wolter J. Mooi, and Anton Berns. 2003. "Induction of Small Cell Lung Cancer by Somatic Inactivation of Both Trp53 and Rb1 in a Conditional Mouse Model." *Cancer Cell*. https://doi.org/10.1016/s1535-6108(03)00220-4.

Meylan, F., E. T. Hawley, L. Barron, J. L. Barlow, P. Penumetcha, M. Pelletier, G. Sciume, et al. 2014. "The TNF-Family Cytokine TL1A Promotes Allergic Immunopathology through Group 2 Innate Lymphoid Cells." *Mucosal Immunology* 7 (4): 958–68.

Meziani, L., M. Mondini, B. Petit, A. Boissonnas, V. Thomas de Montpreville, O. Mercier, M. C. Vozenin, and E. Deutsch. 2018. "CSF1R Inhibition Prevents Radiation Pulmonary Fibrosis by Depletion of Interstitial Macrophages." *The European Respiratory Journal: Official Journal of the European Society for Clinical Respiratory Physiology* 51 (3). https://doi.org/10.1183/13993003.02120-2017.

Milette, S., P. O. Fiset, L. A. Walsh, J. D. Spicer, and D. F. Quail. 2019. "The Innate Immune Architecture of Lung Tumors and Its Implication in Disease Progression." *The Journal of Pathology*. https://doi.org/10.1002/path.5241.

Mirchandani, A. S., A. G. Besnard, E. Yip, C. Scott, C. C. Bain, V. Cerovic, R. J. Salmond, and F. Y. Liew. 2014. "Type 2 Innate Lymphoid Cells Drive CD4+ Th2 Cell Responses." *Journal of Immunology* 192 (5): 2442–48.

Molofsky, A. B., F. Van Gool, H. E. Liang, S. J. Van Dyken, J. C. Nussbaum, J. Lee, J. A. Bluestone, and R. M. Locksley. 2015. "Interleukin-33 and Interferon-Gamma Counter-Regulate Group 2 Innate Lymphoid Cell Activation during Immune Perturbation." *Immunity* 43 (1): 161–74.

Mondini, M., P. L. Loyher, P. Hamon, M. Gerbe de Thore, M. Laviron, K. Berthelot, C. Clemenson, et al. 2019. "CCR2-Dependent Recruitment of Tregs and Monocytes Following Radiotherapy Is Associated with TNFalpha-Mediated Resistance." *Cancer Immunol Res* 7 (3): 376–87.

Monticelli, Laurel A., Gregory F. Sonnenberg, Michael C. Abt, Theresa Alenghat, Carly G. K. Ziegler, Travis A. Doering, Jill M. Angelosanto, et al. 2011. "Innate Lymphoid Cells Promote Lung-Tissue Homeostasis after Infection with Influenza Virus." *Nature Immunology* 12 (11): 1045–54.

Moore, M. W., F. R. Carbone, and M. J. Bevan. 1988. "Introduction of Soluble Protein into the Class I Pathway of Antigen Processing and Presentation." *Cell* 54 (6): 777–85.

Moral, John Alec, Joanne Leung, Luis A. Rojas, Jennifer Ruan, Julia Zhao, Zachary Sethna, Anita Ramnarain, et al. 2020. "ILC2s Amplify PD-1 Blockade by Activating Tissue-Specific Cancer Immunity." *Nature*. https://doi.org/10.1038/s41586-020-2015-4.

Moro, Kazuyo, Hiroki Kabata, Masanobu Tanabe, Satoshi Koga, Natsuki Takeno, Miho Mochizuki, Koichi Fukunaga, Koichiro Asano, Tomoko Betsuyaku, and Shigeo Koyasu. 2015. "Interferon and IL-27 Antagonize the Function of Group 2 Innate Lymphoid Cells and Type 2 Innate Immune Responses." *Nature Immunology* 17 (1): 76–86.

Moro, Kazuyo, Taketo Yamada, Masanobu Tanabe, Tsutomu Takeuchi, Tomokatsu Ikawa, Hiroshi Kawamoto, Jun-Ichi Furusawa, Masashi Ohtani, Hideki Fujii, and Shigeo Koyasu. 2009. "Innate Production of TH2 Cytokines by Adipose Tissue-Associated c-Kit+Sca-1+ Lymphoid Cells." *Nature* 463 (7280): 540–44.

Motomura, Y., H. Morita, K. Moro, S. Nakae, D. Artis, T. A. Endo, Y. Kuroki, O. Ohara, S. Koyasu, and M. Kubo. 2014. "Basophil-Derived Interleukin-4 Controls the Function of Natural Helper Cells, a Member of ILC2s, in Lung Inflammation." *Immunity* 40 (5): 758–71.

Muroyama, Yuki, Thomas R. Nirschl, Christina M. Kochel, Zoila Lopez-Bujanda, Debebe Theodros, Wendy Mao, Maria A. Carrera-Haro, et al. 2017. "Stereotactic Radiotherapy Increases Functionally Suppressive Regulatory T Cells in the Tumor Microenvironment." *Cancer Immunology Research*. https://doi.org/10.1158/2326-6066.cir-17-0040.

Nagashima, H., T. Mahlakoiv, H. Y. Shih, F. P. Davis, F. Meylan, Y. Huang, O. J. Harrison, et al. 2019. "Neuropeptide CGRP Limits Group 2 Innate Lymphoid Cell Responses and Constrains Type 2 Inflammation." *Immunity*. https://doi.org/10.1016/j.immuni.2019.06.009.

Nagata, Y., M. Hiraoka, T. Mizowaki, Y. Narita, Y. Matsuo, Y. Norihisa, H. Onishi, and H. Shirato. 2009. “Survey of Stereotactic Body Radiation Therapy in Japan by the Japan 3-D Conformal External Beam Radiotherapy Group.” *International Journal of Radiation Oncology, Biology, Physics* 75 (2): 343–47.

Nagata, Y., J. Wulf, I. Lax, R. Timmerman, F. Zimmermann, I. Stojkovski, and B. Jeremic. 2011. “Stereotactic Radiotherapy of Primary Lung Cancer and Other Targets: Results of Consultant Meeting of the International Atomic Energy Agency.” *International Journal of Radiation Oncology, Biology, Physics* 79 (3): 660–69.

Nakajima, Takahiro, Takashi Anayama, Yasushi Matsuda, David M. Hwang, Patrick Z. McVeigh, Brian C. Wilson, Gang Zheng, Shaf Keshavjee, and Kazuhiro Yasufuku. 2014. “Orthotopic Lung Cancer Murine Model by Nonoperative Transbronchial Approach.” *The Annals of Thoracic Surgery* 97 (5): 1771–75.

Nakatsuka, Yoshinari, Ai Yaku, Tomohiro Handa, Alexis Vandenbon, Yuki Hikichi, Yasutaka Motomura, Ayuko Sato, et al. 2020. “Profibrotic Function of Pulmonary Group 2 Innate Lymphoid Cells Is Controlled by Regnase-1.” *The European Respiratory Journal: Official Journal of the European Society for Clinical Respiratory Physiology*, January. https://doi.org/10.1183/13993003.00018-2020.

Neill, D. R., S. H. Wong, A. Bellosi, R. J. Flynn, M. Daly, T. K. Langford, C. Bucks, et al. 2010. “Nuocytes Represent a New Innate Effector Leukocyte That Mediates Type-2 Immunity.” *Nature* 464 (7293): 1367–70.

Nicolai, Christopher J., Natalie Wolf, I. Chang Chang, Georgia Kirn, Assaf Marcus, Chudi O. Ndubaku, Sarah M. McWhirter, and David H. Raulet. 2020. “NK Cells Mediate Clearance of CD8$^+$ T Cell–Resistant Tumors in Response to STING Agonists.” *Science Immunology* 5 (45): eaaz2738.

Niknam, S., H. B. Barsoumian, J. E. Schoenhals, H. L. Jackson, N. Yanamandra, M. S. Caetano, A. Li, et al. 2018. “Radiation Followed by OX40 Stimulation Drives Local and Abscopal Antitumor Effects in an Anti-PD1-Resistant Lung Tumor Model.” *Clinical Cancer Research: An Official Journal of the American Association for Cancer Research* 24 (22): 5735–43.

Nolan, Emma, Victoria Louise Bridgeman, Luigi Ombrato, Adam Karoutas, Nicolas Rabas, Celine Angeli Natascha Sewnath, Marcos Vasquez, et al. 2022. “Radiation Exposure Elicits a Neutrophil-Driven Response in Healthy Lung Tissue That Enhances Metastatic Colonization.” *Nature Cancer* 3 (2): 173–87.

Nosaka, T., T. Baba, Y. Tanabe, S. Sasaki, T. Nishimura, Y. Imamura, H. Yurino, et al. 2018. “Alveolar Macrophages Drive Hepatocellular Carcinoma Lung Metastasis by Generating Leukotriene B4.” *Journal of Immunology* 200 (5): 1839–52.

Nurwidya, F., F. Takahashi, and K. Takahashi. 2016. “Gefitinib in the Treatment of Nonsmall Cell Lung Cancer with Activating Epidermal Growth Factor Receptor Mutation.” *Journal of Natural Science, Biology, and Medicine* 7 (2): 119–23.

Ohne, Yoichiro, Jonathan S. Silver, Luann Thompson-Snipes, Magalie A. Collet, Jean Philippe Blanck, Brandi L. Cantarel, Alan M. Copenhaver, Alison A. Humbles, and Yong-Jun Liu. 2016. “IL-1 Is a Critical Regulator of Group 2 Innate Lymphoid Cell Function and Plasticity.” *Nature Immunology* 17 (6): 646–55.

Oliphant, C. J., Y. Y. Hwang, J. A. Walker, M. Salimi, S. H. Wong, J. M. Brewer, A. Englezakis, et al. 2014. “MHCII-Mediated Dialog between Group 2 Innate Lymphoid Cells and CD4(+) T Cells Potentiates Type 2 Immunity and Promotes Parasitic Helminth Expulsion.” *Immunity* 41 (2): 283–95.

Oliphant, Chris J., Jillian L. Barlow, and Andrew N. J. McKenzie. 2011. “Insights into the Initiation of Type 2 Immune Responses.” *Immunology* 134 (4): 378–85.

Olson, B., Y. Li, Y. Lin, E. T. Liu, and A. Patnaik. 2018. “Mouse Models for Cancer Immunotherapy Research.” *Cancer Discovery* 8 (11): 1358–65.

Onn, Amir, Takeshi Isobe, Satoshi Itasaka, Wenjuan Wu, Michael S. O’Reilly, Waun Ki Hong, Isaiah J. Fidler, and Roy S. Herbst. 2003. “Development of an Orthotopic Model to Study the Biology and Therapy of Primary Human Lung Cancer in Nude Mice.” *Clinical Cancer Research: An Official Journal of the American Association for Cancer Research* 9 (15): 5532.

Otto, Karl. 2008. “Volumetric Modulated Arc Therapy: IMRT in a Single Gantry Arc.” *Medical Physics* 35 (1): 310–17.

Overwijk, W. W., and N. P. Restifo. 2001. “B16 as a Mouse Model for Human Melanoma.” *Current Protocols in Immunology / Edited by John E. Coligan ... [et Al.]* Chapter 20 (May): Unit 20 1.

Paez, J. Guillermo, Pasi A. Jänne, Jeffrey C. Lee, Sean Tracy, Heidi Greulich, Stacey Gabriel, Paula Herman, et al. 2004. “EGFR Mutations in Lung Cancer: Correlation with Clinical Response to Gefitinib Therapy.” *Science* 304 (5676): 1497.

Palma, David A., Robert Olson, Stephen Harrow, Stewart Gaede, Alexander V. Louie, Cornelis Haasbeek, Liam Mulroy, et al. 2019. “Stereotactic Ablative Radiotherapy versus Standard of Care Palliative Treatment in Patients with Oligometastatic Cancers (SABR-COMET): A Randomised, Phase 2, Open-Label Trial.” *The Lancet* 393 (10185): 2051–58.

Patel, Dhiren F., Teresa Peiró, Nicoletta Bruno, Juho Vuononvirta, Samia Akthar, Franz Puttur, Chloe J. Pyle, et al. 2019. “Neutrophils Restrain Allergic Airway Inflammation by Limiting ILC2 Function and Monocyte–Dendritic Cell Antigen Presentation.” *Science Immunology* 4 (41): eaax7006.

Patin, Emmanuel C., Magnus T. Dillon, Pablo Nenclares, Lorna Grove, Heba Soliman, Isla Leslie, Davina Northcote, et al. 2022. “Harnessing Radiotherapy-Induced NK-Cell Activity by Combining DNA Damage-Response Inhibition and Immune Checkpoint Blockade.” *Journal for Immunotherapy of Cancer* 10 (3). https://doi.org/10.1136/jitc-2021-004306.

Paun, Alexandra, Amit Kunwar, and Christina K. Haston. 2015. “Acute Adaptive Immune Response Correlates with Late Radiation-Induced Pulmonary Fibrosis in Mice.” *Radiation Oncology* 10 (February): 45.

Pelosi, G., M. Barbareschi, A. Cavazza, P. Graziano, G. Rossi, and M. Papotti. 2015. “Large Cell Carcinoma of the Lung: A Tumor in Search of an Author. A Clinically Oriented Critical Reappraisal.” *Lung Cancer* 87 (3): 226–31.

Platonova, S., J. Cherfils-Vicini, D. Damotte, L. Crozet, V. Vieillard, P. Validire, P. Andre, et al. 2011. “Profound Coordinated Alterations of Intratumoral NK Cell Phenotype and Function in Lung Carcinoma.” *Cancer Research* 71 (16): 5412–22.

Price, A. E., H. E. Liang, B. M. Sullivan, R. L. Reinhardt, C. J. Eisley, D. J. Erle, and R. M. Locksley. 2010. “Systemically Dispersed Innate IL-13-Expressing Cells in Type 2 Immunity.” *Proceedings of the National Academy of Sciences of the United States of America* 107 (25): 11489–94.

Ramirez-Labrada, A. G., D. Isla, A. Artal, M. Arias, A. Rezusta, J. Pardo, and E. M. Galvez. 2020. “The Influence of Lung Microbiota on Lung Carcinogenesis, Immunity, and Immunotherapy.” *Trends in Cancer Research* 6 (2): 86–97.

Reck, M., D. Rodriguez-Abreu, A. G. Robinson, R. Hui, T. Csoszi, A. Fulop, M. Gottfried, et al. 2016. “Pembrolizumab versus Chemotherapy for PD-L1-Positive Non-Small-Cell Lung Cancer.” *The New England Journal of Medicine* 375 (19): 1823–33.

Reck, Martin, Tudor-Eliade Ciuleanu, Manuel Cobo Dols, Michael Schenker, Bogdan Zurawski, Juliana Menezes, Eduardo Richardet, et al. 2020. “Nivolumab (NIVO) + Ipilimumab (IPI) + 2 Cycles of Platinum-Doublet Chemotherapy (Chemo) vs 4 Cycles Chemo as First-Line (1L) Treatment (Tx) for Stage IV/Recurrent Non-Small Cell Lung Cancer (NSCLC): CheckMate 9LA.” *Journal of Clinical Orthodontics: JCO* 38 (15_suppl): 9501–9501.

Regales, L., M. N. Balak, Y. Gong, K. Politi, A. Sawai, C. Le, J. A. Koutcher, et al. 2007. “Development of New Mouse Lung Tumor Models Expressing EGFR T790M Mutants Associated with Clinical Resistance to Kinase Inhibitors.” *PloS One* 2 (8): e810.

Reits, E. A., J. W. Hodge, C. A. Herberts, T. A. Groothuis, M. Chakraborty, E. K. Wansley, K. Camphausen, et al. 2006. “Radiation Modulates the Peptide Repertoire, Enhances MHC Class I Expression, and Induces Successful Antitumor Immunotherapy.” *The Journal of Experimental Medicine* 203 (5): 1259–71.

Roche, Paul A., and Kazuyuki Furuta. 2015. “The Ins and Outs of MHC Class II-Mediated Antigen Processing and Presentation.” *Nature Reviews. Immunology* 15 (4): 203–16.

Rock, Jason R., Mark W. Onaitis, Emma L. Rawlins, Yun Lu, Cheryl P. Clark, Yan Xue, Scott H. Randell, and Brigid L. M. Hogan. 2009. “Basal Cells as Stem Cells of the Mouse Trachea and Human Airway Epithelium.” *Proceedings of the National Academy of Sciences of the United States of America* 106 (31): 12771–75.

Rusthoven, Kyle E., Brian D. Kavanagh, Stuart H. Burri, Changhu Chen, Higinia Cardenes, Mark A. Chidel, Thomas J. Pugh, Madeleine Kane, Laurie E. Gaspar, and Tracey E. Schefter. 2009. “Multi-Institutional Phase I/II Trial of Stereotactic Body Radiation Therapy for Lung Metastases.” *Journal of Clinical Oncology: Official Journal of the American Society of Clinical Oncology* 27 (10): 1579–84.

Salimi, M., R. Wang, X. Yao, X. Li, X. Wang, Y. Hu, X. Chang, P. Fan, T. Dong, and G. Ogg. 2018. “Activated Innate Lymphoid Cell Populations Accumulate in Human Tumour Tissues.” *BMC Cancer* 18 (1): 341.

Santini, F. C., and C. M. Rudin. 2017. “Atezolizumab for the Treatment of Non-Small Cell Lung Cancer.” *Expert Review of Clinical Pharmacology* 10 (9): 935–45.

Saranchova, I., J. Han, R. Zaman, H. Arora, H. Huang, F. Fenninger, K. B. Choi, et al. 2018. “Type 2 Innate Lymphocytes Actuate Immunity Against Tumours and Limit Cancer Metastasis.” *Scientific Reports* 8 (1): 2924.

Sarin, N., F. Engel, G. V. Kalayda, M. Mannewitz, J. Cinatl Jr, F. Rothweiler, M. Michaelis, et al. 2017. “Cisplatin Resistance in Non-Small Cell Lung Cancer Cells Is Associated with an Abrogation of Cisplatin-Induced G2/M Cell Cycle Arrest.” *PloS One* 12 (7): e0181081.

Satoh-Takayama, Naoko, Tamotsu Kato, Yasutaka Motomura, Tomoko Kageyama, Naoko Taguchi-Atarashi, Ryo Kinoshita-Daitoku, Eisuke Kuroda, et al. 2020. “Bacteria-Induced Group 2 Innate Lymphoid Cells in the Stomach Provide Immune Protection through Induction of IgA.” *Immunity*. https://doi.org/10.1016/j.immuni.2020.03.002.

Sceneay, J., M. T. Chow, A. Chen, H. M. Halse, C. S. Wong, D. M. Andrews, E. K. Sloan, et al. 2012. “Primary Tumor Hypoxia Recruits CD11b+/Ly6Cmed/Ly6G+ Immune Suppressor Cells and Compromises NK Cell Cytotoxicity in the Premetastatic Niche.” *Cancer Research* 72 (16): 3906–11.

Schaue, Dörthe, Josephine A. Ratikan, Keisuke S. Iwamoto, and William H. McBride. 2012. “Maximizing Tumor Immunity with Fractionated Radiation.” *International Journal of Radiation Oncology, Biology, Physics* 83 (4): 1306–10.

Schneider, T., H. Hoffmann, H. Dienemann, P. A. Schnabel, A. H. Enk, S. Ring, and K. Mahnke. 2011. “Non-Small Cell Lung Cancer Induces an Immunosuppressive Phenotype of Dendritic Cells in Tumor Microenvironment by Upregulating B7-H3.” *Journal of Thoracic Oncology: Official Publication of the International Association for the Study of Lung Cancer* 6 (7): 1162–68.

Schuijs, M. J., and T. Y. F. Halim. 2018. “Group 2 Innate Lymphocytes at the Interface between Innate and Adaptive Immunity.” *Annals of the New York Academy of Sciences* 1417 (1): 87–103.

Schuijs, Martijn J., Shaun Png, Arianne C. Richard, Anastasia Tsyben, Gregory Hamm, Julie Stockis, Celine Garcia, et al. 2020. “ILC2-Driven Innate Immune Checkpoint Mechanism Antagonizes NK Cell Antimetastatic Function in the Lung.” *Nature Immunology* 21 (9): 998–1009.

Schwartz, C., A. R. Khan, A. Floudas, S. P. Saunders, E. Hams, H. R. Rodewald, A. N. J. McKenzie, and P. G. Fallon. 2017. “ILC2s Regulate Adaptive Th2 Cell Functions via PD-L1 Checkpoint Control.” *The Journal of Experimental Medicine* 214 (9): 2507–21.

Senkus-Konefka, E., R. Dziadziuszko, E. Bednaruk-Mlynski, A. Pliszka, J. Kubrak, A. Lewandowska, K. Malachowski, M. Wierzchowski, M. Matecka-Nowak, and J. Jassem. 2005. “A Prospective, Randomised Study to Compare Two

Palliative Radiotherapy Schedules for Non-Small-Cell Lung Cancer (NSCLC)." *British Journal of Cancer* 92 (6): 1038–45.
Sharabi, A. B., C. J. Nirschl, C. M. Kochel, T. R. Nirschl, B. J. Francica, E. Velarde, T. L. Deweese, and C. G. Drake. 2015. "Stereotactic Radiation Therapy Augments Antigen-Specific PD-1-Mediated Antitumor Immune Responses via Cross-Presentation of Tumor Antigen." *Cancer Immunol Res* 3 (4): 345–55.
Sharma, S. K., N. K. Chintala, S. K. Vadrevu, J. Patel, M. Karbowniczek, and M. M. Markiewski. 2015. "Pulmonary Alveolar Macrophages Contribute to the Premetastatic Niche by Suppressing Antitumor T Cell Responses in the Lungs." *Journal of Immunology* 194 (11): 5529–38.
Sharma, Sherven, Seok-Chul Yang, Li Zhu, Karen Reckamp, Brian Gardner, Felicita Baratelli, Min Huang, Raj K. Batra, and Steven M. Dubinett. 2005. "Tumor Cyclooxygenase-2/Prostaglandin E_2–Dependent Promotion of FOXP3 Expression and $CD4^+CD25^+$ T Regulatory Cell Activities in Lung Cancer." *Cancer Research* 65 (12): 5211.
Shiao, S. L., B. Ruffell, D. G. DeNardo, B. A. Faddegon, C. C. Park, and L. M. Coussens. 2015. "TH2-Polarized CD4(+) T Cells and Macrophages Limit Efficacy of Radiotherapy." *Cancer Immunol Res* 3 (5): 518–25.
Sia, Joseph, Radoslaw Szmyd, Eric Hau, and Harriet E. Gee. 2020. "Molecular Mechanisms of Radiation-Induced Cancer Cell Death: A Primer." *Frontiers in Cell and Developmental Biology* 8 (February): 41.
Silva-Santos, B., S. Mensurado, and S. B. Coffelt. 2019. "Gammadelta T Cells: Pleiotropic Immune Effectors with Therapeutic Potential in Cancer." *Nature Reviews. Cancer* 19 (7): 392–404.
Silver, J. S., J. Kearley, A. M. Copenhaver, C. Sanden, M. Mori, L. Yu, G. H. Pritchard, et al. 2016. "Inflammatory Triggers Associated with Exacerbations of COPD Orchestrate Plasticity of Group 2 Innate Lymphoid Cells in the Lungs." *Nature Immunology* 17 (6): 626–35.
Singhal, S., P. S. Bhojnagarwala, S. O'Brien, E. K. Moon, A. L. Garfall, A. S. Rao, J. G. Quatromoni, et al. 2016. "Origin and Role of a Subset of Tumor-Associated Neutrophils with Antigen-Presenting Cell Features in Early-Stage Human Lung Cancer." *Cancer Cell* 30 (1): 120–35.
Soda, Manabu, Shuji Takada, Kengo Takeuchi, Young Lim Choi, Munehiro Enomoto, Toshihide Ueno, Hidenori Haruta, et al. 2008. "A Mouse Model for EML4-ALK-Positive Lung Cancer." *Proceedings of the National Academy of Sciences* 105 (50): 19893.
Spiotto, Michael, Yang-Xin Fu, and Ralph R. Weichselbaum. 2016. "The Intersection of Radiotherapy and Immunotherapy: Mechanisms and Clinical Implications." *Science Immunology* 1 (3): EAAG1266.
Spits, H., D. Artis, M. Colonna, A. Diefenbach, J. P. Di Santo, G. Eberl, S. Koyasu, et al. 2013. "Innate Lymphoid Cells--a Proposal for Uniform Nomenclature." *Nature Reviews. Immunology* 13 (2): 145–49.
Spits, Hergen, and Jenny Mjösberg. 2022. "Heterogeneity of Type 2 Innate Lymphoid Cells." *Nature Reviews. Immunology*, March, 1–12.
Stanaway, Jeffrey D., Ashkan Afshin, Emmanuela Gakidou, Stephen S. Lim, Degu Abate, Kalkidan Hassen Abate, Cristiana Abbafati, et al. 2018. "Global, Regional, and National Comparative Risk Assessment of 84 Behavioural, Environmental and Occupational, and Metabolic Risks or Clusters of Risks for 195 Countries and Territories, 1990–2017: A Systematic Analysis for the Global Burden of Disease Study 2017." *The Lancet* 392 (10159): 1923–94.
Steer, Catherine A., Laura Mathä, Hanjoo Shim, and Fumio Takei. 2020. "Lung Group 2 Innate Lymphoid Cells Are Trained by Endogenous IL-33 in the Neonatal Period." *JCI Insight*. https://doi.org/10.1172/jci.insight.135961.
Stier, Matthew T., Melissa H. Bloodworth, Shinji Toki, Dawn C. Newcomb, Kasia Goleniewska, Kelli L. Boyd, Marc Quitalig, et al. 2016. "Respiratory Syncytial Virus Infection Activates IL-13–Producing Group 2 Innate Lymphoid Cells through Thymic Stromal Lymphopoietin." *The Journal of Allergy and Clinical Immunology* 138 (3): 814-824.e11.
Strauss, Laura, Mohamed A. A. Mahmoud, Jessica D. Weaver, Natalia M. Tijaro-Ovalle, Anthos Christofides, Qi Wang, Rinku Pal, et al. 2020. "Targeted Deletion of PD-1 in Myeloid Cells Induces Antitumor Immunity." *Science Immunology* 5 (43): eaay1863.
Sung, Hyuna, Jacques Ferlay, Rebecca L. Siegel, Mathieu Laversanne, Isabelle Soerjomataram, Ahmedin Jemal, and Freddie Bray. 2021. "Global Cancer Statistics 2020: GLOBOCAN Estimates of Incidence and Mortality Worldwide for 36 Cancers in 185 Countries." *CA: A Cancer Journal for Clinicians* 71 (3): 209–49.
Sutherland, K. D., N. Proost, I. Brouns, D. Adriaensen, J. Y. Song, and A. Berns. 2011. "Cell of Origin of Small Cell Lung Cancer: Inactivation of Trp53 and Rb1 in Distinct Cell Types of Adult Mouse Lung." *Cancer Cell* 19 (6): 754–64.
Tang, Le, Fang Wei, Yingfen Wu, Yi He, Lei Shi, Fang Xiong, Zhaojian Gong, et al. 2018. "Role of Metabolism in Cancer Cell Radioresistance and Radiosensitization Methods." *Journal of Experimental & Clinical Cancer Research: CR* 37 (1): 87.
Taranova, Anna G., David Maldonado 3rd, Celine M. Vachon, Elizabeth A. Jacobsen, Hiam Abdala-Valencia, Michael P. McGarry, Sergei I. Ochkur, et al. 2008. "Allergic Pulmonary Inflammation Promotes the Recruitment of Circulating Tumor Cells to the Lung." *Cancer Research* 68 (20): 8582–89.
Teresa Pinto, A., M. Laranjeiro Pinto, A. Patricia Cardoso, C. Monteiro, M. Teixeira Pinto, A. Filipe Maia, P. Castro, et al. 2016. "Ionizing Radiation Modulates Human Macrophages towards a Pro-Inflammatory Phenotype Preserving Their pro-Invasive and pro-Angiogenic Capacities." *Scientific Reports* 6: 18765.
Thai, Alesha A., Benjamin J. Solomon, Lecia V. Sequist, Justin F. Gainor, and Rebecca S. Heist. 2021. "Lung Cancer." *The Lancet* 398 (10299): 535–54.

Thio, Christina Li-Ping, Po-Yu Chi, Alan Chuan-Ying Lai, and Ya-Jen Chang. 2018. “Regulation of Type 2 Innate Lymphoid Cell–Dependent Airway Hyperreactivity by Butyrate.” *The Journal of Allergy and Clinical Immunology* 142 (6): 1867-1883.e12.

Thommen, D. S., J. Schreiner, P. Muller, P. Herzig, A. Roller, A. Belousov, P. Umana, et al. 2015. “Progression of Lung Cancer Is Associated with Increased Dysfunction of T Cells Defined by Coexpression of Multiple Inhibitory Receptors.” *Cancer Immunol Res* 3 (12): 1344–55.

Timmerman, R., J. Galvin, J. Michalski, W. Straube, G. Ibbott, E. Martin, R. Abdulrahman, S. Swann, J. Fowler, and H. Choy. 2006. “Accreditation and Quality Assurance for Radiation Therapy Oncology Group: Multicenter Clinical Trials Using Stereotactic Body Radiation Therapy in Lung Cancer.” *Acta Oncologica* 45 (7): 779–86.

Timmerman, R., R. McGarry, C. Yiannoutsos, L. Papiez, K. Tudor, J. DeLuca, M. Ewing, et al. 2006. “Excessive Toxicity When Treating Central Tumors in a Phase II Study of Stereotactic Body Radiation Therapy for Medically Inoperable Early-Stage Lung Cancer.” *Journal of Clinical Oncology: Official Journal of the American Society of Clinical Oncology* 24 (30): 4833–39.

Timmerman, Robert, Rebecca Paulus, James Galvin, Jeffrey Michalski, William Straube, Jeffrey Bradley, Achilles Fakiris, et al. 2010. “Stereotactic Body Radiation Therapy for Inoperable Early Stage Lung Cancer.” *JAMA: The Journal of the American Medical Association* 303 (11): 1070–76.

Tonneau, Marion, Arielle Elkrief, David Pasquier, Thomas Paz Del Socorro, Mathias Chamaillard, Houda Bahig, and Bertrand Routy. 2021. “The Role of the Gut Microbiome on Radiation Therapy Efficacy and Gastrointestinal Complications: A Systematic Review.” *Radiotherapy and Oncology: Journal of the European Society for Therapeutic Radiology and Oncology* 156 (March): 1–9.

Trabanelli, S., M. F. Chevalier, A. Martinez-Usatorre, A. Gomez-Cadena, B. Salome, M. Lecciso, V. Salvestrini, et al. 2017. “Tumour-Derived PGD2 and NKp30-B7H6 Engagement Drives an Immunosuppressive ILC2-MDSC Axis.” *Nature Communications* 8 (1): 593.

Trojan, A., M. Urosevic, R. Dummer, R. Giger, W. Weder, and R. A. Stahel. 2004. “Immune Activation Status of CD8+ T Cells Infiltrating Non-Small Cell Lung Cancer.” *Lung Cancer* 44 (2): 143–47.

Tsoutsou, P. G., and M. I. Koukourakis. 2006. “Radiation Pneumonitis and Fibrosis: Mechanisms Underlying Its Pathogenesis and Implications for Future Research.” *International Journal of Radiation Oncology, Biology, Physics* 66 (5): 1281–93.

Turner, J. E., P. J. Morrison, C. Wilhelm, M. Wilson, H. Ahlfors, J. C. Renauld, U. Panzer, H. Helmby, and B. Stockinger. 2013. “IL-9-Mediated Survival of Type 2 Innate Lymphoid Cells Promotes Damage Control in Helminth-Induced Lung Inflammation.” *The Journal of Experimental Medicine* 210 (13): 2951–65.

Twyman-Saint Victor, C., A. J. Rech, A. Maity, R. Rengan, K. E. Pauken, E. Stelekati, J. L. Benci, et al. 2015. “Radiation and Dual Checkpoint Blockade Activate Non-Redundant Immune Mechanisms in Cancer.” *Nature* 520 (7547): 373–77.

Vanpouille-Box, C., A. Alard, M. J. Aryankalayil, Y. Sarfraz, J. M. Diamond, R. J. Schneider, G. Inghirami, C. N. Coleman, S. C. Formenti, and S. Demaria. 2017. “DNA Exonuclease Trex1 Regulates Radiotherapy-Induced Tumour Immunogenicity.” *Nature Communications* 8: 15618.

Videtic, Gregory M. M., Larry W. Stitt, A. Rashid Dar, Walter I. Kocha, Anna T. Tomiak, Pauline T. Truong, Mark D. Vincent, and Edward W. Yu. 2003. “Continued Cigarette Smoking by Patients Receiving Concurrent Chemoradiotherapy for Limited-Stage Small-Cell Lung Cancer Is Associated with Decreased Survival.” *Journal of Clinical Oncology: Official Journal of the American Society of Clinical Oncology* 21 (8): 1544–49.

Voortman, Johannes, Jih-Hsiang Lee, Jonathan Keith Killian, Miia Suuriniemi, Yonghong Wang, Marco Lucchi, William I. Smith, Paul Meltzer, Yisong Wang, and Giuseppe Giaccone. 2010. “Array Comparative Genomic Hybridization-Based Characterization of Genetic Alterations in Pulmonary Neuroendocrine Tumors.” *Proceedings of the National Academy of Sciences* 107 (29): 13040.

Walker, Jennifer A., and Andrew N. J. McKenzie. 2013. “Development and Function of Group 2 Innate Lymphoid Cells.” *Current Opinion in Immunology* 25 (2): 148–55.

Walle, Thomas, Joscha A. Kraske, Boyu Liao, Bénédicte Lenoir, Carmen Timke, Emilia von Bohlen und Halbach, Florian Tran, et al. 2022. “Radiotherapy Orchestrates Natural Killer Cell Dependent Antitumor Immune Responses through CXCL8.” *Science Advances* 8 (12): eabh4050.

Wallrapp, A., S. J. Riesenfeld, P. R. Burkett, R. E. Abdulnour, J. Nyman, D. Dionne, M. Hofree, et al. 2017. “The Neuropeptide NMU Amplifies ILC2-Driven Allergic Lung Inflammation.” *Nature* 549 (7672): 351–56.

Wang, Yifan, Weiye Deng, Nan Li, Shinya Neri, Amrish Sharma, Wen Jiang, and Steven H. Lin. 2018. “Combining Immunotherapy and Radiotherapy for Cancer Treatment: Current Challenges and Future Directions.” *Frontiers in Pharmacology* 9 (March): 185.

Wculek, S. K., and I. Malanchi. 2015. “Neutrophils Support Lung Colonization of Metastasis-Initiating Breast Cancer Cells.” *Nature* 528 (7582): 413–17.

Weaver, B. A. 2014. “How Taxol/Paclitaxel Kills Cancer Cells.” *Molecular Biology of the Cell* 25 (18): 2677–81.

Wennerberg, E., S. Spada, N. P. Rudqvist, C. Lhuillier, S. Gruber, Q. Chen, F. Zhang, et al. 2020. “CD73 Blockade Promotes Dendritic Cell Infiltration of Irradiated Tumors and Tumor Rejection.” *Cancer Immunol Res* 8 (4): 465–78.

Wild, Christopher, Paul Brennan, Martyn Plummer, Freddie Bray, Kurt Straif, and Jiri Zavadil. 2015. “Cancer Risk: Role of Chance Overstated.” *Science*.

Wirsdorfer, F., and V. Jendrossek. 2016. “The Role of Lymphocytes in Radiotherapy-Induced Adverse Late Effects in the Lung.” *Frontiers in Immunology* 7: 591.

Wojno, E. D., L. A. Monticelli, S. V. Tran, T. Alenghat, L. C. Osborne, J. J. Thome, C. Willis, A. Budelsky, D. L. Farber, and D. Artis. 2015. “The Prostaglandin D(2) Receptor CRTH2 Regulates Accumulation of Group 2 Innate Lymphoid Cells in the Inflamed Lung.” *Mucosal Immunology* 8 (6): 1313–23.

Wong, John, Elwood Armour, Peter Kazanzides, Iulian Iordachita, Erik Tryggestad, Hua Deng, Mohammad Matinfar, et al. 2008. “High-Resolution, Small Animal Radiation Research Platform with x-Ray Tomographic Guidance Capabilities.” *International Journal of Radiation Oncology, Biology, Physics* 71 (5): 1591–99.

Wong, See Heng, Jennifer A. Walker, Helen E. Jolin, Lesley F. Drynan, Emily Hams, Ana Camelo, Jillian L. Barlow, et al. 2012. “Transcription Factor RORα Is Critical for Nuocyte Development.” *Nature Immunology* 13 (3): 229–36.

Woo, E. Y., H. Yeh, C. S. Chu, K. Schlienger, R. G. Carroll, J. L. Riley, L. R. Kaiser, and C. H. June. 2002. “Cutting Edge: Regulatory T Cells from Lung Cancer Patients Directly Inhibit Autologous T Cell Proliferation.” *Journal of Immunology* 168 (9): 4272–76.

Woo, Edward Y., Christina S. Chu, Theresa J. Goletz, Katia Schlienger, Heidi Yeh, George Coukos, Stephen C. Rubin, Larry R. Kaiser, and Carl H. June. 2001. “Regulatory $CD4^+CD25^+$ T Cells in Tumors from Patients with Early-Stage Non-Small Cell Lung Cancer and Late-Stage Ovarian Cancer.” *Cancer Research* 61 (12): 4766.

Wu, Qiuji, Awatef Allouch, Isabelle Martins, Nazanine Modjtahedi, Eric Deutsch, and Jean-Luc Perfettini. 2017. “Macrophage Biology Plays a Central Role during Ionizing Radiation-Elicited Tumor Response.” *Biomedical Journal* 40 (4): 200–211.

Wu, Y., Y. Yan, Z. Su, Q. Bie, X. Chen, P. A. Barnie, Q. Guo, S. Wang, and H. Xu. 2017. “Enhanced Circulating ILC2s and MDSCs May Contribute to Ensure Maintenance of Th2 Predominant in Patients with Lung Cancer.” *Molecular Medicine Reports* 15 (6): 4374–81.

Yang, S., J. J. Zhang, and X. Y. Huang. 2012. “Mouse Models for Tumor Metastasis.” *Methods in Molecular Biology* 928: 221–28.

Yusa, K., L. Zhou, M. A. Li, A. Bradley, and N. L. Craig. 2011. “A Hyperactive PiggyBac Transposase for Mammalian Applications.” *Proceedings of the National Academy of Sciences of the United States of America* 108 (4): 1531–36.

Zappa, C., and S. A. Mousa. 2016. “Non-Small Cell Lung Cancer: Current Treatment and Future Advances.” *Transl Lung Cancer Res* 5 (3): 288–300.

Zhang, H., and J. Chen. 2018. “Current Status and Future Directions of Cancer Immunotherapy.” *Journal of Cancer* 9 (10): 1773–81.

Zhang, Jingjing, Jinxin Qiu, Wenyong Zhou, Jianping Cao, Xuefei Hu, Wenli Mi, Bing Su, Bin He, Ju Qiu, and Lei Shen. 2022. “Neuropilin-1 Mediates Lung Tissue-Specific Control of ILC2 Function in Type 2 Immunity.” *Nature Immunology* 23 (2): 237–50.

Zhang, Kangning, Xingyuan Xu, Muhammad Asghar Pasha, Christian W. Siebel, Angelica Costello, Angela Haczku, Katherine MacNamara, et al. 2017. “Cutting Edge: Notch Signaling Promotes the Plasticity of Group-2 Innate Lymphoid Cells.” *The Journal of Immunology* 198 (5): 1798–1803.

Zhang, Y., S. Huang, D. Gong, Y. Qin, and Q. Shen. 2010. “Programmed Death-1 Upregulation Is Correlated with Dysfunction of Tumor-Infiltrating CD8+ T Lymphocytes in Human Non-Small Cell Lung Cancer.” *Cellular & Molecular Immunology* 7 (5): 389–95.

Zheng, T., Z. Zhu, Z. Wang, R. J. Homer, B. Ma, R. J. Riese Jr, H. A. Chapman Jr, S. D. Shapiro, and J. A. Elias. 2000. “Inducible Targeting of IL-13 to the Adult Lung Causes Matrix Metalloproteinase- and Cathepsin-Dependent Emphysema.” *The Journal of Clinical Investigation* 106 (9): 1081–93.

Zhou, L., J. E. Lopes, M. M. Chong, Ivanov II, R. Min, G. D. Victora, Y. Shen, et al. 2008. “TGF-Beta-Induced Foxp3 Inhibits T(H)17 Cell Differentiation by Antagonizing RORgammat Function.” *Nature* 453 (7192): 236–40.

Zhu, Z., B. Ma, R. J. Homer, T. Zheng, and J. A. Elias. 2001. “Use of the Tetracycline-Controlled Transcriptional Silencer (TTS) to Eliminate Transgene Leak in Inducible Overexpression Transgenic Mice.” *The Journal of Biological Chemistry* 276 (27): 25222–29.